REVIEWS OF
MODERN PHYSICS

Synthesis of the Elements in Stars*

E. MARGARET BURBIDGE, G. R. BURBIDGE, WILLIAM A. FOWLER, AND F. HOYLE

*Kellogg Radiation Laboratory, California Institute of Technology, and
Mount Wilson and Palomar Observatories, Carnegie Institution of Washington,
California Institute of Technology, Pasadena, California*

"It is the stars, The stars above us, govern our conditions";
(King Lear, Act IV, Scene 3)

but perhaps

"The fault, dear Brutus, is not in our stars, But in ourselves,"
(Julius Caesar, Act I, Scene 2)

TABLE OF CONTENTS

I. INTRODUCTION

A. Element Abundances and Nuclear Structure

MAN inhabits a universe composed of a great variety of elements and their isotopes. In Table I,1 a count of the stable and radioactive elements and isotopes is listed. Ninety elements are found terrestrially and one more, technetium, is found in stars; only promethium has not been found in nature. Some 272 stable and 55 naturally radioactive isotopes occur on the earth. In addition, man has been able to produce artificially the neutron, technetium, promethium, and ten trans-uranic elements. The number of radioactive isotopes he has produced now numbers 871 and this number is gradually increasing.

Each isotopic form of an element contains a nucleus with its own characteristic nuclear properties which are different from those of all other nuclei. Thus the total of known nuclear species is almost 1200, with some 327 of this number known to occur in nature. In spite of this, the situation is not as complex as it might seem. Research in "classical" nuclear physics since 1932 has shown that all nuclei consist of two fundamental building blocks. These are the proton and the neutron which are called nucleons in this context. As long as energies below the meson production threshold are not exceeded, all "prompt" nuclear processes can be described as the shuffling and reshuffling of protons and neutrons into the variety of nucleonic packs called nuclei. Only in the slow beta-decay processes is there any interchange between protons and neutrons at low energies, and even there, as in the prompt reactions, the number of nucleons remains constant. Only at very high energies can nucleons be produced or annihilated. Prompt nuclear processes plus the slow beta reactions make it possible in principle to transmute any one type of

TABLE I,1. Table of elements and isotopes [compiled from *Chart of the Nuclides* (Knolls Atomic Power Laboratory, April, 1956)].

Elements		Isotopes	
Stable	81	Stable	272
Radioactive:		Radioactive:	
Natural ($Z \leq 83$)	1[a]	Natural ($A < 206$)	11[d]
($Z > 83$)	9[b]	($A \geq 206$)	44
Natural:		Natural:	
Stable and Radioactive	91	Stable and Radioactive	327
Radioactive:		Radioactive:	
Artificial ($Z \leq 83$)	1[c]	Artificial ($A < 206$)	702
($Z > 83$)	10	($A \geq 206$)	169
Total	102	Total	1198
Neutron	1	Neutron	1
	103		1199

[a] Tc, observed in S-type stars.
[b] Including At and Fr produced in weak side links of natural radioactivity
[c] Pm, not observed in nature.
[d] Including H^3, C^{14}, and Tc^{99}.

nuclear material into any other even at low energies of interaction.

With this relatively simple picture of the structure and interactions of the nuclei of the elements in mind, it is natural to attempt to explain their origin by a synthesis or buildup starting with one or the other or both of the fundamental building blocks. The following question can be asked: What has been the history of the matter, on which we can make observations, which produced the elements and isotopes of that matter in the abundance distribution which observation yields? This history is hidden in the abundance distribution of the elements. To attempt to understand the sequence of events leading to the formation of the elements it is necessary to study the so-called universal or cosmic abundance curve.

Whether or not this abundance curve is universal is not the point here under discussion. It is the distribution for the matter on which we have been able to make observations. We can ask for the history of that particular matter. We can also seek the history of the peculiar and abnormal abundances, observed in some stars. We can finally approach the problem of the universal or cosmic abundances. To avoid any implication that the abundance curve is universal, when such an implication is irrelevant, we commonly refer to the number distribution of the atomic species as a function of atomic weight simply as the atomic abundance distribution. In graphical form, we call it the atomic abundance curve.

The first attempt to construct such an abundance curve was made by Goldschmidt (Go37).† An improved curve was given by Brown (Br49) and more recently Suess and Urey (Su56) have used the latest available data to give the most comprehensive curve so far available. These curves are derived mainly from terrestrial, meteoritic, and solar data, and in some cases from other astronomical sources. Abundance determinations for

† Refer to Bibliography at end of paper.
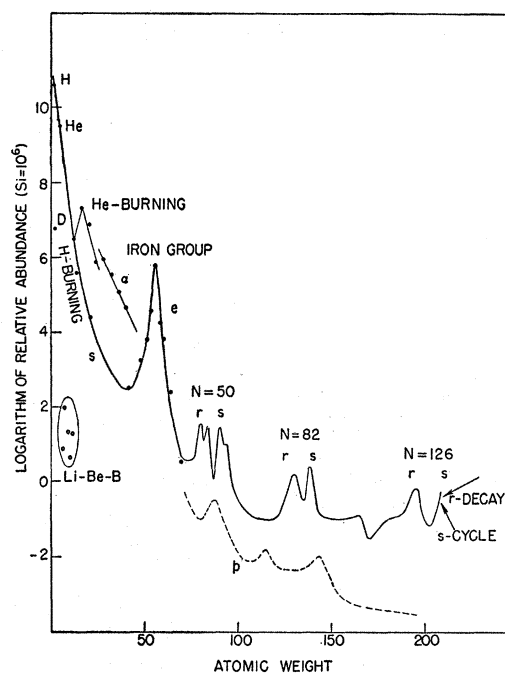
FIG. I,1. Schematic curve of atomic abundances as a function of atomic weight based on the data of Suess and Urey (Su56). Suess and Urey have employed relative isotopic abundances to determine the slope and general trend of the curve. There is still considerable spread of the individual abundances about the curve illustrated, but the general features shown are now fairly well established. These features are outlined in Table I,2. Note the overabundances relative to their neighbors of the alpha-particle nuclei $A = 16, 20, \cdots 40$, the peak at the iron group nuclei, and the twin peaks at $A = 80$ and 90, at 130 and 138, and at 194 and 208.

the sun were first derived by Russell (Ru29) and the most recent work is due to Goldberg, Aller, and Müller (Go57). Accurate relative isotopic abundances are available from mass spectroscopic data, and powerful use was made of these by Suess and Urey in compiling their abundance table. This table, together with some solar values given by Goldberg *et al.*, forms the basic data for this paper.

It seems probable that the elements all evolved from hydrogen, since the proton is stable while the neutron is not. Moreover, hydrogen is the most abundant element, and helium, which is the immediate product of hydrogen burning by the pp chain and the CN cycle, is the next most abundant element. The packing-fraction curve shows that the greatest stability is reached at iron and nickel. However, it seems probable that iron and nickel comprise less than 1% of the total mass of the galaxy. It is clear that although nuclei are tending to evolve to the configurations of greatest stability, they are still a long way from reaching this situation.

It has been generally stated that the atomic abundance curve has an exponential decline to $A \sim 100$ and is approximately constant thereafter. Although this is very roughly true it ignores many details which are important clues to our understanding of element synthesis. These details are shown schematically in Fig. I,1

TABLE I,2. Features of the abundance curve.

Feature	Cause
Exponential decrease from hydrogen to $A \sim 100$	Increasing rarity of synthesis for increasing A, reflecting that stellar evolution to advanced stages necessary to build high A is not common.
Fairly abrupt change to small slope for $A > 100$	Constant $\sigma(n,\gamma)$ in s process. Cycling in r process.
Rarity of D, Li, Be, B as compared with their neighbors H, He, C, N, O	Inefficient production, also consumed in stellar interiors even at relatively low temperatures.
High abundances of alpha-particle nuclei such as O^{16}, $Ne^{20} \cdots Ca^{40}$, Ti^{48} relative to their neighbors	He burning and α process more productive than H burning and s process in this region.
Strongly-marked peak in abundance curve centered on Fe^{56}	e process; stellar evolution to advanced stage where maximum energy is released (Fe^{56} lies near minimum of packing-fraction curve).
Double peaks $\begin{cases} A = 80, 130, 196 \\ \\ A = 90, 138, 208 \end{cases}$	Neutron capture in r process (magic $N = 50$, 82, 126 for progenitors). Neutron capture in s process (magic $N = 50$, 82, 126 for stable nuclei).
Rarity of proton-rich heavy nuclei	Not produced in main line of r or s process; produced in rare p process.

and are outlined in the left-hand column of Table I,2. The explanation of the right-hand column will be given in Sec. II.

It is also necessary to provide an explanation of the origin of the naturally radioactive elements. Further, the existence of the shielded isobars presents a special problem.

B. Four Theories of the Origin of the Elements

Any completely satisfactory theory of element formation must explain in quantitative detail all of the features of the atomic abundance curve. Of the theories so far developed, three assume that the elements were built in a primordial state of the universe. These are the nonequilibrium theory of Gamow, Alpher, and Herman [see (A150)], together with the recent modifications by Hayashi and Nishida (Ha56), the polyneutron theory of Mayer and Teller (Ma49), and the equilibrium theory developed by Klein, Beskow, and Treffenberg (Kl47). A detailed review of the history and development of these theories was given by Alpher and Herman (Al53).

Each of these theories possesses some attractive features, but none succeeds in meeting all of the requirements. It is our view that these are mainly satisfied by the fourth theory in which it is proposed that the stars are the seat of origin of the elements. In contrast with the other theories which demand matter in a particular

primordial state for which we have no evidence, this latter theory is intimately related to the known fact that nuclear transformations are currently taking place inside stars. This is a strong argument, since the primordial theories depend on very special initial conditions for the universe. Another general argument in favor of the stellar theory is as follows.

It is required that the elements, however they were formed, are distributed on a cosmic scale. Stars do this by ejecting material, the most efficient mechanisms being probably the explosive ejection of material in supernovae, the less energetic but more frequent novae, and the less rapid and less violent ejection from stars in the giant stages of evolution and from planetary nebulae. Primordial theories certainly distribute material on a cosmic scale but a difficulty is that the distribution ought to have been spatially uniform and independent of time once the initial phases of the universe were past. This disagrees with observation. There are certainly differences in composition between stars of different ages, and also stars at particular evolutionary stages have abnormalities such as the presence of technetium in the S-type stars and Cf^{254} in supernovae. A detailed discussion of these and other features is given in Secs. XI and XII.

It is not known for certain at the present time whether all of the atomic species heavier than hydrogen have been produced in stars without the necessity of element synthesis in a primordial explosive stage of the universe. Without attempting to give a definite answer to this problem we intend in this paper to restrict ourselves to element synthesis in stars and to lay the groundwork for future experimental, observational, and theoretical work which may ultimately provide conclusive evidence for the origin of the elements in stars. However, from the standpoint of the nuclear physics alone it is clear that our conclusions will be equally valid for a primordial synthesis in which the initial and later evolving conditions of temperature and density are similar to those found in the interiors of stars.

C. General Features of Stellar Synthesis

Except at catastrophic phases a star possesses a self-governing mechanism in which the temperature is adjusted so that the outflow of energy through the star is balanced by nuclear energy generation. The temperature required to give this adjustment depends on the particular nuclear fuel available. Hydrogen requires a lower temperature than helium; helium requires a lower temperature than carbon, and so on, the increasing temperature sequence ending at iron since energy generation by fusion processes ends here. If hydrogen is present the temperature is adjusted to hydrogen as a fuel, and is comparatively low. But if hydrogen becomes exhausted as stellar evolution proceeds, the temperature rises until helium becomes effective as a fuel. When helium becomes exhausted the temperature rises still

further until the next nuclear fuel comes into operation, and so on. The automatic temperature rise is brought about in each case by the conversion of gravitational energy into thermal energy.

In this way, one set of reactions after another is brought into operation, the sequence always being accompanied by rising temperature. Since penetrations of Coulomb barriers occur more readily as the temperature rises it can be anticipated that the sequence will be one in which reactions take place between nuclei with greater and greater nuclear charges. As it becomes possible to penetrate larger and larger barriers the nuclei will evolve towards configurations of greater and greater stability, so that heavier and heavier nuclei will be synthesized until iron is reached. Thus there must be a progressive conversion of light nuclei into heavier ones as the temperature rises.

There are a number of complicating factors which are superposed on these general trends. These include the following.

The details of the rising temperature and the barrier effects of nuclear reactions at low temperatures must be considered.

The temperature is not everywhere the same inside a star, so that the nuclear evolution is most advanced in the central regions and least or not at all advanced near the surface. Thus the composition of the star cannot be expected to be uniform throughout. A stellar explosion does not accordingly lead to the ejection of material of one definite composition, but instead a whole range of compositions may be expected.

Mixing within a star, whereby the central material is mixed outward, or the outer material inward, produces special effects.

Material ejected from one star may subsequently become condensed in another star. This again produces special nuclear effects.

All of these complications show that the stellar theory cannot be simple, and this may be a point in favor of the theory, since the abundance curve which we are trying to explain is also not simple. Our view is that the elements have evolved, and are evolving, by a whole series of processes. These are marked in the schematic abundance curve, Fig. I,1, as H burning, He burning, α, e, r, s, and p processes. The nature of these processes is shown in detail in Fig. I,2; details of this diagram are explained in the following sections.

II. PHYSICAL PROCESSES INVOLVED IN STELLAR SYNTHESIS, THEIR PLACE OF OCCURRENCE, AND THE TIME-SCALES ASSOCIATED WITH THEM

A. Modes of Element Synthesis

As was previously described in an introductory paper on this subject by Hoyle, Fowler, Burbidge, and Burbidge (Ho56), it appears that in order to explain all of the features of the abundance curve, at least eight different types of synthesizing processes are demanded, if we believe that only hydrogen is primeval. In order to clarify the later discussion we give an outline of these processes here (see also Ho54, Fo56).

(i) Hydrogen Burning

Hydrogen burning is responsible for the majority of the energy production in the stars. By hydrogen burning in element synthesis we shall mean the cycles which synthesize helium from hydrogen and which synthesize the isotopes of carbon, nitrogen, oxygen, fluorine, neon, and sodium which are not produced by processes (ii) and (iii). A detailed discussion of hydrogen burning is given in Sec. III.

(ii) Helium Burning

These processes are responsible for the synthesis of carbon from helium, and by further α-particle addition for the production of O^{16}, Ne^{20}, and perhaps Mg^{24}. They are described in detail in Sec. III.

(iii) α Process

These processes include the reactions in which α particles are successively added to Ne^{20} to synthesize the four-structure nuclei Mg^{24}, Si^{28}, S^{32}, A^{36}, Ca^{40}, and probably Ca^{44} and Ti^{48}. This is also discussed in Sec. III. The source of the α particles is different in the α process than in helium burning.

(iv) e Process

This is the so-called equilibrium process previously discussed by Hoyle (Ho46, Ho54) in which under conditions of very high temperature and density the elements comprising the iron peak in the abundance curve (vanadium, chromium, manganese, iron, cobalt, and nickel) are synthesized. This is considered in detail in Sec. IV.

(v) s Process

This is the process of neutron capture with the emission of gamma radiation (n,γ) which takes place on a long time-scale, ranging from $\sim$100 years to $\sim$10^5 years for each neutron capture. The neutron captures occur at a *slow* (s) rate compared to the intervening beta decays. This mode of synthesis is responsible for the production of the majority of the isotopes in the range $23 \leq A \leq 46$ (excluding those synthesized predominantly by the α process), and for a considerable proportion of the isotopes in the range $63 \leq A \leq 209$. Estimates of the time-scales in different regions of the neutron-capture chain in the s process will be considered later in this section, while the details of the nuclear physics of the process are discussed in Secs. V and VI together with the results. The s process produces the abundance peaks at $A = 90$, 138, and 208.

HYDROGEN BURNING ⟶

HELIUM BURNING

NUCLEAR REACTIONS AT EQUILIBRIUM

H^1 —$\frac{p\ p}{CN}$→ He^4

C^{12} — — → C^{13} — — → N^{14} — — → N^{15} — — → C^{12}

O^{16} ⟷ O^{17} O^{18} F^{19}

n

Ne^{20} ⟷ Ne^{21} — → Ne^{22} — → Na^{23} — → Ne^{20}

n

Mg^{24}

s-process on Ne^{22}

P^{31} S^{32} α-process

e-process

Iron Group

Neutron Rich Isotopes

Ti^{50} Ti^{48}

Slow capture (s-process on Fe^{56}) "Tc^{99}"

Heavy Elements

Rapid capture (r-process on Fe^{56}) "Cf^{254}"

Proton Rich Isotopes (p-process) (γ-process)

α-decay fission

Transbismuth Elements (U, Th, etc)

⟶ Main Line: H-burning He-burning

⟶ Less Frequent Processes

⟲ Neutron Capture: s-process r-process

■⟶ Catalytic Process: CN, Ne Na cycles

⟶ Equilibrium: e-process

⟹ Alpha Capture: α-process

- - → Modifying Process: p-process γ-process

—·—► Alpha decay or Fission

Fig. I,2. A schematic diagram of the nuclear processes by which the synthesis of the elements in stars takes place. Elements synthesized by interactions with protons (hydrogen burning) are listed horizontally. Elements synthesized by interactions with alpha particles (helium burning) and by still more complicated processes are listed vertically. The details of the production of all of the known stable isotopes of carbon, nitrogen, oxygen, fluorine, neon, and sodium are shown completely. Neutron capture processes by which the highly charged heavy elements are synthesized are indicated by curved arrows. The production of radio-active Tc[99] is indicated as an example for which there is astrophysical evidence of neutron captures at a slow rate over long periods of time in red giant stars. Similarly Cf[254], produced in supernovae, is an example of neutron synthesis at a rapid rate. The iron group is produced by a variety of nuclear reactions at equilibrium in the last stable stage of a star's evolution.

(vi) r Process

This is the process of neutron capture on a very short time-scale, $\sim$0.01–10 sec for the beta-decay processes interspersed between the neutron captures. The neutron captures occur at a *rapid* (*r*) rate compared to the beta decays. This mode of synthesis is responsible for production of a large number of isotopes in the range $70 \leq A \leq 209$, and also for synthesis of uranium and thorium. This process may also be responsible for some light element synthesis, e.g., S^{36}, Ca^{46}, Ca^{48}, and perhaps Ti^{47}, Ti^{49}, and Ti^{50}. Details of this process and the results of the calculations are discussed in Secs. VII and VIII. The *r* process produces the abundance peaks at $A = 80$, 130, and 194.

(vii) p Process

This is the process of proton capture with the emission of gamma radiation (p, γ), or the emission of a neutron following gamma-ray absorption (γ, n), which is responsible for the synthesis of a number of proton-rich isotopes having low abundances as compared with the nearby normal and neutron-rich isotopes. It is discussed in Sec. IX.

(viii) x Process

This process is responsible for the synthesis of deuterium, lithium, beryllium, and boron. More than one type of process may be demanded here (described collectively as the *x* process), but the characteristic of all of these elements is that they are very unstable at the temperatures of stellar interiors, so that it appears probable that they have been produced in regions of low density and temperature. There is, however, some observational evidence against this which is discussed in Sec. X together with the details of the possible synthesizing processes.

In the upper half of Table II,1 the abundances of different natural groups of elements, taken from the atomic abundance table of Suess and Urey (Su56), have been summed and listed, firstly by number and by fraction of the total, and secondly by weight and by mass fraction of the total. In the lower half of Table II,1, a similar listing has been made, but in this case the isotopes have been grouped according to which mode of synthesis has been responsible for their production. Our method of assignment to these different processes is described in subsection B. In some cases a natural group comprises just the elements built by one process; e.g., the iron group of elements are also the *e*-process isotopes in the lower half of the table, and consequently the same entry appears in both halves. In one case, that of the *r*-process isotopes of intermediate atomic weight, the estimate given is one that has been calculated in Sec. VII.

An auxiliary but indispensable process which is also demanded in our description of element synthesis is a nuclear process which will provide a source of free neutrons for both the *s* process and the *r* process. The first suggestion in this direction was made by Cameron (Ca54, Ca55) and Greenstein (Gr54), who proposed that the $C^{13}(\alpha,n)O^{16}$ reaction would provide such a source. In addition to this the reaction $Ne^{21}(\alpha,n)Mg^{24}$ has also been proposed by Fowler, Burbidge, and Burbidge (Fo55). More detailed work on the rates of these reactions by Marion and Fowler is now available (Ma57) and some discussion is included in Sec. III.

B. Method of Assignment of Isotopes among Processes (i) to (viii)

Of the eight processes which are demanded to synthesize all of the stable isotopes, assignments among hydrogen burning, helium burning, the α process, the *e* process, and the *x* process are comparatively straightforward, and are implicit in previous work and in the discussions in Secs. III, IV, and X. Thus pure hydrogen

TABLE II,1. Atomic abundances of various groups of the elements from Suess and Urey (Su56).

Group	By number	Fraction of total	By weight	Fraction of total
H	4.00×10^{10}	0.928	4.03×10^{10}	0.755
He	3.08×10^{9}	0.071	1.23×10^{10}	0.231
Li, Be, B	1.44×10^{2}	3.3×10^{-9}	1.30×10^{3}	2.4×10^{-8}
Carbon group: C, N, O, Ne	4.01×10^{7}	9.3×10^{-4}	6.5×10^{8}	1.2×10^{-2}
Silicon group: Na$-$Sc	2.65×10^{6}	6.1×10^{-5}	7.3×10^{7}	1.3×10^{-3}
Iron group: $50 \leq A \leq 62$	6.4×10^{5}	1.5×10^{-5}	3.6×10^{7}	6.7×10^{-4}
Middleweight: $63 \leq A < 100$	1.1×10^{3}	2.6×10^{-8}	7.7×10^{4}	1.4×10^{-6}
Heavyweight: $A \geq 100$	28	6.5×10^{-10}	4.6×10^{3}	8.6×10^{-8}
H+He burning: $12 \leq A \leq 22$	4.01×10^{7}	9.3×10^{-4}	6.5×10^{8}	1.2×10^{-2}
α process: 24, 28, $\cdots$48	2.2×10^{6}	5.1×10^{-5}	6.1×10^{7}	1.1×10^{-3}
s process: $23 \leq A \leq 46$	4.7×10^{5}	1.1×10^{-5}	1.3×10^{7}	2.4×10^{-4}
e process: $50 \leq A \leq 62$	6.4×10^{5}	1.5×10^{-5}	3.6×10^{7}	6.7×10^{-4}
s process: $63 \leq A \leq 75$	8.8×10^{2}	2.0×10^{-8}	5.7×10^{4}	1.1×10^{-6}
s process: $A > 75$	1.1×10^{2}	2.6×10^{-9}	1.1×10^{4}	2.1×10^{-7}
r process: intermediate A (calculated)	$\sim 1.5 \times 10^{3}$	$\sim 3.5 \times 10^{-8}$	$\sim 8 \times 10^{4}$	$\sim 1.5 \times 10^{-6}$
r process: $A > 75$	1.5×10^{2}	3.5×10^{-9}	1.4×10^{4}	2.6×10^{-7}
p process:	3.1	7.2×10^{-11}	2.0×10^{2}	3.8×10^{-9}

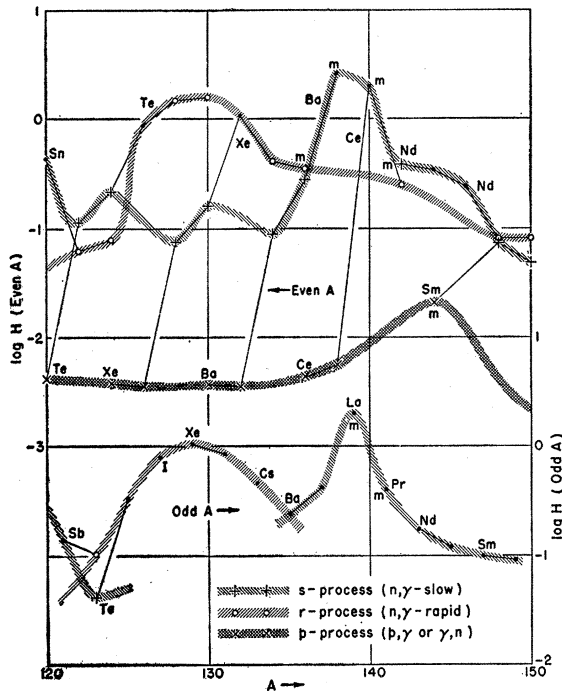Summary: $X(H) = 0.755$, $Y(He) = 0.231$, $Z(A > 4) = 0.014$

Fig. II,1. Logarithm of abundance H (silicon = 6.00, hydrogen = 10.60) of isotopes from $A = 120$ to 150 according to Suess and Urey (Su56). Odd mass numbers are shown in the bottom curve (read right ordinate). Even mass numbers are shown in the top curves (read left ordinate). Isotopes of a given element are connected by light lines (not to be confused with cross-hatched modes of element synthesis). Nuclei are distinguished by their method of synthesis as follows: +, produced only in neutron capture at a slow rate (s process); O, produced only in neutron capture at a rapid rate (r process); ●, produced in both processes but predominant mode of production assigned as discussed in text; X, produced only in proton capture or photoneutron processes (p process). The paths of the three processes are then indicated by the cross-hatching indicated in the figure. The stable nuclei with the magic number of closed shell neutrons, $N = 82$, are indicated by m. The abundance peak near $A = 139$ follows from the low neutron-capture cross section of the magic stable nuclei in the s process. The abundance peak near $A = 129$ follows from the low neutron-capture cross section and slow beta decay in the r process for the magic neutron-rich isobars (for example, $A = 129$, $N = 82$, $Z = 47$) which eventually decay by beta emission to the stable nuclei in this region. These arguments are based on the fact that in "steady flow" the abundance of a given nucleus will be inversely proportional to the rate at which it is transmuted by neutron capture or beta decay. The alternation in abundances exhibited by the sequence Te^{122}, Te^{124}, Xe^{128}, Xe^{130}, and Ba^{134}, Ba^{136} is to be expected in the s process because of the difficulty in adding further neutrons after two have already been captured. In general there is only one isobar at odd mass numbers. However, Te^{123} and Sb^{123} differentiate the r and s processes in an odd A curve. Te^{123} is probably unstable but with a very long lifetime.

burning is responsible for the synthesis of helium, and pure helium burning is responsible for C^{12}, O^{16}, and Ne^{20}. Also, hydrogen burning in these latter products of helium burning accounts for all of the stable isotopes up to Ne^{22} (cf. Sec. III). The only exceptions up to this point are deuterium, lithium, beryllium, and boron, which have therefore been assigned to a radically different type of synthesizing process, the x process. Assignment to the α process for a number of four-structure

nuclei was originally suggested by Hoyle (Ho54). All of these nuclei lie in a region of the abundance curve in which the surrounding nuclei are synthesized by the s process. As described in detail in Sec. VI, a plot of the σN products (neutron capture cross section times abundance) for such nuclei should delineate a smooth curve. However, because of their comparatively large abundances, the nuclei made by the α process all lie above this curve. This result bears out the assignment of these nuclei to the α process. Assignment of the nuclei in the iron peak to the e process was also proposed earlier by Hoyle. The large abundance peak at this point shows clearly that a separate process is demanded and the results of Sec. IV suggest strongly that our assignments to the e process are correct.

As far as assignments among the s, r, and p processes are concerned, the situation is a little more complex. Suess and Urey (Su56) and Coryell (Co56) have already pointed out that the peaks in the abundance curves at stable nuclei with filled neutron shells ($A = 90$, $N = 50$; $A = 138$, $N = 82$; $A = 208$, $N = 126$) strongly indicate the operation of the s process, and the nearby peaks at $A = 80$, 130, and 194, shifted by $\delta A \sim 8$ to 14, similarly require the operation of the r process. Also, calculations of Fowler et al. (Fo55) suggested that apart from the nuclei built by the α process all of the nuclei with $23 \leq A \leq 46$ with the exception of S^{36}, Ca^{46}, and Ca^{48} can be synthesized by the s process.

Certain isotopes of the heavy elements can be built only by the r process while others can be built only by the s process. The two processes differ in this respect because they allow very different times for the occurrence of the beta disintegrations along the chain of nuclei built by the neutron addition. In the s process most beta-active nuclei have time to decay before additional capture occurs. On the other hand, the r process involves neutron captures which take place at a rate much faster than the beta decays which have reaction times of 0.01 to 10 sec.

The need for a third process, the p process, arises because a third set of isotopes cannot be built by either the rapid or the slow capture of neutrons (the reasons for this from the standpoint of nuclear structure are discussed in Sec. V). As an example of the way in which the three processes operate and also of how assignments have been made, we shall consider the eight isotopes of tellurium. The light isotopes $_{52}Te_{70}^{122}$, $_{52}Te_{71}^{123}$, and $_{52}Te_{72}^{124}$ can be synthesized only in the s process, since in the r process, the ultimate beta decays of the neutron-rich isobars at 122, 123, 124, produced by rapid neutron addition, terminate at the stable isotopes $_{50}Sn_{72}^{122}$, $_{51}Sb_{72}^{123}$, and $_{50}Sn_{74}^{124}$, which are on the neutron side of the nuclear stability line. On the other hand, the heaviest isotope Te^{130} can be produced only in the r process, where it is the stable product of the decay of neutron-rich isobars of mass 130. In the s process, radioactive Te^{129} with a half-life of 70 min has time to decay to I^{129} (half-life 2×10^7 years), and after another neutron

capture, the resultant I^{130} decays in 12.6 hr to Xe^{130} which is thus produced in the s chain instead of Te^{130}. The isotopes Te^{125}, Te^{126}, and Te^{128} can be produced in either the s or the r process, although Te^{128} is produced in the slow capture of neutrons only in a weak side link of the chain resulting from the fact that I^{128} decays 5% of the time by positron emission or electron capture. Thus we believe that it is synthesized predominantly by the r process. The rarest and lightest isotope Te^{120} cannot be built by either process and it is for this isotope that the p process is demanded. Te^{120} is about 1% as abundant, and Te^{122}, Te^{123}, and Te^{124} are about 10% as abundant, as Te^{128} and Te^{130}. This suggests that we assign Te^{126}, which has an abundance comparable to Te^{128} and Te^{130}, to the r process. Te^{125} is an intermediate case, but it follows the trend of the r process and to this we assign its production. Assignments between the s, r, and p processes have been made in this way. In Figs. II,1; II,2; and II,3, the separation of the isotopes in the region $120 < A < 150$ is shown. In Fig. II,1 the abundances are plotted logarithmically after the manner of Suess and Urey (Su56). Nuclear species produced in the same process are connected by shaded curves and the general trend of the production becomes clear. In order to show more clearly the great increase in abundance in the peaks, linear plots of the abundances of the odd and even isotopes, respectively, are shown in Figs. II,2 and II,3. The magic-number peaks stand out clearly in both odd-A and even-A nuclei.

C. Abundances and Synthesis Assignments Given in the Appendix

The Appendix contains all of the information we have been able to collect which is relevant to the synthesis
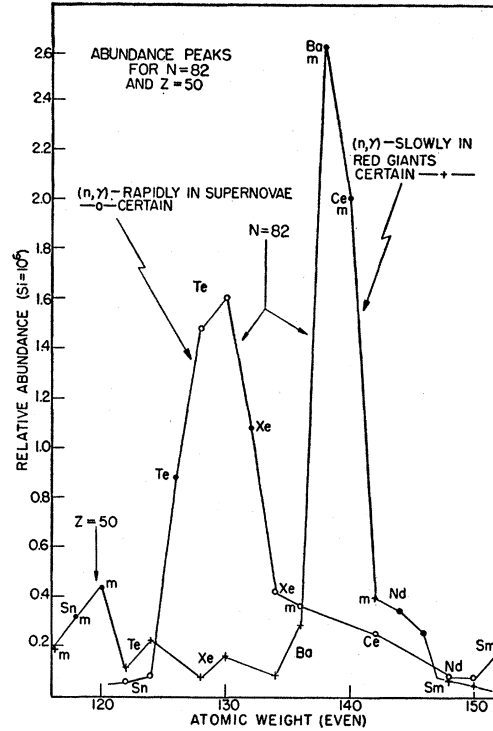
FIG. II,3. The even-A abundance peaks near $A = 130$ and 138 shown on a linear scale. See Fig. II,1 for comments.

problem. All of the stable isotopes in order of increasing A are given in this table. We also include the beta-unstable isotopes which lie on the main neutron-capture chain in the s process, together with a few others which are given for special reasons. The table was originally drawn up to represent the building of elements by the s process. For this reason the left-hand columns follow the main chain of nuclei synthesized by neutron capture in the s process. The right-hand columns give information concerning the isotopes which are either completely by-passed by the s process or which lie in the subsidiary loops of the chain. These loops can be formed in two ways. Either they form at nuclei which beta decay with a half-life such that in the s process a proportion of the nuclei will capture a further neutron before beta decay, while the remainder beta decay directly (the next step in the chain following the nucleus $X_Z{}^A$ being either $X_Z{}^{A+1}$ or $X_{Z+1}{}^A$). Alternatively a loop will be formed if a nucleus can decay either by emitting an electron or by emitting a positron or capturing a K electron (the next step in the chain following the nucleus $X_Z{}^A$ being either $X_{Z+1}{}^A$ or $X_{Z-1}{}^A$). A few isomeric states are also given [an example is $_{48}Cd_{65}{}^{(m)} (\beta^-)$] in cases in which they also lead to the development of loops. In all cases the side of the loop which is in the main chain will be determined by the faster of the reactions (either neutron-capture or beta-decay) which can take place. To distinguish between nuclei which lie in the weak branch of a loop, and those which are completely by-passed
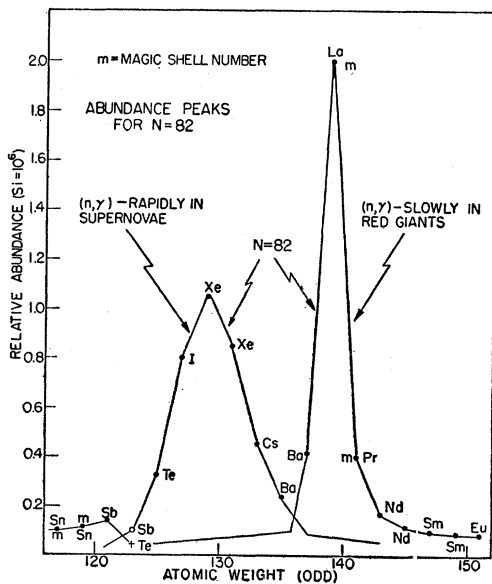

FIG. II,2. The odd A abundance peaks near $A = 129$ and 139 shown on a linear scale. See Fig. II,1 for comments.

in the chain, horizontal lines are drawn to contain each loop.

Although the table was prepared primarily for the s process it is now used to describe all of the modes of element synthesis. For this reason a number of beta-active nuclei which are by-passed in regions of small A are given. This enables us to discuss the r process as it would apply for the very light elements.

Abundances given in the Appendix have been taken predominantly from the table of Suess and Urey (Su56). For the elements scandium, titanium, vanadium, chromium, manganese, iron, cobalt, nickel, copper, and lead, the solar abundances obtained by Goldberg, Aller, and Müller (Go57) are also given in parentheses under those of Suess and Urey. The product of the neutron-capture cross section times the solar abundance is also given in parentheses in the σN column (cf. Sec. VI).

Assignments of all of the stable isotopes to their most probable mode of production are given in the right-hand columns in the table. In the s and the r processes, when the isotope can be made only by one or other of these processes, then they are designated s only or r only. In cases where the isotope is made predominantly by one process though the other may contribute a little—as, for example, where the r process is mainly responsible for synthesis, though the isotope lies in the main s chain—then we write simply r (or s), hydrogen burning, helium burning, α, e, p, x, as the case may be. In some cases more than one process may contribute appreciably to the synthesis of that isotope. In these cases the process which is believed to contribute most is written first, while in the few cases in which the two processes are believed to make equal contributions, an approximate equality sign is used, and in the abundance column ($\frac{1}{2}$) is written. In some other cases $\frac{2}{3}$ of the abundance of an isotope has been attributed to the s process and only $\frac{1}{3}$ to the r process. In these cases ($\frac{2}{3}$) is written in the abundance column (these fractions are only very approximate). Thus, in proceeding from isotopes which can be made solely on the s process to those which are made solely on the r process, the sequence of designations is s only, s, sr, $s \approx r$, rs, r, r only. Magic-number nuclei with closed shells having 14, 20, 28, 50, 82, and 126 neutrons, most of which are synthesized by the s process, are marked in the assignment column of the table by m in parentheses. Similarly, nuclei made by the r process whose progenitors had closed shells having 50, 82, or 126 neutrons are marked by m' in parentheses. A few of the light nuclei undergo nuclear reactions which lead not to heavier element synthesis but to breakup, or to decrease in A (e.g., Li^9). In the table these have been designated return (meaning that they return back down the chain), and in some cases the products of the reactions which are responsible for this are given.

D. Time-Scales for Different Modes of Synthesis

(1) Hydrogen-Burning Time-Scale

Hydrogen burning is responsible for all of the energy production of stars on the main sequence. After stars have evolved off the main sequence following the development of a chemical inhomogeneity, hydrogen burning in a shell still remains an important energy source. Thus the synthesis of elements in hydrogen burning is going on continuously, and the range in time-scales for particular stars is dependent only on their initial masses after condensation, and the point in their evolution at which they eject material which has been synthesized. Thus these time-scales may range from $\sim 10^6$ years for massive O and B stars to times which are of the order of though less than the age of the galaxy (since we have no evidence for the existence today of primeval stars of pure hydrogen).

(2) Helium-Burning Time-Scale

It is believed that helium burning takes place in stars which have evolved onto the giant branch of the HR diagram. In this region central temperatures of $\sim 10^8$ degrees and densities of $\sim 10^5$ g/cc are reached in the helium core, according to the theoretical calculations of Hoyle and Schwarzschild (Ho55), and under these conditions synthesis of C^{12} becomes possible (Sa52, Co57, Sa57). The further helium-burning reactions leading to production of O^{16}, Ne^{20}, and Mg^{24} also can take place under suitable conditions though the amounts of these isotopes synthesized will decrease as the Coulomb barriers get larger (cf. Sec. III). The time-scale for helium burning is therefore governed by the lifetime of stars subsequent to their becoming red giants. Since their mode of evolution off the giant branch is not yet understood, it is difficult to make accurate estimates of this time, but calculations of Hoyle and Schwarzschild and Hoyle and Haselgrove (Ho56a) suggest that a time-scale of $\sim 10^7 - 10^8$ years for stars to evolve in this region is reasonable.

(3) α-Process Time-Scale

This process, since it involves reactions between nuclei of comparatively large Z, demands temperatures of $\sim 10^9$ degrees (cf. Sec. III). Thus it appears that this condition will be reached only when a star is contracting further following the helium burning mentioned above. Consequently we may hypothesize that this situation is reached at a later stage of evolution, after the star has left the giant branch. The time-scale involved is difficult to estimate. It is probably short in comparison with the time taken for the star to evolve in the giant region but long compared with the time-scale for the e, r, and p processes. An argument concerning the synthesis of Ti^{48}, the last nucleus which may be built by this process, suggests that the time-scale for its production from the preceding nucleus is $\gtrsim 20$ years. Details

of this argument are given in Sec. III D. The total time-scale for the whole α process might lie in the range $\sim 10^2$–10^4 years.

(4) Rapid Time-Scales

e process.—As is discussed in Secs. IV and XII, this process takes place under extreme conditions of temperature and density, probably just prior to a supernova outburst. The time-scale involved may be of the order of seconds or minutes.

r process.—The nuclear physics of this process demands that neutrons be added extremely rapidly, so that the total time-scale for the addition of a maximum of about 200 neutrons per iron nucleus is ~ 10–100 sec. It has previously been suggested that the spontaneous fission of Cf^{254} is responsible for the form of the decay light curves of supernovae of Type I which have an exponential form with a half-life near 55 days, so that this is strong evidence for the fact that the r process takes place in such outbursts (Bu56). The time-scale for the explosive phases of such outbursts may well be as short as 100–1000 sec. Further support is given by a comparison of the results of calculations based on this hypothesis with the observed abundances of isotopes built by this process (Secs. VII and VIII).

p process.—It has previously been suggested that this process takes place in the outbursts of supernovae of Type II on a time-scale comparable to that for the r process.

(5) s-Process Time-Scale

In earlier work it was suggested that the s process is currently going on in the interiors of some red giant stars (Ca55, Fo55). The presence of technetium in the atmospheres of S-type stars, observed by Merrill (Me52), and also to a lesser extent in carbon and M-type stars, affords conclusive evidence that nuclear activity involving neutron capture is currently going on in the interiors of these stars. This element is being both synthesized and mixed to the surface of the star in a time which is less than or at least of the same order as the half-life against beta decay of the longest-lived isotope of technetium (Tc^{99} with a half-life of 2×10^5 years). This is compatible with the result that the time taken for the stars to evolve in the giant branch of the HR diagram is $\sim 10^7$ years. Of the reactions $C^{13}(\alpha,n)O^{16}$ and $Ne^{21}(\alpha,n)Mg^{24}$, which can give neutron production, the former will give an adequate supply of neutrons to carry heavy-element synthesis right through to the heaviest nuclei only if there is some mixing between the envelope hydrogen and the products of helium burning in the cores at the red-giant stage. In a previous paper (Fo55) it was pointed out that the $Ne^{21}(\alpha,n)Mg^{24}$ reaction could provide an adequate source of neutrons and also avoid the problem of mixing between core and envelope. In Sec. III F, however, it is pointed out that for this to be the case, certain conditions must be satisfied. The relative importance of these two reactions

for the s process will be discussed in detail in Sec. III F. The evidence from work on theoretical models suggests that a very deep convective zone extending inward from the surface is not unreasonable, so that mixing of the synthesized material to the surface can take place.

As will be seen, there appear to be two time-scales for the s process. These depend on the average times taken for the nuclei to capture neutrons. Thus these times are functions of the neutron density and hence of the rates of the neutron-producing reactions, and also of the capture cross sections. In Sec. V we describe the method of estimating the neutron capture cross sections (σ) given in the appendix. By using these together with the isotopic abundances and the assignments of nuclei to the s process, it is possible to make some estimates of the neutron-capture times at particular points in the slow neutron-capture chain. The method of doing this is as follows.

As pointed out in Sec. II C, if the beta-decay time is greater than a few years then the next link in the chain following $X_Z{}^A$ may be either $X_{Z+1}{}^A$ or $X_Z{}^{A+1}$, the relative importance of the branch depending on the time-scale for neutron capture at this point. We show in the appendix all possible loops corresponding to time-scales between $\sim 10^2$ years and $\sim 10^6$ years. Thus in all cases in which the beta decay takes place in a time $\ll 100$ years we have assumed that all of the nuclei will beta decay and any nuclei which can only be produced if another neutron is captured before the beta decay takes place are by-passed in the s process. If on the other hand the half-life for beta decay is $\gg 10^6$ years we have assumed that the nucleus is effectively stable in the s chain and will always capture a neutron. In cases like this it must be remembered, however, that all of the unstable nuclei with half-lives $\gg 10^6$ years which are effectively stable as far as the s process is concerned will eventually decay into the succeeding stable nuclei long after the s process has ceased operating. For elements in the solar system this will be true for all long-lived but unstable nuclei for which the half-life $< 5 \times 10^9$ years.

There appear to be two indicators for the time-scale for the s process in two regions of A. The first can be obtained from two isotopes of krypton. Both Kr^{80} and Kr^{82} are built only by the s process, being shielded in the r process by Se^{80} and Se^{82}. However, from the appendix we see that there is an s chain loop at Se^{79} which is due to the beta decay of this isotope with a half-life of 7×10^4 years. Thus while Kr^{82} is produced partly in the main chain and partly in the loop, Kr^{80} is only produced in the loop. Now under conditions of steady neutron flow (see Sec. VI) the basic equations for the relative abundances of these isotopes are

$$N(Kr^{80})\lambda_n(Kr^{80}) = 0.92 N(Se^{79})\lambda_\beta(Se^{79})$$

and

$$N(Kr^{82})\lambda_n(Kr^{82}) = N(Se^{79})[\lambda_\beta(Se^{79}) + \lambda_n(Se^{79})],$$

where λ_n and λ_β are the neutron-capture and beta-decay rates respectively. The coefficient 0.92 appears because in the loop the nuclei have to pass through Br^{80} which beta decays only 92% of the time. On dividing these two equations and substituting in terms of the half-lives t_n and t_β instead of the rates, we find that

$$\frac{t_n(Se^{79}) + t_\beta(Se^{79})}{t_n(Se^{79})} = 0.92 \frac{t_n(Kr^{80})}{t_n(Kr^{82})} \frac{N(Kr^{82})}{N(Kr^{80})}.$$

Now $\sigma(Kr^{80}) \backsimeq 2\sigma(Kr^{82})$ so that $\lambda_n(Kr^{80}) \backsimeq 2\lambda_n(Kr^{82})$ and $t_n(Kr^{82}) \backsimeq 2t_n(Kr^{80})$. [In the appendix we put $\sigma(Kr^{80}) = \sigma(Kr^{82})$ and do not in general take into account the factor of ~ 2 which is a result of the fact that the light neutron-poorer isotopes capture neutrons more readily than the heavier ones.] The abundance ratio $N(Kr^{82})/N(Kr^{80})$ is given in the appendix. Thus substituting these values on the right-hand side of the equation we find for Se^{79} that

$$t_n/t_\beta = 1/1.37,$$

and, since $t_\beta = 7 \times 10^4$ years, $t_n = 5.1 \times 10^4$ years. Now this half-life for neutron capture is determined in a region where $\sigma_n = 360$ mb, so that in the region near iron where this neutron chain begins and where $\sigma = 30$ mb the effective half-life is $5.1 \times 10^4 \times 360/30 \backsimeq 6 \times 10^5$ years. The total time demanded to build up the isotopes from iron if this were characteristic of the whole curve would be 10^6–10^7 years since there are many captures involved, but most of these take place on nuclei with larger σ values than that for iron. We show later that this long time-scale for the s process is probably the result of a paucity of neutrons—probably only about five neutrons per iron nucleus are made available. This is reflected in the tendency for the σN product to decrease rather rapidly as A increases.

The second indicator for an s process time-scale comes from consideration of the isotopes of gadolinium at $A = 152$ and 154. Of these isotopes Gd^{154} can only be

made by the s process. On the other hand the majority of Gd^{152} is probably made in the p process (Sec. IX), since its abundance fits in well with the run of abundances of the isotopes made by this process in this region of the curve. We shall arbitrarily suppose that of the total abundance of Gd^{152} of 0.00137 about 0.001 is made by the p process (cf. Fig. IX,1) and the remainder by the s process, since the following argument is in no way critically dependent on this division. The small amount made in the s process must be due to the fact that Gd^{152} is mostly by-passed in the s-process chain. Reference to the appendix shows that the branching which does this cannot take place at Eu^{152} since in 28% of the cases Eu^{152} will decay to Gd^{152} while in 78% of the cases isomeric Eu^{152m} will decay to Gd^{152}. The combination of these two decays shows that in 36% of the cases Eu^{152} will decay to Gd^{152} if the production ratio $Eu^{152}/Eu^{152m} \sim 5$. Thus the branching responsible for this by-pass must take place at Sm^{151} which has a half-life for beta decay of 80 years and which must mainly capture a neutron before beta decay. Thus we must have that

$$\frac{t_n(Sm^{151})}{t_\beta(Sm^{151})} = \frac{N'(Gd^{152})}{N(Gd^{154})},$$

where $N'(Gd^{152})$ is the abundance of Gd^{152} estimated on the supposition that 36% of the decays from Eu^{152} give an abundance of 0.00037. That is, $N'(Gd^{152}) = 0.00037/0.36 \backsimeq 0.001$, and $N(Gd^{154})$ is the abundance of this isotope given in the appendix. Thus substituting for $N'(Gd^{152})$, $N(Gd^{154})$, and $t_\beta(Sm^{151})$ we find that $t_n(Sm^{151}) \backsimeq 5$ years. Using the ratio of the σ's in this region as compared with iron we find that near iron $t_n \sim 10^3$ years. The mean value of σ near $A = 150$ is about 1000 mb whereas $\sigma(Sm^{152}) = 1440$ mb. Thus the mean t_n near $A = 150$ is of the order of 10 years, and the total time for the capture of ~ 200 neutrons is about 2×10^3 years. We show later that this shorter of the two time-scales of the s process is probably due to the fact that plenty of neutrons are available and that the "steady flow" concept can be used. In this case the σN product remains approximately constant.

(6) x-Process Time-Scales

Several alternative processes which may synthesize deuterium, lithium, beryllium, and boron are described in Sec. X. Depending on which of these is the most satisfactory, the time-scale for synthesis may range from a few seconds if a supernova origin is assumed to $\sim 10^9$ years if the surfaces of active stars are considered probable. The time-scale here is important only in as far as it may allow some predictions of the probable distribution of these elements in the solar system and the Galaxy.

In Fig. II,4 we give a schematic diagram showing where the various synthesizing processes take place in a plot of the internal stellar temperature against the
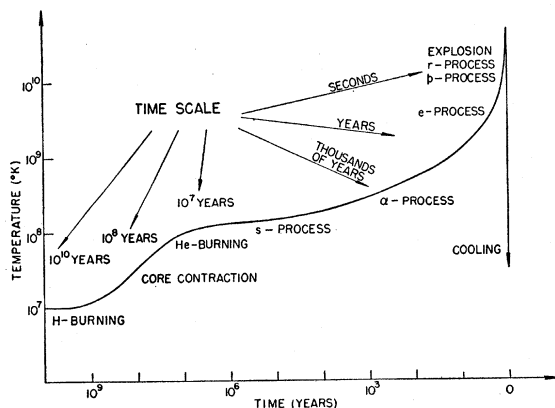

FIG. II,4. The time-scales of the various processes of element synthesis in stars. The curve gives the central temperature as a function of time for a star of about one solar mass. The curve is schematic.

time that the star lives in each temperature range. The estimated time-scales associated with each of these processes are also given very approximately.

III. HYDROGEN BURNING, HELIUM BURNING, THE α PROCESS, AND NEUTRON PRODUCTION

This section and the sections to follow are devoted to detailed elaboration and discussion of the different physical processes introduced in Sec. II. These sections treat quantitatively experimental and theoretical evaluations of the cross sections and reaction rates of the nuclear processes involved in energy generation and element synthesis in stars. The material supplements and extends that published in a series of articles in 1954 (Fo54, Bo54, Ho54), in 1955 (Fo55, Fo55a), and in 1956 (Bu56). In the first part of this section we give a discussion of the relations between nuclear cross sections and nuclear reaction rates in stellar interiors and of the notation used in this and the following sections.

A. Cross-Section Factor and Reaction Rates

The experimental results to be discussed will be used to derive the numerical value of the nuclear cross-section factor for a charged particle reaction defined by

$$S = \sigma(E) E \exp(31.28 Z_1 Z_0 A^{\frac{1}{2}} E^{-\frac{1}{2}}) \text{ kev barns}$$

where $\sigma(E)$ is the cross section in barns (10^{-24} cm^2) measured at the center-of-mass energy E in kev. The charges of the interacting particles are Z_1 and Z_0 in units of the proton charge and $A = A_1 A_0 / (A_1 + A_0)$ is their reduced mass in atomic mass units. S is measured in the center-of-mass system. From measurements made in the laboratory system with incident particle energy E_1 and with target nuclei at rest, the quantity S is given by

$$S = \sigma(E_1) E_1 \frac{A_0}{A_1 + A_0} \exp(31.28 Z_1 Z_0 A_1^{\frac{1}{2}} E_1^{-\frac{1}{2}}) \text{ kev barns.}$$

For a nonresonant or off-resonant reaction S is a slowly varying function of the energy E. Methods for extrapolating to the effective thermal energy E_o in stellar interiors have been given by numerous authors (Sa52a, Fo54, Sa55, Ma57). The effective thermal energy at temperature T is

$$E_o = 1.220 (Z_1^2 Z_0^2 A T_6^2)^{\frac{1}{3}} \text{ kev barns,}$$

where T_6 is the temperature measured in units of 10^6 °K. The width of the effective range of thermal energy is

$$\Delta E_o = 0.75 (Z_1^2 Z_0^2 A T_6^5)^{1/6} \text{ kev.}$$

The mean reaction rate of a thermonuclear process may be expressed as

$$P = \rho r = n_1 n_0 \langle \sigma v \rangle_{Av} = 3.63 \times 10^{47} \rho^2 \frac{x_1 x_0}{A_1 A_0} \langle \sigma v \rangle_{Av}$$

reactions cm^{-3} sec^{-1},

where n_1 and n_0 are the number densities of the interacting particles per cm^3 and $\langle \sigma v \rangle_{Av}$ is the average of the cross section multiplied by the velocity in cm^3 sec^{-1}. The quantity r is the reaction rate per gram per second. The quantities x_1 and x_0 are the amounts of the interacting nuclei expressed as fractions by weight. In terms of $S_o = S(E_o)$ kev barns, it is found for a nonresonant process that

$$P = 7.20 \times 10^{-19} n_1 n_0 f_o S_o (A Z_1 Z_0)^{-1} \tau^2 e^{-\tau}$$

reactions cm^{-3} sec^{-1}

$$= 2.62 \times 10^{29} \rho^2 \frac{x_1 x_0}{A_1 A_0} f_o S_o (A Z_1 Z_0)^{-1} \tau^2 e^{-\tau}$$

reactions cm^{-3} sec^{-1},

where S_o is in kev barns and

$$\tau = 42.48 \left(Z_1^2 Z_0^2 \frac{A}{T_6} \right)^{\frac{1}{3}}$$

(this τ is not to be confused with the mean lifetime of the interacting particles which will always be accompanied by appropriate subscripts, etc.). The term f_o is the electron screening or shielding factor discussed by Salpeter (Sa54), evaluated at E_o. The cross-section factor S_o as customarily calculated does not include allowance for electron screening.

The mean lifetime of the nuclei of type 0 for the interaction with nuclei of type 1 is given by

$$\frac{1}{\tau_1(0)} = p_1(0) = \nu_0 P / n_0$$

$$= 4.34 \times 10^5 \frac{\rho x_1}{A_1} \nu_0 S_o f_o (A Z_1 Z_0)^{-1} \tau^2 e^{-\tau} \text{ sec}^{-1}$$

$$= 7.83 \times 10^8 \frac{\rho x_1}{A_1} \nu_0 S_o f_o \left(\frac{Z_1 Z_0}{A T_6^2} \right)^{\frac{1}{3}} e^{-\tau} \text{ sec}^{-1},$$

where ν_0 is the number of nuclei of type 0 consumed in each reaction. The quantity $p_1(0)$ is the mean reaction rate per nucleus of type 0. If nuclei of type 0 are regenerated in a cycle of reactions then $\tau_1(0)$ becomes the mean cycle time for nuclei of type 0.

The most satisfactory procedure for determining S_o is to make experimental observations on cross sections over a range of energies not too large compared to E_o. The cross-section factor, S, can then be plotted as a function of E and an appropriate extrapolation to find S_o can be made. This is not always possible and computational procedures for several frequently occurring cases will now be given.

(i) For the case in which S_o is to be calculated from the experimentally determined parameters of a reso-

nance at E_r which falls outside the range $E_o \pm 2\Delta E_o$, then

$$\sigma = \pi \lambda^2 \omega \frac{\Gamma_1 \Gamma_2}{(E-E_r)^2 + \Gamma^2/4},$$

and

$$S_o = 3.10 \times 10^3 \frac{\theta_1^2}{A} \frac{1-\alpha_l E_o}{K_{2l+1}^2(x)} \frac{\omega \Gamma_2 E_R}{(E_o - E_r)^2 + \Gamma^2/4} \text{ kev barns.}$$

The corrections for level shift effects are given by Marion and Fowler (Ma57). The various quantities which enter into these expressions are:

λ = reduced De Broglie wavelength of interacting particles 0 and 1
  $= (\hbar^2/2ME)^{\frac{1}{2}} = 144(AE)^{-\frac{1}{2}}$ fermis (10^{-13} cm)
$R/\lambda = (E/E_R)^{\frac{1}{2}}$
R = interaction radius
  $\approx 1.44(A_1^{\frac{1}{3}} + A_0^{\frac{1}{3}})$ fermis
θ_1^2 = dimensionless reduced width for the interaction of particle 1 with particle 0, derivable from the observed width, Γ_1
Γ_1 = width for re-emission of particle 1 with particle 0
  $= 6\theta_1^2(\hbar^2/2MR^2)(R/\lambda)P_l$
  $= 6\theta_1^2(EE_R)^{\frac{1}{2}}P_l$
  $= [3\pi/2K_{2l+1}^2(x)](1-\alpha_l E)\theta_1^2 E_R$
    $\times \exp(-31.28Z_1 Z_0 A^{\frac{1}{2}} E^{-\frac{1}{2}})$
P_l = barrier penetration factor for orbital angular momentum $l\hbar$
  $= [\pi(E_R/E)^{\frac{1}{2}}/4K_{2l+1}^2(x)](1-\alpha_l E)$
    $\times \exp(-31.28Z_1 Z_0 A^{\frac{1}{2}} E^{-\frac{1}{2}})$
Γ_2 = experimental width for emission of reaction product 2 with 3; approximately independent of E.
Γ = total width of resonance $= \Gamma_1 + \Gamma_2 + \cdots$
ω = statistical factor $= (2J+1)/(2J_1+1)(2J_0+1)$
J = angular momentum of resonant state
J_1 = angular momentum of particle 1
J_0 = angular momentum of particle 0
$x = 2(E_C/E_R)^{\frac{1}{2}} = 0.525(AZ_1 Z_0 R)^{\frac{1}{2}}$
$E_R = [1/l(l+1)] \times$ centrifugal barrier height
  $= \hbar^2/2MR^2 = 20.9/AR^2 \times 10^3$ kev
E_C = Coulomb barrier height $= Z_1 Z_0 e^2/R$
  $= (1.44Z_1 Z_0/R) \times 10^3$ kev.

$K_{2l+1}(x)$ = modified Bessel function of order $2l+1$. Convenient tables for K are given in (Br37, 52).

$$\alpha_l = \frac{1}{3E_R}\left[\frac{1}{l+1}\left\{\frac{K_{2l+3}(x)}{K_{2l+1}(x)}\left(1-2l(l+1)\left(\frac{2}{x}\right)^2\right)-1\right\}\right.$$

$$\left. +2l(l+1)(2l+1)\left(\frac{2}{x}\right)^4\right]$$

$$\alpha_{l=0} = \frac{1}{3E_R}\left\{\frac{K_3(x)}{K_1(x)}-1\right\}.$$

For large x (high Coulomb barrier):

$$K_{2l+1}(x) \approx (\pi/2x)^{\frac{1}{2}} \exp\left[-x + \frac{2(l+\frac{1}{2})^2}{x}\right]$$

$$P_l \approx \left[\frac{E_C}{E}\right]^{\frac{1}{2}}(1-\alpha_l E) \exp\left[-31.28Z_1 Z_0 A^{\frac{1}{2}} E^{-\frac{1}{2}}\right.$$

$$\left. +4\left(\frac{E_C}{E_R}\right)^{\frac{1}{2}} - 2(l+\frac{1}{2})^2\left(\frac{E_R}{E_C}\right)^{\frac{1}{2}}\right]$$

$$P_l/P_0 \approx \exp[-2l(l+1)(E_R/E_C)^{\frac{1}{2}}]$$

$$= \exp[-7.62l(l+1)/(AZ_1 Z_0 R)^{\frac{1}{2}}]$$

$$\alpha_{l=0} \approx \frac{2}{3(E_R E_C)^{\frac{1}{2}}} \sim 10^{-3} \text{ (kev)}^{-1}.$$

In principle the cross sections and cross-section factors given above must be summed over all values of the orbital angular momentum, $l\hbar$. The expressions given apply to any one specified l-wave interaction. Because of the low energies involved in nuclear collisions in stellar interiors, s-wave ($l=0$) interactions and in some cases p-wave ($l=1$) interactions are usually the only ones which need to be taken into account. However, whenever selection rules or destructive interference effects reduce the low l-value interactions to zero, then higher l values must be considered. In addition, whenever any particular l-wave interaction is resonant, see (iv), then it must be taken into account. Resonant cross sections can be quite large even for high l values.

(ii) For the case in which the cross section is an average over resonances of the same spin and parity with mean width Γ spaced by an average energy interval equal to D, then averaging over the expression for σ given in (i) yields

$$\bar{\sigma} \approx 2\pi^2 \lambda (2l+1)\Gamma_1 \Gamma_2/D\Gamma.$$

In general, each l wave can form several compound systems of different spins but the same parity. In employing the above approximate relation with the simple statistical factor $(2l+1)$ we assume that these different systems have the same mean widths, Γ, and the same mean level separations, D.

With the foregoing expression for $\bar{\sigma}$, one finds, neglecting $\alpha_l E_o$,

$$S_o \approx 1.94 \times 10^4 \frac{\theta_1^2}{A} \frac{2l+1}{K_{2l+1}^2(x)} \frac{\Gamma_2 E_R}{\Gamma D} \text{ kev barns.}$$

This will prove to be useful for order of magnitude estimates for interactions of charged particles with heavy nuclei ($Z \gtrsim 10$). Blatt and Weisskopf (Bl52) have given a general relation between the particle decay widths, $\Gamma_1 \propto \theta_1^2$, for a given system of resonances and

their mean energy separation. This can be written

$$\theta_1{}^2 = \frac{\lambda_o}{3\pi R}\frac{D}{E_R}\beta(A_0).$$

The function $\beta(A_0)$ varies between ~ 0.3 and 3 for all except a few light and intermediate weight nuclei (Fe54, We57a) and we will set it equal to unity for order of magnitude estimates in what follows. The quantity $\lambda_o \approx 0.7 \times 10^{-13}$ cm is the characteristic reduced De Broglie wavelength of low-energy nucleons once inside nuclei.

We now have, for R in fermis,

$$S_o \sim 1.4 \times 10^3 \frac{2l+1}{ARK_{2l+1}{}^2(x)}\frac{\Gamma_2}{\Gamma} \text{ kev barns.}$$

For $l=0$ and large x we then have

$$S_o(l=0) \sim 1.8 \times 10^3 \frac{1}{AR}\frac{\Gamma_2}{\Gamma}\left(\frac{E_C}{E_R}\right)^{\frac{1}{2}}$$

$$\times \exp\left[+4\left(\frac{E_C}{E_R}\right)^{\frac{1}{2}}\right] \text{ kev barns.}$$

In general for (p,γ) reactions on the light nuclei ($Z=6$ to 12) one finds $S_o \sim 1$ to 100 kev barns. For the (p,α) reactions, $S_o \sim 10^3$ to 10^5 kev barns. On substitution into the expression for the mean lifetime, and setting $\nu_0 = 1$, $f_o = 1$, $l=0$, it is found that

$$\frac{1}{\tau_1(0)} \sim 3.8 \times 10^{11}\frac{\rho x_1}{A_1}\frac{(Z_1 Z_0)^{5/6}}{R^{\frac{1}{3}}A^{5/6}T_6{}^{\frac{2}{3}}}\frac{\Gamma_2}{\Gamma}$$

$$\times \exp\left[+4\left(\frac{E_C}{E_R}\right)^{\frac{1}{2}} - \tau\right] \text{ sec}^{-1}.$$

In cases where this expression is applicable, e.g., (p,γ) or (α,n) reactions on heavy nuclei ($Z \gtrsim 10$) one will in general have $\Gamma \approx \Gamma_2 \gg \Gamma_1$.

(iii) In the case of light nuclei, the interaction energy may fall in the flat minimum in between resonances. For this nonresonant case, order of magnitude estimates may be made by summing the contributions of all resonances of a given type with width Γ spaced by an average energy interval equal to D. The nonresonant cross section for a given l-wave interaction is

$$\sigma_{nr} \approx \pi \lambda^2 (2l+1)(\pi^2 \pm 8)\Gamma_1\Gamma_2/D^2.$$

This expression *assumes* that all except the two nearest resonances have random phases, that is, that their contributions to the cross section can be simply added without compounding amplitudes. The factor (π^2+8) is to be used if the two nearest resonances interfere constructively; the factor (π^2-8) if the two nearest resonances interfere destructively. In fact, it is possible for the cross section for a given l wave to go to zero if all

of the contributing states interfere to give zero reaction amplitude. In this case the next highest l wave must be considered. On the average, for order of magnitude estimates, we can assume that all resonances, including the two nearest ones, are randomly phased in which case the factor $\pi^2 \pm 8$ becomes π^2. The expression for σ_{nr} is then the same as $\bar{\sigma}$ in (ii) with Γ replaced by $2D/\pi$. With this substitution, expressions for S_o and $1/\tau_1(0)$ given in (ii) can be employed. It will be noted, however, that in general $\Gamma_2 < D$ so that an approximation similar to $\Gamma_2 \sim \Gamma$ is not valid in this case. For the light nuclei $D \sim 1$ to 10 Mev, whereas for radiative processes $\Gamma_2 = \Gamma_\gamma \sim 0.1$ to 100 ev so that $10^{-7} < \Gamma_\gamma/D < 10^{-4}$. For particle emission Γ_2/D may be as high as 0.1.

(iv) When a resonance E_r falls within the range $\sim E_o \pm 2\Delta E_o$ the resonant cross section factor S_r, derivable from the resonant cross section σ_r, must be employed. When resonant, even fairly large l-wave interactions must be considered. We have

$$\sigma_r = 4\pi \lambda^2 \omega \Gamma_1 \Gamma_2 / \Gamma^2.$$

We will consider two limiting cases,

$$\sigma_r \to 4\pi \lambda^2 \Gamma_1/\Gamma_2 \text{ for } \Gamma \approx \Gamma_2 \gg \Gamma_1,$$

$$\sigma_r \to 4\pi \lambda^2 \Gamma_2/\Gamma_1 \text{ for } \Gamma \approx \Gamma_1 \gg \Gamma_2.$$

The cross-section factor is

$$S_r = 1.24 \times 10^4 \frac{\theta_1{}^2}{A}\frac{1-\alpha_l E_r}{K_{2l+1}{}^2(x)}\frac{\omega\Gamma_2 E_R}{\Gamma^2}.$$

The two limiting cases become

$$S_r \to 1.24 \times 10^4 \frac{\theta_1{}^2}{A}\frac{1-\alpha_l E_r}{K_{2l+1}{}^2(x)}\frac{\omega E_R}{\Gamma_2} \quad \text{for } \Gamma \approx \Gamma_2 \gg \Gamma_1,$$

$$S_r \to 2.63 \times 10^3 \frac{\omega \Gamma_2}{A\Gamma_1}$$

$$\times \exp(+31.28 Z_1 Z_0 A^{\frac{1}{2}} E_r{}^{-\frac{1}{2}}) \quad \text{for } \Gamma \approx \Gamma_1 \gg \Gamma_2.$$

The resonant reaction rate is for Γ in kev and S_r in kev barns:

$$P = 3.08 \times 10^{-15} n_1 n_0 \frac{f_r}{A^{\frac{1}{2}}T_6{}^{\frac{3}{2}}}S_r\Gamma e^{-\tau_r} \text{ reactions cm}^{-3}\text{ sec}^{-1}$$

$$= 1.12 \times 10^{33}\rho^2\frac{x_1 x_0}{A_1 A_0}\frac{f_r}{A^{\frac{1}{2}}T_6{}^{\frac{3}{2}}}S_r\Gamma e^{-\tau_r}$$

$$\to 1.39 \times 10^{37}\rho^2\frac{x_1 x_0}{A_1 A_0}\frac{\omega E_R f_r \theta_1{}^2}{(AT_6)^{\frac{3}{2}}}\frac{1-\alpha_l E_r}{K_{2l+1}{}^2(x)}e^{-\tau_r}$$

$$\text{for } \Gamma \approx \Gamma_2 \gg \Gamma_1$$

$$\to 2.94 \times 10^{36}\rho^2\frac{x_1 x_0}{A_1 A_0}\frac{\omega\Gamma_2 f_r}{(AT_6)^{\frac{3}{2}}}\exp(-11.61 E_r/T_6)$$

$$\text{for } \Gamma \approx \Gamma_1 \gg \Gamma_2.$$

In the preceding expressions

$$\tau_r = 31.28 Z_1 Z_0 A^{\frac{1}{3}} E_r^{-\frac{1}{3}} + 11.61 E_r/T_6$$

and f_r is the electron shielding factor evaluated at E_r.

The mean reaction time of nuclei of type 0 is

$$\frac{1}{\tau_1(0)} = p_1(0) = 1.86 \times 10^9 \frac{\rho x_1}{A_1} \frac{\nu_0 f_r}{A^{\frac{1}{3}} T_6^{\frac{2}{3}}} S_r \Gamma e^{-\tau_r} \text{ sec}^{-1}$$

$$\rightarrow 2.31 \times 10^{13} \frac{\rho x_1}{A} \frac{\nu_0 \omega E_R f_r \theta_1^2}{(AT_6)^{\frac{2}{3}}} \frac{1 - \alpha_l E_r}{K_{2l+1}^2(x)} e^{-\tau_r}$$

$$\text{for } \Gamma \approx \Gamma_2 \gg \Gamma_1$$

$$\rightarrow 0.49 \times 10^{13} \frac{\rho x_1}{A_1} \frac{\nu_0 \omega \Gamma_2 f_r}{(AT_6)^{\frac{2}{3}}} \exp(-11.61 E_r/T_6)$$

$$\text{for } \Gamma \approx \Gamma_1 \gg \Gamma_2.$$

B. Pure Hydrogen Burning

The point of view that element synthesis begins with pure hydrogen (primordial or continuously produced) condensed in stars is based on the existence of the so-called direct pp chain of reactions by which hydrogen is converted into helium. This chain is initiated by the direct pp reaction

$$p + p \rightarrow d + \beta^+ + \nu_+ + 0.421 \text{ Mev,}$$
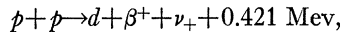
which has good theoretical foundations but which has not yet been observed experimentally in the laboratory because of its extremely low cross section even at relatively high interaction energies. In the above equation and in what follows we use ν_+ for neutrinos emitted with positrons, β^+, and ν_- for antineutrinos emitted with electrons, β^-. *We use nuclear rather than atomic mass differences in expressing the Q values of all reactions.* There is of course practically no difference in atomic and nuclear Q values when positrons or electrons are not involved.

The calculated cross section for the pp reaction is 10^{-47} cm$^2 = 10^{-23}$ barn at 1-Mev laboratory energy. This is much too small for detection with currently available techniques. The yield when a thick hydrogen target is employed can be estimated to be 5×10^{-28} reaction per incident proton or approximately one reaction per 3×10^8 amp sec corresponding at 10^6 volts to 3×10^{14} w sec. Thus only one reaction per *10 Megawatt years* of bombardment can be expected. In an earlier paper (Fo54) it was indicated that the cross section would reach a maximum value at 100 kev. This is not the case if account is taken of the rapid increase in beta-decay probability with increasing beta-decay energy and hence with increasing incident proton energy. At the present time, however, it is not possible to obtain within many orders of magnitude, the necessary amounts of bombardment even at 1 Mev or above. At 100 Mev the cross section becomes 3×10^{-15} barn but very pure hydrogen targets would be necessary to avoid positron production in heavy nuclei as contaminants.

At still higher energy, meson production becomes a complication.

(1) Rate of pp Reaction

Definitive theoretical calculations on the rate of the pp processes were given by Salpeter (Sa52a). These calculations accurately took into account the well-determined phenomenological parameters of the neutron-proton and proton-proton interactions and showed that the main uncertainty in the cross section lay at that time in the uncertainty of the Gamow-Teller beta-decay constant for which the following value was given:

$$g = 7.5 \pm 1.5 \times 10^{-4} \text{ sec}^{-1} \text{ (Sa52a).}$$

This value was adopted by Fowler (Fo54). The 20% uncertainty in the value of the Gamow-Teller coupling constant did not imply any uncertainty in the validity of the Gamow-Teller selection rules for beta-decay transitions. Then, as now, the super-allowed nature of the beta decay, He^6(0$^+$)$\rightarrow$Li^6(1$^+$)$+\beta^-+\nu_-$, which is permitted only by the Gamow-Teller selection rules, serves as a solid empirical foundation for this type of transition. The recent discovery of the nonconservation of parity[‡] in allowed beta decay transitions (Wu57, Le56, Al57) is further substantiation of the existence of Gamow-Teller selection rules. The fore-and-aft asymmetry in the decay of aligned Co^{60} nuclei observed by Wu et al. is not possible for allowed Fermi transitions even with nonconservation of parity.

Experimental data on ft values for super-allowed mirror transitions and 0$\rightarrow$0 transitions in beta decay available in 1956 were employed by Kofoed-Hansen and Winther (Ko56) to evaluate the coupling constants in beta decay with improved accuracy. A recent measurement of the energy of the O^{14}(0$^+$)$\rightarrow$N^{14*}(0$^+$) transition by Bromley et al. (Br57) leads to only a minor change in Kofoed-Hansen and Winther's results. Bromley et al. find 1809.7$\pm$7.8 kev for the transition energy and thus an ft value equal to 3088$\pm$56, which brings O^{14} into agreement with the Al^{26}, Cl^{34}, and K^{38} 0$^+\rightarrow$0$^+$ transitions used by Kofoed-Hansen and Winther.

The quantity g which appears in Salpeter's expression for the rate of the pp reaction is related to the quantities B and x defined by Kofoed-Hansen and Winther (Ko56) through the relation

$$g = 4 \ln 2(x/B) = 2.77(x/B).$$

They find that the best fit to the experimental data yields $B = 2787 \pm 70$ sec, $x = 0.560 \pm 0.012$, so that $B/x = 4980 \pm 150$ sec. With the new O^{14} data we estimate $B = 2818$, $x = 0.544$ so that $B/x = 5180$ and

$$g = 5.35 \pm 0.15 \times 10^{-4} \text{ sec}^{-1} \text{ (new value, 1957),}$$

---

‡ The reader is admonished that parity is still conserved to a high degree of experimental accuracy in reactions involving the strong interactions among nucleons (Ta57) as contrasted with the weak interactions leading to beta decay. The importance of parity conservation in nuclear reactions is illustrated in the discussion of the 3α reaction in Sec. IC(1).

TABLE III,1. Energy generation in pp chain and CN cycle.

T 10^6 °K	E_o kev	$\mathrm{Log}\left(\frac{100}{\rho x_H^2 f_{pp}}\epsilon_{pp}\right)$	E_o kev	$\mathrm{Log}\left(\frac{1}{\rho x_H x_N f_N}\epsilon_N\right)$	E_o kev	$\mathrm{Log}\left(\frac{1}{\rho x_H x_C f_C}\epsilon_C\right)$
		pp chain		CN cycle		
				$N^{14}(p,\gamma)$ determining		$C^{12}(p,\gamma)$ determining
5	2.8	−0.79	13	−11.24	11	−7.71
10	4.5	+0.79	20	−3.47	18	−0.73
15	5.9	1.54	27	+0.30	24	+2.65
20	7.1	2.01	32	2.67	29	4.78
30	9.3	2.58	42	5.63	38	7.45
40	11.3	2.94	51	7.49	46	9.13
50	13.2	3.19	60	8.81	53	10.32
70	16.5	3.54	75	10.72	67	12.0
100	20.8	3.86	94	12.3	84	13.5

which is 29% less than the value given by Salpeter (Sa52a) and used by Bosman-Crespin *et al.* (Bo54) in numerical calculations. These numerical values should thus be reduced by 29%. The over-all probable error, taking other sources of error into account, can be conservatively estimated as 10%. The cross-section factor becomes

$$S = 28.5(1+0.008E)\times 10^{-23} \text{ kev barn } \pm 10\%$$

for E in kev or

$$S_o = 28.5(1+0.008T_6^{\frac{2}{3}})\times 10^{-23} \text{ kev barn } \pm 10\%.$$

The correction term in E or $T_6^{\frac{2}{3}}$ arises from the dependence on energy of the beta-decay transition probability, and in addition from small corrections to the barrier penetrability when a nonzero interaction radius is assumed. It is accurate only for $E < 100$ kev or $T < 10^9$ degrees. At laboratory bombarding energies for $E \gtrsim 1$ Mev, $S \sim 2E^5 \times 10^{-24}$ Mev barn, $\sigma \sim 3E_o^{4.5} \times 10^{-24}$ barn. In the following discussion it is convenient to use a quantity α_{pp}, which is involved in the reaction rate and is given by

$$\alpha_{pp} = \rho f_{pp} T_6^{-\frac{2}{3}}(1+0.012T_6^{\frac{1}{3}}+0.008T_6^{\frac{2}{3}}+0.00065T_6)$$

$$\times \exp(-33.804T_6^{-\frac{1}{3}})\pm 10\%$$

$$\simeq 2.0\times 10^{-7}\rho f_{pp}\left(\frac{T_6}{15}\right)^{3.95} \quad \text{near} \quad T_6 = 15.$$

The electron screening factor, f_{pp}, can be taken as approximately equal to unity for $T_6 \gtrsim 8$. The quantity ρ is the density and x_H is the concentration by mass of hydrogen. The correction terms in $T_6^{\frac{1}{3}}$ and T_6 arise in integrating over all the interaction energies. The first has been discussed by Salpeter (Sa52a) and the second comes when the energy dependence of S is included to first order in the integration. The reaction rate in reactions per gram of material per second is $\alpha_{pp}x_H^2$ multiplied by a numerical factor derivable from S_o, viz.,

$$r_{pp} = 0.833\alpha_{pp}x_H^2 \times 10^{11} \text{ reactions g}^{-1} \text{ sec}^{-1}$$

while the mean reaction rate per proton with *two protons*

consumed per reaction is

$$p_{pp}(H) = -\frac{1}{x_H}\frac{dx_H}{dt} = 2.78(\alpha_{pp}x_H)\times 10^{-13} \text{ sec}^{-1}.$$

If the pp chain is completed then the energy release in the over-all process, $4H^1 \rightarrow He^4$, is 26.22 Mev$=4.201 \times 10^{-5}$ erg, using the atomic masses of Wapstra (Wa55). This value excludes the 2% neutrino energy loss. The expression for the energy generation, ϵ_{pp}, is then given by

$$\epsilon_{pp} = 0.5 \times 4.201 \times 10^{-5}r_{pp} \text{ ergs}$$

or

$$\epsilon_{pp} = 1.75\alpha_{pp}x_H^2 \times 10^6 \text{ ergs g}^{-1} \text{ sec}^{-1} \quad (4H^1 \rightarrow He^4).$$

This energy generation as a function of temperature is tabulated in Table III,1 and is indicated graphically in
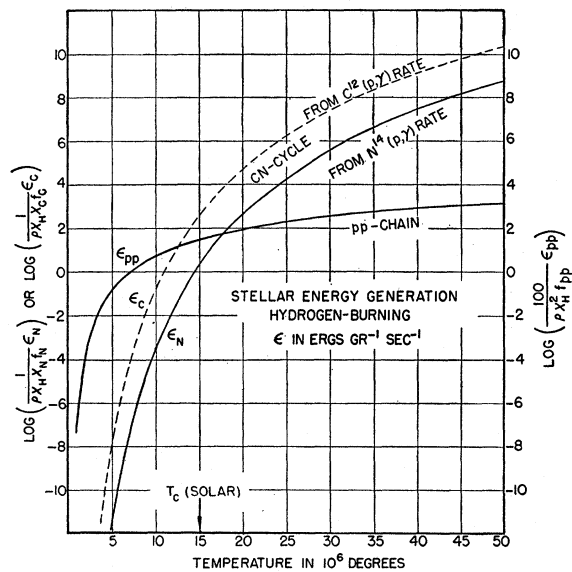
FIG. III,1. Energy generation in ergs g^{-1} sec^{-1} as a function of temperature in the pp chain and the CN cycle. The ordinates give $\log\epsilon$ directly for $\rho x_H^2 f_{pp}=100$ g/cm^3, $\rho x_H x_N f_N=1$ g/cm^3 or $\rho x_H x_C f_C = 1$ g/cm^3. They are thus appropriate for $x_N = x(N^{14})$ or $x_C = x(C^{12}) \simeq 0.8x(C^{12}+C^{13}) = 0.01x_H$. If $N^{14}(p,\gamma)$ is resonant the CN-cycle rate is determined by $C^{12}(p,\gamma)$ and $x_C \simeq 0.8x_{CN}$. If $N^{14}(p,\gamma)$ is nonresonant, it determines the CN-cycle rate and $x_N \approx x_{CN}$.

TABLE III,2. Mean lifetimes or cycle times in hydrogen burning (years).[a]

T 10^6 °K	$\frac{\mathrm{Log}\rho x_C f_C \tau(\mathrm{H})}{\mathrm{H}^1\ \mathrm{C}^{12}(p,\gamma)}$	$\frac{\mathrm{Log}\rho x_N f_N \tau(\mathrm{H})}{\mathrm{H}^1\ \mathrm{N}^{14}(p,\gamma)}$	H^1 pp chain	C^{12}	N^{14}	O^{16}	Ne^{20}	Ne^{21}	Ne^{22}	T $(10^6$ °K)
5	+19.0	+22.5	+12.09	+16.5	20.0					5
10	12.0	14.7	10.51	9.53	12.2					10
15	8.63	11.0	9.76	6.15	8.44	10.8				15
20	6.50	8.61	9.29	4.02	6.07	8.24	+10.92	+12.41	+10.62	20
30	3.83	5.65	8.72	1.35	3.11	4.99	7.28	8.63	6.76	30
40	2.15	3.79	8.36	−0.33	1.25	2.94	5.02	6.25	4.32	40
50	0.96	2.47	8.11	−1.52	−0.07	1.49	3.42	4.55	2.55	50
70	−0.72	0.56	7.76	−3.2	−1.98	−0.50	1.20	2.18	0.05	70
100	−2.22	−1.00	7.44	−4.7	−3.54	−2.37	−0.80	0.02	−2.33	100

Column head spanning C^{12} through Ne^{22}: $\mathrm{Log}(\rho x_H f \tau/100)$

[a] O^{16} and Ne^{20} lifetimes based on results of Ta57a and Pi57a.

Fig. III,1, where it is compared with that for the CN cycle, which is discussed in Sec. III F.

If the chain goes only to He^3, as might be the case in limited times at low temperature, then the energy release in $3\mathrm{H}^1 \rightarrow \mathrm{He}^3$ is 6.68 Mev $= 1.070 \times 10^{-5}$ erg and

$$\epsilon_{pp}' = 0.89\alpha_{pp} \times 10^6 \text{ ergs g}^{-1} \text{ sec}^{-1} \quad (3\mathrm{H}^1 \rightarrow \mathrm{He}^3).$$

The mean lifetime of hydrogen in the pp chain becomes

$$\tau_{pp}(\mathrm{H}) = 1.14(\alpha_{pp}x_H)^{-1} \times 10^5 \text{ years}$$

$$= 1.99(x_H/\epsilon_{pp}) \times 10^{11} \text{ years}$$

$$= \frac{1.99 \times 10^9}{E_{pp}} \frac{100}{\rho x_H} \text{ years,}$$
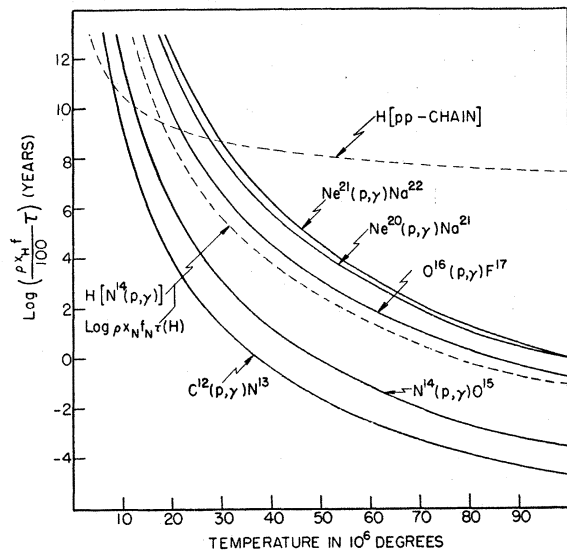
FIG. III,2. Mean lifetimes or cycle times in years for various nuclei in hydrogen burning as a function of temperature. The ordinate gives logτ (years) directly for $\rho x_H f = 100$ g/cm^3 or $\rho x_N f_N = 1$ g/cm^3. The hydrogen lifetime in the CN cycle is calculated from the rate of the nonresonant $\mathrm{N}^{14}(p,\gamma)$ reaction. The mean reaction time of the pp reaction is twice that of the hydrogen since two protons are consumed in each reaction. The latest experimental results (Ta57a) on $\mathrm{O}^{16}(p,\gamma)$ require that the curve for $\tau(\mathrm{O}^{16})$ be lowered by 1.6 in the logarithm. Those on $\mathrm{Ne}^{20}(p,\gamma)$ require that $\tau(\mathrm{Ne}^{20})$ be lowered by 0.8 in the logarithm (Pi57a).

where E_{pp} is the quantity tabulated by Bosman-Crespin et al. (Bo54) decreased by 29%. It will be recalled that $\rho x_H \sim 100$ g/cm^3 at the center of the sun and similar stars. Hydrogen lifetimes at relevant temperatures are given in Table III,2 and Fig. III,2.

The recent detection (Re53, Co56a) of the free antineutrino through absorption by hydrogen in the reaction

$$\nu_- + p \rightarrow \beta^+ + n - 1.804 \text{ Mev}$$
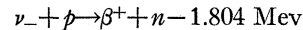
has led to increased confidence in Fermi's neutrino theory of beta decay, and thus in the theoretical calculations of the rate of the pp reaction which have just been discussed. In addition, the interesting possibility arises of investigating antineutrino capture in deuterium in processes which would be inverse to the direct pp reaction. Since antineutrinos are produced in the negative beta decay in a neutron reactor, observation of the following reaction

$$\nu_+ + d \rightarrow p + p + \beta^- - 1.443 \text{ Mev,}$$
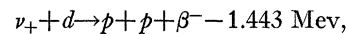
which is directly inverse to the pp reaction, would require that antineutrinos and neutrinos be identical. Recent experiments (Aw56), which show that the half-lives of Ca^{48} and Zr^{96} to double beta decay are $\gtrsim 10^{18}$ years, indicate that this is not the case. In addition, if $\nu_- \neq \nu_+$, the reaction $\mathrm{Cl}^{37} + \nu_- \rightarrow A^{37} + \beta^-$ would not be expected to take place and this has been shown to be the case (Da56). Also, the $\nu_+ + d$ process would be very difficult to detect over background because the energy given to the protons and to the electron will be dissipated promptly in electronic collisions. The process will not have a distinguishing signature as does the antineutrino absorption by protons, where the slowing down of the neutron gives an observable delay up to as much as 17 μsec (Co56a) between the positron annihilation energy release and the neutron capture energy release.

On the other hand, the "mirror-inverse" process to the pp reaction, which is

$$\nu_- + d \rightarrow n + n + \beta^+ - 4.029 \text{ Mev,}$$
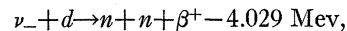
can be induced by reactor antineutrinos of sufficient energy and it will have a signature even more distinctive than that for the absorption in light hydrogen. Only a

small fraction of the reactor antineutrinos have energies above the threshold for this process and thus it will be much more difficult to observe than the absorption by protons. In fact, in the current experiments by Cowan et al. (Co56a) deuterium is used in place of part of the hydrogen in order to show that the observed events are directly proportional to the proton concentration. While this paper has been in preparation, two papers have appeared on the antineutrino disintegration of the deuteron (Mu57, We57) which give the effective cross sections for reactor neutrinos as $\bar{\sigma}(\nu_- + p) = 6 \times 10^{-44}$ cm^2 and $\bar{\sigma}(\nu_- + d) = 2 \times 10^{-45}$ cm^2. These must be multiplied by a factor of 2 in order to account for parity-nonconserving beta transitions. In any case the deuteron disintegration cross section is only 1/30 of that for the proton. However, if the mirror inverse process can ultimately be observed, the observation would constitute fundamental experimental confirmation of the very general ideas underlying the pp process. *Note added in proof.*—Cowan and Reines (Co57a) have not been successful in detecting the $\nu_- + d$ reaction but their experimental upper limit of $\bar{\sigma}(\nu_- + d) = 4 \times 10^{-45}$ cm^2 does not exclude the theoretically expected value given above.

(2) Other Reactions in the pp Chain

New measurements of the cross section for $D^2(p,\gamma)$ have been reported (Gr55) since the review by Fowler (Fo54), but these new values do not necessitate any significant change in the value of the cross-section factor given there ($S_o = 8 \times 10^{-5}$ kev barn). The final results for the He^3(He^3,$2p$)He^4 cross section have been published (Go54). The value of 2.5×10^{-6} barn at $E_{lab} = 200$ kev or $E_{em} = 100$ kev yields a cross section factor equal to 1200 kev barn. Fairly substantial corrections for non-zero radius of interaction in the barrier penetrability energy dependence and for electron shielding effects will increase this to an effective value, $S_o = 2000$ kev barns, at relevant stellar energies.

C. Pure Helium Burning

When hydrogen burning in a star's main-sequence stage leads eventually to hydrogen exhaustion, a helium core remains at the star's center. It has been suggested (Sa52, Sa53, Op51, Op54) that the fusion of helium plays an important role in energy generation and element synthesis in the red-giant stage of the star's evolution. The fusion occurs through the processes
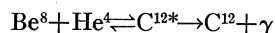
$$\text{He}^4 + \text{He}^4 \rightleftharpoons \text{Be}^8$$
$$\text{Be}^8 + \text{He}^4 \rightleftharpoons \text{C}^{12*} \rightarrow \text{C}^{12} + \gamma$$

or, in a more condensed notation, through

$$3\text{He}^4 \rightleftharpoons \text{C}^{12*} \rightarrow \text{C}^{12} + \gamma.$$
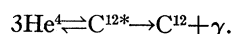
We refer to this as the 3α reaction. These processes are believed to occur at a late stage of the red giant evolution in which the hydrogen in the central core has been largely converted into helium, and in which gravitational contraction (Ho55) has raised the central temperature to $\sim 10^8$ degrees, and the density to $\sim 10^5$ g/cc. Under these conditions, as shown by Salpeter, an equilibrium ratio of Be^8 to He^4 nuclei equal to $\sim 10^{-9}$ is established. This conclusion followed from experimental measurements (He48, He49, To49, Wh41) which established the fact that Be^8 was unstable to disintegration into two alpha particles but only by 95 kev with an uncertainty of about 5 kev.

(1) Rate of the 3α Reaction

Even though very small, the equilibrium concentration of Be^8 is sufficient to lead to considerable production of C^{12} through radiative alpha-particle capture by the Be^8, and of O^{16}, Ne^{20}, etc., by succeeding alpha-particle captures. Salpeter's calculations, in which resonance effects due to the Be^8 ground state were taken into account, indicated a rate for the helium-burning considerably greater at a given pressure and temperature than that previously calculated by Öpik using nonresonant reaction rates (Op54). Detailed consideration of the reaction rates and of the resulting relative abundances of He^4, C^{12}, and O^{16} led Hoyle (Ho54) to the prediction that the foregoing second reaction, in which C^{12} is produced, must exhibit resonance within the range of energies at which the interaction between Be^8 and He^4 effectively occurs. Hoyle's predicted value for the resonance energy was 0.33 Mev, corresponding to an excited state in C^{12} at 7.70 Mev.

It recently has been shown (Fo56, Co57) through the studies of the alpha emission following the beta decay of B^{12} to the second excited state of C^{12}, that this state does decay into three alpha particles through an intermediate stage involving He^4 and the ground state of Be^8. The general reversibility of nuclear reactions thus leads one to expect that C^{12} will be produced in the Salpeter reactions given above and that the second excited state of C^{12} does indeed play a dominant role in the synthesis of elements from helium, as predicted by Hoyle.

The experiments reported (Co57) show that $Q(\text{Be}^8 - 2\text{He}^4) = 93.7 \pm 0.9$ kev, that the excitation energy of C^{12*} is $Q(\text{C}^{12*} - \text{C}^{12}) = 7.653 \pm 0.008$ Mev, that $Q(\text{C}^{12*} - \text{Be}^8 - \text{He}^4) = 278 \pm 4$ kev, $Q(\text{C}^{12*} - 3\text{He}^4) = 372 \pm 4$ kev, and that the most probable spin and parity assignments for C^{12*} are O$^+$. The state must have either even spin with even parity or odd spin with odd parity. Otherwise, by the conservation of angular momentum and parity, it cannot decay into three alpha particles through the ground state of Be^8. Since the Be^8 is in equilibrium, the reaction rate for the conversion of helium into carbon can be calculated simply from the $3\text{He}^4 \rightleftharpoons \text{C}^{12*}$ equilibrium with a small leakage to

stable C^{12}. The reaction rate per alpha particle is

$$p_{3\alpha}(He^4) = \frac{1}{\tau_{3\alpha}(He^4)} = \frac{1}{x_\alpha}\frac{dx_\alpha}{dt}$$

$$= 8\pi^3 3^{\frac{1}{2}}\frac{\hbar^5}{M_\alpha^5(kT)^3}(\rho x_\alpha)^2\frac{\Gamma_\gamma\Gamma_\alpha}{\Gamma_\gamma+\Gamma_\alpha}$$

$$\times \exp(-Q/kT) \text{ sec}^{-1},$$

where the appropriate Q is $Q(C^{12*}-3He^4)=372\pm4$ kev. Numerically:

$$p_{3\alpha}(He^4) = \frac{1}{\tau_{3\alpha}(He^4)} = 2.37$$

$$\times 10^{-4}(\rho x_\alpha)^2\frac{\Gamma_\gamma}{T_8^3}\exp\left(-\frac{43.2}{T_8}\right)\text{ sec}^{-1},$$

where Γ_γ is in ev and T_8 is the temperature in units of 10^8 degrees. Electron screening will increase this rate by a small factor. Using Salpeter's expression for weak screening (Sa54), we find that $f_{3\alpha}\simeq\exp0.88(\rho_5/T_8^3)^{\frac{1}{2}}$, where ρ_5 is the density in 10^5 g/cm³. Kavanagh (Ka56) finds that $\Gamma_\alpha\gg\Gamma_\gamma$ for C^{12*}, so that Γ_α does not appreciably influence the reaction rate numerically. Farrell (Fa57), Salpeter (Sa57), and Hayakawa et al. (Ha56b) have calculated Γ_γ on a reasonable model for states of C^{12} and find $\Gamma_\gamma\sim0.001$ ev. If the γ radiation is highly forbidden then Γ_γ must be replaced by the width for pair emission by C^{12*}. From the inelastic scattering (Fr55) of high-energy electrons by C^{12} this can be calculated (Fr56, Op39) to be $\Gamma_{e\pm}\sim5\times10^{-5}$ ev.

The present rate is in reasonable agreement with that given by Hoyle (Ho54), although it is worth pointing out that two changes have been made from these earlier calculations. Formerly Γ_γ was taken as 1 ev, thereby exaggerating the reaction rate. On the other hand,
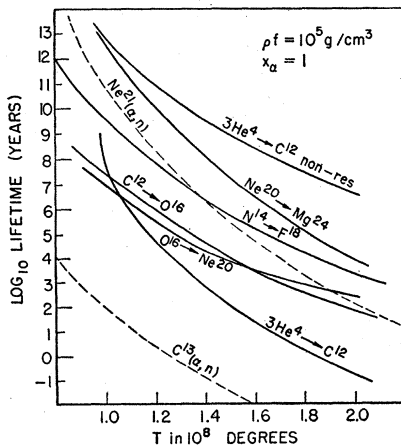
FIG. III,3. Mean lifetimes in years for various nuclei in helium burning as a function of temperature. The curves are drawn in each case for $x_\alpha=1$ and $\rho f=10^5$ g/cm³. The He^4 lifetime to $3He^4\rightarrow C^{12}$ is inversely proportional to $(\rho x_\alpha)^2 f_{3\alpha}$. The other lifetimes are inversely proportional to $\rho x_\alpha f$.

the resonance level was formerly taken such that $Q(C^{12*}-3He^4)=420$ kev. This reduced the reaction rate by an amount that closely compensated for the error in Γ_γ.

The energy generation, with $Q(3He^4-C^{12})=7.281$ Mev $=1.165\times10^{-5}$ erg, becomes

$$\epsilon_{3\alpha}=1.39\times10^{14}(\rho^2 x_\alpha^3)f_{3\alpha}\frac{\Gamma_\gamma}{T_8^3}\exp\left(-\frac{43.2}{T_8}\right)\text{ ergs g}^{-1}\text{ sec}^{-1}.$$

If the C^{12} formation is followed by rapid production of O^{16} and Ne^{20}, then $Q(5He^4-Ne^{20})=19.18$ Mev $=3.072\times10^{-5}$ erg and the numerical coefficient in the above equation becomes 3.66×10^{14}. Salpeter (Sa57) and Hayakawa et al. (Ha56b) have shown that this rate of energy generation is ample to supply the energy emitted by a star while it is on the tip of the red-giant branch when $\rho\sim10^5$ g/cm³, $x_\alpha\sim1$, and $T\sim10^8$ degrees. Under these conditions $\epsilon_{3\alpha}\approx600$ ergs g⁻¹ sec⁻¹ and $\epsilon_{5\alpha}\approx1500$ ergs g⁻¹ sec⁻¹.

(2) Rate of the $C^{12}(\alpha,\gamma)O^{16}$ Reaction

The C^{12} produced in the helium fusion can capture an alpha particle to form O^{16} and thus continue the element synthesis. The binding energy for an alpha particle in O^{16} is 7.148 Mev, so that this process proceeds mainly through the bound state in O^{16} at 7.116 Mev. This state has spin and parity equal to 1^- and thus the alpha capture by $C^{12}(0^+)$ is a p-wave capture and the radiation to the ground state of $O^{16}(0^+)$ is electric dipole. The probability for this radiation is somewhat reduced by the isotopic spin selection rule for $T=0\rightarrow0$ for electric dipole transitions. Swann and Metzger (Sw56) find the mean lifetime of the state to be $0.5_{-0.2}^{+0.8}\times10^{-14}$ sec, or $\Gamma_\gamma\approx0.13$ ev. The reduced alpha particle width for the state can be taken as $\theta_\alpha^2=0.1$ with a probable variation of a factor of 10 either way (Aj55). The cross-section factor becomes

$$S_o=\frac{3.8\times10^7}{(E_o+32)^2}\text{ kev barns}$$

for $E_o=199T_8^{\frac{2}{3}}$ kev. The reaction rate per C^{12} nucleus is

$$\frac{1}{\tau_\alpha(C^{12})}=p_\alpha(C^{12})=-\frac{1}{x_{12}}\frac{dx_{12}}{dt}$$

$$=1.44\times10^7\rho x_\alpha S_o T_8^{-\frac{2}{3}}\exp(-69.19T_8^{-\frac{1}{3}})\text{ sec}^{-1}$$

$$=1.38\times10^{10}\frac{\rho x_\alpha}{T_8^2(1+0.16T_8^{-\frac{2}{3}})^2}$$

$$\times\exp(-69.19T_8^{-\frac{1}{3}})\text{ sec}^{-1}.$$

If a screening term is introduced it will be the same as $f_{3\alpha}$ in the 3α reaction.

(3) Further Alpha-Capture Reactions

The rate of the $O^{16}(\alpha,\gamma)Ne^{20}$ process depends critically on whether the excited states in Ne^{20} at 4.95 and 5.62 Mev have the proper spin and parity (even-even or odd-odd) to be formed by O^{16} and the alpha particles in their ground states. These states probably have even parity and even spin and since they occur at 204 kev and 874 kev, respectively, in $O^{16}+\alpha$ and since $E_o=246T_8^{\frac{2}{3}}$ kev it is clear that for $T \gtrsim 10^8$ degrees they will act as resonances in the conversion of O^{16} into Ne^{20}. Production of Ne^{20} in comparable or greater amounts than O^{16} in helium burning is thus to be expected. Resonances can also be expected to occur in $Ne^{20}(\alpha,\gamma)Mg^{24}$ but the Mg^{24} production will be small because of the large barrier factor for alpha particles.

In Fig. III,3 and Table III,3 we show the mean lifetimes *versus* temperature for the $3He^4 \rightarrow C^{12}$ and $C^{12}(\alpha,\gamma)O^{16}$ reactions as calculated above, as well as the lifetimes for $O^{16}(\alpha,\gamma)Ne^{20}$ and $Ne^{20}(\alpha,\gamma)Mg^{24}$ as calculated by Salpeter (Sa57). Salpeter uses a dimensionless alpha-particle width, $\theta_\alpha^2=0.02$, for $O^{16}(\alpha,\gamma)$. We have taken $\theta_\alpha^2=0.01$ for $Ne^{20}(\alpha,\gamma)$ and have modified his calculations accordingly. We also show in Fig. III,3 the nonresonant $3He^4 \rightarrow C^{12}$ lifetime to illustrate the large factor arising from the resonance predicted by Hoyle.

In comparing the rates of the helium-burning reactions with the atomic abundances of C^{12}, O^{16}, Ne^{20}, and Mg^{24} two points must be borne in mind. In the first place only the rate of the $3He^4 \rightarrow C^{12}$ is known from experimental evidence to better than a factor of ten. The others are very uncertain and one of the most pressing current problems in element synthesis is the need for experimental measurements on $C^{12}(\alpha,\gamma)$, $O^{16}(\alpha,\gamma)$, and $Ne^{20}(\alpha,\gamma)$. Measurements at high energies (2–5 Mev), where the reactions can be easily detected, are needed to serve as guides in extrapolating to lower stellar energies (0.2–0.5 Mev). Such measurements are planned in the near future at the Kellogg Radiation Laboratory.

In the second place, the relative rates of the reactions depend critically on temperature, and thus different astrophysical circumstances will lead to marked differences in abundance ratios. Helium burning can result, for example, in large or small C^{12}/Ne^{20} ratios.

At the same time it is clear from Fig. III,3 that in the region 1.0 to 1.3×10^8 degrees the reaction rates are all of the same order of magnitude within the present uncertainties except for the very slow production of Mg^{24} from Ne^{20}. Thus the atomic abundance ratios of $C^{12}:O^{16}:Ne^{20}:Mg^{24}=1:6:2:0.2$, given by Suess and Urey (Su56), or 1:5:8:1, given by Aller (Al57a) for early-type stars, are reasonable values on the basis of the synthesis of these elements in helium burning. Also other processes are involved. A considerable amount of C^{12} has been converted into N^{14} by the CN cycle (see Secs. III F and XI A); Mg^{24} has been produced in the α process (see Sec. III D) which consumes O^{16} and Ne^{20}, and so on.

D. α Process

As has just been discussed, helium-burning synthesizes C^{12}, O^{16}, Ne^{20}, and perhaps a little Mg^{24}. This occurs at temperatures between 10^8 and 2×10^8 degrees and results in the exhaustion of the helium produced in hydrogen-burning. An inner core of C^{12}, O^{16}, and Ne^{20} develops in the star and eventually undergoes gravitational contraction and heating just as occurred previously in the case of the helium core. Calculations of stellar evolutionary tracks have not yet been carried to this stage, but it is a reasonable extrapolation of current ideas concerning the cause of evolution into the giant stage. Gravitation is a "built-in" mechanism in stars which leads to the development of high temperature in the ashes of exhausted nuclear fuel. Gravitation takes over whenever nuclear generation stops; it raises the temperature to the point where the ashes of the previous processes begin to burn. Implicit in this argument is the assumption that mixing of core and surrounding zones does not occur.

No important reactions occur among C^{12}, O^{16}, and Ne^{20} until significantly higher temperatures, of the order of 10^9 degrees, are attained. Two effects then arise. The γ rays present in the thermal assembly become energetic enough to promote $Ne^{20}(\gamma,\alpha)O^{16}$. This is the first (γ,α) reaction to occur since the alpha-particle binding in Ne^{20} is only 4.75 Mev, while it is 7.37 Mev in C^{12} and 7.15 Mev in O^{16}. The proton and neutron binding energies in these nuclei are 12 to 19 Mev, so that (γ,α) precedes (γ,p) or (γ,n). The alpha

TABLE III,3. Mean lifetimes in helium burning (years).

T 10^6 °K	$\text{Log}\left[\frac{\rho x_\alpha}{10^5}\right]^2 f_{3\alpha}\tau(\text{He}^4)$ $3He^4 \rightarrow C^{12}$	$C^{12}(\alpha,\gamma)$	$N^{14}(\alpha,\gamma)$	$O^{16}(\alpha,\gamma)$	$\text{Log}\frac{\rho x_\alpha f}{10^5}\tau$ $Ne^{20}(\alpha,\gamma)$	$C^{13}(\alpha,n)$	$Ne^{21}(\alpha,n)$
70	+15.47	+11.1	+13.6	11.6	17.9	+5.44	+16.3
100	7.90	7.57	9.60	7.5	12.6	1.93	10.86
120	5.01	5.94	7.78	5.9	10.1	0.31	8.31
150	2.18	4.09	5.70	4.4	7.3	−1.54	5.41
175	0.59	2.90	4.36	3.5	5.5	−2.73	3.59
200	−0.58	1.91	3.26	2.9	4.0	−3.71	2.03
250	−2.16	0.39	1.54	2.0	1.7	−5.23	−0.38
300	−3.18	−0.77	0.23	1.5	−0.1	−6.39	−2.20

particles thus released can now penetrate the Coulomb barrier of the remaining Ne^{20} quite readily at 10^9 degrees, thereby forming Mg^{24}. The resulting transformation is strongly exothermic, viz.:

$$Ne^{20}+\gamma \rightarrow O^{16}+He^4-4.75 \text{ Mev}$$

$$Ne^{20}+He^4 \rightarrow Mg^{24}+\gamma+9.31 \text{ Mev}.$$
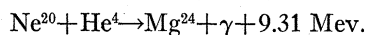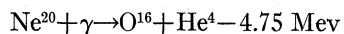
Combining these two equations yields:

$$2Ne^{20} \rightarrow O^{16}+Mg^{24}+4.56 \text{ Mev}.$$

Of course, a proportion of the released alpha particles is consumed in scouring out the C^{12} and forming O^{16}. The result is the formation of additional O^{16} and Mg^{24}; this is highly favored on a statistical basis even though complete equilibrium is not attained.

The addition of the alpha particles released from the Ne^{20} need not be limited to the formation of Mg^{24}. Thus, once some Mg^{24} is produced we also expect $Mg^{24}(\alpha,\gamma)Si^{28}$ to take place, since it is also possible to penetrate the Coulomb barrier of Mg^{24} at temperatures of order 10^9 degrees. Again, once an appreciable concentration of Si^{28} is built up, we expect $Si^{28}(\alpha,\gamma)S^{32}$ to take place in some degree, and so on for the production of A^{36} and Ca^{40}.

This is the α process marked in Figs. I,1 and I,2, and responsible, in our view, for building, in decreasing proportion, the α-particle nuclei Mg^{24}, Si^{28}, S^{32}, A^{36}, and Ca^{40}. Their relative atomic abundances are indicated in Table III,4. The abundance of Ne^{20} is included for comparison. The proportions decrease in general along this sequence, partly because the production of any member of the sequence does not take place in an appreciable amount until the preceding member has first been produced in considerable concentration, and partly because Coulomb effects become increasingly inhibitory as larger and larger values of Z are reached, even at temperatures somewhat above 10^9 degrees.

The nuclei produced in the α process stand out in abundance above other neighboring nuclei. This is made clear in Fig. VI,1 which is discussed in Sec. VI in connection with the neutron-capture s process which synthesizes these nuclei. Mg^{24}, Si^{28}, etc., are much too abundant to have been produced in the s process. The α process is of course, very similar to helium burning. We differentiate the two processes on the basis that the alpha-particle sources are quite different in the two cases. Detailed calculations on the rates of the α-process reactions have been given by Hoyle (Ho54), by Nakagawa et al. (Na56), and by Hayakawa et al. (Ha56b). We estimate that a progression in

temperature from 10^9 to 3×10^9 degrees, either in various regions or at various times in a star, will suffice to bring the rates of the (α,γ) reactions from Mg^{24} to Ca^{40} into reasonable correspondence.

The α process is, of course, an oversimplification as temperatures near 3×10^9 degrees are considered. Interactions between the heavier nuclei themselves must also be taken into account. It is interesting to note that experimental information on the cross sections of these interactions are already becoming available from research with high-energy accelerators equipped with ion sources capable of producing heavy ions (Ha56a).

One interesting elaboration of the α process has not been previously discussed in the literature. The straightforward (α,γ) reactions involving stable nuclei terminate at Ca^{40} since Ti^{44} with an electron capture lifetime of approximately 1000 years (Hu57b) is produced next. We have

$$_{20}Ca^{40}+_2He^4 \rightarrow _{22}Ti^{44}+\gamma$$

$$_{22}Ti^{44}+e^- \rightarrow _{21}Sc^{44}+\nu_+ \qquad \tau_{\frac{1}{2}} \sim 1000 \text{ years}$$

$$_{21}Sc^{44} \rightarrow _{20}Ca^{44}+\beta^++\nu_+ \qquad \tau_{\frac{1}{2}}=3.9 \text{ hours}.$$
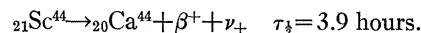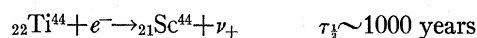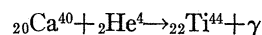
If the alpha-capture lifetimes are greater than 1000 years, then the foregoing decays occur before Ti^{44} captures another alpha particle. Then one has

$$_{20}Ca^{44}+_2He^4 \rightarrow _{22}Ti^{48}+\gamma,$$
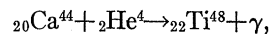
the Ti^{48} being stable. The important point is that Ti^{48} is produced in an interaction with approximately the same barrier height as in the case of Ca^{44} and thus these two should be of roughly equal abundance. This is just the case within a factor of two (favoring Ti^{48}!) in spite of the rapid decrease in abundance evident from Si^{28} to Ca^{44}. Some Ti^{48} may also be produced in the e process discussed in the next section.

A corollary of our argument is that the time-scale of the α process must exceed 1000 years at Ti^{44}. If Ti^{44} captured an alpha particle it would produce Cr^{48} which decays through V^{48} to Ti^{48}. The unconsumed Ti^{44} would eventually decay to Ca^{44}, and in this case one would expect Ca^{44} to be considerably more abundant than Ti^{48}.

E. Succession of Nuclear Fuels in an Evolving Star

Starting with primeval hydrogen condensed into stars, pure hydrogen burning, pure helium burning, and finally the α process successively take place at the stellar center and then move outward in reaction zones or shells. When the star first contracts the generation of energy by hydrogen burning develops internal pressures which oppose gravitational contraction, and the star is stabilized on the main sequence at the point appropriate to its mass. Similarly, the generation of energy in helium burning should lead to a period of

TABLE III,4. Relative abundances of nuclei produced in the α process (Su56).

	$(Ne^{20})^a$	Mg^{24}	Si^{28}	S^{32}	A^{36}	Ca^{40}	Ca^{44}	Ti^{48}
Q_α (Mev)	(9.31)	10.00	6.94	6.66	7.04	5.28	9.40	9.32
Abundance	(8.4)	0.78	1.00	0.39	0.14	0.052	0.0011	0.0019

a Produced in helium burning; included for comparison.

relative stability during the red-giant stage of evolution. It is assumed that mixing does not occur. This is substantiated by the fact that, as hydrogen becomes exhausted in the interior, the star evolves off the main sequence which is the location of stars with homogenous interiors.

At the end of helium burning most of the nuclear binding energy has been abstracted, and indeed the cycle of contraction, burning, contraction . . . must eventually end when the available energy is exhausted, that is, when the most stable nuclei at the minimum in the packing fraction curve are reached, near Fe^{56}. If a star which condensed originally out of pure hydrogen remains stable, it eventually forms the iron-group elements at its center, and this "iron core" continues to grow with time until gravitation, unopposed by further energy generation, leads eventually to a violent instability. This problem of the ultimate instability is discussed, but not solved, in Sec. XII. At this point it suffices only to emphasize that the instability may result in the ejection of at least part of the "iron core" and its thin surrounding shells of lighter elements into the interstellar medium and that in this way a reasonable picture of the production of the abundance peak at the iron-group elements can be formulated. Production of the iron group of elements requires temperatures near 4×10^9 degrees, at which statistical equilibrium is reached, as outlined in Sec. II and discussed in detail in Sec. IV (the e process).

F. Burning of Hydrogen and Helium with Mixtures of Other Elements; Stellar Neutron Sources

In the previous discussion we considered the effect of heating hydrogen and its reaction products to very high temperatures. First, the hydrogen is converted to helium, and the resulting helium is converted to C^{12}, O^{16}, and Ne^{20}. Then α particles released by (γ,α) reactions on the Ne^{20} build the α-particle nuclei Mg^{24}, Si^{28}, S^{32}, A^{36}, Ca^{40}, and also Ca^{44} and Ti^{48}. Finally, at very high temperatures, the latter nuclei are converted into the iron group. Further heating of the iron group, although of astrophysical importance, does not lead directly to any further synthesis. Thus all the remaining elements and isotopes must be provided for otherwise than by a cooking of pure hydrogen.

Very much more complicated reactions arise when we consider the cooking of hydrogen and helium mixed with small concentrations of the elements already provided for, e.g., C^{12}, Ne^{20}, Fe^{56}. It is easy to see how such admixtures can arise. Since stars eject the products of nuclear synthesis into the interstellar gas it seems highly probable that only the "first" stars can have consisted of pure hydrogen. The results of hydrogen cooking in such stars would follow the lines described above. But once the interstellar gas was contaminated by this first cooking, nuclear processes would operate on hydrogen which contains impurities. The eventual

hydrogen exhaustion will lead to helium burning with impurities. As we shall see later, the presence of other nuclei can lead to highly important effects.

In addition, hydrogen and helium may in some cases become adulterated with impurities even in the "first" stars. For example C^{12}, Ne^{20} built in the inner central regions of such stars may be circulated into the outer hydrogen envelopes. The question whether such mixing occurs, and astrophysical observations bearing on the problem, is considered in Secs. XI and XII.

(1) CN cycle

When C^{12} produced in helium burning is mixed with hydrogen at high enough temperatures, hydrogen is converted to He^4 by the CN cycle in addition to the pp chain previously considered. The implications for energy generation in hot main-sequence stars have been considered by numerous authors since Bethe (Be39) and von Weizsäcker (We38). The reactions of the CN cycle are

$$C^{12}(p,\gamma)N^{13}(\beta^+\nu_+)C^{13}$$
$$C^{13}(p,\gamma)N^{14}$$
$$N^{14}(p,\gamma)O^{15}(\beta^+\nu_+)N^{15}$$
$$N^{15}(p,\alpha)C^{12}.$$
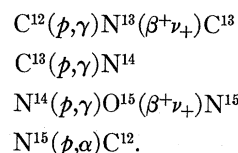
These four reactions produce C^{13}, the heavier stable isotope of carbon, and the two stable forms of nitrogen. For C^{12}, C^{13}, and N^{14} the (p,α) reaction is not exothermic and only the (p,γ) reaction occurs. At N^{15}, the (p,α) reaction becomes exothermic and much more rapid than the (p,γ) reaction, which serves only as a small leak of material to O^{16}. The $N^{15}(p,\alpha)$ reaction reproduces the original C^{12} and a true cycle of reactions is established. Not only does this give rise to the catalytic conversion of hydrogen into helium until hydrogen is exhausted, but it also results in the carbon and nitrogen isotopes *not* being consumed in hydrogen burning.

The cross sections of the CN-cycle reactions have been under experimental investigation in the Kellogg Radiation Laboratory for some years and a review of the reaction rates in stars as known up to 1954 is included in the earlier paper by Fowler (Fo54), with numerical computations by Bosman-Crespin et al. (Bo54). New measurements of the CN-cycle reactions in the 100-kev range of interaction energies are now underway by William A. S. Lamb and Ross E. Hester at the Livermore Radiation Laboratory, who are using an ion source capable of delivering several hundred milliamperes of protons in this energy range, a factor of almost 1000 over the currents used in previous experiments. Results on $C^{12}(p,\gamma)$ are already published (La57) and results have also been obtained on $N^{14}(p,\gamma)$ (La57a). These are the two slowest reactions in the CN cycle and are the ones primarily involved in the over-all rate of this reaction.

In Figs. III,4 and III,5 are shown the yield and
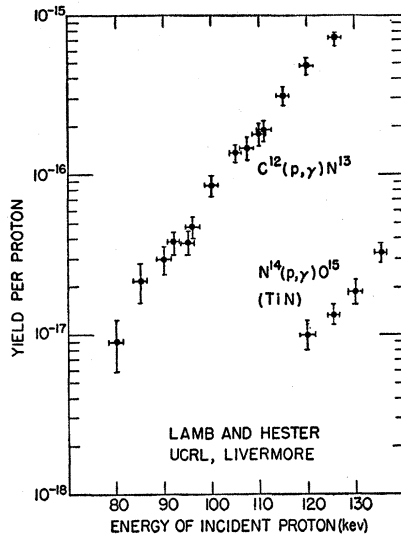
FIG. III,4. Yields of the $C^{12}(p,\gamma)$ and $N^{14}(p,\gamma)$ reactions as a function of bombarding energy obtained by Lamb and Hester (La57) at Livermore. The $N^{14}(p,\gamma)$ results were obtained using a titanium nitride target. In results not illustrated here the yield has been measured down to 100 kev where it has the very low value of only one reaction per 10^{18} incident protons.

cross-section curves for $C^{12}(p,\gamma)$ obtained by Lamb and Hester. For comparison, points obtained originally by Hall and Fowler (Ha50) and by Bailey and Stratton (Ba50) are shown. All of the observations are seen to fit a modification due to Thomas (Th52) of the Breit-Wigner dispersion formula using parameters of the resonance at 456 kev. The new results confirm the original measurements, but more importantly they extend the measurements to cross sections lower by a factor of ten and they do this with increased precision, so that the extrapolation to the lower temperatures relevant to stellar interiors ($E_o \sim 25$ kev) can be made with much more confidence. Their cross section $\sigma = 5.2 \times 10^{-11}$ barn at 90 kev is a representative one and yields

$$S = \left(\frac{12}{13} \times 90 \times 5.2 \times 10^{-11}\right) \exp\{+188.4/(90)^{\frac{1}{2}}\}$$

$= 1.7$ kev barns.

Extrapolation to stellar energies yields

$$S_o = 1.2 \pm 0.2 \text{ kev barns for } C^{12}(p,\gamma)N^{13}$$

as found by Hall and Fowler (Ha50), so that no change in the numerical calculations of Bosman-Crespin et al. is required.

Experimental results for the reaction $N^{14}(p,\gamma)$ have also been obtained and are also shown in Figs. III,4 and III,5. Lamb and Hester find a representative value $\sigma = 7.0 \pm 1.0 \times 10^{-11}$ barn at 125 kev. This corresponds

to a cross-section factor

$$S = \left(\frac{14}{15} \times 125 \times 7.0 \times 10^{-11}\right) \exp\{+219.8/(125)^{\frac{1}{2}}\}$$

$= 2.8$ kev barns.

Their value, $\sigma = 0.9 \times 10^{-11}$ barn, at 100 kev is the smallest charged particle cross section measured up to the present time.

This and their other values correspond to a cross-section factor at stellar energies equal to $S_o = 3.2$ kev barns. In the Kellogg Radiation Laboratory Pixley (Pi57) has made measurements on this reaction from 220 kev up to 650 kev. His results can be interpreted as indicating that a narrow resonance at 278 kev, with width $\Gamma = 1.7$ kev, is superimposed on a non-resonant background which increases with the energy just as the calculated Coulomb barrier penetration factor times the usual $1/v$-term. The nonresonant cross section varies from 1.44×10^{-7} barn at 450 kev to 4.74×10^{-7} barn at 650 kev. The measured cross sections correspond to a cross-section factor at low energies given by $S_o = 2.8$ kev barns. The two sets of experiments indicate that the nonresonant background is characterized by a relatively constant S from 130 to 650 kev. Averaging the two values given above we have, with a reasonable allowance for systematic errors,

$$S_o = 3.0 \pm 0.6 \text{ kev barns for } N^{14}(p,\gamma)O^{15}.$$

This result is 12% of the value derived from the measurements of Woodbury, Hall, and Fowler (Wo49) near 124-kev bombarding energy, and confirms the finding of Duncan and Perry (Du51) that this old value could not be attributed to the effects of known resonances from 278 kev to 2.6 Mev. Fowler (Fo54) attributed the large value at 124 kev to the resonance effects of a bound level at 6.84 Mev in O^{15}, which is 543 kev below the $N^{14} + p$ threshold, and Bosman-Crespin et al. (Bo54) accordingly used, near $T = 10^7$ degrees, the value $S_o = 33$ kev barns for $N^{14}(p,\gamma)$. There is now no basis for this value. Accordingly, the tabulated values of Bosman-Crespin et al. for N^{14}-$(p,\gamma)O^{15}$ must be multiplied by ~ 0.09. On this basis the $N^{14}(p,\gamma)$ reaction is very much slower than $C^{12}(p,\gamma)$.

Lamb and Hester (La57) obtain preliminary values for the cross section for $C^{13}(p,\gamma)$ which are about twice those which were obtained by Woodbury and Fowler (Wo52). Until this discrepancy is cleared up it is recommended that the reaction rates given by Fowler (Fo54) be employed with some caution. No new measurements are available on $N^{15}(p,\alpha)$ and the rates given by Fowler (Fo54) can be employed. Cross-section factors given by Fowler (Fo54) are:

$$S_o = 6.1 \pm 2 \text{ kev barns for } C^{13}(p,\gamma)N^{14},$$

$$S_o = 1.1 \pm 0.3 \times 10^{6} \text{ kev barns for } N^{15}(p,\alpha)C^{12}.$$

In spite of the concordance of the new off-resonant measurements for $N^{14}(p,\gamma)$ there still exists the vexing problem as to whether resonance occurs in $N^{14}(p,\gamma)O^{15}$ in the region of stellar energies corresponding to an excitation energy in O^{15} near 7.37 ± 0.03 Mev. Known levels in O^{15} near this excitation occur at 6.84, 6.90, 7.61 ($\frac{1}{2}^+$), and 8.33 Mev ($\frac{3}{2}^+$). The spin and parity assignments for the last two levels come from studies of the $N^{14}(p,p)$ scattering by Pixley (Pi57) and by Hagedorn et al. (Ha57). The 7.61-Mev level is the level investigated in detail at 278-kev bombarding energy by Pixley. It is too narrow and too far removed to influence the cross section at 7.37 kev. In the mirror nucleus N^{15}, which has been investigated more completely, levels occur at 7.16 ($\frac{7}{2}^+$), 7.31 ($\frac{3}{2}^+$), 7.58 ($\frac{5}{2}^+$?), 8.32 ($\frac{1}{2}^+$), and 8.57 Mev ($\frac{3}{2}^+$). The spin and parity assignments are the results of a recent comparison of shell model calculations with experiment by Halbert and French (Ha57a). In the light of the spins and parities and of the expected large level shifts (Th52) it can be convincingly argued that the last two levels correspond to the last two indicated above for O^{15}. One of the other three has not been found in O^{15}. Considerable work has been done on this problem in the last few years, but no new level has been found in this region in O^{15}, and a possible explanation lies in the level shift phenomenon. However, the research has not been exhaustive and it is still possible that a level falls in the range 7.37 ± 0.03 Mev, where it would serve as a resonance at stellar energies and thus would possibly enhance by a considerable amount the $N^{14}(p,\gamma)$ reaction rate in main-sequence stars.

If resonance in $N^{14}(p,\gamma)$ occurs then the reaction could be much more rapid than $C^{12}(p,\gamma)$, in which case the over-all rate of the CN cycle is determined by this last process. In this case the energy generation is that given as ϵ_C by Bosman-Crespin et al. (Bo54),

$$\epsilon_C = (3.18\pm0.54)\alpha_C x_H x_C \times 10^{27} \text{ ergs g}^{-1} \text{ sec}^{-1},$$

where x_C is the fraction by mass of C^{12}. This is about 81% of the total carbon, C^{12} plus C^{13}, and there will be very little nitrogen. Thus $x_C \approx 0.8 x_{CN}$. The quantity α_C is given by

$$\alpha_C = \rho f_C (T_6^{-\frac{2}{3}}+0.017) \exp(-136.9 T_6^{-\frac{1}{3}})$$

$$\simeq 1.4\times10^{-25}\rho f_C \left(\frac{T_6}{15}\right)^{17.9} \quad \text{near } T_6=15,$$

with the electron shielding factor given by Salpeter's strong screening formula (Sa54) as $f_C = \exp(0.98\rho^{\frac{1}{3}}/T_6)$.

The mean lifetime of hydrogen becomes

$$\tau_C(H) = 1.90(x_H/\epsilon_C)\times10^{11} \text{ years}$$
$$= 0.60(\alpha_C x_C)^{-1}\times10^{-16} \text{ year},$$

while for C^{12} the mean cycle time is

$$\tau_H(C^{12}) = 0.63(x_C/\epsilon_C)\times10^{11} \text{ years}$$
$$= 0.20(\alpha_C x_H)^{-1}\times10^{-16} \text{ year}.$$
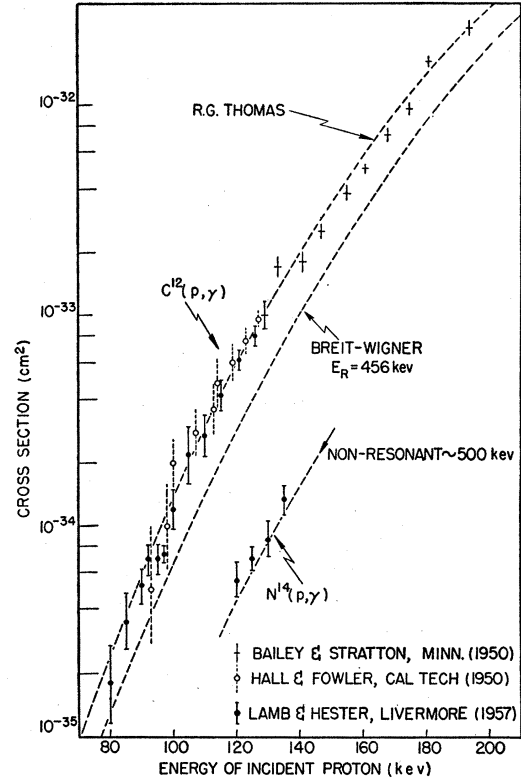
FIG. III,5. The cross sections of the $C^{12}(p,\gamma)$ and $N^{14}(p,\gamma)$ reactions at low bombarding energies. The early results on $C^{12}(p,\gamma)$ of Bailey and Stratton (Ba50) at the University of Minnesota, and of Hall and Fowler (Ha50) at the California Institute of Technology are compared with the new and more accurate results of Lamb and Hester (La57) obtained at the University of California Radiation Laboratory, Livermore. A modification of the Breit-Wigner dispersion formula by Thomas (Th52) based on the parameters of the resonance at 456 kev is found to fit the experimental result very well. Note the extremely low cross section of 10^{-11} barn measured experimentally by Lamb and Hester.

On the other hand, if resonance does not occur in $N^{14}(p,\gamma)$ then we must use the new value for S_o already given. Ignoring all small correction terms and defining

$$\alpha_N = \rho f_N T_6^{-\frac{2}{3}} \exp(-152.3 T_6^{-\frac{1}{3}})$$

$$\simeq 2.5\times10^{-28}\rho f_N \left(\frac{T_6}{15}\right)^{19.9} \quad \text{near } T_6=15,$$

with the electron shielding factor given by Salpeter's strong screening expression as $f_N = \exp(1.11\rho^{\frac{1}{3}}/T_6)$, then the reaction rate of the CN cycle per gram of material per second becomes

$$r_N = (1.96\pm0.39)(\alpha_N x_H x_N)\times10^{32} \text{ reactions g}^{-1} \text{ sec}^{-1},$$

where x_N is the fraction by mass of N^{14}. In this case almost all of the carbon and nitrogen will be in the form of N^{14}. Thus $x_N \approx x_{CN}$. The mean reaction rate per proton with four protons consumed per cycle is

$$p_N(H) = -\frac{1}{x_H}\frac{dx_H}{dt} = (1.31\pm0.26)(\alpha_N x_N)\times10^9 \text{ sec}^{-1}.$$

The energy release per cycle, excluding the 6% neutrino energy loss, is 25.04 Mev = 4.011×10^{-5} erg using Wapstra's masses (Wa55), so that the rate of energy generation can be written

$$\epsilon_N = (0.786 \pm 0.16)(\alpha_N x_H x_N) \times 10^{28} \text{ ergs g}^{-1} \text{ sec}^{-1}.$$

The mean lifetime of hydrogen becomes

$$\tau_N(H) = 1.90(x_H/\epsilon_N) \times 10^{11} \text{ years}$$
$$= (2.42 \pm 0.48)(\alpha_N x_N)^{-1} \times 10^{-17} \text{ year},$$

while for N^{14} the mean *cycle* time is

$$\tau_H(N) = 0.55(x_N/\epsilon_N) \times 10^{11} \text{ years}$$
$$= (0.70 \pm 0.14)(\alpha_N x_H)^{-1} \times 10^{-17} \text{ year}.$$

At the present time the rate of energy generation by the CN cycle can be taken as lying between the wide limits given by ϵ_N and ϵ_C. Since resonance has not been established in $N^{14}(p,\gamma)$, the best guess is ϵ_N. Values for ϵ_C and ϵ_N and the various lifetimes and cycle times are given in Figs. III,1 and III,2 and in Tables III,1 and III,2.

Because of the uncertainty in the resonance problem in $N^{14}(p,\gamma)$ it is reasonable to employ astrophysical arguments in search of a more definite answer concerning the rate of the CN cycle. Let it be assumed that the observed cosmic abundances of N^{14} and C^{13} have been produced at equilibrium at temperature T from C^{12} in the CN cycle. Then if $S_o = 33$ kev barns (Fo54) for $N^{14}(p,\gamma)$ and $S_o = 6.1$ kev barns (Fo54) for $C^{13}(p,\gamma)$ it can be calculated that the relative numbers of nuclei are given by

$$N^{14}/C^{13} = [133/T_6]^2.$$

The relative abundance given by Suess and Urey (Su56) is
$$N^{14}/C^{13} = 168.$$

The temperature giving this ratio is approximately 10^7 degrees. At this temperature the C^{12} cycle time is 3×10^9 years for $\rho x_H = 100$ g/cm³, so conversion of C^{12} to C^{13} or N^{14} will occur only in old stars.

With the lower limit of $S_o = 3.0$ kev barns for N^{14} (p,γ) it is found that

$$N^{14}/C^{13} = [440/T_6]^2.$$

The temperature corresponding to the observed relative abundance is $\sim T = 3.4 \times 10^7$ degrees. This value is close to the temperature believed to hold in the hydrogen-burning shells surrounding the helium cores of red giant stars (Ho55). It is perhaps reasonable astrophysically to argue that this constitutes the last situation in which C^{13} and N^{14} are in equilibrium under hydrogen-burning. The C^{13} and N^{14} from these shells will be ejected into space when instability arises in the stellar interior. C^{13} and N^{14} which remain in the helium region after the exhaustion of hydrogen are consumed in helium burning by $C^{13}(\alpha,n)$ and $N^{14}(\alpha,\gamma)$. On the basis, then, of this

argument, the lower limit for S_o would seem to be the preferred value.

With the new value for S_o for $N^{14}(p,\gamma)$ it is found that the CN cycle rate will exceed that for the pp chain only in stars with central temperatures over 18×10^6 degrees. The existence of nitrogen-rich peculiar stars, as discussed in Sec. XI, is to be expected on this basis since at equilibrium in the CN cycle we now have

$$N^{14}/C^{12} = [200/T_6]^2$$

so that $N^{14} \gg C^{12}$ at all reasonable temperatures ($T_6 < 40$) for hydrogen burning. Stars in which carbon from the helium-burning cores has been passed slowly enough through hydrogen-burning zones and then mixed into the outer atmosphere will show a much greater over-abundance of nitrogen than of carbon. The C^{12}/C^{13} ratio by number should be 4.6 for the carbon in such stars. On the other hand, stars in which C^{12}, O^{16}, and Ne^{20} from helium-burning zones were mixed quickly without hydrogen-burning into the envelope would show anomalous abundances of these isotopes and not necessarily of N^{14} or C^{13}. The ratio of C^{12}/C^{13} might be quite large in such stars. These points have been emphasized by Greenstein (Gr54a); see also Sec. XI A.

Finally, with the new nonresonant value for N^{14}-(p,γ) the CN cycle is very slow in the sun. The recent inhomogeneous model calculations of Schwarzchild, Howard, and Härm (Sc57) which use only the pp chain need not be modified to include CN cycle processing of hydrogen except for the cases involving rather low values of the initial hydrogen content. D. E. Osterbrock (private communication) has kindly made differential corrections to the calculations of Schwarzschild et al. using the pp reaction and $N^{14}(p,\gamma)$ reaction rates given in this paper. He finds $T_c = 15.4 \times 10^6$ degrees and $\rho_c = 147$ g/cm³ for an original hydrogen content of 80% by mass. These values replace $T_c = 14.8 \times 10^6$ degrees and $\rho_c = 132$ g/cm³. For the present values $x_H = 0.30$ and $x_{CN} = 0.003$ at the solar center he finds $\epsilon_{pp} = 5.25$ ergs g⁻¹ sec⁻¹ and $\epsilon_{CN} = 0.20$ erg g⁻¹ sec⁻¹. Thus the CN-cycle energy generation is only about 4% of that of the pp chain at the center and is less than this value on the average.

(2) Other Hydrogen-Burning Reactions

The reactions of protons and other light nuclei have been discussed by Fowler (Fo54) and by Salpeter (Sa55) and most recently by Marion and Fowler (Ma57). The rapid destruction of the lithium, beryllium, and boron isotopes in hydrogen burning, the end result being the production of helium, is well known and will not be discussed here, though some of the problems which this raises for synthesis of these elements are discussed in Sec. X.

At the temperatures occurring in the hydrogen-burning shells of red giant stars O^{16} is converted to

N^{14} by

$$O^{16}(p,\gamma)F^{17}(\beta^+\nu_+)O^{17}$$

$$O^{17}(p,\alpha)N^{14}+1.20 \text{ Mev (exothermic)}.$$
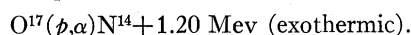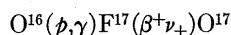
The N^{14} is then processed by the CN cycle. When the small leakage due to $N^{15}(p,\gamma)O^{16}$ from the CN cycle is taken into account with the above reactions one has a generalized CNO cycle.

For $O^{16}(p,\gamma)$ Tanner and Pixley (Ta57a) give the preliminary value

$$S_o = 4 \pm 2 \text{ kev barns for } O^{16}(p,\gamma)$$

so that the lifetime for O^{16} in hydrogen burning becomes

$$\tau_H(O^{16}) = 0.5(\alpha_0 x_H)^{-1} \times 10^{-17} \text{ year},$$

where

$$\alpha_0 = \rho T_6^{-\frac{2}{3}} \exp(-166.7 T_6^{-\frac{1}{3}}).$$

Here we have neglected the weak electron shielding expected to hold in high-temperature, low-density shells. Since $O^{16}(p,\gamma)$ is followed rapidly by $O^{17}(p,\alpha)$ and by hydrogen processing in the CN cycle, the hydrogen lifetime will be the same as that for O^{16}. Whenever O^{16} burning is not complete, a small amount of O^{17} ($\sim 10^{-3} \times O^{16}$) remains in equilibrium with O^{16}. This may be sufficient to account for the small concentration of $O^{17} = 4 \times 10^{-4} \times O^{16}$ observed in the oxygen isotope ratios. Apparently, not all of the O^{16} and O^{17} have been destroyed in the hydrogen-burning shells of the giant stars during the relatively short life of this evolutionary stage. On the other hand, $O^{18} = 2 \times 10^{-3} \times O^{16}$ is not produced in sufficient abundance by $O^{17}(p,\gamma)F^{18}(\beta^+\nu_+)O^{18}$ since the (p,α) reaction is much faster than the (p,γ) for O^{17}.

The burning of Ne^{20} in hydrogen is followed by the NeNa cycle which is somewhat similar to the CN cycle,

$$Ne^2(p,\gamma)Na^{21}(\beta^+\nu_+)Ne^{21}$$

$$Ne^{21}(p,\gamma)Na^{22}(\beta^+\nu_+)Ne^{22}$$

$$Ne^{22}(p,\gamma)Na^{23}$$

$$Na^{23}(p,\alpha)Ne^{20}.$$
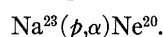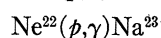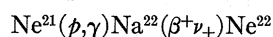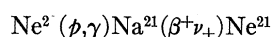
New calculations based on recent experimental information have been made for the rates of the NeNa-cycle reactions by Marion and Fowler (Ma57). It is found that $Na^{23}(p,\alpha)$ is considerably faster than $Na^{23}(p,\gamma)$, so that little leakage from the cycle occurs to Mg^{24}. A method of obtaining the reduced nucleon emission widths for the corresponding levels of mirror nuclei is presented and is used in particular in the calculation of the $Ne^{20}(p,\gamma)$ reaction rate. It is found that a bound level in Na^{21} at $Ne^{20}+p-26$ kev markedly enhances the rate of this reaction and that $S_o \approx 12$ kev barns at the temperatures of hydrogen-burning shells. Results of preliminary measurements by Pixley, Hester, and Lamb (Pi57a) increase this to

$$S_o \sim 75 \text{ kev barns for } Ne^{20}(p,\gamma)Na^{21}.$$

Substantial quantities of Ne^{21} are produced at the elevated temperatures occurring just before the hydrogen is exhausted in such shells. This will be true only if the carbon, nitrogen, and oxygen isotopes are relatively rare so that hydrogen is not processed too rapidly before the Ne^{20} can be burned. The Ne^{21} thus formed becomes important in the subsequent helium burning when the reaction $Ne^{21}(\alpha,n)Mg^{24}$ may serve as a source of neutrons for heavy element synthesis.

The mean lifetimes or cycle times of the light nuclei in hydrogen-burning are summarized in Table III,2 and Fig. III,2.

(3) Helium Burning with Reaction Products; Stellar Neutron Sources

The primary products of pure helium burning are C^{12}, O^{16}, and Ne^{20}. When these are subjected to further hydrogen burning, production of all of the stable isotopes from C^{12} to Na^{23}, with the exception of N^{15}, O^{18}, and F^{19}, is accounted for. Production of these three exceptions is treated at the end of this section. In hydrogen burning, cyclic processes are established which transform the hydrogen into helium without consuming the cycling, catalytic nuclei. Exceptions are O^{16} and O^{17}; these nuclei are consumed in hydrogen burning so it is clear that a proportion of these isotopes originally produced has not been subjected to terminal hydrogen burning.

Exhaustion of the hydrogen by the cyclic processes eventually means that the unconsumed isotopes of carbon, nitrogen, neon, sodium, and perhaps oxygen, will be mixed with helium. Upon contraction the mixture comes to a temperature at which helium begins to interact with these nuclei. Numerous reactions occur but by far the most significant are the exothermic (α,n) reactions which provide a source of neutrons for the s and r processes by which the heavy elements can be synthesized.

The first stellar neutron source was proposed by Greenstein (Gr54) and by Cameron (Ca54, Ca55), namely the *exothermic* reaction:

$$C^{13}(\alpha,n)O^{16}+2.20 \text{ Mev}.$$
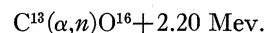
To this, Fowler et al. (Fo55) added the *exothermic* (α,n) reactions involving the $A=4n+1$ nuclei, viz.,

$$O^{17}(\alpha,n)Ne^{20}+0.60 \text{ Mev}$$

$$Ne^{21}(\alpha,n)Mg^{24}+2.58 \text{ Mev}$$

$$Mg^{25}(\alpha,n)Si^{28}+2.67 \text{ Mev}$$
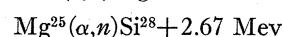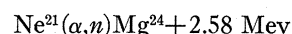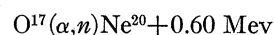
and the special case,

$$Mg^{26}(\alpha,n)Si^{29}+0.04 \text{ Mev}.$$
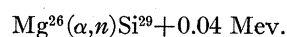
The next $A=4n+1$ reaction, $Si^{29}(\alpha,n)S^{32}$, is *endothermic* by 1.53 Mev, and $S^{33}(\alpha,n)A^{36}$ is *endothermic* by 2.0 Mev.

Insofar as neutron sources for the s process in red giants are concerned, we must confine our attention to C^{13} and Ne^{21}. Very little O^{17} remains for helium burning

because it is destroyed by $O^{17}(p,\alpha)$ in hydrogen burning. Mg^{25} and Mg^{26} are not produced in hydrogen burning because the hydrogen is consumed in other processes before $Mg^{24}(p,\gamma)$ becomes operative.

Marion and Fowler (Ma57) have recently discussed the rates of the $C^{13}(\alpha,n)$ and $Ne^{21}(\alpha,n)$ reactions. For the $C^{13}(\alpha,n)$ reaction they find $S_o = 2.1 \times 10^{11} T_6^{-\frac{4}{3}}$ kev barn so that the C^{13} lifetime is

$$\tau_{\alpha n}(C^{13}) = 4.9 \times 10^{-28} \frac{T_6^2}{\rho x_\alpha} \exp(323 T_6^{-\frac{1}{3}}) \text{ years.}$$

For the $Ne^{21}(\alpha,n)$ reaction they find $S_o = 1.6 \times 10^{13}$ kev barns so that the Ne^{21} lifetime is

$$\tau_{\alpha n}(Ne^{21}) = 5.6 \times 10^{-30} \frac{T_6^{\frac{2}{3}}}{\rho x_\alpha} \exp(468 T_6^{-\frac{1}{3}}) \text{ years.}$$

A reaction rate of importance in the following discussion is that of $N^{14}(\alpha,\gamma)$, for which it was found that $S_o = 1.2 \times 10^7 T_6^{-\frac{4}{3}}$ kev barn and

$$\tau_{\alpha\gamma}(N^{14}) = 8.2 \times 10^{-24} \frac{T_6^2}{\rho x_\alpha} \exp(360 T_6^{-\frac{1}{3}}) \text{ years.}$$

The above lifetimes are indicated graphically in Fig. III,3 and are tabulated in Table III,3.

Neither $C^{13}(\alpha,n)$ nor $Ne^{21}(\alpha,n)$ are wholly free from objection as stellar neutron sources. Cameron (Ca55) and Fowler et al. (Fo55) have discussed the problems which arise if the $C^{13}(\alpha,n)O^{16}$ reaction is taken as the principal source of neutrons for heavy element synthesis in helium burning during the giant stage of a star's evolution. The essential difficulty lies in the fact that only a small amount of C^{13} is produced at equilibrium in the carbon-nitrogen cycle; $C^{13}/C^{12} = 1/4.6$ by number at equilibrium. As a result too few neutrons are produced when C^{13} begins to interact with the helium. The cosmic abundance ratio $C^{12}/Fe^{56} = 6.4$ implies that $6.4/4.6 = 1.4$ neutrons will become available per iron nucleus and these will only be sufficient to build nuclei slightly heavier than Fe^{56}. Another difficulty is the fact that N^{14} is the most abundant of the isotopes at equilibrium in the CN cycle; $N^{14}/C^{13} = 168$ even at the high temperature of 3.4×10^7 degrees for a hydrogen-burning shell. The reaction $N^{14}(n,p)C^{14}$ consumes a large fraction of the neutrons produced in the $C^{13}(\alpha,n)O^{16}$ reaction. These difficulties can be avoided, as emphasized by Cameron, with the C^{13}-$(\alpha,n)O^{16}$ reaction as the neutron source, if it is postulated that considerable mixing between core and envelope takes place during the giant stage. In this case hydrogen from the envelope interacts with C^{12} produced by $3He^4 \rightarrow C^{12}$ in the core and constantly replenishes the C^{13} supply but at such a rate that little N^{14} is produced by the $C^{13}(p,\gamma)N^{14}$ reaction. In addition if C^{12}, produced in the hot center of a core, is mixed into the cooler

outer regions of the core where C^{13} is burning, then the C^{12} captures the protons from $N^{14}(n,p)$ and replenishes the C^{13}, thus permitting the full quota of neutrons to be made available for heavy element synthesis just beyond Fe^{56}.

Fowler et al. proposed the $Ne^{21}(\alpha,n)Mg^{24}$ reaction as an alternative source of neutrons which would avoid the foregoing difficulties without calling upon core-envelope mixing with its attendant stability problems. In this proposal it is assumed that Ne^{20}, previously produced during helium burning at an earlier stage of galactic evolution, is converted into Ne^{21} in the hydrogen-burning shells at $30-50 \times 10^6$ degrees surrounding the helium-burning cores of red-giant stars. When the shell hydrogen is converted into what then becomes core helium, the Ne^{21} interacts with helium to produce neutrons. The neutrons are captured by iron-group nuclei, also previously synthesized, to produce heavy elements. The atomic abundance ratio $Ne^{20}/Fe^{56} = 14$ is taken as indicating that ∼14 neutrons will become available per iron nucleus, a sufficient number for considerable heavy element synthesis. This suggestion thus requires that:

(i) The reactions $Ne^{20}(p,\gamma)Na^{21}(\beta^+\nu_+)Ne^{21}$ produce Ne^{21} faster than it is destroyed by the $Ne^{21}(p,\gamma)Na^{22}$ reaction.

(ii) The Ne^{21} is produced before the hydrogen mixed with the Ne^{20} is exhausted by the pp chain or the CN-cycle reactions.

(iii) The N^{14} is depleted by the $N^{14}(\alpha,\gamma)F^{18}$ reaction before the $Ne^{21}(\alpha,n)Mg^{24}$ reaction supplies the neutrons.

(iv) The Ne^{21} is consumed by $Ne^{21}(\alpha,n)Mg^{24}$ before helium is depleted in the core.

Because of the uncertainty in the reaction-rate calculations presented here, it is not possible to give unequivocal answers as to whether these conditions are satisfied; however, the following qualified statements can be made. With regard to (i) the results incorporated in Table III,2 and Fig. III,2 indicate that Ne^{21} is indeed produced from Ne^{20} faster than it is destroyed. If the NeNa cycle reaches equilibrium, then about 90% of the Ne^{20} could have been converted into Ne^{21} along with small amounts of Ne^{22} and Na^{23}. With regard to (ii), it is clear that the conversion of Ne^{20} into Ne^{21} will not occur before the hydrogen is exhausted by the CN cycle or oxygen reactions unless there is only a small concentration of carbon, nitrogen, and oxygen, perhaps 0.1% that of hydrogen by weight. This is ∼8% the normal abundance but could occur in some stars. With regard to (iii) it may be seen from Table III,3 and Fig. III,3 that N^{14} will be fairly well scoured out at low temperatures before Ne^{21} begins to interact, although there is again considerable uncertainty in this conclusion.

With regard to (iv), Table III,3 and Fig. III,3 show that $Ne^{21}(\alpha,n)$ will compete with other helium reactions only at elevated temperatures near 2×10^8

degrees in the core. Even then it is about a hundred times slower than the consumption of He^4 by $3He^4 \rightarrow C^{12}$ as long as helium is abundant. However, there is a factor of x_α^2 in the rate of $3He^4 \rightarrow C^{12}$ relative to Ne^{21}-(α,n), where x_α is the concentration by weight of the helium. Thus when $x_\alpha < 0.1$, the Ne^{21} will be consumed. Indeed, we can expect that as x_α decreases the core temperature will rise to maintain the energy generation and eventually the last He^4 nuclei will rapidly scour out the Ne^{21} at high temperature. In any case, even if the Ne^{21} remains impervious to helium burning it will lose its loosely-bound neutron in the subsequent interactions of the medium-weight nuclei.

With the above considerations in mind a tentative picture of the generation of neutrons in red giant cores is as follows. We assume that the core will spend some 10^7 to 10^8 years at low temperature $(20-40 \times 10^6$ degrees) while the star slowly progresses into the giant stage, some 10^5 years at 50 to 100×10^6 degrees, and then only a brief period, say 10^3 years, at 200×10^6 degrees as it rapidly exhausts helium and burns the middle weight elements. The C^{13} lifetime to the (α,n) reaction is about 10^5 years at 75×10^6 degrees, so that C^{13} will be consumed at this stage. Thus a few neutrons per Fe^{56} become available on a time-scale of about 10^5 years. We have seen in Sec. II that a time-scale $\lesssim 10^5$ years per neutron capture is demanded to produce the early part of the abundance distribution built by the s process; this is discussed further, in Sec. VI. With the consumption of the C^{13} in its central regions, the core now heats to greater temperatures and rapidly processes He^4 by $3He^4 \rightarrow C^{12}$, etc. Toward the end of the helium burning, instability may well set in and mixing may occur throughout the core and with the envelope hydrogen. New C^{13} is produced, Ne^{21} burns, and a great flux of neutrons is produced in the final period of about 10^3 years. In Sec.II we showed that a shorter time-scale was necessary to account for the s-process abundance distribution for elements with $A \gtrsim 100$, where the atomic abundance curve becomes relatively flat. This is discussed further in Sec. VI, and in Sec. XI in connection with the observed overabundances of heavy elements in stars believed to have recently undergone s-process synthesis in their interiors.

Finally, we turn to neutron sources on a very short time-scale, ~ 10 seconds, as in supernovae. A mechanism by which neutrons could arise in the hot envelope of a supernova following core collapse was proposed by Burbidge, Hoyle, Burbidge, Christy, and Fowler (Bu56). This mechanism is thought to occur in four stages:

(i) A collapse of the inner regions of a highly evolved star occurs leading to the conversion of gravitational energy into other forms of energy, particularly in the envelope of the star where it is converted into thermal energy. A possible cause of such a collapse is discussed in detail in Sec. XII. The imploding envelope reaches 2×10^8 degrees as a result of the conversion of gravitational energy into thermal energy. The density rises to $\sim 10^5$ g/cm^3.

(ii) The onset of reactions of the type $C^{12}(p,\gamma)N^{13}$, $O^{16}(p,\gamma)F^{17}$, $Ne^{20}(p,\gamma)Na^{21}$, $Mg^{24}(p,\gamma)Al^{25}$ take place in the outer parts of the star. These occur very rapidly at 2×10^8 degrees. The mean energy production from these reactions may be taken as approximately 2 Mev per proton. With a composition characteristic of a highly evolved star, consisting of approximately equal abundances (by number) of hydrogen, helium, and light nuclei, the energy released in these reactions is sufficient to raise the temperature of the material to a value $\sim 10^9$ degrees as the hydrogen is consumed. If all of the nuclear energy were converted into particle energy, a temperature of 6×10^9 degrees would be attained. This maximum temperature will not be reached, however, because of the conversion of energy into radiation, turbulence, growing magnetic fields and the general expansion of the eventually exploding envelope. However, 10^9 degrees will probably be reached during the initial implosion of the envelope into the region vacated by the collapsing core. A radiation temperature of $\sim 10^9$ degrees will result from the hydrogen consumption if $\rho = 10^5$ g/cm^3.

(iii) At this high temperature, alpha-particle reactions become important, and the crucial neutron-producing reaction is $Ne^{21}(\alpha,n)Mg^{24}$, which follows very rapidly on the 23-second beta decay of Na^{21}. The mean reaction time for Ne^{21} is of the order of 10^{-5} sec if $T \simeq 10^9$ degrees and $\rho \simeq 10^5$ g/cm^3. The (α,n) reactions on C^{13} and O^{17} are not operative under these conditions since N^{13} requires 14 min in the mean to decay to C^{13} and F^{17} requires 100 sec to decay to O^{17}. A series of neutron-producing reactions from combined hydrogen and helium burning on Ne^{20} and heavier nuclei are shown in Fig. III,6. All of the beta decays shown in this diagram are reasonably short. In general (p,γ) reactions compete with positron emission until proton addition is no longer possible and positron emission must occur.

(iv) The neutrons produced in hydrogen and helium burning are rapidly thermalized $(kT \simeq 100$ kev) and then they are captured primarily by the abundant nuclei of the iron group which were initially present in the envelope. We have supposed that their abundances at this stage total about 1% by mass. If the envelope was very underabundant in these elements the neutrons would be captured by the light elements. This rapid neutron capture process, the r process, will be discussed in detail in Secs. VII and VIII. For this discussion we require to know the neutron density. This will now be estimated.

The neutrons become available in the mean lifetime of Na^{21} (33 sec), or Mg^{22} (7 sec) and Al^{26} (10 sec). Thus a reasonable mean time for the neutron production during the imploding high-density stage is about 10

HYDROGEN BURNING ⟶

$Ne^{20}(p,\gamma)Na^{21}(p,\gamma)Mg^{22}(\beta^{+}\nu_{+})Na^{22}(p,\gamma)Mg^{23}(p,\gamma)Al^{24}(\beta^{+}\nu_{+})Mg^{24}(p,\gamma)Al^{25}$

~5 SEC   2.3 SEC

$(\beta^{+}\nu_{+})$ 23 SEC $(\beta^{+}\nu_{+})$ ~5 SEC $(\beta^{+}\nu_{+})$ 12 SEC $(\beta^{+}\nu_{+})$ 7.3 SEC

$Ne^{21}(p,\gamma)Na^{22}$ Na^{23} Mg^{25}

HELIUM BURNING

(α,n) (α,γ) (α,p) (α,n)

$Mg^{24}(p,\gamma)Al^{25}$ Al^{26} Si^{28}

$(\beta^{+}\nu_{+})$ 7.3 SEC $(\beta^{+}\nu_{+})$ 6.5 SEC

Mg^{25} Mg^{26}

(α,n) (α,n)

Si^{28} Si^{29}
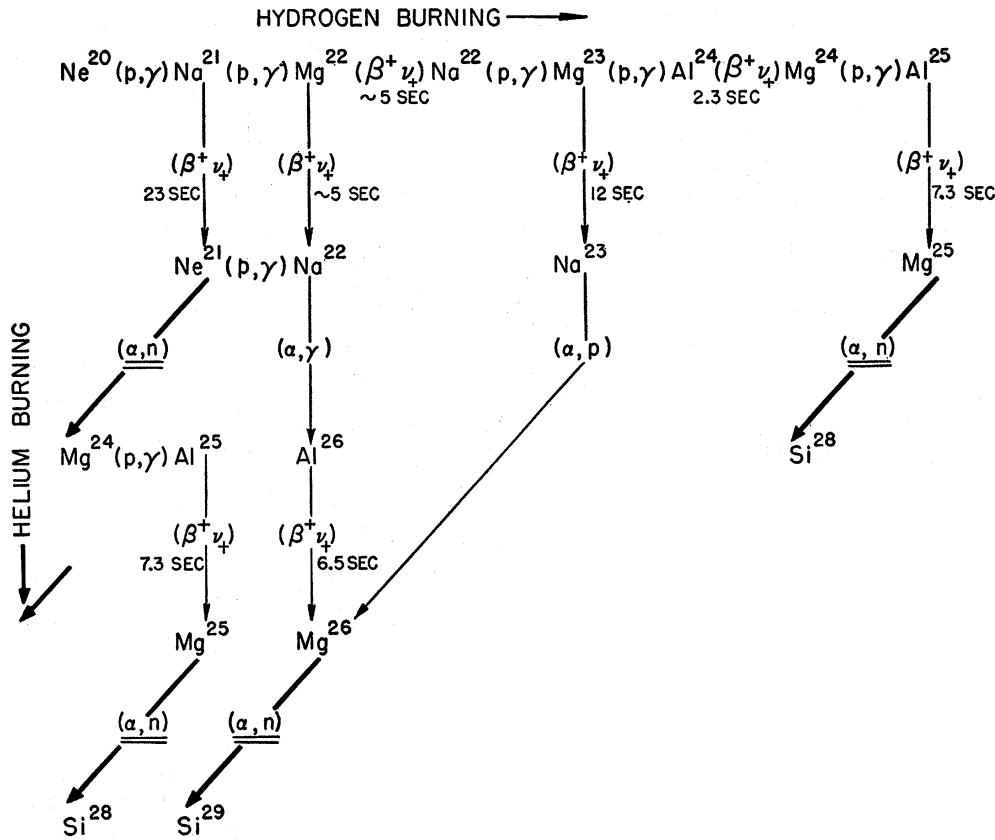
FIG. III,6. Neutron-producing reactions as a result of hydrogen and helium reactions in supernova envelopes. Note that all beta-decay lifetimes are quite short, and that neutrons are produced as long as hydrogen is 1 to 5 times as abundant as Ne²⁰.

sec. There will be one neutron produced for each Ne^{20} nucleus present, and on the assumption that there are approximately equal number densities of hydrogen, helium, and light nuclei, and that perhaps one-third of the light nuclei are together C^{12}, O^{16}, and Ne^{20}, each having equal abundance, the number density of Ne^{20} is $\sim10^{22}\rho$. It has been earlier stated that a reasonable value for $\rho\simeq10^{5}$ g/cm³, during the implosive stage. However, the neutron captures will occur during the later expanding stage when $\rho\simeq100$ g/cm³, so that the neutron density during this stage will be $\sim10^{24}$ neutrons/cm³. We assume that the radiation temperature remains at the high value of $\sim10^{9}$ degrees during the capture process. As we shall see in Sec. VII, this means that captures occur until the neutron binding energy is reduced to ~2 Mev. Further captures must wait until beta emission occurs with lifetimes for the neutron-rich nuclei of about 3 sec. Each beta decay is followed by about 3 captures so that the total time for ~200 captures ($Fe^{56}\rightarrow Cf^{254}$) is ~200 sec. Thus the capture time is long as compared with the total neutron production time and we are justified in assuming that the initial neutron density is that given by the original Ne^{20} density.

To conclude, in our discussion of the r process in supernova envelopes we put the neutron density n_{n} $\simeq10^{24}$/cm³ and the temperature $T\simeq10^{9}$ degrees. The thermal neutron velocity at $kT\simeq100$ kev is approximately 4×10^{8} cm/sec, so that the neutron flux $(nv)_{n}$ $\simeq4\times10^{32}$ neutrons/cm² sec.

In Secs. X and XII brief mention is made of a further possible neutron source in a very highly collapsed stellar core.

(4) Origin of N^{15}, O^{18}, and F^{19}

The concentration of N^{15} given by the CN cycle is far too low, as compared with that of N^{14}, to explain the ratio $N^{15}/N^{14}=1/270$ in the atomic abundance distribution. It is too low by a factor ~100, assuming the very slow rate for $N^{14}(p,\gamma)O^{15}$, discussed above in Sec. III F (1). Hence it appears that N^{15} must be produced by reactions other than those of the normal CN cycle. Let us consider the reaction $C^{13}(\alpha,n)O^{16}$, occurring in the presence of N^{14}, derived previously from the CN cycle, and also in the presence of a strong excess of C^{12} derived from helium burning. This requires mixing of material in a helium-burning core. Protons liberated by $N^{14}(n,p)C^{14}$ are, in the main, converted back to neutrons by the reactions C^{12}-$(p,\gamma)N^{13}(\beta^{+}\nu_{+})C^{13}$ and $C^{13}(\alpha,n)O^{16}$, since the C^{12}, in excess over its CN cycle abundance, will capture most of the protons. Nor are neutrons lost by the reaction $C^{12}(n,\gamma)C^{13}$, again because of the occurrence of the reaction $C^{13}(\alpha,n)O^{16}$. Thus the neutrons tend to cycle,

either through $N^{14}(n,p)C^{14}$, or through $C^{12}(n,\gamma)C^{13}$, the latter reaction being important because of the excess of C^{12}.

Neutrons are eventually lost, however, through capture in reactions with smaller probability. Important among these is $N^{14}(n,\gamma)N^{15}$. If the C^{12} excess is great enough for all protons, released by $N^{14}(n,p)C^{14}$, to be absorbed in $C^{12}(p,\gamma)N^{13}$, the ultimate result is to produce an N^{15} concentration comparable with that of the original C^{13} concentration. Since $C^{13}/N^{14}=1/168$, this implies the possibility of $N^{15}/N^{14}\sim1/168$. As noted above, the isotopic ratio is $N^{15}/N^{14}=1/270$. It appears, therefore, that the present process, dependent on an excess of C^{12} becoming mixed with the products of the CN cycle in helium burning, is capable of providing for the origin of N^{15}.

At somewhat higher temperatures than are required to promote the above reactions, F^{19} is then produced by $N^{15}(\alpha,\gamma)F^{19}$. At the same time O^{18} is produced by $N^{14}(\alpha,\gamma)F^{18}(\beta^{+}\nu_{+})O^{18}$. It would then follow that $F^{19}/O^{18}\sim N^{15}/N^{14}$. This is the case within a factor of 10.

To conclude, detailed mechanisms have been advanced for the production of the nuclei C^{12}, C^{13}, N^{14}, N^{15}, O^{16}, O^{17}, O^{18}, Fe^{19}, Ne^{20}, Ne^{21}, Ne^{22}, Na^{23} in combination hydrogen-helium-burning in stars. These mechanisms are illustrated graphically in Fig. I,2.

IV. e PROCESS

At temperatures above $\sim3\times10^{9}$ degrees all manner of nuclear processes occur in great profusion, i.e., (γ,α), (γ,p), (γ,n), (α,γ), (p,γ), (n,γ), (p,n) reactions as well as others involving heavier nuclei. Such reactions allow the conversion of a nucleus A, Z to a nucleus A', Z', even in cases in which Z and Z' are large; i.e., even though considerable Coulomb barriers may be involved in the conversion. This is the physical condition for statistical balancing to occur among the nuclei. In previous papers (Ho46, Ho54), it was shown that the abundances of the elements in the iron peak could be synthesized under conditions of temperature and density such that statistical equilibrium between the nuclei and the free protons and neutrons was achieved. In this section this question is re-examined using the more accurate nuclear and abundance data now available, and taking into account the appropriate excited nuclear states, the energies and spins for which are available now from the work of Way, King, McGinnis, and Lieshout (Wa55a).

Under conditions of statistical equilibrium the number density $n(A,Z)$ of the nucleus A, Z is given by

$$n(A,Z)=\omega(A,Z)\left[\frac{AMkT}{2\pi\hbar^{2}}\right]^{\frac{3}{2}}\frac{(n_{n})^{A-Z}(n_{p})^{Z}}{2^{A}}$$

$$\times\left[\frac{2\pi\hbar^{2}}{MkT}\right]^{3A/2}\exp\frac{Q(A,Z)}{kT}, \quad (1)$$

where n_{n}, n_{p} are the number densities of free neutrons and protons, M is the atomic mass unit, and $\omega(A,Z)$

is the statistical weight factor given by

$$\omega(A,Z)=\sum_{r}(2I_{r}+1)\exp(-E_{r}/kT),$$

where E_{r} is the energy of the excited state measured above the ground level, and I_{r} is the spin. $Q(A,Z)$ is the binding of the ground level of the nucleus A, Z, and is given by

$$Q(A,Z)=c^{2}[(A-Z)M_{n}+ZM_{p}-M(A,Z)],$$

where M_{n}, M_{p}, and $M(A,Z)$ are the masses of the free neutron, free proton, and nucleus A, Z, respectively. Writing $\theta=\log(n_{p}/n_{n})$, and measuring T in units of 10^{9} degrees (T_{9}), (1) can be expressed in the form

$$\log n(A,Z)=\log\omega(A,Z)+33.77$$
$$+\tfrac{3}{2}\log(AT_{9})+\frac{5.04}{T}Q(A,Z)$$
$$+A(\log n_{n}-34.07-\tfrac{3}{2}\log T_{9})+Z\theta. \quad (2)$$

This is the form given by Hoyle (Ho46) except that formerly the approximation was made of putting $\omega(A,Z)=2$, and a slight numerical change of 0.01 in the numerical term in the right-hand side of the equation has been made. Logarithms are to the base 10. The nuclear data required to calculate $Q(A,Z)$, $\omega(A,Z)$ are available, so that explicit values of $n(A,Z)$ for various A, Z can be worked out if n_{n}, θ, T_{9} are specified. Thus it might seem, at first sight, as if abundances of the nuclei under statistical equilibrium are functions of three independent parameters. This is not the case, however. Two parameters are sufficient to determine the system. This can be understood best from taking ρ, the density, and T_{9} as the independent parameters, although we shall see later that θ, T_{9} give a more convenient choice of parameters from an arithmetical point of view. If ρ is given, the abundances calculated from the above equation must satisfy the condition

$$\sum M(A,Z)n(A,Z)+\sum M_{p}n_{p}+\sum M_{n}n_{n}=\rho, \quad (3)$$

the contribution of the electrons present in the system being neglected. The contribution of the free protons and free neutrons is also negligible for the values of ρ, T_{9} used below, although values of ρ, T_{9} could be chosen for which this would not be so. Equation (3) can be interpreted in a number of ways, for instance as determining $\log n_{n}$ in terms of ρ, T_{9}, θ. A second condition determining θ in terms ρ, T_{9}, arises in one or other of two alternative ways. If the time-scale is long enough, equilibrium between protons and neutrons is established through the operation of beta processes among the nuclei. This equilibrium is expressed by the equations

$$\frac{n_{n}}{n_{p}}=10^{-\theta}=\frac{n_{e}}{2}\left(\frac{2\pi\hbar^{2}}{m_{e}kT}\right)^{\frac{3}{2}}\exp(Q_{0}/kT),$$

$$n_{e}=\sum_{A,Z}Zn(A,Z)+n_{p}, \quad\quad\Bigg\} \quad (4)$$

$$Q_{0}=c^{2}(M_{p}+m_{e}-M_{n})=-0.78\text{ Mev},$$

m_e being the electron mass, and n_e the electron number density.

If, on the other hand, the time-scale is not long enough to establish equilibrium between neutrons and protons, then (4) must be replaced by the condition that the ratio of the number of neutrons per unit volume (bound and free together), to the number of protons per unit volume must be a specified constant with a value determined by the initial state of the material. That is to say

$$\sum_{Z,A} (A-Z)n(A,Z)+n_n= \text{(specified constant)}$$
$$\times [\sum_{Z,A} Zn(A,Z)+n_p]. \quad (5)$$

Before proceeding to a numerical discussion of the above scheme of equations it is desirable to relate them very briefly to astrophysical considerations, particularly to the temperature evolution and time-scales shown schematically in Fig. II,4. So long as the time-scale is longer than a few months (4) are applicable, but in the final rise of temperature to the explosion point shown in Fig. II,4, and during the cooling that follows explosion, the time-scale is far too short to admit of the use of (4). During these phases (5) must be employed. An examination of (5) has shown that it requires θ to stay nearly constant at a value determined by the constant that appears on the right-hand side of the equation. This constant is in turn determined by the values of $n(A,Z)$, n_p, n_n that are operative at the last moment of applicability of (4).

We can now give a description of the physical and mathematical conditions that determine the abundances of the nuclei of the iron peak. Astrophysical reasons, discussed in Sec. XII, require a temperature evolution of the form shown in Fig. II,4 to take place in certain types of star. As previously pointed out, when T rises above about 3×10^9 degrees the statistical equations become applicable. So long as the time-scale is long enough, beta processes establish the equilibrium that satisfies (4). The decay of Mn^{56} with a half-life of 2.58 hours is important in this connection, as also is Co^{57} with a half-life of 267 days. The Co^{57} turns out to be a fairly abundant nucleus and its decay has the effect of changing protons to neutrons. The Mn^{56}, on the other hand, changes neutrons to protons. The time-scale for an appreciable interchange between neutrons and protons, or vice versa, turns out to be of the order of months. This time is determined by two considerations, the half-lives of the beta-decaying nuclei and their abundances. In the case of Co^{57} the lifetime is long but the abundance fairly high, as has been mentioned. In the case of Mn^{56} the lifetime is short but the abundance comparatively low. For the values of ρ, T of interest in the present section the free neutron density n_n is too low for free neutron decay to be of much importance in establishing (4).

Reference to Fig. II,4 shows that the time-scale

becomes too short to maintain (4) as the explosion point is approached. Equation (5) must then be used, the constant on the right-hand side being obtained by the values of $n(A,Z)$, n_p, n_n that are operative in (4) at the time that we switch from (4) to (5). This statement implies a discontinuous transition between (4) and (5). A rigorous treatment would provide for a continuous transition so that in this sense the present arguments are approximate. Throughout the remaining evolution to the explosion point, and in the subsequent cooling, θ remains approximately constant. The basic reason for this is that although complete equilibrium between prompt nuclear reactions is obtained the neutron-proton ratio is determined by the beta-decay rates and the majority of these decays no longer have time to take place. The question now arises as to what this constant value of θ should be. The values of $n(A,Z)$, n_p, n_n at the time (4) ceases to be operative would be sufficient to determine θ, in addition to determining the constant on the right-hand side of (5). The values of $n(A,Z)$, n_p, n_n in question are in turn determined by the values of ρ, T_9 that are operative at the stage at which (4) ceases to hold good. Thus if these values of ρ, T_9 were known, θ could be calculated. Unfortunately the relevant values of ρ and T_9 are not known a priori. Only accurate quantitative calculations of stellar evolution can provide this information, and such calculations have not yet been made.

Our method of solution has been to carry out a series of abundance calculations for a network of values of θ and T_9 and to obtain the values of θ and T_9 which give the best fit to the observed relative abundances. To do this it is convenient to determine the abundances of all of the isotopes relative to Fe^{56}, which is shown later to be the most abundant nucleus. The equation for Fe^{56} is obtained by substituting $A=56$, $Z=26$ in (2); equations for the abundances of the other isotopes relative to Fe^{56} are then obtained by eliminating n_n between the equation for Fe^{56} and the general equation (2). We then obtain

$$\log\frac{n(A,Z)}{n(56,26)} = \frac{A-56}{56}\left\{\log\frac{n(56,26)}{\omega(56,26)} - 33.77\right.$$

$$\left. -\tfrac{3}{2}\log T_9 - \tfrac{3}{2}\log 56\right\}$$

$$+\frac{5.04}{T_9}\left\{Q(A,Z) - \frac{A}{56}Q(56,26)\right\}$$

$$+\log\frac{\omega(A,Z)}{\omega(56,26)} + \theta\left(Z - \frac{26}{56}A\right)$$

$$+\frac{3}{2}\log\frac{A}{56}. \quad (6)$$

A considerable simplification can now be effected at the expense of only a slight approximation. This rests on two points, first that $A=56$, $Z=26$ is the most abundant nucleus, and second that the application of (6) is confined to values of A not very different from 56, since nuclei with appreciably different A turn out to possess only negligible abundances; the exception to this is obtained when $A=4$, $Z=2$, so that the present approximation cannot be made if it is desired to work out the He⁴ abundance. In this approximation $A/56$ is close to unity and the last term on the right-hand side of (6) may be neglected. More important, the quantity $(A-56)/56$ is small compared to unity, a circumstance that enables us to approximate to the factor that multiplies $(A-56)/56$. For values of ρ between 10^4 g/cm³ and 10^9 g/cm³, which covers the range of density of present interest, we write

$$\frac{A-56}{56}\left\{\log\frac{n(56,26)}{\omega(56,26)}-33.77-\tfrac{3}{2}\log T_9-\tfrac{3}{2}\log 56\right\}$$

$$\simeq 0.183(56-A).$$

The coefficient 0.183 is strictly correct for $T_9=3$, $\rho=2\times10^5$ g/cm³, but a change to $\rho=10^7$ g/cm³ only alters the coefficient to 0.153. This approximate term is in any case of comparatively minor importance in its effect on the value of $\log n(A,Z)$. We now have

$$\log\frac{n(A,Z)}{n(56,26)}=0.183(56-A)$$

$$+\frac{5.04}{T_9}\left[Q(A,Z)-\frac{A}{56}Q(56,26)\right]$$

$$+\log\frac{\omega(A,Z)}{\omega(56,26)}+\theta(Z-0.464A). \quad (7)$$

Reference to Fig. II,4 shows that the temperature increases up to the explosion point and cools thereafter. Through the increase of temperature the equilibrium abundances will change in accordance with (7). The abundances will also change during the early part of the cooling. But eventually the temperature will fall so low that the nuclear reactions slow up and the isotopes become "frozen." Freezing occurs when (γ,α), (γ,n), and (γ,p) reactions become insufficient to provide a ready supply of alpha particles and free neutrons and protons. Because the thresholds for these reactions differ from one nucleus to another, freezing will not occur simultaneously for all nuclei, and so it will occur over a range of temperature. Thus the particular value of the temperature that we find to give the best fit to the observed abundances should be interpreted as the *mean freezing temperature*.

Calculations of relative abundances have been carried out for values of T ranging from 2.52×10^9
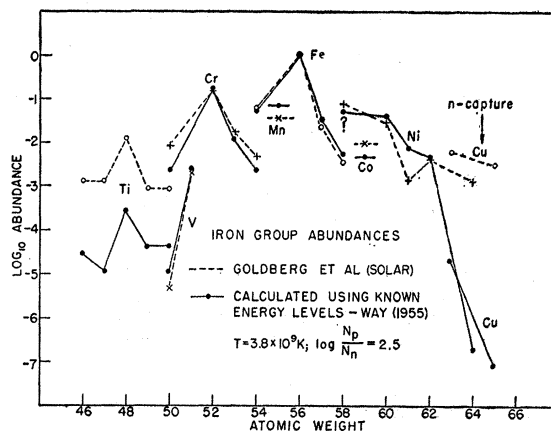
FIG. IV,1. Logarithmic abundance curve for the iron group isotopes relative to the abundance of Fe⁵⁶. The points connected by dashed lines are the solar abundances determined by Goldberg *et al.* (Go57) using terrestrial isotope ratios to calculate isotope abundances. The points connected by solid lines are calculated from equilibrium theory using partition functions calculated from the energy level data of Way *et al.* (Wa55a) and using a temperature of 3.8×10^9 degrees and a ratio of protons to neutrons equal to ~300.

degrees to 7.56×10^9 degrees, and values of θ of 1.5, 2.5, and 3.5. The binding energies $Q(A,Z)$ have been obtained from the tables of Wapstra and Huizenga (Wa55, Hu55), and the weight factors $\omega(A,Z)$ have been estimated from the level diagrams of Way *et al.* (Wa55a). In one case, that of Ni⁵⁸, an additional binding of 0.84 Mev over that given by Wapstra and Huizenga has been used to bring the Q into agreement with the mass-spectrometer value.

The best fit is obtained for $T=3.78\times10^9$ degrees and $\theta=2.5$. This value of θ corresponds to a density of the order of 10^5 g/cc. Results of this calculation are shown in Table IV,1 and in Fig. IV,1. To determine the final abundances of the stable isotopes the last reactions, i.e., the freezing reactions, have to be taken into account, together with the beta processes which take place after the freezing reactions have occurred. These reactions are given in column 4 of Table IV,1. The particular freezing reactions which we have taken into account are V⁴⁹(γ,p), Mn⁵³(γ,p), Co⁵⁷(γ,p), and Cu⁶³(γ,p), all of which have fairly low thresholds of 6–7 Mev and which will freeze at a lower temperature than the (γ,α) and (γ,n) reactions. We have arbitrarily supposed that in these cases half of each of these isotopes have gone to Ti⁴⁸, Cr⁵², Fe⁵⁶, and Ni⁶², respectively. In columns 6 and 7 of the table and in Fig. IV,1, these calculated abundances relative to Fe⁵⁶ have been compared with the solar element abundances given by Goldberg *et al.* (Go57) taken together with the well-known isotopic abundances. For $50\leq A\leq62$ the fit is very good indeed, the standard deviation between calculated and observed values being 0.3 in the logarithm in this region. The binding energies are in general uncertain to within 0.2 Mev, and this uncertainty is sufficient to introduce deviations of the same order as those found.

TABLE IV,1. Comparison between $\log_{10}$ observed and calculated abundances in the iron peak (relative to Fe^{56}); $T=3.78\times10^9$ degrees, $\log_{10}n_p/n_n=2.5$.

	Z	A	Equilibrium abundance	Freezing reactions	Final calculated	Observed solar	Observed − calculated
Ti	22	46	−4.53		−4.54	−2.88	+1.66
		47	−4.95		−4.96	−2.89	+2.07
		48	−3.61	$V^{49}(\gamma,p)$	−3.56	−1.92	+1.64
		49	−5.06	$V^{49}(\beta^+)$	−4.37	−3.04	+1.33
		50	−4.36		−4.37	−3.06	+1.31
V	23	50	−4.96		−4.97	−5.31	−0.34
		51	−3.14	$Cr^{51}(\beta^+)$	−2.62	−2.71	−0.09
Cr	24	50	−2.64		−2.65	−2.09	+0.56
		52	−0.80	$Mn^{53}(\gamma,p)$	−0.78	−0.82	−0.04
		53	−2.60	$Mn^{53}(\beta^+)$	−1.93	−1.76	+0.17
		54	−3.30	$Mn^{54}(\beta^+)$	−2.64	−2.32	+0.32
Mn	25	55	−2.06	$Fe^{55}(\beta^+)$	−1.16	−1.44	−0.28
Fe	26	54	−1.26		−1.27	−1.21	+0.06
		56	0	$Co^{57}(\gamma,p)$	0	0	STAN.
		57	−1.94	$Co^{57}(\beta^+)$	−1.49	−1.63	−0.14
		58	−2.36	$Co^{58}(\beta^+)$	−2.27	−2.46	−0.19
Co	27	59	−2.62	$Ni^{59}(\beta^+)$	−2.33	−2.00	+0.33
Ni	28	58	−2.42		−1.31	−1.11	+0.20
		60	−1.35		−1.36	−1.52	−0.16
		61	−2.11		−2.12	−2.85	−0.73
		62	−2.34	$Cu^{63}(\gamma,p)$	−2.35	−2.38	−0.03
		64	−6.86	$Cu^{64}(\beta^+)$	−6.70	−2.88	+3.82
Cu	29	63	−4.36	minus $Cu^{63}(\gamma,p)$	−4.67	−2.17	+2.50
		65	−7.06		−7.07	−2.51	+4.54

A similar uncertainty is also present because of our assumption of a unique freezing temperature.

For $A<50$ and $A>62$ there are gross discrepancies between observed and calculated values and because of these we conclude that other modes of synthesis are demanded for these isotopes. Beyond $A=62$, the nuclei Ni^{64}, Cu^{63}, and Cu^{65} have all been assigned in the appendix to the s process and in Sec. VI and in Fig. VI,3, it will be seen that the (σN) products for Cu^{63}, Ni^{64}, Zn^{64}, and Cu^{65} are all comparable $(\sigma N\sim10^4)$ as is expected in the first part of the s-process chain which runs from $63\leq A\leq209$. The σN product would not be expected to be constant if these nuclei had been synthesized by the equilibrium process. Below $A=50$, the titanium isotopes have been assigned as follows: Ti^{46} to the s process, Ti^{48} to the α process, and Ti^{47}, Ti^{49}, Ti^{50} probably to the r process. In this region of A, $46\leq A \leq50$, where the s, α, e, and r processes all intersect, details of the exact contributions from each process are not easy to determine. In particular, the r-process calculations in this region are very approximate (cf. Sec. VII).

V. s AND r PROCESSES: GENERAL CONSIDERATIONS

The eventual aim is to compare calculated abundances with observed abundances both for the s and the r processes. Our method of assignment to these processes is described in Sec. II. Before we describe in detail the ways in which the two processes can be handled, it is necessary to digress in order (i) to review briefly the reasons from the standpoint of nuclear stability why all three processes, the s, the r, and the p, are demanded, and (ii) to describe our neutron capture cross sections, σ, which are given in the appendix and are demanded in the discussion of the s process alone.

A. "Shielded" and "Shielding" Isobars and the s, r, p Processes

Let us consider nuclei of the same A but different Z. In Fig. V,1 we show the well-known schematic plot of the stability of such nuclei as a function of Z. In this diagram, Z_A is the charge of the most stable isobar at a given A as given by the smooth Weizsäcker mass law (We35). It can occur near an odd or even integral value of Z. The coefficient in the quadratic dependence of the mass $M(A,Z)$ on $(Z-Z_A)^2$ is $B_A/2$. For odd A (top diagram) there is only one parabola and the nucleus with charge Z closest to Z_A is the stable isobar. Those with smaller Z are electron-antineutrino emitters, while those with greater Z capture electrons and emit neutrinos or emit a positron with a neutrino. In a few cases two nuclei near the bottom of the parabola will apparently be stable, one with a very long but detectable half-life or with too long a half-life to be measured. Rb^{87} is an example of this type; it decays to Sr^{87} with a half-life of 4.3×10^{10} years. An odd-A nucleus produced in neutron capture will always decay eventually to the most stable isobar.

For even A there are two mass parabolas. Those nuclei that have odd Z, odd N $(=A-Z)$ lie on a parabola separated from that for nuclei with even Z, even N by the pairing energy, δ_A. As shown in the two bottom

diagrams, one, two, or three nuclei can be stable, depending on the ratio of δ_A to B_A. Double beta decay is possible for all but the most stable, but this is a very slow process with half-life $>10^{18}$ years. An example of cases where there are three stable isobars is given by Sn^{124}, Te^{124}, and Xe^{124}. On the other hand, there is only one stable nucleus for each even A for $A \leq 34$ and two stable nuclei for $36 \leq A \leq 76$. For $A \geq 78$ there may be two or three stable nuclei for each value of A. In a neutron-capture process at a rate rapid compared to negative beta decay (the r process), the nuclei produced lie far up the left-hand side of the parabolas shown. At the termination of the process β^- decay leads to the stable isobar with smallest Z. This is the *shielding* isobar, and the other one or two stable isobars with the same A are said to be *shielded*. In a neutron-capture process at a rate slow compared to negative beta decay (the s process), the isobar on the left is sometimes produced, that in the middle is sometimes produced, but never the isobar on the right. Those not produced are said to be *by-passed* in the s process. It is to produce the isobar on the right, that having the greatest value of Z, that a third process, the p process involving the addition of protons on already existing heavy nuclei, is demanded. Details of this process are described in Sec. IX.

B. Neutron-Capture Cross Sections

In the third column of the appendix we give either the neutron-capture cross sections or, in the case of unstable nuclei, the half-lives against beta decay. The cross sections (σ) which are given in millibarns (10^{-27} cm^2) are mostly cross sections for neutron capture with emission of gamma radiation (n,γ). For small A a few cross sections for other reactions initiated by neutrons, in which there is no increase in A [(n,p) reactions] or a decrease in A [(n,α) reactions], are given. All of the values are for a neutron energy of 15 kev which is reasonable if the s process is taking place in the interiors of red-giant stars at $T = 1 - 2 \times 10^8$ degrees. To obtain the cross sections several sources were used:

(i) Many of the σ's for the lighter nuclei have been obtained from the Brookhaven tables (Hu55a). Others have been obtained from the thermal cross sections (1/40 ev) by extrapolation, using a 1/v law, where this law is thought to apply (designated 0.1% of thermal in the appendix). Where σ does not drop as rapidly as 1/v in the kilovolt region we have taken 1% of thermal (designated this way in the appendix) to be a reasonably accurate value. In a few cases the σ's have been marked extr. meaning extrapolated from nearby experimental values, or exp. meaning experimentally measured.

(ii) The majority of the remaining σ's have been obtained from the pile reactivity measurements made by Snyder *et al.* (Sn55), in which reactivity changes due to different materials are measured. Since the reactivity measure is given in units of cents per mole, normaliza-
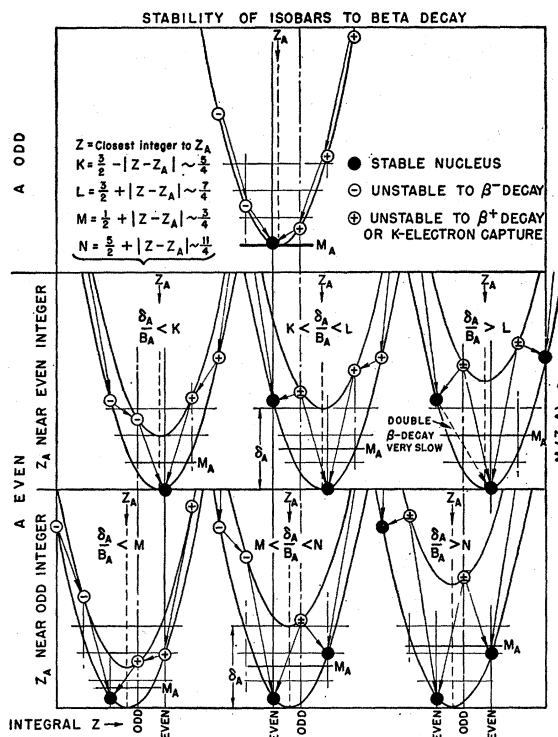
FIG. V,1. The stability of nuclear isobars to beta decay. Z_A is the charge of the most stable isobar at a given A as given by the smooth Weizäcker mass law (We35). It can occur near an odd or even integral value of Z. The coefficient in the quadratic dependence of $M(Z,A)$ on $(Z-Z_A)^2$ is $B_A/2$. For odd A (top diagram) there is only one parabola and the nucleus with charge Z closest to Z_A is the stable isobar. Those with smaller Z are electron-antineutrino emitters while those with greater Z capture electrons and emit neutrinos or emit a positron with a neutrino. In a few cases two nuclei near the bottom of the parabola will apparently be stable, one with a half-life too long to be measured. An odd A nucleus produced in neutron capture will decay eventually to the most stable isobar.

For even A there are two mass parabolas, those nuclei with odd Z, odd N lying on a parabola separated from that for even Z, even N nuclei by the pairing energy δ_A. As can be seen from the two bottom diagrams one, two, or three nuclei can be stable depending on the ratio of δ_A to B_A. Double beta decay is possible for all but the most stable, but this is a very slow process with half-life $> 10^{18}$ years. In a neutron-capture process at a rapid rate (r process) compared with negative beta decay the nuclei produced lie far up the left-hand side of the parabolas shown. At the termination of the process the negative beta decay leads to the stable isobar with smallest Z. This is the *shielding* isobar and the other one or two are said to be *shielded*. In a neutron-capture process at a slow rate (s process) compared with negative beta decay, the isobar on the left is sometimes produced, that in the middle is sometimes produced, but the isobar on the right is never produced. Those not produced are said to be *by-passed* in the s process.

tion has been carried out by using the $B^{10}(n,\alpha)$ reaction which has a cross section of 1 barn at 15 kev. No reactivity measures have been given for isotopes with $Z < 17$, and so we have made a reasonable extrapolation of the reactivity curves of Snyder *et al.* using the independently measured cross section for Al^{27} of 5.2 mb. The normalization by means of the $B^{10}(n,\alpha)$ reaction for isotopes with $Z > 17$ has been carried out by putting

1 barn equal to 24 cents per mole for nonmagic isotopes with odd A, the original normalization of Snyder *et al.*, and 1 barn equal to 8 cents per mole for the even A and the nuclei with closed neutron shells. This latter renormalization has been carried out after comparison of the cross sections obtained from the reactivity measurements with experimental activation measurements for a neutron energy of "25 kev" made at Oak Ridge (La57b) and at Livermore (Bo57). These latter cross sections are shown in Table VI,1, and they are discussed further in Sec. VI when the σN products are considered. In the appendix the cross sections of both even and odd isotopes with closed neutron shells were increased over the original estimates, using the original normalization of Snyder *et al.*, in order to avoid making the even A cross sections exceed the odd A cross sections at these magic-neutron numbers. A further effect which must arise and which cannot presently be estimated from the reactivity measures is the variation in σ within isotopes of even A. This variation must be in the sense that the lightest isotopes will tend to have larger cross sections

than the heavier ones. Trends such as these, which may affect the run of the σN products, are discussed further in Sec. VI.

The reason for differentiating between σ's for odd and even A instead of differentiating between nuclei with odd and even numbers of neutrons is the following. The results of Hurwitz and Bethe (Hu51) show that neutron capture occurs through a compound nuclear state whose effective excitation should be measured without regard for special pairing effects in the ground state of this nucleus. Thus only odd-even effects in the ground state of the target nucleus are relevant. The even A-even Z-even N target nuclei capture neutrons with less excitation and thus smaller σ's than the odd A target nuclei. In particular, the value of σ for odd A nuclei is the same for the odd Z-even N case as for the even Z-odd N case. Snyder *et al.*, have taken this effect into account, and in fact their plotted curves give a large odd-even effect. The difference between the normalizations that we have used for odd and even A is in order to *diminish* the odd-even effect
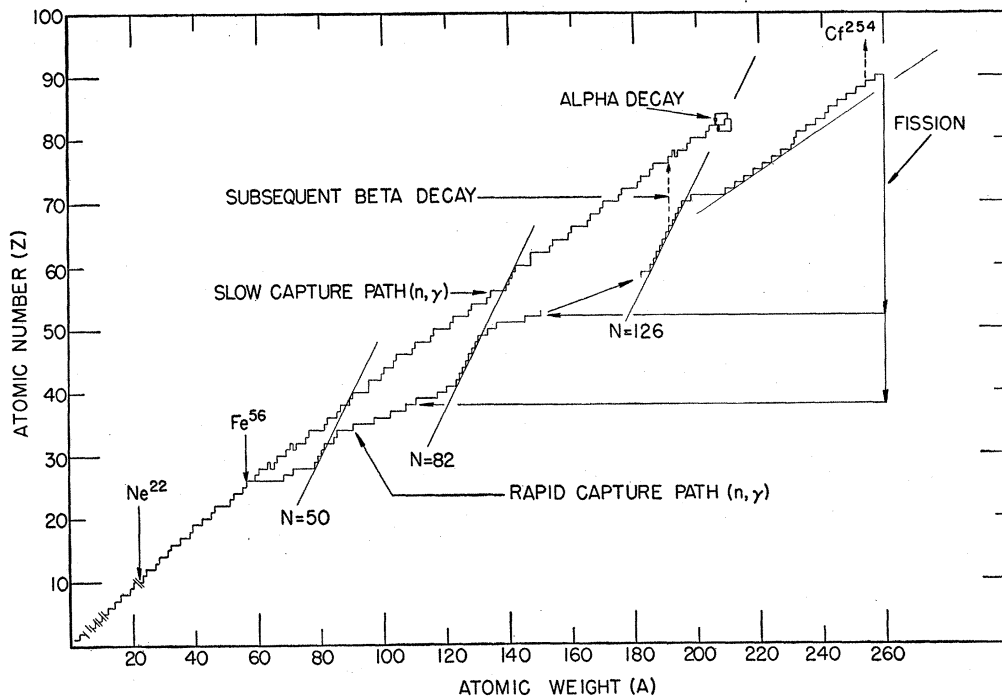
FIG. V,2. The neutron capture paths of the s process and the r process. Ne^{22}, as a typical light nucleus, and Fe^{56} as the most abundant member of the iron group are indicated as "seed" nuclei at which synthesis begins. The capture path of the s process (slow compared with β^- decay) wanders along the stability line in the Z, A plane and finally terminates in alpha decay above bismuth. The r process (rapid compared to β^- decay) is caused by an intense neutron flux which drives the nuclear matter to the neutron-rich side of the stability line. For a temperature of 10^9 degrees the nuclei add neutrons until the neutron binding energy decreases to 2 Mev. At these "waiting points" β decay must occur before further neutrons can be added. Note the "staircase" effects at neutron magic numbers, N, which is due to the difficulty, at this point, of adding the $(N+1)$th neutron. When the path thus moves closer to the stability line the β^- decay lifetime at the waiting points increases and the material builds to an excess abundance. Thus this effect at $N=50$, 82, 126 leads to relatively sharp peaks in the abundance curve. These peaks occur with a smaller Z and A (proton-poor) than is associated with the stable nuclei with magic N and they are thus displaced 6 to 10 units in A below the magic peaks produced in the s process. The r process path is terminated by neutron-induced fission at $A \sim 260$ and the nuclear matter is fed back into the process at $A \sim 108$ and $A \sim 146$. Thus cycling and true steady flow occurs above $A \sim 108$.

given by their curves, because we are dealing with neutrons of higher energy than they were using (15 kev instead of $\lesssim 1$ kev).

(iii) For the few cross sections for which estimates are not available either from the thermal measurements or the reactivity measurements, we have interpolated from a smooth curve through the reactivity measurements for $A > 40$ and the thermal measurements for $A < 20$. In this interpolation we have maintained a ratio of ~ 3 for $\sigma(\text{odd } A)/\sigma(\text{even } A)$ with a minimum at the isotopes with a magic number of 14 neutrons.

C. General Dynamics of the s and r Processes

In the buildup of nuclei by the s and the r processes the reactions which govern both the rate of flow and the track followed in the (A,Z) plane are the (n,γ) and (γ,n) reactions, beta decay, and, at the ends of the tracks, alpha decay in the case of the s process and neutron-induced fission in the case of the r process. We denote the rates of the (n,γ), (γ,n) and beta process as λ_n, λ_γ, λ_β, where

$$\lambda_n = 1/\tau_n = \sigma_n v_n n_n,$$
$$\lambda_\beta = 1/\tau_\beta = \text{const}/W_\beta{}^5, \qquad (8)$$
$$\lambda_\gamma = 1/\tau_\gamma = \sigma_\gamma c n_\gamma,$$

and σ_n and σ_γ are the cross sections for the (n,γ) and (γ,n) reactions, respectively; v_n and n_n are the velocity and density of neutrons responsible for the (n,γ) reactions; n_γ is the density of γ radiation; and W_β is the beta-decay energy.

The general equation for the buildup of nuclei in the s-process is then

$$dn(A,Z)/dt = \lambda_n(A-1, Z)n(A-1, Z) - \lambda_n(A,Z)n(A,Z)$$
$$+ \lambda_\beta(A, Z-1)n(A, Z-1) - \lambda_\beta(A,Z)n(A,Z)$$
$$+ \text{termination terms due to alpha}$$
$$\text{decay at } A > 209. \quad (9)$$

The general equation for the r process is

$$dn(A,Z)/dt = \lambda_n(A-1, Z)n(A-1, Z) - \lambda_n(A,Z)n(A,Z)$$
$$+ \lambda_\beta(A, Z-1)n(A, Z-1) - \lambda_\beta(A,Z)n(A,Z)$$
$$+ \lambda_\gamma(A+1, Z)n(A+1, Z) - \lambda_\gamma(A,Z)n(A,Z)$$
$$+ \text{termination terms due to fission}$$
$$\text{for } A \gtrsim 260. \quad (10)$$

For the s process, we have, in general,

$$\lambda_n < \lambda_\beta(\tau_n > \tau_\beta).$$

For the r process, we have

$$\lambda_n > \lambda_\beta(\tau_n < \tau_\beta).$$

As long as $\lambda_n > \lambda_\beta$ buildup continues with Z constant and λ_n continuously decreases until $\lambda_n(A,Z) \approx \lambda_\gamma(A+1, Z)$. At this point no further buildup can take place until
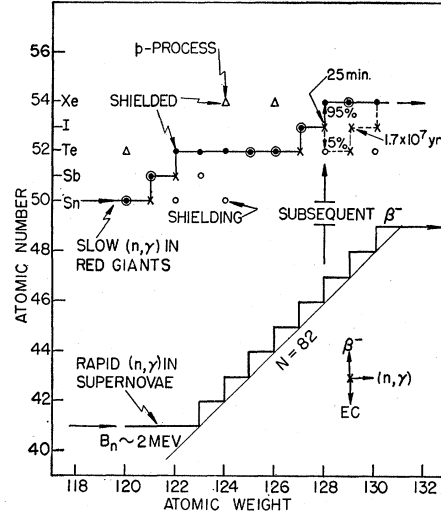
FIG. V,3. Detail of Fig. V,2 showing the s-process and r-process paths from $A = 120$ to 130. Note that the s process builds through one stable isobar, except when branching in the beta decay occurs as at $A = 128$. The nuclei not built are said to be *by-passed*. In the r process the capture path involves those neutron-rich nuclei with binding energy ~ 2 Mev. The path runs parallel to the stability line except at a magic number such as $N = 82$, when it turns toward the stability line producing waiting points with greater β^- lifetimes. The subsequent β^- decay in the freezing of the r process produces only the *shielding* and not the *shielded* isobars. It will be clear from the diagram that certain nuclei are not produced in either the s or r processes. These are very rare in abundance as might be expected, and are produced by a secondary process, the p process, which is described in Sec. IX.

beta decay occurs, thereby increasing Z. The effective rate of neutron addition at this point is such that

$$[\lambda_n(A,Z) - \lambda_\gamma(A+1, Z)] < \lambda_\beta(A,Z).$$

The tracks of both the s and the r processes in the (A,Z) plane are shown in Figs. V,2 and V,3, and were obtained by methods described in the following sections.

VI. DETAILS OF THE s PROCESS

Excluding the alpha-decay terms, and remembering that $\lambda_n < \lambda_\beta$, so that the beta decay takes place in a time short compared with neutron capture, we have from (9)

$$\frac{dn(A)}{dt} = \lambda_n(A-1)n(A-1) - \lambda_n(A)n(A). \quad (11)$$

The large λ_β terms in (9) serve only to produce the most stable Z at each A. Equations (11) determine for the synthesis of the s-process nuclei as a function of time. In order to use this type of equation for calculation it is convenient to use the capture cross sections $\sigma(A,Z)$ and to use, instead of t, the number of neutrons injected per standard nucleus, since this is a number which can be calculated from the abundances of the nuclei in the neutron-producing reactions. Thus Eqs.

(11) can be rewritten (Fo55),

$$\frac{dn(A)}{dn_c} = \frac{\sigma(A-1)n(A-1) - \sigma(A)n(A)}{\sum_A \sigma(A)n(A)}, \quad (12)$$

where n_c is the number of neutrons captured.

The properties of these equations can be thought of in terms of a hydrodynamical analogy. Consider a river bed with a number of depressions in it, each depression corresponding to a value of A, and proportional in its volume to σ^{-1}. Suppose that water starts at A_i and flows in the direction of increasing A. Water does not reach (A_i+2) until the depression at (A_i+1) has been filled. Similarly, water does not reach (A_i+3) until the depression at (A_i+2) is filled. Moreover, if there is a final reservoir at A_f, water only reaches A_f when all of the depressions are filled. Thereafter there is steady flow, water going from A_i to A_f without change at intermediate points. This analogy is not complete since in the hydrodynamic case there is no flow at all beyond

FIG. VI,1. Plot of the abundances of the isotopes times their neutron-capture cross sections (σN products) for $22 \leq A \leq 50$. This plot should be compared with an earlier one given by Fowler *et al.* (Fo55). With the exception of those for $A > 46$, the points marked by filled circles represent isotopes made predominantly by the s process. Those marked by crosses lie above the other points because of the large abundances of these isotopes, and thus we attribute the synthesis of these isotopes to the α process. The curves are those calculated by R. Tuttle for different numbers of neutrons made available per Ne^{22} nucleus. It can be seen that the best fit to the observed points is given by the curve for n_c/Ne^{22} = 2.1. The departure of the calculated curve from the plotted points beyond $A \simeq 45$ suggests that other processes must be responsible for synthesis in this region.

a particular depression until this depression has been filled, whereas in the nuclear case there is always a finite probability that some flow occurs.

The saturation or steady-flow abundance of a particular isotope is reached when $dn(A)/dn_c = 0$, i.e., when

$$\frac{n(A)}{n(A-1)} = \frac{\sigma(A-1)}{\sigma(A)}.$$

If a sufficient number of neutrons is available, the last of the isotopes in the s chain will achieve the full value of $n(A)$ given by this equation and we shall have

$$n(A)\sigma(A) = \text{constant}$$

over the range of isotopes built by the s process, apart from those immediately at the beginning of the chain in which the σN product will decrease unless these nuclei are continuously augmented during the s process. However, if an insufficient number of neutrons is made available, we find that a plot of the $n(A)\sigma(A)$ product is a monotonic function of A, smoothly decreasing as A increases.

There are two separate regions in the abundance curve where a considerable proportion of the isotopes are made by the s process. The region $22 < A < 50$ has been discussed previously (Fo55) and it was found that in this region steady flow was not attained, but that with a supply of neutrons such that $n_c/n(\text{Ne}^{22}) = 2.8$, the abundances of the isotopes built in the s chain up to Ti^{50} could be reasonably well reproduced. However, some modification of these results can now be made with the cross sections which are given in the appendix. A new plot of σN against A is shown in Fig. VI,1. The effect of the improved cross sections is to show very clearly that σN is truly a very smooth function of A for all of the isotopes built predominantly by the s process in the range of atomic weight $23 < A < 46$, thus bearing out the correctness of our assignment of these nuclei. One point of special interest is the case of scandium. This has only a single isotope, Sc^{45}, and is made according to the appendix by the s process. However, when the σN product is plotted by using the abundance given by Suess and Urey (Su56) the point falls below the curve delineated by the surrounding points. On the other hand, the solar abundance determined by Goldberg *et al.* (Go57) is larger than that given by Suess and Urey by a factor ~ 20, and this σN product (which is the one plotted) lies above the curve. This strongly suggests to us that in the case of scandium the true abundance lies between the solar abundance and the estimate from terrestrial and meteoritic data. The points which lie above the curve, designated by crosses instead of filled circles, are due to the nuclei which have $A = 24$, 28, 32, 36, 40, 44, and 48. Their values of σN are higher than those of their neighbors because their abundances are far larger. These are the nuclei which are built predominantly by the α process. The neutron-

capture cross sections, σ, clearly have no significance in their case.

Calculations similar to those carried out previously (Fo55) using the new cross section estimates have been carried out by Tuttle (private communication) and curves showing these results are also shown in Fig. VI,1. The best fit is obtained for $n_c/\mathrm{Ne}^{22}=2.1$, as compared with the value of $n_c/\mathrm{Ne}^{22}=2.8$ obtained in the original calculations. This new calculated curve fits the observed σN values only out to $A=43$, whereas in the earlier calculations it appeared that a reasonable fit out to $A=50$ was obtained. Thus, unless the cross section estimates in the region $45<A<50$ are considerably in error, we conclude from these new results that Ti^{47}, Ti^{48}, Ti^{49}, and Ti^{50} are not built predominantly by the s process, because their abundances are larger than we should expect on the basis of this theory. As described in Sec. III D, Ti^{48} is built by the α process, and Ti^{47}, Ti^{49}, and Ti^{50} have been tentatively ascribed to the r process. This region of A is the region where the α, s, e, and r processes all intersect, a point which was emphasized at the end of Sec. IV. Ti^{46} is assigned partly to the s process and partly to the e process but its atomic abundance is higher than expected on this basis.

The second region in the abundance curve where many isotopes are made by the s process is the region $63\leq A\leq209$. In this region, as described in Sec. II, assignments are more complicated because in many cases both the s and the r process contribute to the synthesis of an isotope. The correctness of our assignments can be tested by plotting both the σN products and also by plotting N and $1/\sigma$ as a function of A. These plots are shown in Figs. VI,2 and VI,3. In Fig. VI,2, which shows the plots of N and $1/\sigma$ for isotopes of odd A only, the major peaks in both N and $1/\sigma$ at magic neutron numbers $N=50$ and 82, the approach towards the peak at the double magic numbers $Z=82$ and $N=126$, and the minor peaks at $Z=50$ and $A=180$ are well defined. The run of the points throughout these curves shows that there are no major inconsistencies in our assignments. For a more detailed comparison we use the plot of σN against A (Fig. VI,3). In this plot isotopes made solely by the s process are distinguished from those in which the s process and the r process both contribute roughly equal amounts or in which the s process dominates. In the latter two cases the σN product has been corrected by assuming that either $\frac{1}{2}$ or $\frac{2}{3}$ of the abundance is due to the s process. In cases
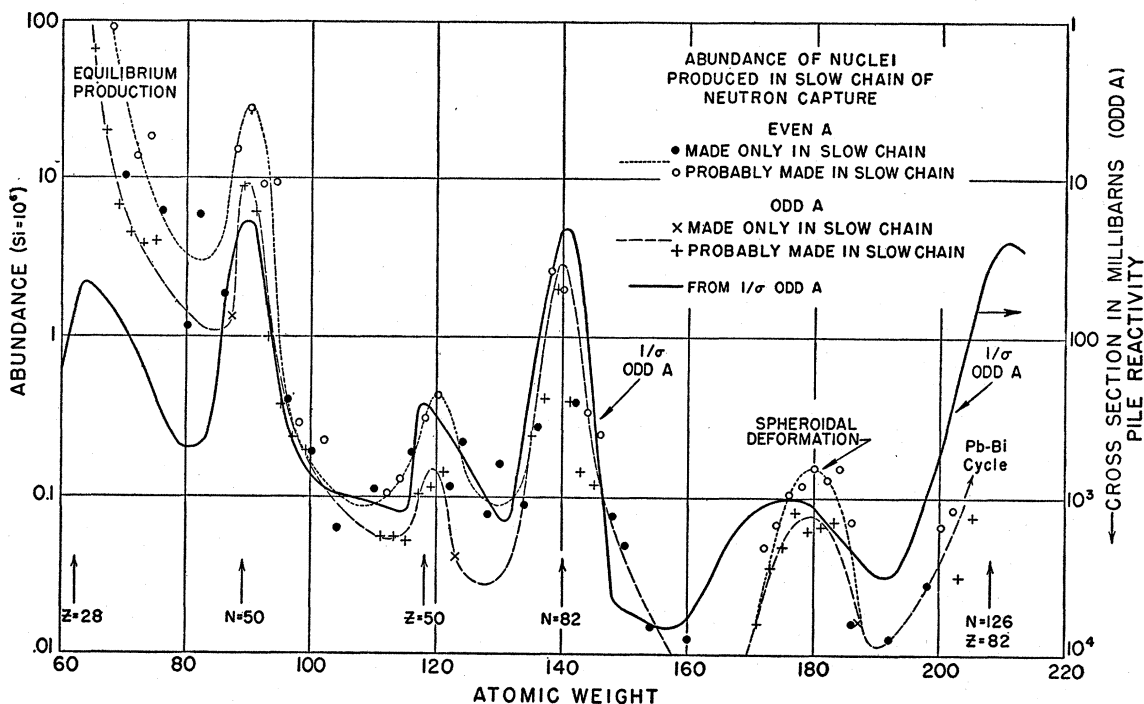
FIG. VI,2. The filled circles and diagonal crosses represent the abundances of even-A and odd-A isotopes, respectively, in the range of atomic weight $63\leq A\leq209$ which are made only in the s process; open circles and vertical crosses represent abundances of even- and odd-A isotopes, respectively, which are probably made in the s process. The abundance scale is given on the left-hand ordinate. Two curves are drawn schematically through the even- and odd-A points separately to show the trends of these abundances. The continuous curve which is also given is a plot of σ^{-1}, the reciprocal of the neutron capture cross section for isotopes of odd A, this scale being given by the right-hand ordinate. It will be seen that the peaks at the neutron magic numbers $N=50$ and 82, the proton magic number at $Z=50$, and the rise to the doubly-magic peak at $N=126$, $Z=82$, together with the broader rise due to the spheroidal deformation effect near $A=180$, are all shown by these curves, reflecting the effect that in local regions the σN product is constant, though over the whole range of A which is displayed, the σN product shows considerable variation (cf. Fig. VI,3).
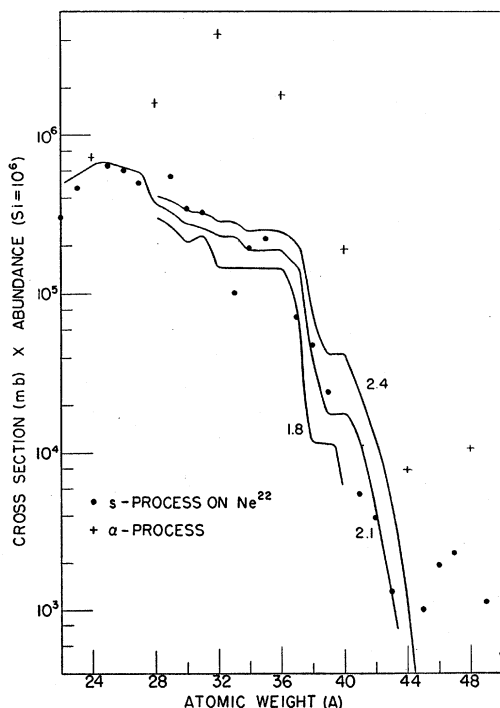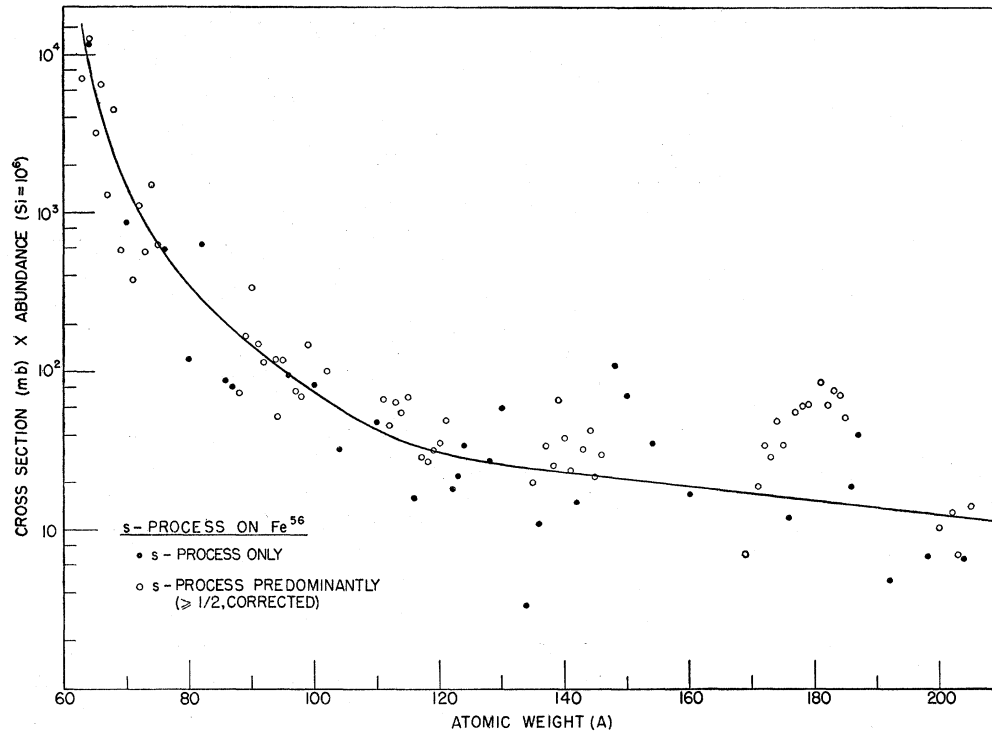
FIG. VI,3. Plot of the abundances of the isotopes times their neutron-capture cross sections (σN products) for $63 \leq A \leq 209$. The points marked by filled circles represent isotopes made by the s process only, while those points marked by open circles represent isotopes made by the s process predominantly; in cases in which it has been estimated that a certain fraction of the abundance is made by the s process (perhaps $\frac{1}{2}$ or $\frac{2}{3}$) this fraction was used in computing σN. The curve which is drawn is purely schematic.

where a smaller proportion than $\frac{1}{3}$ of the abundance has been estimated to be made by the r process, no correction has been applied and the total σN product has been plotted. The curve shows a steep decline from $A \sim 63$ to $A \sim 100$. Beyond this point, the slope appears to decrease more gradually, and it may tend to level off completely; however, the scatter of the points in this region, particularly beyond $A \sim 170$, makes the exact trend hard to determine. A large part of the scatter in this plot is most likely due to uncertainties in the estimated values of σ and also, to a lesser extent, uncertainties in the relative abundances of some elements in the rare earth region. Thus, in particular, the very low points at Ba^{134} and Pt^{192} are probably due in part to an underestimate of σ, since as has previously been mentioned, no account has been taken of the fact that the lightest even isotope of an element will have a larger σ than heavier even isotopes. Again, the high values of σN obtained for Sm^{148} and Sm^{150} may indicate that our estimates of all of the σ's for the samarium isotopes have been consistently too high.

The relative abundances of the isotopes of barium show in a very striking way how the s-process operates. The light isotopes Ba^{130} and Ba^{132} cannot be made on the s or r processes and are indeed very rare with atomic abundances 0.0037 and 0.00356, respectively. The fact that they are almost equal can be well understood on the basis of their production in the p process (cf. Sec. IX). They result from the decay of positron-emitting progenitors at 130 and 132, made in equal abundance in the p process. On the other hand, the

isotopes from Ba^{134} to Ba^{138} show much greater abundances, with a marked increase with increasing number of neutrons. Ba^{134} and Ba^{136} can only be made in the s process, Ba^{138} is magic in this process, and Ba^{135} and Ba^{137} are predominantly made in the s process. The marked rise in abundances from Ba^{134} to Ba^{138}, i.e., 0.0886, 0.241, 0.286, 0.414, 2.622 can be understood on the basis of the decreasing neutron capture cross section. This is to be expected as more neutrons are added, and culminates in the very low cross section and large abundance expected for Ba^{138} with magic $N = 82$. Our estimates of cross sections in the appendix do not take the gradual rise with N into account, but it is strongly indicated by the Oak Ridge results. It will be interesting to see if neutron activation measurements on Ba^{134} (producing 29 hr Ba^{135m}), and on Ba^{136} (producing 2.6 min Ba^{137m}), bear out the ratios expected relative to Ba^{138}. The expected cross sections are $11.4 \times 2.622/0.0886 = 336$ mb for Ba^{134} and $11.4 \times 2.622/0.286 = 109$ mb for Ba^{136}. Unfortunately, the isomeric states may be produced with only a small fraction of these cross sections and this will lead to some ambiguity in interpreting the experimental result. Unambiguous results would be obtained by measuring the total absorption cross sections, but this is very difficult experimentally. It is our view, however, that such measurements would serve as a crucial test of the validity of the s process.

The steep part of the curve shown in Fig. VI,3, followed by part which tends to level off, suggests that the curve has a composite character and that the abundances in the solar system of s-process isotopes

have been produced in more than one stellar synthesis process. Thus, the simplest possibility is that one process is responsible for the part of the curve in the range $63 < A \lesssim 100$ and that this part is similar in shape to the σN plot for the isotopes in the range $33 < A < 46$, shown in Fig. VI,1, falling to zero very rapidly beyond $A \sim 100$. This part of the curve shows that there have not been enough neutrons available per Fe^{56} nucleus to build the nuclei to their saturation abundances. Thus, it may be that in this region the $C^{13}(\alpha,n)O^{16}$ reaction has been the neutron source. A second process may be responsible for that portion of the curve beyond $A \sim 100$. In this case, since this latter slope is small or zero, this is strongly suggestive of steady flow being achieved and of all of these nuclei reaching their saturation abundances. The rates at which the neutrons are released by $C^{13}(\alpha,n)O^{16}$ and $Ne^{21}(\alpha,n)Mg^{24}$ are discussed in Sec. III. The time-scales obtained from arguments based on particular isotopes in the s-process chain are given in Sec. II, where it was shown that these time-scales were compatible with the result that the σN product falls steeply to $A \sim 100$, implying a paucity of neutrons, and then levels off, the abundances reaching their saturation values. Thus at the end of the s-process chain we expect that cycling among the lead isotopes, following the alpha decays at Po^{211}, Bi^{210}, and Bi^{211} which are shown in the appendix and illustrated in Figs. V,2 and V,3 has taken place, so that the lead isotopes which are included in the cycle, Pb^{206}, Pb^{207}, and Pb^{208}, have been built up to a far greater extent than Pb^{204} which is not in the cycle. Some lead is also produced by the r process, and if this contribution is taken into account we can calculate the amount of cycling which has taken place, and also predict a total abundance of lead. This question is discussed in Sec. VIII, following detailed explanation of r-process dynamics.

If this curve in Fig. VI,3 is a composite of two curves, it is also clear that the degrees of dilution of the abundances in the two parts are different, since larger over-abundance ratios are demanded to obtain complete saturation than if saturation is not achieved. Such a situation is entirely possible, since the two different processes might have occurred in two different red-giant stars, in which the dilution was a function both of the original composition, the mixing to the surface, and the ejection into the interstellar medium. Alternatively, they might have occurred in a single star at different evolutionary stages in which the structures and hence these same parameters would be changed. To study this question further it is important to investigate the composition of a star in which it is believed that the s process has recently been occurring. The S-type stars and the so-called Ba II stars fall into this category, and the results of such an investigation are described in Sec. XI D.

Finally, in Table VI,1 we show the σN products for just those isotopes for which experimental measures of

TABLE VI,1. "25 kev" cross section (La57b, Bo57) ×abundance (Su56).

	σ (mb)	N (Si $=10^6$)	σN	Assignment
I. Synthesized on Ne^{22}				
Na^{23}	1	4.38×10^4	4.38×10^4	H burning, s
Mg^{26}	<14	1.00×10^5	$<1.4 \times 10^6$	s(m)
Al^{27}	1.4	9.48×10^4	1.3×10^5	s(m)
Cl^{37}	1.1	2180	2.4×10^3	s(m)
K^{41}	19	219	4.2×10^3	s
II. Synthesized on Fe^{56}				
Cu^{63}	116	146	1.7×10^4	s
Ni^{64}	8	318(0.61)	1.6×10^3	s
Cu^{65}	46	66	3.0×10^3	s
Ga^{71}	68	4.54	3.1×10^2	s
Ge^{74}	54	18.65	1.0×10^3	s
As^{75}	590	4.0(2/3)	1.6×10^3	sr
Y^{89}	25	8.9	2.3×10^2	s(m)
Zr^{94}	243	9.48	2.3×10^3	s
Mo^{98}	209	0.581(1/2)	60	s=r
Ru^{102}	386	0.467(1/2)	90	s=r
In^{115}	805	0.105(1/2)	42	s=r
Sb^{121}	950	0.141	130	s
Ba^{138}	11.4	2.622	30	s(m)
La^{139}	50	2.00	100	s(m)
Ce^{140}	31	2.00	62	s(m)
Pr^{141}	546	0.40	218	s(m)
Hf^{180}	441	0.155	68	s
Re^{185}	2650	0.05(1/2)	66	s=r(m')
Hg^{202}	57	0.0844(2/3)	3.2	sr
Bi^{209}	1.4	0.144(?)	0.2(?)	$\begin{cases} s(m)\text{-cycle} \\ r\text{-decay} \end{cases}$

cross sections at "25-kev" neutron energies have been made at Oak Ridge (La57b) and at Livermore (Bo57), and which have been assigned to the s process or in which the contributions of the r process have been estimated. Five of the isotopes lie in the range $23 \leq A \leq 46$, while the remainder have $A \geq 63$. This table shows the same effects as are shown in Figs. VI,1 and VI,3.

VII. DETAILS OF THE r PROCESS

The essential feature of the r process is that a large flux of neutrons becomes available in a short time interval for addition to elements of the iron group, or perhaps, in cases where the abundances in the iron group are abnormally small, for addition to light nuclei such as Ne^{22}.

From the point of view of the present section, the precise source of the neutrons is not important; any source capable of supplying a large neutron flux on a short time-scale of order 10–100 sec, would meet the requirements. In Sec. III F we discussed the possibility that a neutron density of $10^{24}/cm^3$ and a flux of $4 \times 10^{32}/cm^3$ sec might be produced in supernova envelopes at temperatures $\sim 10^9$ degrees. We assume these conditions in the following discussion of the path of the r process and of the abundances produced by it. Fong (Fo57), using a hydrodynamical analogy, has previously calculated abundances produced by an r process. Our method is somewhat different in that we include the (γ,n) as well as (n,γ) and β^- decay in our calculations.

A. Path of the r Process

A nucleus of fixed Z cannot add neutrons indefinitely even in the presence of an intense neutron flux. The energy of binding of each successive neutron becomes progressively weaker as more and more neutrons are added, until ultimately the binding falls to zero. This sets an upper limit to neutron addition at fixed Z. Moreover, not even this limit will be attained because of the incidence of (γ,n) reactions at the temperature necessary to produce the neutrons by charged particle interactions. The effect of (γ,n) reactions can readily be understood from statistical considerations. Write $n(A,Z)$ and n_n for the number densities of nuclei A, Z and of neutrons respectively, and let $Q_n(A,Z)$ be the neutron binding to the nucleus $X(A,Z)$ in the reaction,

$$X(A,Z)+n \rightleftharpoons X(A+1, Z)+\gamma+Q_n(A,Z),$$
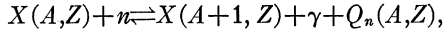
such that

$$Q_n(A,Z)=B_n(A+1, Z)$$
$$=c^2[M(A,Z)+M_n-M(A+1, Z)]. \quad (13)$$

Note that Q_n for nucleus A, Z is equal to the neutron binding energy B_n (taken positive) in nucleus $A+1$, Z. With T in units of 10^9 degrees, Q_n in Mev, and neglecting weight factors of order unity, the statistical balance in this reaction is expressed by

$$\log\frac{n(A+1,Z)}{n(A,Z)}=\log n_n-34.07-\tfrac{3}{2}\log T_9+\frac{5.04}{T_9}Q_n \quad (14)$$

with all logarithms to the base 10. For neutron addition to be highly effective we require $n(A+1,Z)/n(A,Z)\gg1$. When $n(A+1, Z)/n(A,Z)\sim1$, neutron addition is less effective. When $n(A+1, Z)/n(A,Z)\ll1$, neutrons are scarcely added at all. As an approximation, adequate for the present discussion, we may consider that neutrons are added or not added according to whether $n(A+1, Z)/n(A,Z)\geq1$ is satisfied or not, i.e., according to whether

$$Q_n\geq\frac{T_9}{5.04}(34.07+\tfrac{3}{2}\log T_9-\log n_n) \quad (15)$$

is satisfied or not. With $T_9\sim1$ and $n_n\sim10^{24}$ as found in Sec. III F, we have

$$Q_n\gtrsim2 \text{ Mev.}$$

Larger Q_n values would be required at higher temperatures or at lower neutron densities. $n(A+1, Z)/n(A,Z)$ is very sensitive to small changes in Q_n or T_9. Under the conditions discussed above $5.04Q_n/T_9\approx10$. Hence a ten percent change in Q_n, namely by 0.2 Mev, or a ten percent change in T_9, namely by 10^8 degrees, will change $n(A+1, Z)/N(A,Z)$, by a factor of ten. Conversely, for given Q_n, T_9, and Z the distribution in abundance will exhibit a sharp peak where $n(A+1, Z)=n(A,Z)$. This peak will be at most two or three units in A in width.

We have said that Q_n decreases as more and more neutrons are added at fixed Z. This statement ignored neutron pairing effects. Thus Q_n is higher for odd $N=A-Z$ by 1.5 to 3 Mev (depending on A) than it is for even $N=A-Z$. This means that instead of a simple monotonic decrease of Q_n with increasing A (Z fixed) we have two decreasing sequences, one for N odd, the other for N even, the two sequences being separated by about 2 Mev in the range of A of interest in this discussion.

Consider the effect of these two sequences on the criterion for neutron addition. Evidently the pairing effect makes it substantially more difficult for Q_n to satisfy the criterion when N is even, and hence neutron addition must always be expected to cease when N is even. Thus if a neutron can be added at N even, then a further neutron will always be added, since an additional energy approximately equal to 2 Mev is then available for binding the second neutron. On the other hand, when a neutron is added at odd N, the situation is reversed—a second neutron would in that case be less strongly bound by ~2 Mev—so that, although the first neutron might satisfy our criterion, the second is a good deal less likely to do so, and eventually, when N becomes large enough, will not in fact do so. Thus we expect that neutron addition will always cease with N at an even value, so that if A is odd Z must be odd, and if A is even Z must be even.

These remarks all refer to a fixed value of Z. Now Z must increase by unity from time to time, since the neutron-rich nuclei at present under consideration are all unstable against negative beta decay, the lifetimes being ~0.01–10 sec. When Z thus increases, the energy of binding of the next neutron increases quite substantially, so that one or more neutrons can again be added. Once again, however, neutron addition will cease at some even N. Neutron addition cannot then proceed until Z increases by a further unit—and so on. We therefore obtain a clear picture of how the nuclei evolve, by repeated neutron addition interspersed with β^- processes, the nuclei always being obliged to "wait" for a β^- process when neutron addition decreases Q_n to the limit allowed by our criterion. The process is shown schematically in Fig. V,2. A detail of this figure for $118<A<132$ is shown in Fig. V,3.

The s and r processes differ in a very crucial way. In the s process, neutrons are made available very slowly so that the neutron density is always low. In such circumstances the addition of neutrons to the nuclei is controlled by their (n,γ) cross sections. That is to say, the various nuclei compete among themselves for the capture of a slow trickle of neutrons, the abundances of the nuclei being governed by the flow equation (11)

$$dn(A)/dt=-\lambda_n(A)n(A)+\lambda_n(A-1)n(A-1),$$

where $n(A)$ is the abundance of that beta-stable isobar at A which occurs in the s-process capture path. In the r process, on the other hand, we are concerned with a

situation in which there is no neutron shortage, and neutron addition is limited not by (n,γ) cross sections but by (γ,n) competition and by "waiting" for β^- processes to take place. Essentially, we assume that equilibrium is reached between the rapid (n,γ) and (γ,n) processes, viz., n, $\gamma \rightleftharpoons \gamma$, n, and that the slow beta-decay processes constitute a slow leakage from this equilibrium. The corresponding flow equation in the r process, derived from the general equation (10), takes the form

$$dn(Z)/dt = -\lambda_\beta(Z)n(Z) + \lambda_\beta(Z-1)n(Z-1), \quad (16)$$

where $n(Z)$ is the density of that isotope of element Z at which waiting for negative beta decay occurs, i.e., the isotope for which $Q_n \sim 2$ Mev. The quantity $\lambda_\beta(Z)$ is related to the beta-decay mean lifetime, τ_β, and half-life, t_β, by $\lambda_\beta = 1/\tau_\beta = 0.693/t_\beta$. The condition for steady flow in the r process is

$$\lambda_\beta(Z)n(Z) = \lambda_\beta(Z-1)n(Z-1) = \text{const}$$

or

$$n(Z) \propto \lambda_\beta^{-1}(Z) = \tau_\beta(Z).$$

This is the analog of the steady-flow condition in the s process, namely,

$$\lambda_n(A)n(A) = \lambda_n(A-1)n(A-1) = \text{const}$$

or

$$n(A) \propto \lambda_n^{-1}(A).$$

Just as the abundances of the s nuclei suggest that steady flow has occurred in the s process, so the abundances of the r nuclei suggest that steady flow has occurred in the r process.

The $n(Z)$ given by the flow equations cannot immediately be interpreted as atomic abundances. At first sight it might seem as if only certain values of A are concerned in the r process, namely the values of A at which the nuclei "wait." In Figs. V,2 or V,3, if nuclei of charge Z wait at A, nuclei of charge $Z+1$ wait at $A+\Delta A$, where ΔA equals the number of neutron captures at $Z+1$ after beta decay at Z. Thus it might appear that only atomic weights A, $A+\Delta A$, etc., are likely to be produced in any appreciable abundances by the r process. This would be the case if there were a unique track of the kind shown in Figs. V,2 and V,3. But this is scarcely likely to be the case, since there will certainly be a spread in A, Z values about this path, simply due to the statistical nature of Eq. (14). Thus a small scatter in the values of atomic weights at which waiting for beta decay occurs is only to be expected. This suggests that we convert the n_Z abundances to n_A abundances by

$$n(A) = n(Z)(\Delta A)^{-1} = n(Z)(dZ/dA), \quad (17)$$

where ΔA is the number of unit steps in A for a single step in Z along the typical track of the form shown in Fig. V,2, and dZ/dA is the slope of the track in the Z, A plane. That is to say, we "spread" the abundances accumulated at the "waiting points" over the intervals

of A that occur between the waiting points. This treatment is of course approximate, but it is thought adequate for the present purpose, since the present analysis contains other simplifications that are explained at a later stage. We arbitrarily take the spread from a given waiting point at A to the next higher waiting point at $A+\Delta A$ rather than in the reverse direction. Physically, this corresponds to the assumption that, in freezing, the material accumulated at a waiting point with given A, Z is spread out, as γ radiation dies out, by final neutron captures over an interval in A up to the waiting A for $Z+1$. The equation for the equilibrium between (n,γ) and (γ,n) reactions is much more sensitive to T, (linear dependence), than to n_n, (logarithmic dependence). Thus, as T and n_n decrease, the equilibrium is displaced toward slightly greater A values, representing the capture of the last neutrons.

The solution of the dynamical problem in the r process falls into two parts. The first part consists in a determination of the track shown schematically in Fig. V,2, the second consists in estimating the beta-decay waiting time. The relative abundances given by steady flow then follow immediately from

$$n(A) \propto \frac{\tau_\beta(A,Z)}{\Delta A} = \tau_\beta(A,Z)\frac{dZ}{dA},$$

where $\tau_\beta(A,Z)$ is now the mean beta-decay lifetime at the waiting point, A, for a given Z. A determination of the track demands a precise specification of the criterion for neutron addition. This criterion can be written as $Q_n \geq Q_o$, where Q_o is to be a specified quantity, of order 2 Mev, which depends on n_n, T in accordance with the inequality (15).

The problem of the determination of the track is that of obtaining Q_n as a function of A, Z from nuclear data. Assuming for the moment this to be done, we then have $Q_n(A,Z) \geq Q_o$ as the condition for neutron addition. We now wish to determine the waiting values of A for various Z by using the following criteria.

With Z specified, $N = A - Z$ must be even, and

$$Q_n(A,Z) \geq Q_o,$$
$$Q_n(A+2,Z) < Q_o.$$

In this way the waiting points A, $A+\Delta A$, $\cdots$ corresponding to Z, $Z+1$, $\cdots$ can be found. A further necessary condition is that the waiting points increase monotonically with Z.

We have not found it possible to determine the waiting points solely from the current empirical nuclear data on neutron binding energies. This is to be expected, if it is recalled that one must know the binding energy of the very neutron-rich nuclei along the neutron capture path with considerable precision ($\sim$0.2 Mev) in order to specify the path precisely. Even the binding energies of the stable nuclei on which careful mass measurements have been made are rarely known to this

precision. Furthermore, the extrapolation to the neutron-rich nuclei involves considerable uncertainty. For these reasons we have been forced to resort to a method of calculating r-process abundances which establishes a few parameters semiempirically on the basis of certain salient features of the abundance curve itself. We now outline a method of calculation which may eventually be capable of yielding a theoretical abundance curve on the basis of nuclear data alone.

First, we consider the determination of $Q(A,Z)$ on the basis of the smooth Weizsäcker atomic mass formula (We35), neglecting shell, pairing and quadrupole deformation effects:

$$M(A,Z)=(A-Z)M_n+ZM_H-\frac{1}{c^2}\left[\alpha A-\beta\frac{(A-2Z)^2}{A}\right.$$
$$\left.-\gamma A^{\frac{2}{3}}-\epsilon\frac{Z(Z-1)}{A^{\frac{1}{3}}}\right],\quad(18)$$

where M_n and M_H are the masses of the neutron and of the hydrogen atom and α, β, γ, and ϵ are constants in energy units, to be determined empirically. They represent, respectively, volume, isotopic, surface, and Coulomb energy parameters. In the following discussion we use $\alpha=15.3$, $\beta=22.6$, $\gamma=16.7$, and $\epsilon=0.69$, all in Mev, as determined by Fowler, Hornyak, and Cohen (Fo47). Equation (18) can be alternatively written as

$$M(A,Z)=M_A+\frac{1}{2c^2}B_A(Z-Z_A)^2,\quad(18a)$$

where

$$Z_A\simeq\frac{1}{2}A\left(1+\frac{\epsilon}{4\beta}A^{\frac{2}{3}}\right)^{-1}\quad(19)$$

is the value of Z at a given mass number, A, for which $M(A,Z)$ has the minimum value, M_A. Z_A is not necessarily integral, and both M_A and Z_A can be determined in terms of the empirical constants by setting $\partial M/\partial Z=0$, keeping A constant. The coefficient B_A appears in the well-known parabolic dependence of $M(A,Z)$ on Z and can be evaluated from

$$B_A=\frac{8\beta}{A}\left[1+\frac{\epsilon}{4\beta}A^{\frac{2}{3}}\right]\simeq\frac{4\beta}{Z_A}.\quad(20)$$

Alternatively, M_A, Z_A, and B_A can be taken as quantities to be determined as empirical functions of A.

Returning to Eq. (18), we can determine $Q_n(A,Z)$ as follows

$$Q_n(A,Z)=c^2[M_n+M(A,Z)-M(A+1,Z)]$$
$$=\alpha-\beta\left(1-4\frac{Z^2}{A^2}\right)-\frac{2}{3}\gamma A^{-\frac{1}{3}}+\frac{\epsilon}{3}\frac{Z(Z-1)}{A^{\frac{4}{3}}}$$
$$\simeq\alpha-\beta-\frac{2}{3}\gamma A^{-\frac{1}{3}}+4\beta\frac{Z^2}{A^2}\left[1+\frac{\epsilon}{12\beta}A^{\frac{2}{3}}\right].\quad(21)$$

The terms in the second line in Eq. (21) can be identified successively as due to volume, isotopic, surface, and Coulomb effects in atomic masses. Equating Q_n to a specified Q_o in Eq. (21) gives A as a smooth function of Z. The plot of Z against A runs approximately parallel to the stability line, but it is depressed below this line by an amount that depends on the value of Q_o. For $Q_o=2$ Mev the depression amounts to about 7 units in Z at $A\sim100$ and about 11 units in Z at $A\sim200$. If the nuclear masses were really given by the Weizsäcker formula the nuclei would evolve along this line, not completely in a smooth fashion because of the discrete nature of A, but smoothly within one unit of A. There would be no gross deflections of the line, such as are implied in Figs. V,2 and V,3. In addition, the values of τ_β and dZ/dA would also be a smooth function of A, so that the theory would be incapable of explaining the peaks and troughs of the abundance curve for the r nuclei. Evidently an improved expression must be used for $M(A,Z)$ if the theory is to provide this degree of detail. We have not attempted a complete treatment but have been content to approximate in a degree that does not seem to have too serious an impact on the calculated results. A fuller treatment of the form of $M(A,Z)$ is at present being investigated by Dr. Forrest Mozer at the California Institute of Technology, and improved results should be forthcoming from its use.

Our treatment is based on modifying the above expression for $M(A,Z)$ so that we have

$$M(A,Z)=M_W(A,Z)-\frac{1}{c^2}[f(N)+g(Z)],\quad(22)$$

where $M_W(A,Z)$ represents the Weizsäcker expressions given in Eq. (18). That is to say, we subtract a sum of two functions, one of the neutron number and the other of the proton number. Insofar as they are functions of N and Z separately, this procedure takes into account the important effects on nuclear masses of (i) neutron or proton shell structure, (ii) spheroidal quadrupole deformation of partially filled shells, and (iii) pairing of neutrons and pairing of protons. Products of two such functions are not included. The quantities $f(N)$ and $g(Z)$ will be discontinuous functions at magic closed shell numbers for N or Z respectively. The sign is taken negative so that $f(N)$ and $g(Z)$, as positive quantities, decrease the mass and add to the stability of a nucleus.

We now obtain

$$Q_n(A,Z)=\alpha-\beta-\frac{2}{3}\gamma A^{-\frac{1}{3}}$$
$$+4\beta\frac{Z^2}{A^2}\left[1+\frac{\epsilon}{12\beta}A^{\frac{2}{3}}\right]+f'(A-Z),\quad(23)$$

where

$$f'(A-Z)=f'(N)=\frac{df(N)}{dN}=f(A+1-Z)-f(A-Z).$$

Note that $g(Z)$ drops out of Q_n. Care must be exercised in evaluating f' at magic numbers where f is discontinuous. Our criterion $Q_n \geq Q_o$, with Q_o a specified number ~ 2 Mev, now gives a track in the Z, A plane that depends on $f'(A-Z)$.

The capture path is changed considerably on taking $f'(A-Z)$ into account. The plot of Z against A for the r process follows a smooth curve approximately parallel to the stability line if the Weizsäcker mass formula, Eq. (18), is used. The plot of Z against A, shown in Fig. V,2, departs from such a smooth curve, however. Deviations are introduced by the function $f(A-Z)$. Most notably, this function causes the curve to swing upwards towards the stability line whenever $A-Z$ equals a neutron magic number. The physical reason for this is that the energy of binding of the next neutron decreases sharply by about 2 Mev at neutron shell closure. Consider neutron shell closure at $N=A-Z=82$, $A=123$, $Z=41$ (cf. Fig. V,3). The 82nd neutron is added with a binding of 2 Mev, or perhaps somewhat more than this, the value of Z being some 12 units below the stability line at this stage. An 83rd neutron cannot then be added at such a depth below the stability line because of the sharp fall of binding after shell closure. Indeed, an 83rd neutron at $Z=41$ would scarcely be bound at all. Further evolution then depends on a β^- process, which decreases $A-Z$ to 81. An 82nd neutron can then be added, but an 83rd again cannot. A further β^- process must therefore take place, when once again an 82nd neutron can be added. In this way the nucleus climbs a staircase with Z and A both increasing by unity at each step. Eventually, however, the climb up the staircase carries the nucleus close enough to the stability line for an 83rd neutron to be added at a binding energy ~ 2 Mev. This occurs for $Z=49$, $A=131$. Subsequently Z increases by one unit, not for a one-unit increase of A, as on the staircase, but for an increase of some three or more units in A. The differential in A must be an odd integer since waiting occurs only for even N. We refer to the values of A and Z for a magic N at which more than one capture occurs as the "break-through" values at the abundance peaks. Break-through pairs are (82, 32), (131, 49), and (196, 70) at $N=50$, 82, and 126, respectively, and staircases similar to the one at $N=82$ occur at $N=50$ and 126. These staircases are associated with the rising sides of major peaks in the abundance curve for the r process. More subtle effects of proton shells and spheroidal deformations are discussed later.

From the above discussion it would seem that the capture path cannot be determined without explicit knowledge of $f(A-Z)$, but this is not so, as the following device shows. Let A_e, Z_e be a nucleus with empirically known neutron-binding energy, and with

$$N_e = A_e - Z_e = A - Z = N.$$

Then we have

$$Q_n(A_e, Z_e) = \alpha - \beta - \tfrac{2}{3}\gamma A_e^{-\tfrac{1}{3}}$$

$$+ 4\beta \frac{Z_e^2}{A_e^2}\left[1 + \frac{\epsilon}{12\beta}A_e^{\tfrac{2}{3}}\right] + f'(A_e - Z_e), \quad (23a)$$

where

$$f'(A_e - Z_e) = f'(A-Z).$$

Subtracting Eq. (23a) from (23), we have

$$Q_n(A,Z) = Q_n(A_e, Z_e) + \tfrac{2}{3}\gamma(A_e^{-\tfrac{1}{3}} - A^{-\tfrac{1}{3}})$$

$$+ 4\beta \frac{Z^2}{A^2}\left[1 + \frac{\epsilon}{4\beta}A^{\tfrac{2}{3}}\right] - 4\beta \frac{Z_e^2}{A_e^2}\left[1 + \frac{\epsilon}{4\beta}A_e^{\tfrac{2}{3}}\right]$$

$$\simeq Q_n(A_e, Z_e) - 4\beta\left[\frac{Z_e^2}{A_e^2} - \frac{Z^2}{A^2}\right] - 0.4. \quad (24)$$

In the last approximate expression we have evaluated in Mev the differences in the surface and Coulomb terms for the cases which will be found to be of interest. The isotopic term in β is by far the largest term in the difference in neutron binding energy for two nuclei with the same N. The important result of the foregoing analysis is that $g(Z)$ does not appear in (23) for $Q_n(A,Z)$ and $f(N)$ and $f'(N)$ do not appear in (24). This follows from our assumptions that to first order the deviations from the Weizsäcker mass law are separable in N and Z.

If the values of $Q(A_e, Z_e)$ were always accurately known the present procedure would be simple of application. Unfortunately, individual empirical values of $Q(A_e, Z_e)$ contain sufficient inaccuracies to cause serious difficulties if employed singly. The difficulties can be overcome, in part, by a suitable form of smoothing, except for values of $A-Z$ between ~ 84 and ~ 110, in which range the empirical mass data seem to be too poorly known even to admit of smoothing.

Smoothing is effected by constructing the quantity

$$\Delta\langle f'(A_e - Z_e)\rangle_{\mathrm{Av}} \simeq \Delta\left[Q_n(A_e, Z_e) - 4\beta\frac{Z_e^2}{A_e^2}\right]_{\mathrm{Av}}.$$

The quantity in square brackets is first calculated for each nucleus for which empirical values of Q_n are available, and then averaged over all cases having the specified value of $N=A_e-Z_e$. The Δ indicates that the values are calculated relative to those at the beginning of the appropriate neutron shell. Thus $\Delta\langle f'\rangle$ is the excess neutron binding energy to nuclei with a specified N over that given by the smooth Weizsäcker mass formula normalized to zero at the beginning of the shell in which N lies. We have used the nuclear mass tables of Wapstra (Wa55) and Huizenga (Hu55) for this purpose. When this has been done for various N the resulting average values have been plotted against N, as in Fig. VII,1. A second form of averaging is then effected by drawing a smooth curve through the points obtained in this way, values being finally read off the curve.
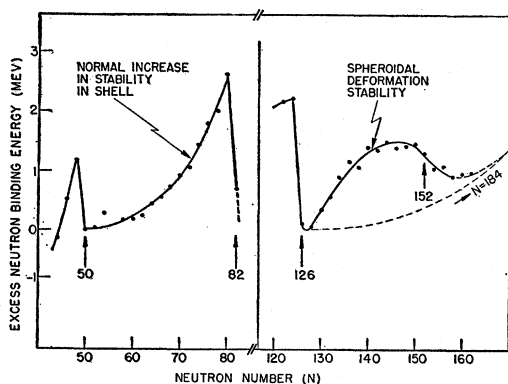
FIG. VII,1. The average excess neutron binding energy *to* nuclei with neutron number N, over that given by the smooth Weizsäcker atomic mass formula (We35). Each value has been normalized to the value at the beginning of the shell in which N lies. Empirical mass data for the $N=82$ to 126 shell are not accurate enough to yield the portion of the curve in this region.

We interpret the "quadratic" rise in the neutron binding excess between $N=50$ and 82 as the normal behavior as a neutron shell is filled. The last neutrons interact with a greater number of nucleons and are bound by about 2.6 Mev more than the first neutrons in this shell. In the $N=126$ to 184 shell there is a rapid rise to great stability early in the shell, a flattening off, and eventually a decrease having a maximum slope near $N=152$. We assume that eventually the curve rises again to a high value at shell closure. The early rise may be attributed to the ability of these heavy nuclei to take up spheroidally deformed shapes which have lower energy levels for extra neutrons than the spherical shape at the beginning of the shell. Maximum deformation is reached apparently near $A\sim144$ and then the shell becomes spherical again on closure, with the normal shell effect coming into play. The effect of spheroidal deformations on quadrupole moments and on rotational level structure in heavy nuclei has been brilliantly developed by Bohr and Mottelson (Bo53) and extensive calculations of energy levels in spheroidal

potentials have been made by Nilsson (Ni55). Nuclei in the $N=51$ to 82 shell do not show these effects in a pronounced manner, and thus "normal" shell behavior can be expected. The effects are well known in the heavier $N=82$ to 126 shell, for which, unfortunately, masses accurate enough for our purposes are not available. The effects can be expected to be highly developed in the $N=126$ to 184 shell. The influence of the enhanced stability on the r process is discussed in detail in what follows. *Note added in proof.*—The recent mass spectroscopic data of W. H. Johnson, Jr., and V. B. Bhanot (Jo57) yield a curve in the range $N=82$ to 126 similar to the right-hand curve in Fig. VII,1.

A difficulty which arises in determining the $Q_n(A,Z)$ from the empirical $Q_n(A_e,Z_e)$ lies in the isotopic parameter β for which we have taken the value 22.6 Mev. This is the value which gives the correct dependence of Z_A on A if the Coulomb coefficient ϵ is taken as 0.69 Mev. Fowler *et al.* (Fo47) found this value for ϵ to be necessary to fit the rise of the packing fraction curve for nuclei with $A>70$, and Green has confirmed this point (Gr54b). This value for ϵ is somewhat larger than that found in early attempts to adjust the smooth Weizsäcker formula to nuclear masses but is in keeping with the smaller values of nuclear radii found in electron scattering experiments by Hofstadter and his collaborators (Ho56c). However, in determining $Q_n(A,Z)$ from $Q_n(A_e,Z_e)$ we really need "local" values of β at $N=A-Z=A_e-Z_e$, not the average value determined by the best fit to Z_A over all A. This implies that β is not constant, as is indeed found to be the case if one adjusts the Weizsäcker formula or its alternative form in M_A, B_A, Z_A to local regions. Unfortunately, the empirical values for $Q_n(A_e,Z_e)$ do not cover a sufficient spread in A_e and Z_e to give accurate determinations of the local values for β, and thus the extrapolation to A,Z values far from the stability line involves considerable uncertainty.

To elaborate, let us consider the accuracy with which we must compute Q_n for the waiting point, A, at a given Z value along the capture path not near any magic

TABLE VII,1. Parameters of the r process at magic neutron numbers.

N	A	Z	Process	Q_n[a] Mev	Z_A	B_A Mev	$\frac{1}{2}\delta_A$ Mev	W_β Mev	τ_β sec	A	n(calc)	n(obs)
50	80	30	$(\beta^-\nu_-)$	1.9	35.0	1.90	1.43	3.82	12.3	1	42.6	33.8
	81	31	$(\beta^-\nu_-)$	2.4	35.4	1.88	$\cdots$	4.07	8.96	3	10.4	6.62
	82	32	(n,γ)	2.9[a]				Break-through point				
82	128	46	$(\beta^-\nu_-)$	1.0	54.5	1.36	1.18	7.48	0.43	1	Stan.	1.48
	129	47	$(\beta^-\nu_-)$	1.4	54.9	1.36	$\cdots$	7.84	0.34	1	1.17	1.05
	130	48	$(\beta^-\nu_-)$	1.7	55.3	1.35	1.16	5.82	1.50	3	1.73	$\cdots$
	131	49	(n,γ)	2.0[a]				Break-through point				
126	194	68	$(\beta^-\nu_-)$	1.2	77.9	1.16	0.77	8.31	0.25	1	0.87	0.533
	195	69	$(\beta^-\nu_-)$	1.4	78.3	1.16	$\cdots$	8.39	0.24	3	0.28	0.548
	196	70	(n,γ)	1.6[a]				Break-through point				

[a] The values for Q_n, at which (n,γ) occurs at the recognizable break-through points of the magic-neutron-number peaks in the atomic abundance curve, have been used to establish a smooth dependence of Q_n on atomic weight.

shell number in N. We evaluate

$$\frac{\partial Q_n}{\partial A}\bigg|_Z \simeq -\frac{8\beta Z^2}{A^3} \sim -0.25 \text{ to } -0.1 \text{ Mev},$$

where the numerical values have been determined near $A=100$ and $A=200$, respectively. Since the Q_n can hardly be specified to better than 0.5 Mev an uncertainty in A of several units is to be expected. The break-through points near magic shell numbers for N can be evaluated from

$$\frac{\partial Q_n}{\partial A}\bigg|_N \simeq +\frac{8\beta Z N}{A^3} \sim 0.5, 0.3, 0.2 \text{ Mev},$$

where the numerical values have been determined at $N=50, 82, 126$, respectively. Again an uncertainty of one or more units in A arises from uncertain knowledge of the Q_n.

With these difficulties in mind, we have chosen to establish a few key points in the track of the r process by using the values for the atomic weights at those peaks in the atomic abundance curve which are attributed to the r process. On the leading edges of these peaks there is no arbitrariness, except in the value of A (or Z) at which a given magic N is reached, and in the value of A (or Z) at which break-through occurs. The break-through points at which neutron capture without a preceding beta decay becomes possible occur just beyond the maxima of the magic-neutron-number abundance peaks. We have chosen these break-through points to give the best fit to the three abundance peaks due to magic neutron-numbers and have then adjusted the path determined by our criterion $Q_n(A,Z) \geq Q_0$ to fit the three points and to give a smooth run of waiting points between these break-through points. Thus the r-process path has been determined by a smooth curve for Q_0 passing through the break-through values at $N=50, 82$, and 126. These key values are shown in Table VII,1, where we list the Q_n values calculated by the smoothing procedures, using $\beta=22.6$ Mev. These Q_n values show a systematic decrease from 2.9 Mev at $N=50$, through 2.1 Mev at $N=82$ to 1.6 Mev at $N=126$. These values correspond to temperatures of 1.45, 1.0, and 0.8×10^9 degrees, respectively, for $n_n=10^{24}$. Whether or not this systematic decrease is real is a matter which cannot be answered with present knowledge of nuclear masses and binding energies. In attempting to use estimated local values for β we have found that the differences in Q_n and thus T are only accentuated. It is clear that the conditions, n_n and T, for the production of the three peaks were not greatly different. A small difference, if real, would be very significant in our understanding of the astrophysical circumstances under which the r-process elements were synthesized. We return to this matter later in our discussion and in Sec. XII. The capture path from Fe^{56} to

TABLE VII,2. The path of the r process and calculations of r-process abundances.

N	A	Z	Z_A	B_A Mev	$\frac{1}{2}\delta A$ Mev	W_β Mev	τ_β sec	ΔA	Atomic abundances
30	56	26	...	...	...	...	...	...	Starting point
42	68	26	30.3	2.40	1.40	3.42	21.4	3	First waiting point
44	71	27	31.4	2.20	...	4.68	4.45	7	2.20
50	78	28	34.2	1.94	1.42	6.26	1.04	1	3.61
	79	29	34.6	1.92	...	6.45	0.90	1	3.11
	80	30	35.0	1.90	1.43	3.82	12.3	1	42.6
	81	31	35.4	1.88	...	4.07	8.96	3	10.4
52	84	32	37.4	1.80	1.44	4.28	6.96	1	24.2
	85	33	37.8	1.78	...	4.59	4.91	5	3.40
56	90	34	39.8	1.70	1.44	4.67	4.50	7	2.23
62	97	35	42.5	1.60	...	8.50	0.225	5	0.156
66	102	36	44.5	1.55	1.41	8.39	0.241	5	0.167
70	107	37	46.5	1.50	...	11.00	0.062	3	0.072
72	110	38	47.7	1.47	1.35	9.73	0.115	7	0.057
78	117	39	50.5	1.41	...	13.19	0.025	3	0.029
80	120	40	51.7	1.39	1.27	12.02	0.040	3	0.046
82	123	41	52.8	1.38	...	13.33	0.024	1	0.083
	124	42	53.1	1.37	1.23	11.05	0.061	1	0.211
	125	43	53.5	1.37	...	11.46	0.051	1	0.176
	126	44	53.8	1.37	1.20	9.30	0.144	1	0.500
	127	45	54.2	1.36	...	9.61	0.122	1	0.423
	128	46	54.5	1.36	1.18	7.48	0.427	1	1.48
	129	47	54.9	1.36	...	7.84	0.338	1	1.17
	130	48	55.3	1.35	1.16	5.82	1.50	3	1.73
84	133	49	57.6	1.33	...	8.61	0.211	3	0.244
86	136	50	57.6	1.31	1.08	6.10	1.18	9	0.454
94	145	51	60.6	1.28	...	9.59	0.123	5	0.085
126	185	59	74.9	1.18	...	16.31	0.009	1	0.030
	186	60	75.3	1.18	0.78	14.82	0.014	1	0.049
	187	61	75.6	1.18	...	14.78	0.014	1	0.049
	188	62	75.9	1.17	0.78	13.06	0.026	1	0.091
	189	63	76.3	1.17	...	13.14	0.025	1	0.088
	190	64	76.6	1.17	0.78	11.54	0.049	1	0.170
	191	65	76.9	1.16	...	11.40	0.052	1	0.180
	192	66	77.3	1.16	0.77	9.94	0.103	1	0.357
	193	67	77.6	1.16	...	9.90	0.105	1	0.364
	194	68	77.9	1.16	0.77	8.31	0.252	1	0.874
126	195	69	78.3	1.16	...	8.39	0.240	3	0.278
128	198	70	80.4	1.16	0.76	8.90	0.180	11	0.056
138	209	71	83.9	1.16	...	12.56	0.032	3	0.037
140	212	72	84.9	1.16	0.75	11.81	0.043	3	0.050
142	215	73	86.0	1.16	...	12.68	0.030	3	0.035
144	218	74	87.0	1.16	0.75	11.93	0.041	3	0.048
146	221	75	88.1	1.16	...	12.80	0.029	3	0.034
148	224	76	89.1	1.16	0.74	12.06	0.039	3	0.045
150	227	77	90.2	1.16	...	12.91	0.028	3	0.032
152	230	78	91.3	1.16	0.73	12.30	0.036	1	0.123
	231	79	91.6	1.16	...	12.22	0.037	1	0.127
	232	80	91.9	1.16	0.73	10.67	0.072	3	0.084
154	235	81	93.0	1.16	...	11.52	0.049	3	0.057
156	238	82	93.4	1.16	0.72	10.10	0.095	3	0.110
158	241	83	94.5	1.16	...	10.94	0.064	1	0.221
158	242	84	94.8	1.16	0.72	9.41	0.136	3	0.157
160	245	85	95.9	1.16	...	10.24	0.089	3	0.103
162	248	86	97.0	1.16	0.72	9.64	0.120	3	0.139
164	251	87	98.0	1.16	...	10.36	0.084	3	0.097
166	254	88	99.0	1.16	0.72	9.64	0.120	3	0.139
168	257	89	100.1	1.16	...	10.48	0.029	3	0.091
170	260	90	101.2	1.16	0.71	9.87	0.107	5	0.074a
174	265	91	102.9	1.16	...	11.40	0.052	7	0.026a

a Probably depleted by neutron-induced fission.

$A=265$ which we have used is given in Table VII,2 and is illustrated in Figs. V,2 and V,3. The path is complete except for a gap from $A=150$ to $A=185$, in which region the empirical masses are so poorly known that there is no guide at all even to the trend of the capture track.

B. Calculation of r-Process Abundances

We now pass to the conclusion of our problem, namely, calculation of the relative abundances of the elements produced in the r process. This involves determination of $\Delta A = \partial Z/\partial A$ and τ_β at the waiting points. The capture path calculated from the criterion $Q_n(A,Z) \geq Q_o$ yielded nonintegral values of Z and A and thus a fairly smooth $\partial Z/\partial A$ along the track which we used as a guide as discussed above. In the track we

have finally chosen in Table VII,2, and in the "actual" track, Z and A change by integral values, and so we have chosen to use the integral ΔA listed in Table VII,2, in calculating $n(A)$. In Table VII,2 the various parameters needed in the abundance calculations are also listed.

The mean beta-decay lifetimes at the waiting points have been calculated from the Fermi expression

$$\tau_\beta = \frac{1}{\lambda_\beta} = \frac{10^4}{W_\beta{}^5} \text{ sec,}$$

where W_β, measured in Mev, is the effective beta-decay energy at the waiting point. It includes the kinetic energy of the electron and neutrino and the rest-mass equivalent energy (0.5 Mev) of the electron. The numerical constant has been determined by using an allowed transition $\log_{10} ft$ value of 3.85, where

$$f = \frac{1}{30} \left[\frac{W_\beta}{m_o c^2} \right]^5 \simeq W_\beta{}^5$$

if W_β is measured in Mev, and $t = 0.693\tau_\beta$ is the beta-decay half-life. The method described below for evaluating W_β leads in general to an underestimate, so that our values of τ_β could be too large by a factor of as much as 10. However, the relative values and thus the relative abundances should not be uncertain by such a large factor.

The determination of W_β as a function of the waiting point charge, Z, and mass, A, is a matter of some complexity. The total kinetic energy, Q_β, available in the beta transition to the ground state of the daughter nucleus is calculable from the atomic mass expression given in Eq. (22) and becomes

$$Q_\beta = c^2 [M(A,Z,N) - M(A, Z+1, N-1)].$$

Since the masses are atomic rather than nuclear, no allowance need be made for the beta-electron mass. We thus have,

$$Q_\beta = B_A (Z_A - Z - 0.5) + \frac{dg}{dZ} - \frac{df}{dN}. \qquad (25)$$

In this expression dg/dZ and df/dN explicitly appear. However, since they appear as a difference their influence on Q_β cannot be too great. Except at shell numbers, g and f increase with Z and N, respectively. If g and f were linear in Z and N with the same coefficient, then $dg/dZ - df/dN$ would be zero. Actually, g and f are approximately quadratic in the nuclear excess over magic-number values. Since there is a neutron excess in negative beta decay, in general $df/dN > dg/dZ$ and Z_A and B_A are usually smaller than the values calculated from the smooth formula. Z_A changes discontinuously at magic numbers, increasing after N magic and decreasing at Z magic. Actually, the residual effect of these terms can be taken into account by using just the

first term of Eq. (25) for Q_β with local values for B_A and Z_A, particularly for Z_A. Local values for Z_A have been given by Coryell (Co53) and we have used these values as tabulated in Table VII,2. Z_A is not only a function of A but also of the shell in which Z and N fall. Coryell chose the smooth Weizsäcker relation between local values of B_A and Z_A, namely $B_A Z_A \simeq 4\beta$, but we have not found this to be sufficiently accurate for our purpose. Accordingly, we made an independent analysis in order to obtain the values of B_A listed in Table VII,2. To do this we used Coryell's Z_A at a given A and determined B_A from the empirical Q_β differences calculable at a given A from the masses of Wapstra (Wa55) and Huizenga (Hu55). These values of B_A are shown as a function of A in Fig. VII,2.

We thus have

$$Q_\beta = B_A (Z_A - Z - 0.5),$$

where B_A and Z_A are now the "local" values for these quantities taking into account all deviations from the Weizsäcker mass law except odd-even effects, which must be treated separately, as discussed below, for nuclei with odd A and even A. It is emphasized that Z_A must be chosen to correspond to the shells in which Z and N lie.

The beta-ray transition to the ground state of the daughter nucleus will rarely be allowed. Allowed transitions occur to excited states of the daughter nucleus having spins differing by zero or unity from those of the parent ground state and having the same parity. Of these allowed transitions perhaps one is favored by a large matrix element indicating considerable similarity in the initial and final states as to spin, isobaric spin, and orbital characteristics. The excitation of this favored state will in general be lower at larger A, since the level density increases with A. It can be argued that the amount of excitation ought to be proportional to, and of the order of magnitude of, the isobaric parameter B_A. We have arbitrarily chosen $2B_A$ as the excitation energy of the excited state to which the beta transition effectively occurs. With this choice, the relative heights of the abundance peaks at $N = 50$, 82, and 126 are approximately reproduced as indicated by a comparison of the columns giving $n(\text{obs})$ and $n(\text{calc})$ in Table VII,1. The choice of $2B_A$ probably errs on the high side, so that our estimates for W_β may be somewhat low.

We can now write down W_β as soon as pairing energy or odd-even terms are clarified. If δ_A is used to designate the pairing energy term, and if odd A nuclei are taken as arbitrary standards for which no pairing correction is made, then for the mass of the ground states of even A, even Z, even N nuclei we must subtract $\delta_A/2$, and for even A, odd Z, odd N nuclei we must add $\delta_A/2$. Our waiting nuclei all have even N, so that for odd A no correction is necessary and for even A we must subtract $\delta_A/2$. On the other hand, the special symmetry properties of the ground states of nuclei insofar as pairing

effects are concerned do not apply to the excited states. This has been shown by Hurwitz and Bethe (Hu51) in connection with their analysis of the neutron capture cross section of odd A and even A nuclei. Hence, we neglect pairing energy terms in the daughter nuclei. As a final result, then,

$$W_\beta = B_A(Z_A - Z - 2.5) + 0.5 \begin{cases} +0 & A \text{ odd}, Z \text{ odd} \\ -\tfrac{1}{2}\delta_A & A \text{ even}, Z \text{ even}. \end{cases}$$

This prescription leads if anything to an underestimate of W_β, as indicated above, so that our values for $\tau_\beta \sim W_\beta^{-5}$ may be high by as much as a factor of ten. The term $m_0c^2 = 0.5$ Mev has been added to give the total kinetic plus rest mass energy of the effective beta decay. For $\delta_A/2$ we use the empirical values tabulated by Coryell (Co53). His values of $\delta_A/2$ as a function of A are shown in Fig. VII,2. The resulting values of W_β are given in column 7 of Table VII,2 and have been used to calculate the values of τ_β given in column 8. These in turn have been used to calculate the abundances given in column 10, arbitrarily taking the abundance of $_{52}\text{Te}_{76}^{128}$ near the $N=82$ peak as standard at 1.48 on the Suess and Urey scale. The calculated abundances are shown as a histogram for comparison with Suess and Urey abundances which are plotted as points in Fig. VII,3. The results of the calculations, extended into the range above $A=209$, are shown in Fig. VII,4.

From Fig. VII,3 reasonable but not exact agreement with observed abundances is obtained on the basis of the theory of the r process that has been outlined. The
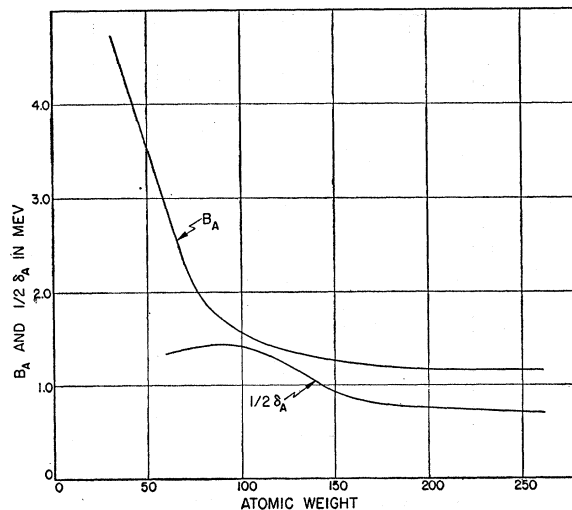
FIG. VII,2. The parameters B_A and $\delta_A/2$ as a function of atomic weight. B_A was calculated by the method described in the text, while $\delta_A/2$ is taken from the work of Coryell (Co53).

break-through values for A were established from the rounding-off points of the three observed abundance peaks ascribed to $N=50$, 82, and 126, respectively. However, the rapid rise in abundance below the peak point is unambiguously given by the rapid decrease in beta-ray energy as the track is held in the Z, A plane to the magic N numbers until break-through is finally attained. The relative abundances of the peaks come out quite well on our calculations, but this can be attributed to our arbitrary choice of the excitation energy, $2B_A$,
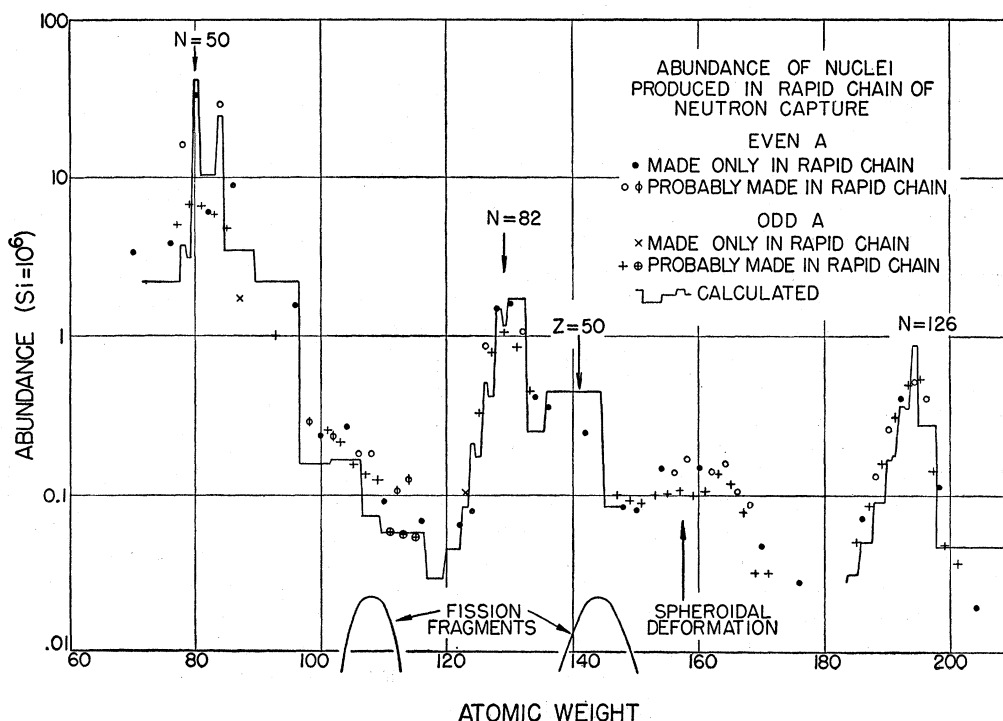
FIG. VII,3. Abundances of nuclei produced in the r process. The empirical points are taken from Suess and Urey (Su56). The histogram is a curve calculated by the methods described in the text. The free parameters have been adjusted to yield the correct relative heights of the three abundance peaks for magic neutron numbers $N=50$, 82, and 126.
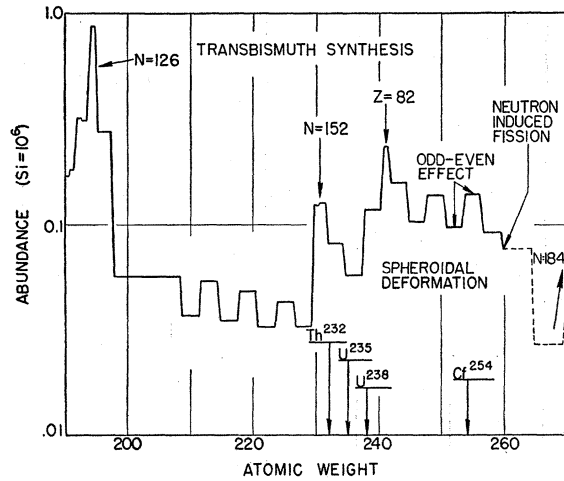
FIG. VII,4. Abundances of heavy nuclei produced in the r process. The method of calculation was the same as that used in calculating the abundance histogram shown in Fig. VII,3. It is assumed that neutron-induced fission terminates the r process at $A=260$.

in the residual nucleus after beta decay. We can conclude as follows: on the basis of the r-process track shown in Fig. V,2 which passes through neutron-rich nuclei with neutron-binding energies of the order of 2 Mev, and on the basis of beta-decay lifetimes for these nuclei computed from reasonable local values for the parameters B_A, Z_A, and $\delta_A/2$, it has been possible to compute a satisfactory caricature of the abundances of those nuclei which have been produced predominantly in the r process.

Let us discuss a few special features of the calculated histogram of Fig. VII,3. In the first place, the $N=50$ peak is really a double peak with maxima at $A=80$ and $A=84$. The empirical validity of this double peaking rests on the ratios $Se^{80}/Se^{82}=33.8/5.98$ and $Kr^{83}/Kr^{84}/Kr^{86}=5.89/29.3/8.94$, determined by the mass spectroscope. Changing the Se/Kr ratio, which might be possible in view of the divergent methods of obtaining their individual abundances, does not lead to a solution of the problem. It is also difficult to question the assignment of these isotopes to the r process. This situation can be caricatured in the r process by (i) letting $A=80$, $Z=30$ be the last nucleus at $N=50$ for which beta decay is followed by only one neutron capture; (ii) letting break-through occur at $A=81$, $Z=31$, with beta decay followed by three neutron captures to $A=84$, $Z=32$, $N=52$; (iii) making this last described nucleus a waiting point followed by only one neutron capture, in keeping with the empirical fact that the binding energy of the 53rd neutron is as small as that of the 51st neutron. Beyond this point the abundance curve trails off gradually as the neutron binding energy for increasing N gradually increases up to $N=82$ and the capture process slowly returns to the off-peak path.

The backside of the $N=126$ peak is very precipitous, in keeping with the fact that the neutron-binding energy

rapidly increases after the drop at $N=126$, and the rapid return to the very neutron-rich nuclei gives a small dZ/dA ($dN/dA\sim1$), a small τ_β, and hence a small abundance. As noted previously, the rapid increase in neutron-binding energy after $N=126$ can be attributed to the fact that the first neutrons in the $N=127$ to $N=184$ shell can distort the closed nucleon shells ($N=126$, $Z=82$) in such a way as to lead to a spheroidal deformation considerably more stable than the spherical shape at the end of the preceding shell. When maximum deformation is reached, further neutron addition does not lead to greater stability, and the neutron-binding energy curve reaches a plateau. This results in the r-process path moving somewhat closer to the stability line in the Z, A plane. This leads in turn to somewhat greater values of τ_β and dZ/dA and thus to a moderate increase in abundance. It is to this spheroidal deformation effect that we attribute the abundance hump from $A=230$ to 260 in Fig. VII,4. Additional discussion of this feature is given in Sec. VIII. We also attribute the abundance hump near $A=160$, which is evident in Fig. VII,3, to this same effect, even though we have not been able to make detailed calculations in this region. It is well known that the stable nuclei in this region show large quadrupole moments consistent with the fact that the most stable forms of the ground states are spheroidal rather than spherical in shape.

The precipitous drop expected on the backside of the $N=82$ peak is masked by the appearance of a peak due to the magic number of protons, $Z=50$. It might be thought that in a neutron capture process, proton magic numbers would be irrelevant. However, a proton magic number does affect the beta-decay lifetime by slowing down the transition to the nucleus containing a proton outside the closed shell. Another way of expressing this is to note that, for example, Z_A does not increase when Z changes from 49 to 50 in Table VII,2, and thus W_β decreases, τ_β increases, and the abundance hump evident at $A=140$ in Fig. VII,3 is to be expected. Since dZ/dA becomes quite small at Z magic, as numerous neutrons are added before decay to the proton in the next shell occurs, we find that the abundance value established at the waiting point ($A=136$) is spread out over a considerable interval of atomic weights up to $A=145$.

C. Time for the r Process: Steady Flow and Cycling

The r-process abundances have been calculated on the assumption that a steady state is reached in which the abundances are proportional to the beta-decay lifetimes at the waiting points. The circumstances under which the steady state is a good approximation can be elucidated by considering the individual beta decay times and total time for the r process. From Table VII,2 Fe^{56}, taken as the source nucleus, rapidly captures some 12 neutrons to produce Fe^{68}, the first waiting point in

the "typical" capture path. Here Q_n is less than Q_o ($\sim$3 Mev in this region) for the first time and beta decay occurs with a lifetime of $\sim$21 sec. This is longer than all the succeeding lifetimes and is in fact $\sim$25% of the total time for the r process. This latter quantity is just the sum of all the τ_β in Table VII,2, plus a rough estimate of 3 sec for the region $A = 150$ to 185, and is therefore $\sim$80 sec. After passing Fe^{68}, the material spends $\sim$40 sec in the $N = 50$ (and 52) peak. Thus the long-lived "source" and first "sink" control the flow for a considerable period during which the heavier, shorter-lived products come into, and remain in equilibrium with, these long-lived predecessors. It is significant that the Fe^{68} lifetime plus the $N = 50$ peak lifetime is long as compared with the 5 to 23 sec lifetimes of Mg^{22}, Na^{21}, etc., which control the production of the neutrons. It is also significant that the total time for the r process is comparable to the $\sim$100-sec expansion and cooling time for the supernova envelope.

From the correspondence of the calculated abundances with those in the atomic abundance distribution, it would seem that this distribution was produced under conditions in which steady flow was just reached and maintained. Other conditions can pertain in different circumstances. The establishment of steady flow requires about 38 neutrons per capturing Fe^{56}, since the average atomic weight in the distribution given in Fig. VII,3 is $\simeq$94. For fewer than 38 neutrons per Fe^{56}, the upper end of the abundance curve will not reach its full value. For a greater number of neutrons, as will certainly be the case in some supernovae, the abundances of high atomic weight will be enhanced over those illustrated in Fig. VII,3. This enhancement occurs over the entire region above $A\sim$110 because of cycling resulting from the neutron-induced fission process near $A\sim$260. For asymmetric fission, one-half of the flow is returned near $A\sim$110 and the full flow is maintained above $A\sim$150. Thus the abundances above $A\sim$110 grow relative to those below $\sim$110, with a factor of two marking the growth above $A\sim$150 relative to that for $A\sim$110 to 150. For a neutron to iron-group abundance ratio $\gtrsim$100, practically all of the original "seed" nuclei will be cycling in the region $A\sim$110 to 260 and increasing in abundance with average atomic weight $A\simeq$174. Under these circumstances the peaks at $N = 82$ and $N = 126$ have about the same abundances, since only one half of the material is returned to the $N = 82$ peak in the cycling. In Sec. XII we consider the case of enhanced production above $A\sim$110 to be typical for certain supernovae.

D. Freezing of the r-Process Abundances

Implicit in our comparison of calculated abundances with those observed is the assumption that the unstable nuclei produced at mass number A in the r process subsequently decay only by beta decay to their stable isobars with the same mass number. This is indeed the predominant final step in the synthesis of a stable nucleus by the r process as the temperature and neutron flux decrease and the r process abundances are "frozen in." In some cases beta decay can occur to a state of the residual nucleus in the final chain of beta decays which is so highly excited that it is unstable to neutron emission. This is similar to the delayed emission of neutrons following fission. Since this mode of decay is not the main one, we have neglected it in our calculations. We note here, however, that delayed neutron emission occurs for even-even nuclei, since the depression of their ground states results in the availability of higher excited states when they are produced. Thus, this process favors odd A production over even A, since some even A mass chains switch to odd by delayed neutron emission. This point tends to compensate for the fact that even A abundances are somewhat greater than odd A abundances before the freezing occurs.

Smart (Sm48, Sm49) suggested, in connection with primordial synthesis of the elements, that (γ,n) reactions compete with negative beta decay in the freezing after a rapid neutron capture process. In this way the shielded isobars could be produced. In stellar synthesis the shielded isobars are produced separately in a second process which we have labeled the s process and which we suggest has occurred during the giant stage of stellar evolution. It is our belief that (γ,n) reactions subsequent to the r process, primordially or in supernovae, cannot have produced the shielded isobar abundances found in the atomic abundance curve.

It has been noted in Sec. VI that the barium isotope ratios and absolute abundances are consistent with p- and s-process production. Let us now consider the difficulties arising in an attempt to explain the observed barium abundances, for example, on the basis of (γ,n) reactions in the freezing of the r process. In the first place the possibility can be considered that the neutron flux suddenly ceases while the temperature is still high and that (γ,n) reactions rather than negative beta decays return the material to the stability line. This would require the ejection of some 10 to 30 neutrons per product nucleus and would obviously be self-defeating in that it would almost restore the original neutron flux. Furthermore it would invalidate the explanation for the r-process peak abundances given in this section and would require double abundance humps to have been produced in the r-process path near $A\sim$100, 140, and 200, for which there are no known reasons.

A more reasonable possibility is that suggested by Smart; after the original very fast beta decays bring the nuclei close to the stability line, the beta lifetimes become long and the (γ,n) process competes in the final adjustments. Thus in the case of barium, material produced at A just greater than 138 might stop, after fast beta decay, in the long-lived unstable barium isotopes $_{56}Ba_{83}^{139}$ (85 min), $_{56}Ba_{84}^{140}$ (12.8 days), and $_{56}Ba_{85}^{141}$ (18 min). Then (γ,n) processes would scour out the

loosely bound 85th, 84th, and 83rd neutrons and pile up the material in $_{56}Ba_{82}{}^{138}$ with its tightly bound 82nd neutron. Some leakage to the lighter isotopes could occur and a general tailing off in abundance from $_{56}Ba_{82}{}^{138}$ to $_{56}Ba_{74}{}^{130}$ would be expected. This is indeed found with the important exception that $_{56}Ba_{74}{}^{130}$ is even slightly more abundant than $_{56}Ba_{76}{}^{132}$, which is not to be expected at all. Furthermore, if the (γ,n) process does occur at barium, why does it not occur for xenon? On the basis of this process one would expect magic $_{54}Xe_{82}{}^{136}$ to be the most abundant of the xenon isotopes, with a tailing off to $_{54}Xe_{70}{}^{124}$. This is not found to be the case. $_{54}Xe_{78}{}^{132}$ is the most abundant isotope of xenon and is 2 to 3 times as abundant as $_{54}Xe_{80}{}^{134}$ and $_{54}Xe_{82}{}^{136}$. On the other hand, this is just what is to be expected if it is supposed that the s and r processes are operating separately. $_{54}Xe_{78}{}^{132}$ is the heaviest stable isotope of xenon which can be produced in the s process, and presumably it has the smallest (n,γ) cross section. $_{54}Xe_{80}{}^{134}$ and $_{54}Xe_{82}{}^{136}$ are made only in the r process, and they are low in abundance in keeping with the general ratio of the r-process abundances to the s-process abundances in this region.

Returning to the case of barium, we must finally emphasize that in the Suess and Urey distribution Ba^{138} is very abundant compared to its neighbors. If it were made by (γ,n) reactions following the r process, this would require an abundance peak in the primary path at A just greater than 138, for which no explanation can be given in terms of known "magic" properties. On the other hand its great production in the s process is understood in terms of its own magic properties.

VIII. EXTENSION AND TERMINATION OF THE r PROCESS AND s PROCESS

A. Synthesis of the Naturally Radioactive Elements

Because of its long time-scale and because it builds through the beta-stable nuclei, the s process is incapable of producing the naturally radioactive elements beyond bismuth. Bismuth $(Z=83)$ is the heaviest of the elements with an isotope which does not decay by electron emission, alpha-particle emission, or fission. As is discussed in detail later, the short-lived alpha-emitting isotopes of polonium, which are produced after bismuth, terminate the s process by cycling its products back to lead.

On the other hand, just because of its short time-scale and because it builds through charge-poor, neutron-rich nuclei, the r process can produce transbismuth elements. These proton-poor nuclei are relatively more stable to alpha emission and fission than their stable isobars at a given A.

A convincing experimental demonstration of this was given by the production of Cf^{254} and other nuclei in the November, 1952, thermonuclear hydrogen bomb test at Bikini, as reported by Fields et al. (Fi56). These nuclei were synthesized by the instantaneous irradiation of U^{238} by an intense neutron flux. The successive addition of neutrons to U^{238} built U^{254} and other neutron-rich uranium isotopes. After the explosion, the U^{254} decayed rapidly to beta-stable Cf^{254}. The Cf^{254} was detected in the test debris through its spontaneous decay by the fission process. The energy release in the spontaneous fission is 220 Mev per decay, which is very large compared to the energy emitted in alpha decay (~ 5 Mev) or beta decay (~ 1 Mev). Fields et al. reported the half-life of Cf^{254} as 55 days. More recent measurements by Thompson and Ghiorso (Th57) yield a preliminary value of 61 days while Huizenga and Diamond (Hu57) have recently obtained a value of 56.2 ± 0.7 days.§ The Cf^{254} is unique in that it is the only beta-stable nucleus which decays predominantly by spontaneous fission with a half-life between a few days and 10^4 years.

The authors and their collaborators (Bu56, Ba56) have associated the r process astrophysically with the explosion of supernovae of Type I. A characteristic feature of supernovae of Type I is that after an initial period of 50–100 days the light curve exhibits an exponential decline corresponding to about 0.0137 magnitudes daily or a half-life of 55 days. The uncertainties in this half-life are discussed in Sec. XII. The close correspondence between this value and that for Cf^{254} suggested that Cf^{254} was produced in the supernova explosion along with the other products of the r process. Because of its large energy release per decay it was supposed in this earlier work that the Cf^{254} would dominate the radioactive energy input into the supernova debris for the order of a year after the original outburst. In the following part of this section we discuss the radioactive decay of the r-process products which give the radioactive energy input for Type I supernovae. The connection between the energy input and the light curve for Type I supernovae is discussed in Sec. XII. The source of the great flux of neutrons required in supernovae has been discussed in Sec. III.

B. Extension and Termination of the r Process

(1) Radioactive Energy Input in Type I Supernovae

Certain of the calculations necessary for computing the radioactive energy release by r-process products have been made by Schuman (Sc57a). He has analyzed the mode of decay and calculated the total decay energy for the longest-lived neutron-rich nuclei produced in each mass chain where the r process extends beyond the stable nuclei $(A > 209)$. His results, modified by new data, are incorporated in Table VIII.1. The total decay

§ The calculations which are described in this section have all been made using a half-life of Cf^{254} of 61 days, since the authors were not aware of the work of Huizenga and Diamond when they were made. Clearly, the value obtained by them is in better agreement with the original result of Baade for the half-life of the light curve of the supernova in IC 4182.

energy includes all subsequent shorter-lived activities which quickly come into equilibrium with the decay listed. Neutrino kinetic energy is not included; 45% of the energy released in each beta decay is assigned to the electrons. In addition we list in Table VIII,1 all mass chains produced in the r process below $A = 209$ which beta decay with maximum half-lives in excess of 3 days. In the table all chains with maximum half-lives less than 3 days are neglected, except for the fast spontaneous fission decays at the end of the table, which are designated (SF) in column 4; (n,f) indicates neutron-induced fission.

Table VIII,1 illustrates the fact that after the rapid beta decays in a given mass chain which immediately follow the termination of an r-process event, the beta-stable nuclei above bismuth decay either by fission to the middle of the periodic table, or by alpha emission and further beta decay to the long-lived nuclei listed. Those above uranium then decay to Th^{232} ($4n$ naturally radioactive series), Np^{237} ($4n+1$ series), U^{238} ($4n+2$ series), and U^{235} ($4n+3$ series), and eventually to Pb^{208}, Bi^{209}, Pb^{206}, and Pb^{207}. The tabulated results confirm the uniqueness of Cf^{254}. It is the only beta-stable, neutron-rich nucleus which decays predominantly by spontaneous fission with a half-life between 10 days and 10^4 years. The table clearly indicates that the energy released by any fission decay exceeds the energy release of any alpha-plus-beta chain by a factor of five, and thus qualitatively the dominance of the radioactive energy release by Cf^{254} is assured.

It is important to consider the empirical evidence which underlies this matter of the uniqueness of Cf^{254}. Ghiorso (Gh55) has presented a graphic display of this evidence by plotting spontaneous fission and alpha-emission half-lives versus neutron numbers for the transuranium nuclei. Ghiorso's diagram is shown in Fig. VIII,1. The spontaneous fission half-lives decrease precipitously in value for all elements beyond the "magic" neutron number $N = 152$. In what way 152 is magic, we discuss below. For $N < 152$, the fission half-lives for a given Z show the characteristic rise with increasing N, to be expected from the well-understood increase in lifetime with decreasing value of the fission parameter, $Z^2/A = Z^2/(Z+N)$ (Bo39). This parameter is proportional to the ratio of the nuclear Coulomb energy to the nuclear surface energy. The alpha-emission half-lives also decrease at $N = 152$, but then recover and resume their normal increase with N, since the essential nuclear bindings increase with N, while the Coulomb energy, upon which the alpha-particle decay energy is linearly dependent, remains essentially constant. The result is the sudden occurrence, within one isotope or two for each element, of spontaneous fission as the predominant mode of decay rather than alpha emission. Ghiorso's diagram, with its ordinate of some 28 factors of ten in half-life, shows that the sudden dominance of this mode of decay occurs over a wide spectrum of half-lives for the various transuranium elements.
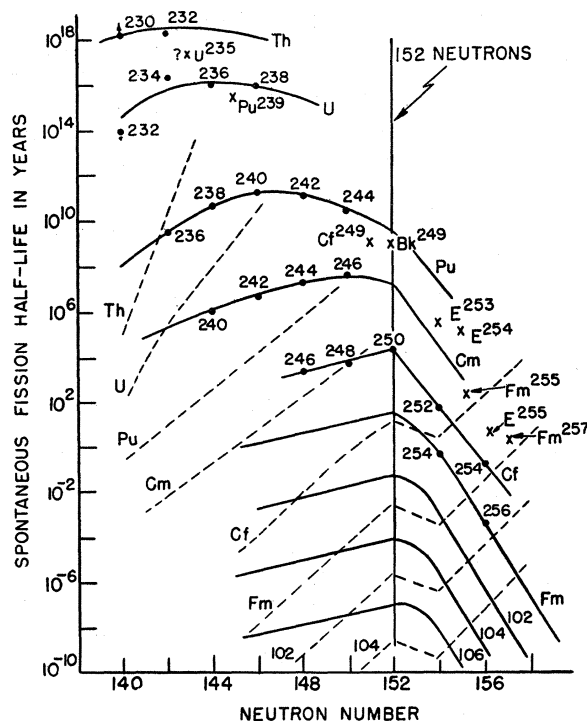
FIG. VIII,1. The analysis by Ghiorso (Gh55) of the spontaneous fission half-life (solid lines) against neutron number. Dotted lines indicate the experimentally observed alpha half-life variation except in the cases of elements 102 and 104.

Only for $_{98}Cf^{254}$ does it occur when the fission lifetime is anywhere near 55 days. For fermium it occurs at Fm^{256} with a fission lifetime of 3 hours (measured), while for curium it occurs at $_{96}Cm^{250}$ with a fission lifetime of 10^4 years (estimated). For the other relevant californium isotopes, Cf^{250} has $t_\alpha = 3 \times 10^4$ years and $t_{SF} = 10^4$ years, so that it decays by spontaneous fission a considerable proportion of the time, while Cf^{252} has $t_\alpha = 2.2$ years and $t_{SF} = 66$ years, so that it decays 3% of the time by spontaneous fission. For Cf^{254}, on the other hand, $t_{SF} = 56$ days while $t_\alpha \geq 100$ years (estimated). The fission activity predominates to the extent that alpha decay has not yet been observed for Cf^{254}.

As an empirical rule the spontaneous fission lifetime for $N \geq 152$ is a function primarily of A. Thus it is 2×10^9 sec for $A = 252$, 5×10^6 sec for $A = 254$, 10^4 sec for $A = 256$, ~ 10 sec for $A = 258$, and $\sim 10^{-3}$ sec for $A = 260$.

To obtain a quantitative measure of the energy released by radioactivity by the products of the r-process event, we must multiply Schuman's calculations and those which we have made of the energy release for each mass chain, by an estimate of the relative production of the fast-decaying progenitor of that chain in the event itself. This is done in Table VIII,1, where the last columns give the total energy released, and the initial energy released measured in Mev/day. In his original calculations Schuman assumed that equal amounts of

TABLE VIII,1. Radioactive energy release of mass chains produced in the r process with half-life >3 days.

A	Element	Longest half-life, seconds, days or years	Decay type	Decay energy Q Mev	Initial abund. n_0 (Si $=10^6$)	Total energy n_0Q Mev	Initial en. rate $0.7\ n_0Q/t^{\frac{1}{2}}$ Mev/day
3	H	12.26y	β	0.01		for reference only	
10	Be	2.7×10^6y	β	0.25		for reference only	
14	C	5600y	β	0.08		for reference only	
32	Si	~300y	β	0.82	50	40.8	~1.1×10^{-4}
33	P	25d	β	0.12	50	5.95	0.165
35	S	87d	β	0.08	50	3.75	0.0299
39	A	260y	β	0.22	50	12.8	9.3×10^{-5}
45	Ca	160d	β	~0.11	1	~0.11	~4.8×10^{-4}
47	Ca	4.7d	β	1.83	100	183	26.9
59	Fe	45d	β	1.36	30	40.8	0.628
60	Fe	~3×10^5y	β	~0.05	30	~0.15	~9.4×10^{-9}
63	Ni	80y	β	~0.03	10	~0.3	~7×10^{-6}
79	Se	7×10^4y	β	~0.08	3.1	~0.248	~6.7×10^{-9}
85	Kr	10.4y	β	0.31	3.4	1.05	1.9×10^{-4}
89	Sr	54d	β	0.66	3.4	2.24	0.0287
90	Sr	28y	β	1.26	2.2	2.77	1.9×10^{-4}
91	Y	58d	β	0.70	2.2	1.54	0.0183
93	Zr	9×10^5y	β	~0.03	2.23	~0.067	~1.4×10^{-10}
95	Zr	65d	β	1.73	2.2	3.81	0.0408
99	Tc	2.1×10^5y	β	~0.13	0.156	~0.02	~1.8×10^{-10}
103	Ru	40d	β	0.6	0.167	0.10	0.0017
106	Ru	1y	β	1.61	0.17	0.274	5.2×10^{-4}
107	Pd	7×10^6y	β	~0.02	0.072	~0.0014	~4×10^{-13}
111	Ag	7.5d	β	~0.5	0.57	~0.28	~0.026
125	Sn	10d	β	~1.2	0.176	~0.21	~0.015
126	Sb	28d	β	~0.9	0.50	~0.45	~0.011
127	Sb	3.88d	β	~0.8	0.42	~0.34	~0.06
131	I	8.05d	β	0.50	1.73	0.865	0.0745
132	Te	3.21d	β	2.5	1.73	4.32	0.933
133	Xe	5.27d	β	~0.2	0.24	~0.048	~0.0063
135	Cs	2×10^6y	β	~0.1	0.244	~0.024	~2.3×10^{-11}
137	Cs	30y	β	~0.55	0.45	~0.25	~1.6×10^{-5}
140	Ba	12.8d	β	~2.4	0.45	~1.08	~0.058
141	Ce	32d	β	~0.27	0.45	~0.12	~0.0026
143	Pr	13.8d	β	~0.42	0.45	~0.189	~0.0095
144	Ce	285d	β	~1.5	0.45	~0.68	~0.0016
147	Nd	11.6d	β	0.45	0.09	0.040	0.0024
151	Sm	80y	β	~0.045	0.09	~0.004	~1×10^{-7}
155	Eu	1.7y	β	~0.12	0.1	~0.012	~1.3×10^{-5}
156	Eu	15d	β	~1.2	0.14	~0.17	~0.0078
161	Tb	7d	β	~0.3	0.15	~0.045	~0.0045
166	Dy	3.42d	β	~1	0.11	~0.11	~0.0223
169	Er	9.4d	β	~0.15	0.1	~0.015	~0.0011
171	Tm	1.9y	β	~0.05	0.05	~0.002	~2×10^{-6}
175	Yb	4.2d	β	~0.23	0.03	~0.007	~0.0011
177	Lu	6.8d	β	~0.2	0.03	~0.006	~6.1×10^{-4}
181	Hf	46d	β	~0.5	0.03	~0.015	~2.3×10^{-4}
182	Ta	112d	β	0.8	0.057	0.046	2.85×10^{-4}
183	Ta	5.2d	β	~0.6	0.03	~0.018	~0.0024
185	W	74d	β	0.19	0.031	0.006	6.0×10^{-5}
188	W	65d	β	1.0	0.09	0.09	9.6×10^{-4}
189	Re	~200d	β	0.1	0.09	0.009	~3.1×10^{-5}
191	Os	16d	β	~0.15	0.18	~0.027	~0.0012
194	Os	~2y	β	1.01	0.88	0.889	~8.4×10^{-4}
196	Ir	9.7d	β	~0.6	0.278	~0.17	~0.012
199	Au	3.15d	β	~0.23	0.056	~0.013	~0.0028
203	Hg	48d	β	~0.23	0.056	~0.013	~1.9×10^{-4}
210	Pb	20y	$\alpha+\beta$	5.8	0.17	0.986	9.36×10^{-5}
222	Em	3.8d	$\alpha+\beta$	23.1	0.034	0.785	0.143
223	Ra	11.6d	$\alpha+\beta$	28.6	0.034	0.972	0.058
224	Ra	3.6d	$\alpha+\beta$	28.7	0.045	1.29	0.248
225	Ra	14.8d	$\alpha+\beta$	27.9	0.045	1.26	0.059
226	Ra	1620y	$\alpha+\beta$	31.6	0.045	1.42	1.66×10^{-6}
227	Ac	22y	$\alpha+\beta$	34.8	0.032	1.11	9.57×10^{-5}
228	Ra	6.7y	$\alpha+\beta$	35.2	0.032	1.13	3.2 ×10^{-4}
229	Th	7300y	$\alpha+\beta$	33.8	0.032	1.08	2.8 ×10^{-5}
230	Th	8×10^4y	$\alpha+\beta$	36.4	0.123	4.48	1.06×10^{-7}
231	Pa	3.4 ×10^4y	$\alpha+\beta$	39.9	0.127	5.07	2.83×10^{-7}
232	Th	1.39×10^{10}y	$\alpha+\beta$	39.3	0.641	25.2	3.43×10^{-12}

TABLE VIII,1.—*Continued.*

A	Element	Longest half-life, seconds, days or years	Decay type	Decay energy Q Mev	Initial abund. n_0 (Si $=10^6$)	Total energy n_0Q Mev	Initial en. rate $0.7\ n_0Q/t_{\frac{1}{2}}$ Mev/day
233	U	1.62×10^5y	$\alpha+\beta$	38.9	0.084	3.27	3.83×10^{-8}
234	U	2.50×10^5y	$\alpha+\beta$	41.2	0.084	3.46	2.63×10^{-8}
235	U	$7.1\ \times10^8y$	$\alpha+\beta$	44.6	0.663	29.6 .	7.93×10^{-11}
236	U	2.39×10^7y	α	4.6	0.167	0.768	6.10×10^{-11}
237	Np	$2.2\ \times10^6y$	$\alpha+\beta$	43.9	0.617	27.1	2.34×10^{-8}
238	U	4.51×10^9y	$\alpha+\beta$	46.3	0.405	18.8	7.90×10^{-12}
239	Pu	2.43×10^4y	α	5.2	0.267	1.39	1.08×10^{-7}
240	Pu	$6.6\ \times10^3y$	α	5.3	0.110	0.583	1.68×10^{-7}
241	Am	$470y$	α	5.6	0.221	1.24	5.01×10^{-6}
242	Pu	3.8×10^5y	α	5.0	0.260	1.30	6.49×10^{-9}
243	Am	$7600y$	$\alpha+\beta$	5.4	0.157	0.848	$2.0\ \times10^{-7}$
244	Pu	7.5×10^7y	$\alpha+\beta$	15.2	0.393	5.97	1.41×10^{-10}
245	Cm	1.1×10^4y	$\alpha+\beta$	11.4	0.430	4.90	8.43×10^{-7}
246	Cm	$4000y$	α	5.5	0.103	0.566	2.69×10^{-7}
247	Cm	$>4\times10^7y$	$\alpha+\beta$	16.3	0.103	1.68	$<7.76\times10^{-10}$
248	Cm	4.3×10^5y	α, SF(10%)	23.4	0.236	5.52	2.62×10^{-8}
249	Cf	$470y$	α	6.3	0.139	0.876	3.45×10^{-6}
250	Cm	7.5×10^3y	α, SF(75%)	170	0.139	23.6	5.97×10^{-6}
251	Cf	$700y$	α	6.2	0.236	1.46	3.96×10^{-6}
252	Cf	$2.2y$	α, SF(3%)	12.9	0.097	1.25	0.0011
253	E	$20d$	$\alpha+\beta$	6.7	0.188	1.26	0.0436
254	Cf	61 or $56.2d$	SF	220	0.139	30.6	0.349
255	E	$24d$	$\alpha+\beta$	7.3	0.139	1.01	0.0292
256	All	$\sim10^4s$	SF	$\cdots$	$\cdots$	$\cdots$	$\cdots$
257	Fm	$\sim10d$	α, SF(6%)	18.5	0.091	1.68	~0.116
258	All	$\sim10s$	SF, (n,f)	$\cdots$	$\cdots$	$\cdots$	$\cdots$
259	All	$\sim10s$	SF, (n,f)	$\cdots$	$\cdots$	$\cdots$	$\cdots$
260	All	$\sim10^{-2}s$	SF, (n,f)	$\cdots$	$\cdots$	$\cdots$	$\cdots$

odd A nuclei were produced, and that equal amounts of even A nuclei were produced, and that the ratio of production of odd to even A was 1:3. We feel that this assumption can be improved upon by using the results of Table VII,2. Table VII,2 includes the abundances which we have calculated for the r process in the range $A=71$ to 209. Estimates to be discussed later have been made for $A\leq70$. Above $A=209$ we include our calculations for the production of transbismuth mass numbers using exactly the same methods as those which were employed to calculate the abundance histogram shown in Fig. VII,3. The extended results are shown graphically in Fig. VII,4.

Some comments on the calculations above $A=209$ are appropriate. No guiding landmarks such as the observed magic number peaks are available above $A=209$. On the other hand, the relative masses of the nuclei near the beta-stable region are quite well established through extensive measurements of the alpha- and beta-decay energies of the naturally occurring and artificially produced radioactive nuclei from $A=210$ to ~260. This is amply demonstrated by the smoothness of the neutron binding energy excess curve shown in Fig. VII,1 for neutron numbers above $N=126$. The general increase in the neutron binding energy following the closure of the $N=126$ shell is apparent, as well as the rapid and considerable enhancement of stability which is to be attributed to the ability of the nucleons in nuclei with $N>126$ to take up spheroidal as con-

trasted to spherical distributions. The loss in neutron stability, after the maximum spheroidal deformation is reached at $N\sim140$ to 150, leads to a pseudo-shell effect|| near $N=152$ for which there is considerable experimental evidence (Fig. VIII,1) in the sudden onset of spontaneous fission itself at this neutron number. The decrease in neutron binding energy leads to increased nuclear masses, and the energy available for fission suddenly increases. This increase, coupled with the already deformed shape which is the first step toward fission, leads to the catastrophic decline in spontaneous fission lifetimes.

Referring to Fig. VIII,3, the calculated and observed abundance curves just above the $N=126$ shell peak at $A=194$ show the precipitous drop expected from the rapid return to stability arising from the fact that the first neutrons in the $N=126-184$ shell deform these nuclei spheroidally. The greater neutron binding energy in the beta-stable region means that neutrons are readily captured, and that the capture path at $Q_n\sim2$ Mev passes through nuclei far removed from the stability line, the beta-decay energy at waiting points is enhanced, and the lifetimes and the resulting abundances are decreased $(A=200$ to $A=230)$. Eventually, however, the maximum deformation is passed, and at $N=152$ the neutron binding energy is decreasing rapidly

---

|| The next magic number expected after 126 on the shell model with strong spin-orbit splitting is $N=\frac{1}{3}[(n+1)^3+5(n+1)]=184$ for the $n=7$ shell.
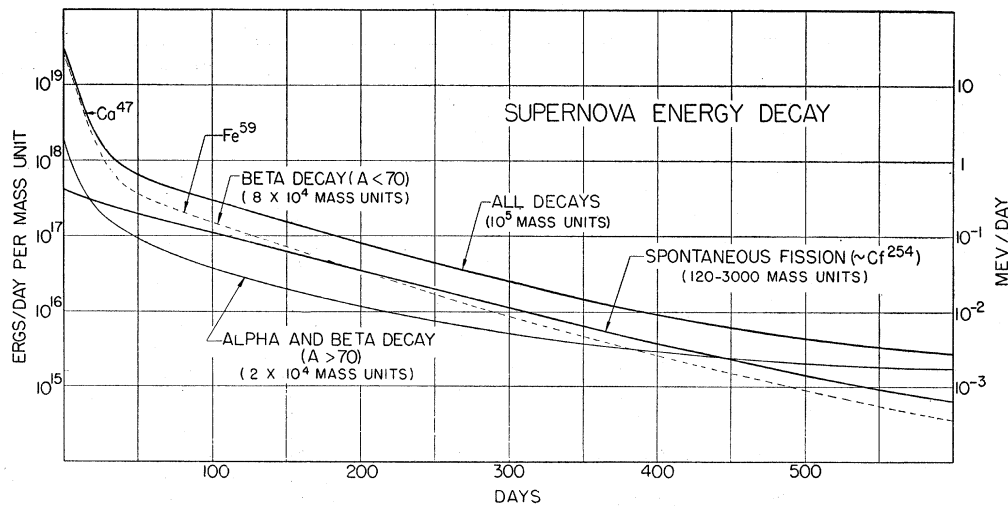
FIG. VIII,2. The radioactive energy release of the products of the r process. Radioactivity with half-lives less than 3 days has been neglected. Individual curves are shown for the beta decays of products with $A < 70$, for alpha and beta decay for the products with $A > 70$, for the products which decay by spontaneous fission, for the sum of all of these cases, and for Fe[59] alone. The label for each curve includes the total mass in atomic mass units which produces the energy release measured in Mev/day on the right-hand ordinate. The scale of energy release in ergs/day, given in the left-hand ordinate, is for an amount of material measured in grams and equal numerically to the number of mass units indicated.

(Fig. VII,1), the r-process path moves toward the stability line, the beta decay waiting energy decreases, and the broad hump in the abundance curve from $A = 230$ to ~ 260 corresponding to $N = 152$ to 170 occurs. Included in this abundance hump is the progenitor of Cf[254] at $A = 254$. Superimposed on this broad hump is the minor peak expected at the closure of the $Z = 82$ shell. Our calculations do not take into account the influence of the closing of the proton shell at $Z = 82$ upon the neutron spatial distribution, which may tend to become more spherical at this point. This effect may well enhance, for the neutron-rich nuclei, the pseudo-shell effects at $N = 152$, since some nuclei which lie in the r-process path fall close to having $N = 152$ and $Z = 82$ simultaneously.

Above $N = 170$, $A = 260$ the closing of the shell as N advances toward 184 would be expected to yield a deep minimum in the abundance curve just before a rise to another major peak at $N = 184$, $A \sim 280$. However, the r process terminates before this minimum and subsequent rise can occur. This is because of the onset of neutron-induced fission (n,f) near $A \sim 260$, which will become more probable than neutron capture (n,γ) and will shunt the r-process products back to the middle of the periodic table at $A \sim 110$ and ~ 150, if we assume that asymmetric fission is the rule. These fission fragments are swept up in the general flow of the r process and in this way a cycling, steady flow will be established.

The sudden onset of neutron-induced fission is to be expected for exactly the same reasons as those previously enunciated to explain the onset of spontaneous fission. Even if neutron-induced fission were ignored, the 10^{-3} sec spontaneous fission lifetime will destroy the $A = 260$ progenitors in an explosion for which the time-

scale is 10–100 seconds. Even the mass chains at $A = 257$, 258, 259 may not be produced in full measure. The onset of neutron-induced fission is delayed until $A \simeq 260$ only because the r process builds through neutron-rich nuclei for which the fission-inducing parameter Z^2/A is abnormally low, and also because the average neutron energy is moderately low $(kT \sim 100$ kev at $T \sim 10^9$ degrees). These last points constitute the central explanations underlying the difference between the fission decay curve of the californium fraction of the Bikini thermonuclear debris and the energy input curve expected for a Type I supernova. In the Bikini debris the 2.2-year Cf[252] activity dominated the fission decay curve after about 200 days (Fi56) and indicated that 50 times as much Cf[252] was produced as Cf[254]. This factor of 50 is required because Cf[252] decays only 3% of the time by spontaneous fission. In the thermonuclear test the capture path started with U[238] and was limited to the neutron-rich isotopes of uranium $(Z = 92)$ even as it built through the progenitors of the beta-stable californium isotopes at 252 and 254. For the r process we see from Table VII,2 and Fig. V,2 that $Z = 87$ and 88 at $A = 252$ and $A = 254$, respectively. Thus, the progenitors in the Bikini explosion had relatively higher Z and were more susceptible to neutron-induced fission as compared to neutron capture than are the progenitors in an r-process event. In addition, they were almost certainly subject to a neutron flux containing a high-energy component in the many Mev range and for this reason interacted relatively more often through fission than through capture. The result was certainly that the Bikini synthesis of the neutron-rich uranium isotopes (which ultimately decay to Cf[252], Cf[254], etc.) occurred only through an infrequent (1–10%) capture

event relative to fission at each mass number in the build-up from $A = 238$ to 254. This competition with fission explains in a very plausible manner why, even though the high-energy neutron-capture cross section remained constant at the geometrical size of the neutron-rich isotopes of uranium, yet the relative synthesis must have decreased markedly with increasing A so as to have produced Cf^{254} only in the observed 2% of the amount of Cf^{252}. Thus, in the fission decay curve of the Bikini californium fraction, the Cf^{252} decay with its 2.2-year half-life should dominate, as it does, after about 200 days. This will not at all be the case in the r process where, as shown in Table VII,2, Cf^{252} and Cf^{254} are produced in the ratio of 0.097 to 0.139, essentially one to one.

We now return to the quantitative calculation of the radioactive energy decay curve which follows an r-process event. In Fig. VIII,2 is shown the energy release in ergs/day as a function of time for (i) the beta decays of nuclei with $A < 70$, (ii) the alpha and beta decays with $A > 70$, (iii) the spontaneous fission decay, and (iv) the total sum for these three cases. This figure is based on the calculations given in Table VIII,1, and these in turn are based on the abundance distribution for steady-state flow but without cycling from $A = 110$ to 260. Figure VIII,2 thus represents the radioactive energy decay curve for an r-process event, such as might take place in a supernova outburst, which would have produced the atomic abundance distribution of Figs. VII,3 and VII,4 plus an extension to atomic weights below $A = 70$. The main contributions to the energy release after the first few days through the first two years come from Ca^{47}, Fe^{59}, Ra^{228}, Cf^{252}, and Cf^{254}. These contributions are summarized in Table VIII,2.

Figure VIII,2 shows that the total energy release parallels the spontaneous fission release from 50 to 450 days. The spontaneous fission release during this period is almost entirely due to Cf^{254}. In the labels for each curve in Fig. VIII,2 we also include the total mass, in atomic mass units, involved in the production of each of the three types of decay given as (i), (ii), and (iii) above. Thus, the alpha- and beta-decay energy for $A > 70$ in Mev/day (right-hand ordinate) is that for 2×10^4 atomic mass units of material which has been computed by multiplying the abundances of Table VII,2 by the appropriate atomic weights, A, and summing over $A > 70$. In the left-hand ordinate we have obtained the energy release in ergs/day for the same numerical amount of material in grams by multiplying by 1.6×10^{-6} erg/Mev and dividing by 1.66×10^{-24} gram/atomic mass unit. The number of mass units producing the beta decay for $A < 70$ is estimated to be 8×10^4 by extending the calculations of Table VII,3 in an approximate manner to $A < 70$. Two estimates are given for the amount of mass associated with the spontaneous fission curve. If only the Cm^{250}, Cf^{254}, and Fm^{257} which actually undergo fission are counted, the total mass is some 120 atomic mass units. However, it is not possible to suppose that these fissionable products are produced alone and thus for another estimate we associate with them the production of all of the mass chains above $A = 110$. This is the appropriate model for the situation discussed previously in which the neutron flux is great enough to move all of the material into the region $A = 110$ to 260 and cycle it there. The yield from $A = 110$ to 150 must be multiplied by one-half because only half of the fission fragments return to this region.

These considerations show that the energy release per gram of r product is much greater for fission than for alpha and beta decay. This is illustrated graphically in Fig. VIII,3 where the energy release is plotted for three different cases in which the same amount of material, namely, 1% of a solar mass (2×10^{31} g), is converted to r products. In Fig. VIII,3 the ordinate has been expressed in absolute magnitude with zero magnitude corresponding to 2.3×10^{40} ergs/day; this is done to facilitate comparison with actual supernova light curves which are shown and discussed in Sec. XII. A total

TABLE VIII,2. Principal radioactive decays of Table VIII,1.

A	Element	Longest half-life, days or years	Decay type	Decay energy Q Mev	Initial abund. n_0 (Si $=10^6$)	Total energy n_0Q Mev	Initial en. rate $0.7\ n_0Q/t_{\frac{1}{2}}$ Mev/day
33	P	$25d$	β	0.12	50	5.95	0.165
47	Ca	$4.7d$	β	1.83	100	183	26.9
59	Fe	$45d$	β	1.36	30	40.8	0.628
85	Kr	$10.4y$	β	0.31	3.4	1.05	1.9×10^{-4}
89	Sr	$54d$	β	0.66	3.4	2.24	0.0287
91	Y	$58d$	β	0.70	2.2	1.54	0.0183
95	Zr	$65d$	β	1.73	2.2	3.81	0.0408
131	I	$8.05d$	β	0.50	1.73	0.865	0.0745
140	Ba	$12.8d$	β	$\sim$2.4	0.45	$\sim$1.08	$\sim$0.058
144	Ce	$285d$	β	$\sim$1.5	0.45	$\sim$0.68	$\sim$0.0016
194	Os	$\sim$2y	β	1.01	0.88	0.889	$\sim$8.4$\times 10^{-4}$
225	Ra	$14.8d$	$\alpha+\beta$	27.9	0.045	1.26	0.059
228	Ra	$6.7y$	$\alpha+\beta$	35.2	0.032	1.13	3.2×10^{-4}
250	Cm	7.5×10^3y	α, SF(75%)	170	0.139	23.6	5.97×10^{-6}
252	Cf	$2.2y$	α, SF(3%)	12.9	0.097	1.25	0.0011
254	Cf	61 or $56.2d$	SF	220	0.139	30.6	0.349
257	Fm	$\sim$10d	α, SF(6%)	18.5	0.091	1.68	$\sim$0.116
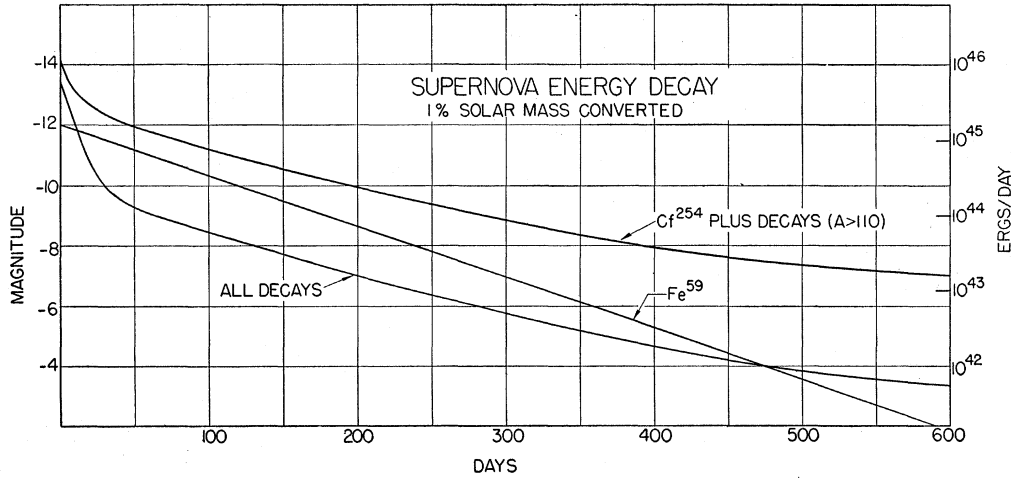
FIG. VIII,3. The radioactive energy release of the products of the r process calculated by assuming that one percent of a solar mass (2×10^{31} g) of these products is produced. Three cases are illustrated; (i) the energy release for all alpha, beta, and fission decays in relative abundances similar to those found for r-process products in the atomic abundance curve, (ii) the energy release for an extreme r-process event in which all of the converted material is moved into the region above $A = 110$ and cycled there, and (iii) the energy release from Fe^{59}, when this isotope is produced in maximum quantity in a process in which only a few neutrons are made available per iron group nucleus. Compare with Fig. XII,1.

mass of one percent of a solar mass is taken simply as a reference point in this diagram. The total mass necessary to be converted to produce the observed light curves of supernovae is discussed for two specific cases, the Crab Nebula and the supernova in IC 4182, in Sec. XII.

The three cases which have been treated in Fig. VIII,3 are as follows. One case is the energy release for all activities in equilibrium with half-lives greater than 3 days, produced in an r process which would give an abundance distribution similar to that necessary to account for the r-process isotopes in the atomic abundance curve. This would occur, as indicated previously, if steady flow was achieved but no cycling occurred in the region above $A = 110$. Another case illustrated is the energy release just for the activities produced above $A = 110$. This is then the type of energy curve expected for a supernova in which the neutron flux was so great that all of the converted material was pushed into the region above $A = 110$ and cycled there (one half cycling $A = 110$ to 150). In this curve the Cf^{254} fission decay dominates the curve from 56 to 450 days but other activities take over after 450 days. The relation between this energy decay curve and the light curve of the supernova in IC 4182, which was observed for about 600 days after maximum, is also considered in Sec. XII.

The third case shown in Fig. VIII,3 is one calculated for the special case in which only a few neutrons are made available per iron group nucleus. In this case the most important activity produced is that of Fe^{59}, which has a half-life of 45 days. It is produced in maximum abundance when $n_c/Fe^{56} = 3$, in which case 20% of the Fe^{56} is converted into Fe^{59} (Fo55a, Appendix II) and the remainder into nearby nuclei. The conditions under

which the decay curve produced by Fe^{59} could explain an observed supernova light curve are discussed in Sec. XII, although from the astrophysical standpoint we do not consider this to be a very likely occurrence.

(2) Abundance Yield in the r Process below $A = 70$; the Production of Titanium; Discussion of Short-Period Radioactivity Following the r Process

We have postponed to this point discussion of our estimate for the r-process yields below $A = 70$. Two important activities, 4.8-day Ca^{47} and 45-day Fe^{59}, occur in this region. We have mentioned Fe^{59} above in discussion of a rather special possibility. Here we discuss its production in a steady-state r process similar to that discussed in Sec. VII when the abundances above $A = 70$ were calculated. There is one important difference, however. When Fe^{56} is taken as the starting point (infinite source) in the r process, the first waiting point is at $A = 68$, and no production below this atomic weight is achieved. Thus, the source material for building isotopes below $A \sim 70$ must be the light elements rather than the iron group elements. This leads to considerable uncertainty in estimating the r-process yields below $A = 70$.

Another reason why detailed calculations have not been made on the r process below $A = 70$ is the fact that the s, e, and α processes are the major contributors in this region. Only for S^{36}, Ca^{46}, and Ca^{48} in this region is there no other method of production than the r process. It is also possible that Ti^{47}, Ti^{49}, and Ti^{50} should be assigned to this process. All of these isotopes except Ca^{46} have abundances ~ 100 (Su56). Thus empirical data in this region are lacking. Although good mass data are

available, we have hesitated to use our expression for the effective W_β for light nuclei in calculating τ_β and hence abundances, since it assumes a high density of levels in the daughter product. Since the abundance is proportional to W_β^{-5}, one can expect considerable fluctuations for the r-process products. This may explain the behavior illustrated by the abundance ratios $Ca^{46}:Ti^{47}:Ca^{48}=1.6:189:88$. An abundance peak for $N=28$ in the r process might be expected at somewhat lower A, and thus the abundance of Ca^{46} seems definitely low and must be attributed to a fluctuation in the value of W_β at the progenitor for $A=46$. Ti^{47} may also be produced in the s process or possibly in the e process. The abundance produced in the s process should be considerably less than the abundances of Sc^{45} and Ti^{46}, which are 63 and 194, respectively, since the s process is dropping rapidly in this region. It should also be produced less abundantly than $Ti^{46}(194)$, $Ti^{49}(134)$, and $Ti^{50}(130)$ in the e process. Thus it would seem reasonable to attribute to the r process a part of the mass-chain at $A=47$ comparable in abundance to Ca^{48} rather than to the abnormally low Ca^{46}. Ca^{47} is in this chain and we round off its abundance to about 100 as given in Table VIII,1. As indicated in Fig. VIII,2, this gives rather a large contribution in the early part of the energy decay curve. However, as discussed in Sec. XII, the early part of the supernova light curve may not be simply a radioactive energy decay curve, since it may represent cooling of the expanding envelope for a short period after the explosion.

The amount of production of the mass-chain at $A=59$, and of Fe^{59} in particular, is very difficult to estimate. We can expect that the nucleus produced directly in the r process might have $Z=20$. An atomic abundance estimate of 30 is a reasonable value. The energy release in the decay of the Fe^{59} is slightly larger than that in the decay of the Cf^{254} when the atomic abundance yield of the Fe^{59} is assumed to be 30. The abundances are in the ratio $30/0.139\simeq220$ while the energy release ratio is $1.35/220=1/160$. The Ca^{47} energy release is ~5 times that of Cf^{254}. This, of course, will not be the case in a supernova in which a large ratio of neutrons to iron is available and only activities with $A>110$ are produced. However, this illustrates the fact that in any case the energy release in the Cf^{254} is only a small part of the *total* energy release from the radioactivity following a supernova explosion. In each mass-chain there will be very rapid beta decays releasing some 10 Mev in beta-ray energy. We estimate that the Cf^{254} is only about 0.05 to 0.5% by number of all the nuclei produced in the r process. Thus the total energy released radioactively is 10 to 100 times that from Cf^{254} but is emitted within a matter of a few minutes or hours of the initial explosion. The main point is this: If the Cf^{254} release is $\sim10^{47}$ ergs, which is a reasonable estimate, then the total radioactive energy release will be 10^{48} to 10^{49} ergs. This is indeed a large value, but it does not exceed the total energy available, some 10^{50} ergs,

from the hydrogen and helium reactions which take place in the envelope of the supernova.

(3) Abundance of Fission Fragments Produced in the r Process

At this point a remark concerning the contribution of fission fragments to the atomic abundance distribution is in order. Termination of the r process by very rapid spontaneous fission and neutron-induced fission during the supernova explosion will occur at $A\sim260$, $Z\sim90$. Fission of such neutron-rich nuclei will probably result in the production of more neutrons than are observed for beta-stable nuclei; we estimate ~6. On the assumption that the fission is asymmetrical in charge and mass we then expect fragments which are spread about $A\sim108$, $Z\sim38$, and $A\sim146$, $Z\sim52$, as shown diagrammatically in Fig. V,2, although we have rounded off these numbers to $A=110$ and 150 in preceding discussions. The neutron-rich fragments are very similar to the nuclei involved in the capture path and are swept up into the r process and do not produce any particular effects near $A\sim108$ or 146. They tend to cycle material above $A\sim108$ and to establish steady-state abundances in this region, even though they are far from the iron group elements and light elements with which the synthesis starts. The neutrons released in the fission are recaptured as the r process proceeds.

On the other hand, the ultimate decay by spontaneous fission of Cm^{250}, Cf^{252}, Cf^{254}, and Fm^{257} produces a total yield of both light and heavy fragments equal to $0.75\times0.139+0.03\times0.097+0.139+0.06\times0.091=0.252$ on the $Si=10^6$ scale (see Tables VII,2 and VIII,1). This abundance is spread out over the usual distribution in fragments and the peak yield can be expected to be about 8% of the total or about 0.020. This is illustrated graphically in Fig. VII,3, where it will be noted that the fission fragment abundance is small compared to that produced directly in the r process.

C. Age of the Elements and of the Galaxy

Transuranium elements are produced by the r process. Those with atomic weights of the form $235+4m$, $m=0, 1, 2, 3\cdots$ are progenitors of U^{235} provided alpha decay is more probable than fission. From Table VIII,1 this appears to be the case for $m\leq5$ but for $m>5$ it seems that fission must dominate. Thus there are six progenitors of U^{235} at atomic weights 235, 239, 243, 247, 251, and 255. The number of progenitors of U^{238}, of atomic weights $238+4m$, is even more restricted. As can be seen in Table VIII,1 the beta-stable nuclei at $A=238$, 242, and 246 decay by alpha emission while that at $A=250$ decays 25% of the time by alpha emission and 75% by fission. Starting with Cf^{254}, nuclei of atomic weights 254, 258, etc., decay predominantly by fission. This information is summarized in Table VIII,3, where we also list the progenitors of the other parents of the radioactive series, Th^{232} and Np^{237}.

TABLE VIII,3. Production of parents of radioactive series; progenitors decaying by alpha emission rather than spontaneous fission.

Half-life	$_{90}Th^{232}(4n)$ 1.39×10^{10}y		$_{93}Np^{237}(4n+1)$ 2.2×10^{6}y		$_{92}U^{238}(4n+2)$ 4.51×10^{9}y		$_{92}U^{235}(4n+3)$ 7.13×10^{8}y	
	A	Yield	A	Yield	A	Yield	A	Yield
	232	0.084	237	0.057	238	0.110	235	0.057
	236	0.057	241	0.221	242	0.157	239	0.110
	240	0.110	245	0.103	246	0.103	243	0.157
	244	0.157	249	0.139	250(25%)	0.035	247	0.103
	248	0.139	253	0.097			251	0.097
	252(97%)	0.094					255	0.139
Total yield		0.641		0.617		0.405		0.663

Ratio U^{235}/U^{238}=0.663/0.405=1.64
Th^{232}/U^{238}=0.641/0.405=1.58

If the abundances produced by the r process were the same for all progenitors, the ultimate abundance of U^{235}, after alpha and beta decays at 239, 243, etc., would exceed that of U^{238} by a factor of 6/3.25=1.85. Calculations discussed in the previous sections make it possible to improve upon this factor by totaling the yield of the progenitors for the individual radioactive parents, U^{235}, U^{238}, and Th^{232}, Np^{237} as well. Yields for the progenitors and the totals after alpha and beta decay are given in Table VIII,3. The ratio of U^{235}/U^{238} produced by the r process and subsequent decay is 1.64, slightly less than the ratio of the number of progenitors. This is to be expected since the even-A progenitors of U^{238} will individually be produced in greater abundance than the odd-A progenitors of U^{235} because of the even-odd pairing term which decreases the beta-decay energy of even-A waiting points and thus increases even-A waiting point abundances. This effect is most clearly demonstrated by the calculations in Sec. VII which show peaks at $A=130$ and 194, where each A is a waiting point. We digress, in order to discuss this effect more fully.

For the $A=130$ peak, results of the calculations given in Table VII,2 are that $W_\beta=11.46$, 9.30, and 9.61 Mev at $A=125$, 126, and 127, respectively. For $A=126$ the value would have been $W_\beta=10.50$, i.e., it would have been intermediate between the values for 125 and 127, if we had not subtracted $\delta_A/2=1.20$ Mev from this value. The calculated abundances were then found to be 0.18, 0.50, and 0.42, and these values must be compared with the observed values for Te^{125}, Te^{126}, and I^{127}, i.e., 0.328, 0.874, and 0.80. The computed values are low but are relatively correct. Empirically, we can estimate the even-odd pairing effect from 2Te^{126}/(Te^{125}+I^{127})=1.55. The main uncertainty in this calculation arises from the uncertainty in the abundance ratio of tellurium to iodine.

Three osmium isotopes are produced in the rising portion of the $A=194$ peak. Using $\delta_A/2=0.78$ Mev, we find that $W_\beta=13.06$, 13.14, and 11.54 Mev at $A=188$, 189, and 190, respectively. The predicted abundances are then 0.09, 0.09, and 0.17, and these are in good agreement with the observed abundances of Os^{188}, Os^{189}, and Os^{190}, which are 0.133, 0.161, and 0.264, respec-

tively. In this case, on the basis of relative isotopic abundances alone, the even-odd pairing term is given by (Os^{190}+Os^{188})/(2×Os^{189})=1.23. Incidentally, the observed abundance ratio of the two osmium isotopes Os^{190}/Os^{188}=1.98 represents a substantial check on our calculated abundances (proportional to W_β^{-5}), which give a ratio of 1.85. This agreement indicates that our choice of parameters B_A and Z_A and our use of $W_\beta=B_A(Z_A-Z-2.5)$+pairing term has some empirical validity. Off the abundance peaks, the even-odd effects are not so clear cut in our method of calculation, since odd-A nuclei can result from even-A waiting points and vice versa. However, there is some correlation along even and odd lines as is clear from a perusal of Table VII,2.

An even-odd effect of 1.13 yields the change from 1.85 to 1.64 discussed above for the uranium isotopes, and this seems to be a reasonable value. It neglects the effect of delayed neutron emission from excited states of the nuclei in the decay of the various mass chains to their stable isobars. This is a small effect, but does give some transfer of even-A material to odd-A material since the most highly excited states result in beta transitions from odd Z-odd N-even A nuclei to even Z-even N-even A nuclei. If the even-odd effect were as high as 1.55, as it is at the $A=130$ peak, the production ratio would be 1.20. By a selective choice of parameters entering into our calculation the ratio could be reduced in extremum to a value as low as unity. It is our considered opinion that it is highly unlikely for the ratio to be less than this value. A reasonable value for an upper limit would be 2.

With these estimates of the production ratio of U^{235}/U^{238} in the r process, we are now able to calculate the age of these uranium isotopes (and by inference of the other r-process isotopes) using their presently observed terrestrial abundance ratio.

(i) Let us suppose that all of the uranium were produced in a single r-process event (e.g., one supernova) at one moment of time, $t_0\times10^9$ years ago. Then, using a present-day ratio of U^{235}/U^{238}=0.0072, and using half-lives of 7.13×10^8 years and 4.51×10^9 years for U^{235} and U^{238}, respectively, we have the following equa-

tion for the abundance ratio U^{235}/U^{238} as a function of t_0

$$\frac{U^{235}(t_0)}{U^{238}(t_0)}=0.0072\times 2^{t_0[(1/0.713)-(1/4.51)]}=0.0072\times 2^{1.18t_0}.$$

This relationship is plotted in Fig. VIII,4. At the formation of the solar system 4.55×10^9 years ago U^{235}/U^{238} $=0.29$, which is definitely below the lower limit of unity for the production ratio discussed above. We find $U^{235}/U^{238}=1$, 1.64, and 2 at $t_0=6.0$, 6.6, and 6.9×10^9 years, respectively. Our best value for the time of a single-event synthesis of U^{235} and U^{238} is thus 6.6×10^9 years ago. If these isotopes were produced in a single supernova, this is its date. For each change of a factor of two in the production ratio of the uranium isotopes, this figure changes by 0.85×10^9 years.

There is some confirmatory evidence for the above calculations in the Th^{232}/U^{238} abundance ratio, which is, however, much more uncertain than the U^{235}/U^{238} ratio. Suess and Urey estimate that the present-day ratio $Th^{232}/U^{238}=3$ to 3.5. Our production ratio is $0.641/0.405=1.58$. From these data we find $t_0=6.2$ to 7.7×10^9 years. This time estimate is obviously quite sensitive to the value taken for the present thorium to uranium ratio but is not inconsistent with the value of t_0 obtained from the U^{235}/U^{238} ratio.

(ii) Alternatively, let us consider the problem on the basis that production of uranium started a time $t_0\times 10^9$ years ago and that, instead of production being confined to just one moment, production took place at a constant rate until a time $t_1\times 10^9$ years ago, after which no more production occurred. This model corresponds to production in a series of supernovae with uniform mixing of their products over the interval t_0 to t_1. Let $U^{235}(t)$ and $U^{238}(t)$ be the abundances at any time, t, and let λ_{235} and λ_{238} be the production rates taken as independent of time. If t is taken as the time measured backward from the present epoch, we then have

$$\left.\begin{array}{l}-\dfrac{dU^{235}(t)}{dt}=\lambda_{235}-\dfrac{0.693}{0.713}U^{235}(t)\\[2ex]-\dfrac{dU^{238}(t)}{dt}=\lambda_{238}-\dfrac{0.693}{4.51}U^{238}(t)\end{array}\right\}\ \ t_0\geq t\geq t_1.$$

These equations taken together with the boundary conditions

$$U^{235}(t_0)=U^{238}(t_0)=0$$

integrate to give

$$\frac{U^{235}(t)}{U^{238}(t)}=\frac{0.713\lambda_{235}[1-2^{-[(t_0-t)/0.713]}]}{4.51\lambda_{238}[1-2^{-[(t_0-t)/4.51]}]}\ \ t_0\geq t\geq t_1.$$

This result, together with the condition that the free decay of U^{235} and U^{238} from t_1 to the present day must yield a ratio equal to 0,0072, determines the following
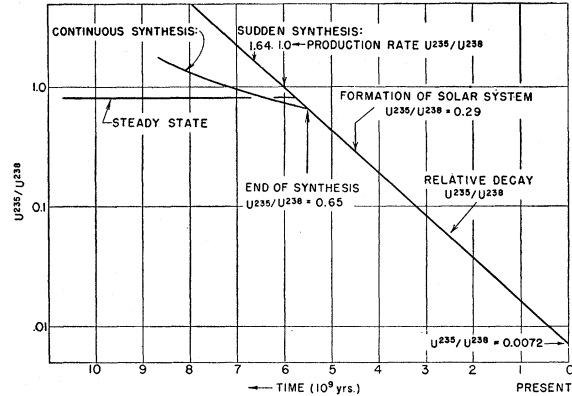

FIG. VIII,4. The ratio U^{235}/U^{238} as a function of time. This curve has been employed to determine the age of terrestrial uranium by the method described in Sec. VIII C.

relation between t_1 and t_0

$$\frac{U^{235}(0)}{U^{238}(0)}=\frac{0.713\lambda_{235}[1-2^{-[(t_0-t)/0.713]}]2^{-t_1/0.713}}{4.51\lambda_{238}[1-2^{-[(t_0-t)/4.51]}]2^{-t_1/4.51}}=0.0072.$$

With

$$\lambda_{235}/\lambda_{238}=1.64,$$

this reduces to

$$\frac{[1-2^{-[(t_0-t_1)/0.713]}]}{[1-2^{-[(t_0-t_1)/4.51]}]}\times 2^{-1.18t_1}=\frac{0.0072\times 4.51}{1.64\times 0.713}=0.0278.$$

The values of t_0 corresponding to a set of values of t_1 are given in the following tabulation, along with values of $U^{235}(t_1)/U^{238}(t_1)$:

t_1 (in 10^9 years)	4.5	5.0	5.5	6.0	6.6
t_0 (in 10^9 years)	18	11.5	8.5	7.4	6.6
$U^{235}(t_1)/U^{238}(t_1)$	0.29	0.43	0.65	0.98	1.64

The computed value for t_0 is very sensitive to t_1 if t_1 is chosen near the time of formation of the solar system at about 4.5×10^9 years ago. On the other hand, t_0 does not change rapidly once t_1 exceeds 5.5×10^9 years ago, since t_0 must equal t_1 at 6.6×10^9 years, the computed time for a single-event synthesis. Evidence on the time interval between nucleogenesis and the formation of the meteorites of the solar system has been given by Wasserburg and Hayden (Wa55b). Following Suess and Inghram they argue that Xe^{129} would be abnormally abundant in meteorites if the meteorites crystallized before I^{129}, with an observed half-life of 1.7×10^7 years, had all decayed. They did not find abnormal amounts of Xe^{129} in the Beardsley chondrite and concluded that it crystallized at least 23.7 half-lives or 4.1×10^8 years after the production of the I^{129}. In their argument they assume that I^{129} and I^{127} were produced in equal amounts. This is consistent with our point of view that I^{129} is a progenitor of Xe^{129} and Suess and Urey's abundance ratio $Xe^{129}/I^{127}=1.05/0.80=1.30$. Our calculations in Table VII,2 yield $I^{129}/I^{127}=1.17/0.42=2.8$ in

the r process. Actually, the calculations of Wasserburg and Hayden are quite insensitive to the I^{129}/I^{127} ratio, our calculated value raising their lower limit only to 4.3×10^8 years.

On this basis it would seem justified to choose $t_1 \geq 5.0 \times 10^9$ years, and therefore t_0 lies between 11.5 and 6.6×10^9 years. For nucleogenesis in a continuous and uniform series of supernovae occurring between the formation of the galaxy and the time of formation of the cloud of gas or protostar from which the sun condensed, we can take 10^{10} years as a round figure for the beginning epoch. On this point of view the age of our galaxy is thus $\sim 10^{10}$ years.

There is one point of view in which the above ideas must be somewhat modified. In the steady-state cosmologies of Hoyle (Ho49) and of Bondi and Gold (Bo48) it may be expected that the U^{235}/U^{238} ratio in a sufficiently large volume will remain constant due to supernova activity, in spite of the apparent universal expansion and the constant dilution by the addition of matter in the form of hydrogen which is necessitated in order to keep the mass energy content of the specified volume at a fixed value. The characteristic time involved for the removal by expansion of one-half of a particular type of matter from a fixed volume is $0.693T/3$, where T is the reciprocal of Hubble's constant. Taking T as 5.4×10^9 years we have for our characteristic half-life 1.25×10^9 years. The decay lifetime for any radioactive material must be properly corrected for this value. The effective lifetimes of U^{235} and U^{238} become 0.45×10^9 and 0.98×10^9 years, respectively.

On the steady-state point of view $t_0 = \infty$, and after a long period of production one would expect that at time t_1, after which no further contribution to solar system material occurred, we should have

$$\frac{U^{235}(t_1)}{U^{238}(t_1)} = \frac{0.45\lambda_{235}}{0.98\lambda_{238}} = 0.75.$$

This is just the value expected from the present-day ratio of $U^{235}/U^{238} = 0.0072$ now if the solar system material has been isolated for some 5.7×10^9 years. We may conclude that the present abundance ratio of the uranium isotopes is consistent with the steady-state cosmology if the method of production of their isotopes is the r process as described. We do not wish to overemphasize this conclusion, but rather to emphasize that studies concerning the origin of the radioactive elements may lead to objective tests of the various cosmological theories.

It can also be noted that there exists an approximate indication of the epoch of synthesis by the s process. The radioactive isotope K^{40} is in the main line of the s process. Figure VI,1 shows that for this isotope $\sigma N \sim 10^4$ for σ in mb and N on the scale $Si = 10^6$. We estimate in the appendix that $\sigma \sim 100$ mb so at the time of K^{40} production $N \sim 100$. It is now, $N = 0.38$. Using the known K^{40} half-life of 1.3×10^9 years we find that the

K^{40} was produced $\sim 10^{10}$ years ago. This calculation could be made with great assurance if the capture cross sections for 15-kev neutrons were measured accurately for K^{39}, K^{40}, and K^{41}. Our calculation assumes the K^{40} cross section to be 12.5 times that of K^{39} which has a closed shell of neutrons.[20] Even if this factor has the very high value of 100 the epoch for K^{40} formation will be reduced only to 6.5×10^9 years ago.

In any case we consider the minimum age of the isotopes of uranium, namely 6.6×10^9 years with an uncertainty on the low side of at most 0.6×10^9 years, to be significantly greater than the age of the solar system, 4.5×10^9 years. This age is indeed comparable to the ages, 6.5×10^9 years, of the oldest known clusters in the galaxy (Jo56, Ho55, Ha56c). Since our age is a minimum for that of the elements and thus, on the hypothesis of stellar nucleogenesis, for the galaxy, it would not be unexpected if still older objects were eventually found in the galaxy.

D. Termination of the s Process; the Abundances of Lead, Bismuth, Thorium, and Uranium

The s process is terminated at Bi^{209} by the onset of natural alpha-particle radioactivity. Detailed discussion of the termination has been postponed to this point so that it can be applied, along with the discussion of the r-process termination, to calculation of the abundances of lead, bismuth, thorium, and uranium, which can be expected to be produced in the s and r processes.

As illustrated in Fig. VIII,5, the s process proceeds through the mercury isotopes to stable Tl^{203} and thence by neutron capture to Tl^{204} which decays 98% by beta emission to Pb^{204} and 2% by electron capture to Hg^{204}. We can neglect this last branching. The half-life of Tl^{204} is 4.1 years, which we shall take to be short compared to its mean neutron-capture time. At Pb^{204} neutron capture leads to Pb^{205} which decays by electron capture with a lifetime of approximately 5×10^7 years to Tl^{205}.

Pb^{205} is essentially stable on the time-scale of individual captures in the s process, and the neutron capture continues through the stable lead isotopes Pb^{206}, Pb^{207}, and Pb^{208} to beta-active Pb^{209}. After the s process finally ends, the Pb^{205} produced in the capture chain eventually does decay to Tl^{205}. Pb^{209} decays in 3.3 hours to stable Bi^{209} which, upon neutron capture, forms the 2.6×10^6-year alpha-particle-emitting ground state of Bi^{210} or the 5.0-day electron-emitting isomeric state, RaE. For slow neutrons the capture results 44% of the time in the ground state and 56% of the time in the isomeric state. It is reasonable to assume that this branching ratio will hold for the 15-kev neutrons involved in the s process. The RaE decays quickly before neutron capture to Po^{210} which is an alpha-particle emitter with 138.4-day half-life, fast compared to neutron capture times. Thus Pb^{206} is

ALPHA DECAY (138 d)

84 — Po

83 — Bi

82 — Pb

81 — Tℓ

80 — Hg

ATOMIC NUMBER

β^- (5 d)

56% — RaE

44%

β^- (4 y) | 98% | EC(10^6 y)

β^- (5 m)

ALPHA DECAY (2 m)

EC 2%

TERMINATION OF THE s-PROCESS

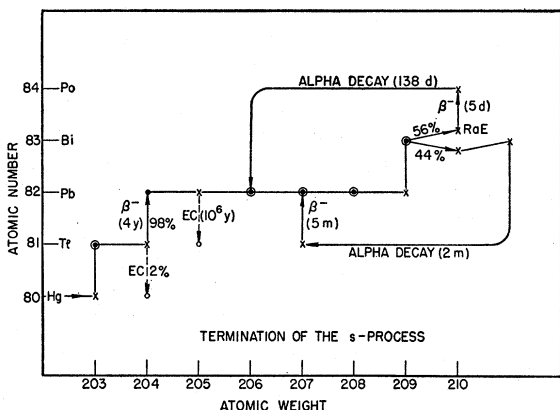203   204   205   206   207   208   209   210
ATOMIC WEIGHT

FIG. VIII,5. This diagram shows the details of the termination of the s process. The half-life for electron capture in Pb^{205} should be changed to $\sim 5 \times 10^7$ years.

formed and this branch of the termination of the s process can result in a cycling process between Pb^{206} and Bi^{210}. The long half-life of the ground state of Bi^{210} means that it captures a neutron before decaying, so that in this case the termination is delayed until Bi^{211} is formed; this then decays rapidly through Tl^{207} to Pb^{207}, which can then cycle back through lead and bismuth. The result is a steady production of Pb^{206}, Pb^{207}, Pb^{208}, and Bi^{209} by the s process. The steady-flow relative abundances of these nuclei are then given by

$$an_{204}\sigma_{204} = an_{205}\sigma_{205} = 1.8n_{206}\sigma_{206}$$

$$= n_{207}\sigma_{207} = n_{208}\sigma_{208} = n_{209}\sigma_{209},$$

where the σ's represent neutron capture cross sections, a is the factor for the number of terminal cycles, and the factor $1.8 = 1 + 44/56$ arises because Pb^{206} is replenished in only 56% of the cycling processes.

The capture cross section for 15-kev neutrons have been discussed in Sec. V and are given in the appendix. These cross sections are 100 and 50 mb for the odd isotopes Pb^{205} and Pb^{207}, 25 mb for the even isotope Pb^{206}, 10 mb for the even doubly-magic isotope Pb^{208}, and 15 mb for the odd magic Bi^{209}. These values are consistent with the energies gained on neutron addition, i.e., 8.10, 7.38, 6.73, 3.87, and 4.67 Mev, respectively. There is a problem concerning the neutron addition energy and the capture cross section for Pb^{204}. The reactivity measurements do not distinguish between even isotopes. From Huizenga's masses (Hu55) the energy is 6.80 Mev but has a considerably larger error than that for the other lead isotopes. It can be argued that Pb^{204}, with fewer neutrons than Pb^{206}, should more readily capture neutrons than Pb^{206}, and so the Pb^{204} cross section has been estimated as 50 mb. On this basis one-half as much Pb^{204} should be produced on the s process as Pb^{206}, as long as cycling is neglected. To see whether such a ratio is reasonable, we may compare it with the abundance ratios of other pairs of even isotopes which have been made in a similar

way, i.e., by steady flow in the s process without cycling. We find, for example, that the abundance ratios $Te^{122}/Te^{124} = 0.52$, $Xe^{128}/Xe^{130} = 0.47$, $Ba^{134}/Ba^{136} = 0.31$, and $Sm^{148}/Sm^{150} = 1.52$.

An alternative way of estimating the relative lead capture cross sections is by comparison with the barium capture cross sections deduced from the relative abundances of the barium isotopes 134, 135, 136, 137, and 138. These lead to the completion of the $N = 82$ neutron shell just as Pb^{204} to Pb^{208} lead to the completion of the $N = 126$ shell. Ba^{134} and Ba^{136} are shielded, that is, they are made only in the s process, Ba^{138} is magic in the s process and all of its yield can be attributed to this process, while for Ba^{135} and Ba^{137} we have attributed two thirds of their abundances to the s process.

Thus, on the basis of our two independent estimates, the relative abundances of the lead isotopes produced in the s process are as follows:

	Pb^{204}	Pb^{205} (Tl^{205})	Pb^{206}	Pb^{207}	Pb^{208}	Bi^{209}
From reactivity σ	1	0.5	1.1a^a	a	5a	3.3a
From barium abundances	1	1.8	1.8a^b	3.1a	29.6a	$\cdots$

a In case $a = 1$, use 2 in place of 1.1a.
b In case $a = 1$, use 3.2 in place of 1.8a.

Having discussed the relative abundances of the lead isotopes and bismuth expected to be produced by the s process, we must now calculate the relative abundance production expected in the r process. This can be done for Pb^{206}, for example, by first adding the abundances given in Table VII,2 for the mass chains 206, 210, 214, . . . 234, which decay fairly rapidly to Pb^{206}. For Pb^{206} this sum is 0.48 on our customary scale. If we wish to compare our results with the "nonradiogenic" lead isotope abundances at the time of formation of the solar system, we must add to this sum the amount of Pb^{206} resulting from the decay of U^{238} in the period between element production and solar system formation. This value depends somewhat on whether the element formation was continuous, or occurred in a single event, but for simplicity we have chosen the latter alternative. The decay period is then $(6.6 - 4.5) \times 10^9 = 2.1 \times 10^9$ years, so that 27% of the U^{238} will have decayed. From Table VIII,3 we see that this adds 0.11 to the Pb^{206} abundance, bringing the total to 0.59. These abundances are summarized in Table VIII,4 which also includes the results of similar calculations for Pb^{207}, Pb^{208}, and Bi^{209}. Since Np^{237} decays rapidly as compared with the time scales involved here, the Bi^{209} abundance is just the sum over all mass chains 209, 213 . . . 253.

For the nonradiogenic lead isotope abundances it is customary to take the isotopic abundances observed in iron meteorites, which have the lowest observed proportions of radiogenic leads, and which are assumed to have crystallized without including parents of the radioactive series [see discussion on p. 68 of (Su56)]. For the present-day average for lead, Suess and Urey

recommend the chondritic meteorite ratios. According to Patterson et al. (Pa53, Pa55, Pa55a) the ratios are

	$\dfrac{Pb^{206}}{Pb^{204}}$	$\dfrac{Pb^{207}}{Pb^{204}}$	$\dfrac{Pb^{208}}{Pb^{204}}$	$\dfrac{\text{Total Pb}}{Pb^{204}}$
Iron meteorites, 4.5×10⁹ yr ago	9.5	10.3	29.2	50.0
Chondrites "now"	19.4	15.9	38.6	74.9

Now Pb^{204} is not produced directly in the r process, since it is shielded by Hg^{204} and it does not result from any radioactive decay of r products. From the capture cross sections in the s process it may be expected that it will be produced to a lesser extent than the other isotopes, and this will be especially true if the s process does not just terminate at Bi^{209}, but cycles to some extent, thus building up Pb^{206}, Pb^{207}, and Pb^{208}. Thus the observed ratios given above are entirely reasonable on the basis of s process and r process synthesis of the elements.

On the other hand, these processes will have produced much more lead than commonly accepted in abundance estimates. This can be seen as follows. Pb^{204} is produced in the regular flow of the s process, and should have the corresponding abundance, which may be calculated as follows. The average value of σN, read off the curve in Fig. VI,3, is about 10 in the vicinity of $A = 204$. The estimate given above for the cross section is 50 mb, and hence $N = 0.20$. The cross-section estimate is probably high rather than low, so this abundance is, if anything, a lower limit. This leads to a total lead abundance of 10 for the iron meteorites and 15 for the chondrites. These values are much larger, for example, than those given by Suess and Urey, namely 0.31 and 0.47, respectively. On the other hand, our values are in good agreement with the solar abundance obtained by Goldberg et al. (Go57), i.e., a value of about 20 from the lead/hydrogen ratio and 10 from the lead/silicon ratio on the silicon = 10⁶ scale. Our view is that the meteoritic abundance of lead may be exceptionally low due to a fractionating process that took place when the meteorites were formed.

TABLE VIII,4. Production of Pb^{206}, Pb^{207}, Pb^{208}, and Bi^{209} in the r process.

	Pb^{206}	Pb^{207}	Pb^{208}	Bi^{209}
Long-lived parent	U^{238}	U^{235}	Th^{232}	(Np^{237})
Parent:				
Originally	0.405	0.663	0.641	0.617
4.5×10⁹ years ago	0.295	0.083	0.577	0.0
Now	0.146	0.001	0.462	0.0
From long-lived parent:				
4.5×10⁹ years ago	0.110	0.580	0.064	0.617
Now (no fractionation)	0.259	0.662	0.179	0.617
Short-lived progenitors	0.477	0.369	0.266	0.317
Total:				
4.5×10⁹ years ago	0.587	0.949	0.330	0.934
Now (no fractionation)	0.736	1.031	0.445	0.934
Radiogenic	0.149	0.082	0.115	0.0

On the basis of our analysis of the lead produced in the s and r processes we can calculate lead isotope ratios, the only uncertainty being in the cycling factor a. Using the two estimates of the cross sections discussed above, i.e., those derived from the reactivity measurements and those derived from the barium abundances [with $\sigma(Pb^{204}) = 50$ mb], and choosing $a = 6$ in the first case and $a = 1$ in the second, we have the following values for the three isotopic ratios:

	$\dfrac{Pb^{206}}{Pb^{204}}$	$\dfrac{Pb^{207}}{Pb^{204}}$	$\dfrac{Pb^{208}}{Pb^{204}}$	$\dfrac{Bi^{209}}{Pb^{204}}$
From reactivity $\sigma(a=6)$	9.5	10.7	31.6	24.7
From barium abundances $(a=1)$	6.2	7.8	31.2	$\cdots$
Iron meteorites (obs)	9.5	10.3	29.2	$\cdots$

In this calculation we have taken into account the amount of lead produced by the decay of r-process isotopes before the freezing of the material of the meteorites 4.5×10⁹ years ago. Thus for the first case $(a=6)$, $Pb^{206}/Pb^{204} = 1.1 \times 6 + 0.587/0.2 = 9.5$. There is little to choose between the two sets of calculations, but we are inclined to favor the first since it would be rather accidental if the s process terminated at bismuth without some cycling at its termination.

In addition to obtaining a high abundance of lead through these calculations, we also find that the abundance of bismuth is high. Using the reactivity cross sections and the cycling factor $a = 6$, we find that Bi^{209} should be produced with an abundance 20 times that of Pb^{204} in the s process. An additional contribution of $0.934/0.2 = 4.7$ comes from the r process (Table VIII,4). Thus, Bi^{209} should have an abundance of $24.7 \times 0.2 = 4.94$ on the silicon = 10⁶ scale whereas Suess and Urey, using a value due to the Noddacks, give 0.144.

On the other hand, our calculation of the abundances of the isotopes of thallium is in fair agreement with the abundances given by Suess and Urey. Thus Tl^{203}, with a cross section of 276 mb, has a calculated s-process abundance of $10/276 = 0.036$, to which must be added 0.057 from the r process, yielding a total of 0.093 which is only a factor of 3 higher than the Suess and Urey value of 0.0319. Tl^{205} results from the decay of Pb^{205} produced in the s process and thus the Pb^{205} cross section of 100 mb must be used in calculating its s-process abundance, i.e., $10/100 = 0.10$. Adding 0.057 for the r-process abundance, we obtain 0.157 which is about twice the value of 0.0761 given by Suess and Urey.

Our values for the mercury isotopes, as compared with the values of Suess and Urey, are shown in the following:

	s process	r process	Total	Suess and Urey
Hg^{196}	0.0	0.0	(p process)→0.00045	
Hg^{198}	0.042	0.057	0.099	0.0285
Hg^{199}	0.015	0.057	0.072	0.0481
Hg^{200}	0.042	0.057	0.099	0.0656
Hg^{201}	0.015	0.057	0.072	0.0375
Hg^{202}	0.042	0.057	0.099	0.0844
Hg^{204}	0.000	0.057	0.057	0.0194
			0.498	0.284

STARS SHOWING RESULTS OF:

| NiII | FeII CoII | CrII HI8 | HII,VII | HeI | SiII HeI,H8 | CaII HeI |
| 3577 | 3621 | 3678 3692 | 3771 | 3820 | 3856 3889 | 3934 3965 |

I. HYDROGEN - BURNING

MgI CaII H8
3838 3934,3968 4102   Hγ HeI   Hβ
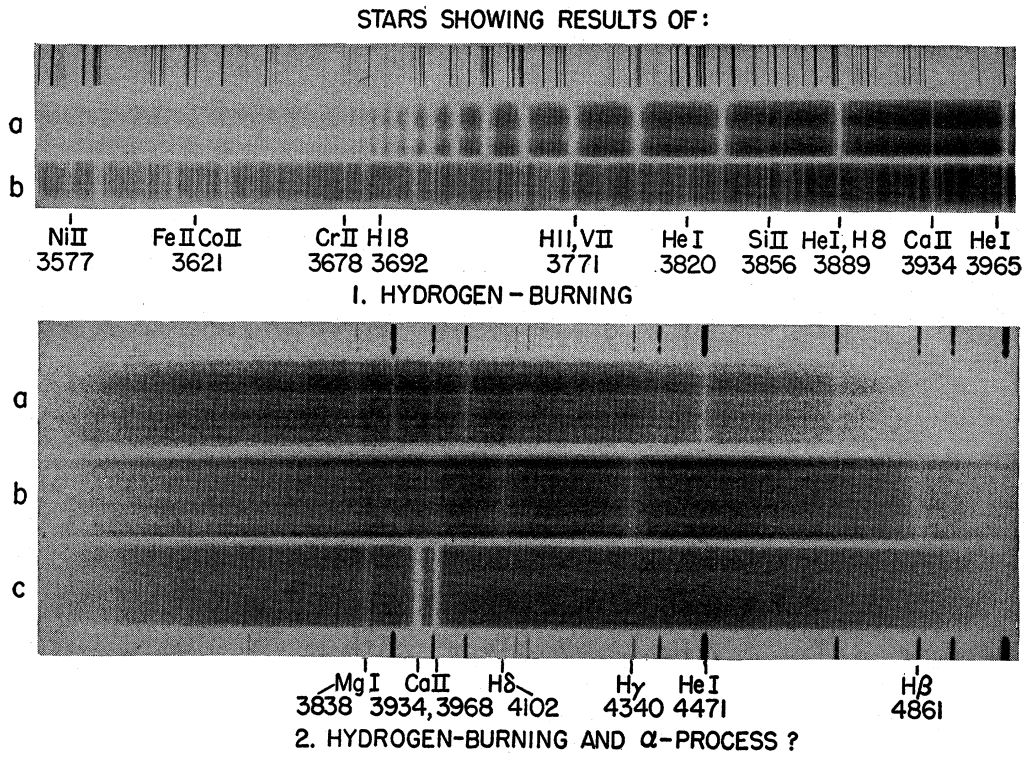   4340 4471   4861

2. HYDROGEN-BURNING AND α-PROCESS ?

PLATE I.

PLATE 1. Portions of the spectra of stars showing the results of hydrogen burning and possibly the α process. Upper: (a) Normal A-type star, η Leonis, showing strong Balmer lines of hydrogen and a strong Balmer discontinuity at the series limit. (b) Peculiar star, υ Sagittarii, in which hydrogen has a much smaller abundance than normal. Lower: (a) White dwarf, L 1573–31, in which hydrogen is apparently absent. The comparison spectrum above the star is of a helium discharge tube; note the lines of helium in the star's spectrum. (b) White dwarf, L 770–3, which shows broad lines due to hydrogen only, for comparison with (a) and (c). (c) White dwarf, Ross 640, which shows only the two lines due to Ca II and a feature due to Mg I. All the spectrograms in this plate were obtained by J. L. Greenstein; the upper two are McDonald Observatory plates and the lower three are Palomar Observatory plates.
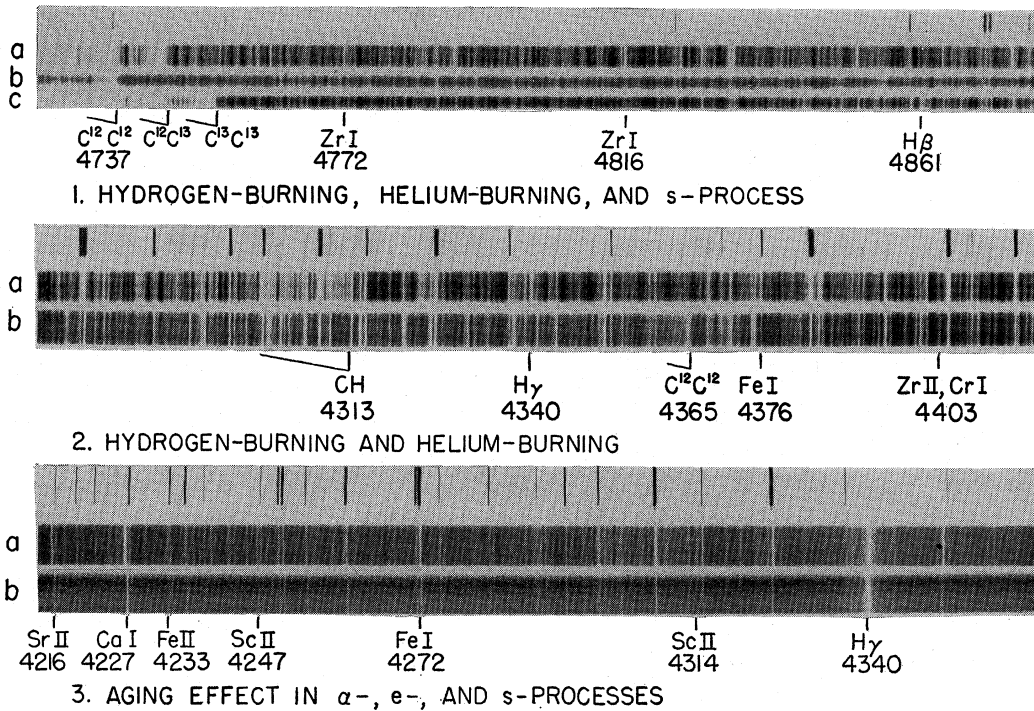
STARS SHOWING RESULTS OF:

a
b
c

$C^{12}C^{12}$ $C^{12}C^{13}$ $C^{13}C^{13}$ ZrI   ZrI   Hβ
4737   4772   4816   4861

I. HYDROGEN-BURNING, HELIUM-BURNING, AND s-PROCESS

a
b

CH   Hγ $C^{12}C^{12}$ FeI   ZrII, CrI
4313   4340   4365 4376   4403

2. HYDROGEN-BURNING AND HELIUM-BURNING

a
b

SrII   CaI   FeII   ScII   FeI   ScII   Hγ
4216   4227   4233   4247   4272   4314   4340

3. AGING EFFECT IN α-, e-, AND s-PROCESSES

PLATE 2.

PLATE 2. Portions of the spectra of stars showing different aspects of element synthesis. Upper: (a) Normal carbon star, X Cancri, which has $C^{12}/C^{13} \sim 3$ or 4. (b) Peculiar carbon star, HD 137613, which shows no C^{13} bands, and in which hydrogen is apparently weak. (c) Normal carbon star, HD 52432, which has $C^{12}/C^{13} \sim 3$ or 4. Note that ZrI lines appear to be strongest in (a). Middle: (a) Normal carbon star, HD 156074, showing the CH band and Hγ. (b) Peculiar carbon star, HD 182040, in which CH is not seen, although the weak band of C_2 at λ 4365 is visible. Hγ is also very weak, indicating that hydrogen has a low abundance. Lower: (a) Normal F-type star, ξ Pegasi. (b) Peculiar star, HD 19445, which has a slightly lower temperature than ξ Pegasi, yet all lines but hydrogen are much weakened, showing that the abundances of α-, e-, and s-process elements are much lower than normal ("aging" effect). The middle two spectra were obtained by J. L. Greenstein, the remainder, with the exception of HD 137613, by E. M. and G. R. Burbidge.
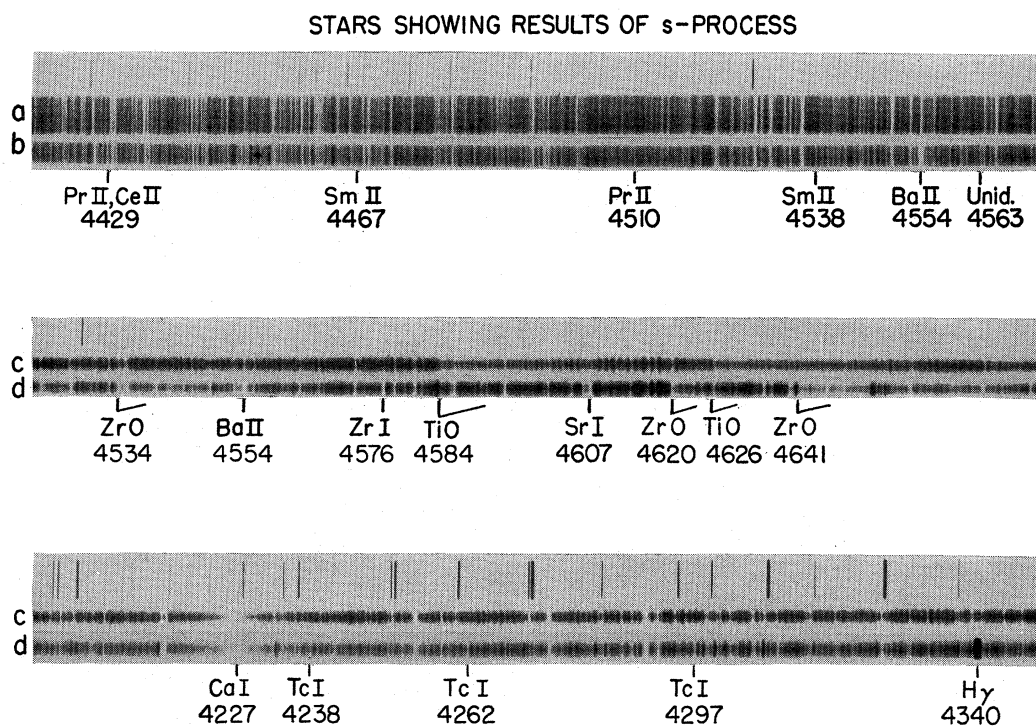
STARS SHOWING RESULTS OF s-PROCESS

PLATE 3.

PLATE 3. Portions of the spectra of stars showing the results of the s process. Upper: (a) Normal G-type star, κ Geminorum. (b) Ba II star, HD 46407, showing the strengthening of the lines due to the s-process elements barium and some rare earths. Middle: (c) M-type star, 56 Leonis, showing TiO bands at λλ 4584 and 4626. (d) S-type star, R Andromedae, showing ZrO bands which replace the TiO bands. Lines due to Sr I, Zr I, and Ba II are all strengthened. Lower: (c) Another spectral region of the M-type star, 56 Leonis; note that Tc I lines are weak or absent. (d) R Andromedae; note the strong lines of Tc I. The spectrum of R Andromedae was obtained by P. W. Merrill, and the upper two spectra by E. M. and G. R. Burbidge.

Crab Nebula

Supernova in IC 4182

(a)

(b)

(c)

PLATE 4. Left: The Crab Nebula, photographed in the wavelength range λ6300–λ6750. The filamentary structure stands out clearly at this wavelength, which comprises light mainly due to the Hα line. Right: The supernova in IC 4182, photographed (a) September 10, 1937 at maximum brightness—exposure 20 m; (b) November 24, 1938, about 400 days after maximum—exposure 45 m; (c) January 19, 1942, about 1600 days after maximum, when the supernova was too faint to be detected—exposure 85 m. Note that the lengths of the three exposures are different. These plates were taken by W. Baade, to whom we are indebted for permission to reproduce them.

Thus the calculated abundance is in fair agreement with that given by Suess and Urey. The expected decrease in cross sections with increasing N, neglected here, would give the observed gradual rise in abundance with N up to Hg^{202}. The drop in abundance at Hg^{204} is to be expected since it is not produced in the s process.

The large abundance of lead which we have derived from both the s and the r process results in considerable difficulties from the geological standpoint. Thus it is worthwhile to consider ways in which this conflict might be avoided. The most convincing evidence that the s process has been fully operative is the fact that the observed relative abundance of Pb^{208}, for which the r-process contribution is only 5%, and Pb^{204}, produced only by the s process, agree with the predictions of the s-process theory. Thus, the large Pb^{208}/Pb^{204} abundance ratio is attributable partly to the small neutron-capture cross section expected for magic Pb^{208} and partly to some cycling at the end of the s process. On the other hand, Pb^{204} might have an anomalously large cross section or might not be produced at all if Tl^{204} had such a large cross section that it captured a neutron and formed Tl^{205} instead of decaying to Pb^{204}. Neither of these possibilities seem likely, but they must be borne in mind as possible ways out of the conflict with geological evidence. It may be remarked that the total predicted lead production by the r process alone is 1.15 as compared with Suess and Urey's value of 0.47.

Finally, we consider the abundances of thorium and uranium. The recent results of Turkevich, Hamaguchi, and Reed (Tu56), using the neutron activation method, indicate that there is only a small amount of uranium in the Beddgelert chondrite. Urey (Ur56) has analyzed these results, which give an abundance of 0.007 on the scale of Suess and Urey. His results also give an atomic abundance of 0.02 for thorium. Our predicted r-process abundances are 0.147 for uranium and 0.462 for thorium. Thus, our calculations would seem to indicate that thorium and uranium as well as lead and bismuth have been reduced in abundance by some fractionation process in the formation of the planets and meteorites. As previously stated, of these four elements only lead has had its abundance in the sun determined (Go57), and in this case the solar abundance is in agreement with our calculated abundance and is very much higher than the abundance given by Suess and Urey.

In conclusion, the expected yield of radiogenic lead from the decay of thorium and uranium during the period since the formation of the meteorites would result in ratios of $(Rd\ Pb^{206})/Pb^{204}$, $(Rd\ Pb^{207})/Pb^{204}$, and $(Rd\ Pb^{208})/Pb^{204}$ equal to 0.75, 0.41, and 0.57, respectively (see last line of Table VIII,4; Pb^{204} is taken as 0.2). These values are obtained by assuming no uranium-lead-thorium fractionation at formation. The Rd Pb^{206} and Rd Pb^{207} ratios are clearly consistent with Patterson's determinations of the radiogenic

leads in chondrites and the Nuevo Laredo meteorite since we have used 4.5×10^9 years as the age of the meteorites. On the other hand, the ratios to Pb^{204} are considerably smaller than those found for radiogenic leads, indicating that lead was removed preferentially relative to uranium and thorium in chondrites and especially in the Nuevo Laredo meteorite. However, the iron meteorites could well contain the small amount of radiogenic leads which would be expected if no fractionation of lead relative to uranium and thorium occurred when they were formed.

IX. p PROCESS

In Sec. V it was pointed out that the proton-rich isotopes of a large number of heavy elements cannot be built by either the s or the r process, and particular examples of this difficulty are discussed in Sec. II, in connection with our assignments to one or the other of the synthesizing processes. With the exceptions of In^{113} and Sn^{115}, all of these isotopes have even A. From the Appendix we see that in the cases of Mo^{94}, Cd^{108}, and Gd^{152}, in addition to synthesis by the p process, these isotopes can also be made in weak loops of the s-process chain. In addition, In^{113}, Sn^{114}, and Sn^{115} may also be built in a weak loop of the s-process chain which is begun by decay from an isomeric state of Cd^{113}. In Fig. IX,1 a plot of the abundances of the p-process isotopes is given. The black dots represent isotopes which are made only by the p process, while the open circles represent isotopes which might have a contribution from the s process as well. A smooth curve has been drawn through the points merely to show the trends and positions of the peaks. This curve shows the same general trend as that of the main abundance curve, and the fact that the open circles lie predominately near the curve defined by the other points suggests that in no case is the s process an important contributor to the abundance. All of the isotopes are rare in comparison with the other isotopes of the same element, and it appears that only about 1% of the material has been processed by reactions which give rise to these isotopes (see Table II,1). The reactions which must be involved in synthesizing these isotopes are (p,γ) and possibly (γ,n) reactions on material which has already been synthesized by the s and the r processes.

The astrophysical circumstances in which these reactions can take place must be such that material of density $\gtrsim 10^2$ g/cm^3 and containing a normal or excessive abundance of hydrogen is heated to temperatures of 2–3×10^9 degrees. It has been suggested (Bu56) that these conditions are reached in the envelope of a supernova of Type II. Alternatively they might be reached in the outermost parts of the envelope of a supernova of Type I in which the r process has taken place in the inner envelope. These possible situations are explored further in Sec. XII.

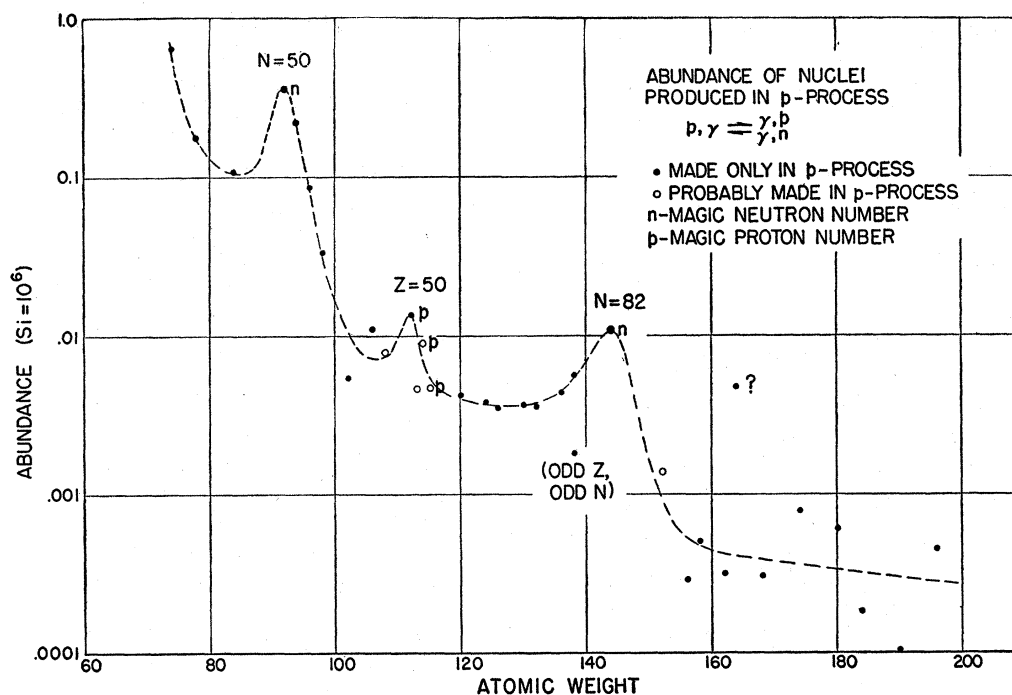We suppose that for a short period quasi-statistical

Fig. IX,1. Here we show a plot of the abundances of the isotopes made in the p process. The isotopes with magic N or magic Z are marked n and p, respectively. A curve has been drawn through the points to show the general trends. Note the peaks at $N=50$ and 82 and the lesser peak at $Z=50$.

equilibrium is reached between (p,γ), (γ,p), and (γ,n) reactions, i.e. $(p,\gamma)\dfrac{\rightarrow(\gamma,p)}{\rightarrow(\gamma,n)}$. Since the initiating reaction is (p,γ), the flux of free neutrons built up by any (γ,n) reactions will not become comparable with the proton flux, so that complete equilibrium cannot be set up between protons, neutrons, and gamma radiation. In Fig. IX,2 we give a schematic diagram which shows what the effect of (p,γ) and (γ,n) reactions on nuclei which originally lie on the stability curve in the Z, A plane will be. These reactions tend to drive nuclei off the curve of greatest stability in the direction of increasing A and Z in the case of (p,γ) reactions and decreasing A in the case of (γ,n) reactions. Qualitative arguments suggest that the values of ΔA and ΔZ, the displacements off the main stability curve, will be small. The reasons for this are as follows. In the cases of ruthenium, cadmium, xenon, barium, cerium, and dysprosium, the two lightest isotopes built by the p process have roughly equal abundances or at least ratios which never exceed ~3. In the case of tin, three isotopes, Sn^{112}, Sn^{114}, and Sn^{115}, have abundances in the ratio $\sim3:2:1$. Now if it were supposed that (γ,n) reactions on the heavier isotopes were mainly responsible for the production of those proton-rich isotopes we might expect, because of the cross-section effect, that in the case of tin, for example, the ratio would be more nearly like $1:x:x^2$ where $x\gg1$. If, on the other hand, we supposed that (p,γ) reactions were responsible for driving the nuclei

a very long way from the main stability line so that contributions from many nuclei were responsible for the tin isotopes, we would also expect that the ratios would not be small. Thus our qualitative conclusion is that (p,γ) reactions are responsible but the nuclei are only displaced in general two or three units of A and Z from the stability line. The existence of the nuclei Mo^{92} and Sm^{144} which have closed shells of 50 and 82 neutrons respectively and which show up as peaks in Fig. IX,1 suggests that these have been made directly from progenitors with closed neutron shells which form peaks in the normal abundance curve; i.e. in the case of Mo^{92}, these would be Zr^{90}, Y^{89}, Sr^{88}, etc., while the progenitors of Sm^{144} would be Nd^{142}, Pr^{141}, Ce^{140}, etc. The case of Er^{164} remains an anomaly, since the ratio $Er^{164}/Er^{162}\simeq15$ is very large and is out of line with the results for the other pairs of isotopes. There appear to be no peculiarities in the possible progenitors of Er^{164} which might explain this large abundance.

A simple calculation can be made to see whether these qualitative results deduced from the observed abundances are correct. The equation of statistical equilibrium is

$$\log\frac{n(A+1, Z+1)}{n(A,Z)}=\log n_p - 34.07$$
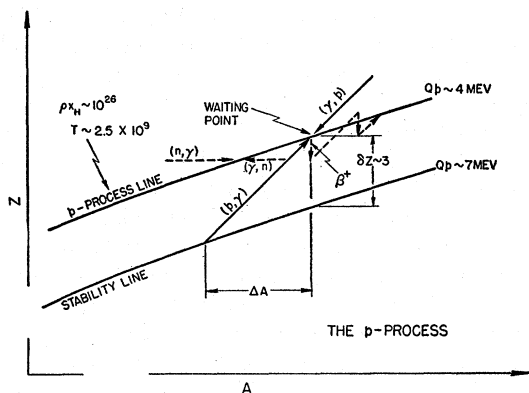$$-\tfrac{3}{2}\log T_9+\frac{5.04}{T_9}Q_p, \quad (26)$$

FIG. IX,2. The path of the p process in the Z, A plane. Material on the stability line (produced previously by the r or s process) is subjected to a hydrogen density of 10^{26} protons/cm^3 and a temperature of $\sim 2.5 \times 10^9$ degrees. The (p,γ) reactions give an increase $\Delta A = \Delta Z = 4$ or 5 until stopped by the (γ,p) reaction at nuclei with a proton binding energy, $Q_p \sim 4$ Mev. The (γ,n) reactions also produce a displacement onto the p-process line. Along this line positron emission must occur before further synthesis can take place. In general the lifetime of this emission is $\sim 10^3$ sec which is longer than the p-process conditions hold (100 sec). Thus a displacement $\delta Z \sim 3$ off the stability line (slope $\sim\frac{1}{3}$) at a given A occurs. This displacement by proton capture will occur even at large $A \sim 200$ in a time $\lesssim 1$ sec which is short compared to the time for the p process. Thus the displacement is terminated by the positron emission and not by decreasing Coulomb barrier penetrability so that it will be substantially independent of A. The p-process abundances as shown in Fig. I,1 and Fig. IX,1 should parallel the main abundance curve. The abundances will be 10^{-2} to 10^{-3} of those produced in the s and r processes.

where n_p is the number density of protons, Q_p is the proton binding energy, and T_9 is the temperature in units of 10^9 degrees. This equation is analogous to (14) in Sec. VII. Putting $n_p = 10^{26}$/cm^3 and $T_9 = 2.5$, the binding energy of the last proton such that $n(A+1, Z+1) \approx n(A,Z)$ is obtained by putting the left-hand side of (26) equal to zero. We find $Q_p = 4.3$ Mev. Now the proton binding energy is given by

$$Q_p(A,Z) = \alpha - \beta\left(1 - \frac{4N^2}{Z^2}\right) - \frac{2}{3}\gamma A^{-\frac{1}{3}}$$
$$- 2\epsilon\frac{Z}{A^{\frac{1}{3}}} + \frac{\epsilon}{3}\frac{Z^2}{A^{\frac{4}{3}}} + g'(Z). \quad (27)$$

This equation is analogous to (23) of Sec. VII for the neutron binding energy; the symbols have the same meaning.
Thus

$$\left.\frac{\partial Q_p}{\partial A}\right|_N \approx -8\beta\frac{N^2}{A^3} \approx 0.6 \quad \text{for} \quad 100 < A < 200.$$

The binding energy of a proton in a nucleus on the main stability curve in this range of A is about 7 Mev. Thus $\Delta Q_p \sim 2.7$ Mev and $\Delta A \sim 4$ to 5. Thus ΔZ is also 4 to 5. However, we wish to know the deviation in Z of the new point from the stability line at $A + \Delta A$.

We call this δZ and calculate it as follows. In Fig. IX,2 the slope of the line joining nuclei (A,Z) and $(A+1, Z+1)$ in the Z, A plane is 1. On the other hand, the change in Z corresponding to ΔA is just the change in the Z ordinate. Now the slope of the curve of maximum stability is $\sim\frac{1}{3}$. Thus δZ is given by

$$\delta Z = \frac{2}{3}\Delta A \sim 3.$$

Whether the nuclei are driven off the main line to this maximum extent will depend on (i) whether sufficient protons are available, and (ii) whether the equilibrium conditions endure for sufficient time to allow the unstable nuclei to positron-decay so that the maximum number of protons can be added. The lifetime against positron emission is given by

$$\tau_{\beta+} \simeq \frac{10^6}{W_{\beta+}^5} \quad \text{(forbidden transition)},$$

where

$$W_{\beta+} = B_A(\delta Z - 0.5) + 0.5.$$

Now $B_A \simeq 1.5$ Mev near $A = 100$. The coefficient of B_A in this equation is $(\delta Z - 0.5)$ instead of $(\delta Z - 2.5)$ (which is used in Sec. VII) because we assume that the positron emission takes place by a forbidden transition to the ground state instead of by an allowed transition to an excited state as is the case for beta decay discussed in Sec. VII. In that case a mean value $\bar{W}_\beta$ was calculated.

Thus $W_\beta \simeq 4.2$, and $\tau_{\beta+} \simeq 1000$ sec. Now the duration of a supernova outburst has been estimated to be 10–100 sec, and the time during which the p process takes place may be of the same order as or shorter than this explosion time. Consequently, it appears that the number of protons which can be added to the heavy nuclei is limited by the positron decay times and the synthesis to the limit of proton stability at this temperature will not be reached. Thus we conclude that the qualitative argument based on the observed abundances, that $\Delta A \sim 2$ or 3 and $\Delta Z \sim 1$ or 2, is borne out by this calculation.

The number of protons available to be captured by the heavy elements is determined by the number which are captured by the light and abundant elements. A typical example is C^{12}. Addition of two protons produces O^{14} whose half-life for positron emission is 72 sec. Thus it is probable that the maximum number of protons which can be added to C^{12} through the duration of the p process is only two. If we suppose that in the envelope in which the process occurs the H/C^{12} ratio is normal and equal to $\sim 10^4$, it is clear that even when we take into account all of the light elements which capture protons they can take only a small fraction of the total available, so that proton capture among the heavy nuclei is not limited by the number of protons available.

The mean reaction time for a (p,γ) reaction on a heavy nucleus A_0, Z_0 is given approximately by [see

Sec. III A, case (ii)]

$$\frac{1}{\tau}=3.1\times10^9\rho\frac{Z_0^{5/6}}{A_0^{1/6}T_9^{\frac{2}{3}}}$$

$$\times\exp\left[1.26\{AZ_0(A_0^{\frac{1}{3}}+1)\}^{\frac{1}{2}}-4.25\left(\frac{Z_0^2A}{T_9}\right)^{\frac{1}{3}}\right]\text{ sec}^{-1},$$

where $A=A_0/(A_0+1)$. For example, for $_{80}\text{Hg}^{200}$, we have

$$\frac{1}{\tau}=3.0\times10^{23}\frac{\rho}{T_9^{\frac{2}{3}}}\exp(-78.8T_9^{-\frac{1}{3}})\text{ sec}^{-1}.$$

Thus for $T_9=2.5$ and $\rho=10^2$ g/cm^3, $1/\tau=10$ sec^{-1}, so that the capture rate is rapid and is not a limiting factor in the proton addition.

X. x PROCESS

We have given the name x process collectively to mechanisms which may synthesize deuterium, lithium, beryllium, and boron. Some discussion of the problems involved in the x process are discussed in this section.

A. Observational Evidence for the Presence of Deuterium, Lithium, Beryllium, and Boron in our Galaxy

From the appendix the number ratios of deuterium, Li^6, Li^7, Be^9, B^{10}, and B^{11} relative to hydrogen are 1.4×10^{-4}, 1.8×10^{-10}, 2.3×10^{-9}, 5×10^{-10}, 1.1×10^{-10}, and 4.9×10^{-10}, respectively. Thus deuterium is rare as compared with its neighbors hydrogen and helium in the atomic abundance table, but as far as the remainder of the elements are concerned is very abundant and comparable with iron. Lithium, beryllium, and boron are all extremely rare as compared with their neighbors helium, carbon, nitrogen, and oxygen, and are only about 100 times as abundant as the majority of the heavy elements (see Fig. I,1). It should be emphasized for these elements particularly that all of these values have been obtained from terrestrial and meteoritic data and thus they may not be at all representative of the cosmic abundances of these elements.

A number of attempts have been made to detect deuterium in the sun. The latest, by Kinman (Ki56), shows that the abundance ratio of deuterium to hydrogen in the atmosphere is less than 4×10^{-5}. Attempts have also been made to detect the radio spectral line at 327 Mc/sec due to neutral deuterium in interstellar gas, and the most recent results by Stanley and Price (St56) and Adgie and Hey (Ad57) lead to the conclusion that the deuterium to hydrogen ratio does not exceed 5×10^{-4}.

The abundances of lithium and beryllium in the solar atmosphere have been investigated by Greenstein and Richardson (Gr51) and Greenstein and Tandberg-Hanssen (Gr54c). They found that while the isotope ratio Li^6/Li^7 could well be normal, the lithium to hy-

drogen ratio lies in the range $1.6\times10^{-11}-7\times10^{-12}$ or about 100 times smaller than the meteoritic value. The beryllium to hydrogen ratio$=10^{-10}$, a value which is reasonably well in agreement with that of Suess and Urey. An upper limit to the beryllium to hydrogen ratio of 10^{-10} has been obtained for a magnetic star by Fowler, Burbidge, and Burbidge (Fo55a). Estimates of the upper limits to the interstellar abundances of lithium and beryllium have been made by Spitzer (Sp49, Sp55). He has estimated that the upper limit to the lithium to sodium ratio is about 0.1, so that if sodium has normal abundance the lithium to hydrogen ratio is less than 10^{-7}. The beryllium to hydrogen ratio is found to be $\leq10^{-11}$. This is an order of magnitude lower than that found in meteorites, and Spitzer has concluded that some beryllium may be locked up in interstellar grains.

Lithium, probably in variable amounts, has been detected through the presence of the Li I resonance doublet at λ 6707.8 in a wide variety of late-type stars. Certain carbon stars show this feature very strongly in their spectra (Mc40, Mc41, Mc44, Sa44, Fu56), while it is also present in S-stars (Ke56, Te56), and in M-type dwarfs and giants (Gr57). No relative abundances are yet available.

Boron is spectroscopically unobservable.

In the primary cosmic radiation the abundances of lithium, beryllium, and boron are comparable with those of carbon, nitrogen, and oxygen (Go54a, Ka54, No55, No57).

B. Nuclear Reactions Which Destroy Deuterium, Lithium, Beryllium, and Boron

First we outline the reactions which destroy these light elements in a hydrogen-burning zone. At temperatures commonly found in the interiors of main-sequence stars the reactions which destroy deuterium are $D^2(d,p)H^3(\beta^-)He^3$, $D^2(p,\gamma)He^3$, and $D^2(d,n)He^3$. In the same way the reactions which destroy lithium are Li$^6(p,\alpha)$He^3 and Li$^7(p,\alpha)$He^4. Beryllium is destroyed by Be$^9(p,d)$Be$^8\rightarrow$2He^4 and $D^2(p,\gamma)$He^3, or Be$^9(p,\alpha)$Li$^6(p,\alpha)$He^3. Boron is destroyed by B$^{10}(p,\alpha)$Be$^7(EC)$-Li$^7(p,\alpha)$He^4 and B$^{11}(p,\alpha)$Be$^8\rightarrow$2He^4. Thus the net result is always to convert these elements into helium through proton bombardment, and the rates of the reactions are such that in all conditions before a star evolves off the main sequence all of the deuterium, lithium, beryllium, and boron in the volume which contains the vast majority of the mass will be destroyed (Sa55).

C. Synthesis of Deuterium, Lithium, Beryllium, and Boron

The foregoing considerations make it appear probable that these elements have been synthesized in a low-temperature, low-density environment in the universe, or conceivably in a region in which hydrogen was

absent. The alternative is a situation in which the synthesis was followed extremely rapidly by an expansion of the material resulting in cooling and decreased density so that the reactions leading to destruction were avoided, or else by a rapid transfer of the synthesized material to a low-temperature, low-density environment. Recent work of Heller (He57) shows very clearly the conditions of density and temperature under which a deuterium to hydrogen ratio $\simeq 10^{-4}$ can be preserved. Now the regions in our Galaxy in which such conditions are present are (i) in stellar atmospheres and (ii) in gaseous nebulae.

(i) This possibility was explored (Fo55a, Bu57) in connection with nuclear reactions which may take place in the atmospheres of magnetic stars (see Sec. XI). Besides having large magnetic fields and thus large sources of magnetic energy which may be available for particle acceleration and hence nuclear activity, the magnetic stars have one other feature which makes the results of elements synthesis in their atmospheres observable. It seems probable that their atmospheres do not mix appreciably with the lower layers. Thus the light elements synthesized there will not be mixed into the interiors and destroyed. However, the abundance of deuterium produced following the release of neutrons by (p,n) reactions on the light elements in such an atmosphere can never exceed a deuterium to hydrogen ratio $\sim 10^{-2}$. The use of different nuclear cross sections than those employed in Fo55a might conceivably raise this upper limit to $\sim 10^{-1}$. Because of the rarity of the magnetic stars and because of the small mass of their atmospheres, ejection of such atmospheres into the interstellar gas will lead to an interstellar deuterium to hydrogen ratio $\leq 10^{-10}$. If a more widespread class of stars such as the red dwarfs are proposed as stars in which deuterium can be made in the same way, a maximum interstellar ratio of 10^{-6} might be achieved. Thus since the lower limit to the interstellar abundance ratio so far determined is 5×10^{-4}, this explanation might be satisfactory. However, it leaves the terrestrial abundance to be explained by circumstances peculiar to the solar system, e.g., through electromagnetic activity in an early stage of formation of the solar nebula, a situation which is rather unsatisfactory.

Production of lithium, beryllium, and boron in a stellar atmosphere can take place through spallation reactions on abundant elements such as carbon, nitrogen, oxygen, and iron. Thus, if we believe that stellar atmospheres are the places of origin of these elements, it is also probable that they are a major source of the primary cosmic radiation, a conclusion which is consistent with observed abundances of primary nuclei mentioned earlier. Since energies $\gtrsim 100$ Mev/nucleon are demanded for spallation reactions it has been suggested that these reactions take place in regions fairly high in the stellar atmospheres. If it is supposed that these reactions go on only in magnetic stars, and that all the material synthesized is ejected, then the interstellar

ratios of lithium, beryllium, and boron to hydrogen which can be obtained are all about 10^{-18}. However, if the red dwarfs are proposed as stars in whose atmospheres spallation reactions can go on at the same rates, ratios $\sim 10^{-10}$ can reasonably be predicted for the interstellar gas. Lithium has been found to be quite strong in the spectrum of T Tauri (He57a).

Thus we conclude that if the x process takes place in stellar atmospheres, a further process is demanded to synthesize the deuterium in the solar system, though the interstellar abundances of lithium, beryllium, and boron might be produced.

(ii) We shall now consider in a qualitative fashion the possibility that the x process takes place at some point in the evolution of gaseous nebulae. The current sources of energy in the bright gaseous nebulae are in general the highly luminous stars which are embedded in them. However, the discovery in recent years that some gaseous nebulae (not necessarily optically bright) are strong sources of nonthermal radio emission has shown that another source of energy must be present. There is strong support for the theory that this radiation is synchrotron emission by high-energy electrons and positrons moving in magnetic fields in these sources. The reservoirs of energy which must be present in such sources in the form of *high-energy particles and magnetic flux* are as large as the total amounts of energy which are released in supernova outbursts. Thus the energetic conditions that are demanded to produce a flux of free neutrons, which can then be captured to form deuterium and can also spallate nuclei to form lithium, beryllium, and boron, are also present. Unfortunately, the mean densities in such radio sources are so low ($\sim 10^{-21}$ g/cc) that at the present time the amount of activity leading to synthesis must be negligible. On the other hand, the situation in the early life-history of such nebulae may have been more conducive to such synthesis.

Recently the light from another star of the T Tauri class, NX Monocerotis, has been found to be largely polarized, thus indicating the presence of a considerable amount of synchrotron radiation (Hu57c). High-energy particles and a magnetic field must therefore be present. Stars in the T Tauri class are thought to be young stars, recently formed and not yet stabilized on the main sequence, and are embedded in dense interstellar matter. The observation of lithium in T Tauri itself and synchrotron radiation in NX Monocerotis support the idea that the x process (by spallation) is occurring here.

Of the strong radio emitters in our own galaxy, the Crab is known to be a supernova remnant, and it may be that some of the other sources are supernova remnants as well. In the context of the theory described in this paper, supernovae are the sources both of the r process and the p process, while a supernova outburst may well follow the e-process production of elements. Now if, in the early stages of a supernova outburst, after these other processes have taken place and the

envelope is beginning to expand so that the densities fall below those in which deuterium, for example. will be destroyed, the envelope can be subjected to a large flux of neutrons, it is possible that the x process could take place. However, as pointed out by Heller, if the source of neutrons which is demanded to synthesize deuterium is $C^{13}(\alpha,n)O^{16}$ or $Ne^{21}(\alpha,n)Mg^{24}$ (in Sec. III it was pointed out that there are strong reasons for rejecting $C^{13}(\alpha,n)O^{16}$ and using $Ne^{21}(\alpha,n)Mg^{24}$ as the source of neutrons here), then a high temperature $\sim10^{9}$ degrees is demanded to produce sufficient neutrons, but a low density $\sim10^{-4}-10^{-5}$ g/cm^3 is demanded to preserve the deuterium; this appears to be an improbable situation. Thus a more plausible mode of synthesis would obtain if a large flux of neutrons from a high-energy, high-temperature region could be injected into an envelope of cool hydrogen at an early stage of the expansion. The following situation may be envisaged. As discussed in Sec. XII, at temperatures in excess of 5×10^{9} degrees and densities $\geq10^{8}$ g/cm^3 the stellar core will reach a configuration in which there can easily be a transition from a core made of iron to a core consisting primarily of helium with a fraction of free neutrons. If some portion of this core can be ejected into a surrounding, relatively cool, shell, the neutrons will be moderated and captured to form deuterium. The condition that they are captured before decaying is that $\bar{\rho} \geq 10^{-10}$ g/cm^3.

The very advanced stage of evolution in which a star might possess a neutron core might also provide a suitable source of neutrons for deuterium production, though this question will not be explored further here.

In Sec. XII it is shown that one percent of a supernova shell may be converted to the heavy elements in the r process. If the total mass of material is taken to be $\sim1M\odot$, then dilution by a factor of the order of 10^4 is demanded to produce the correct abundances, relative to hydrogen, in the solar system, which is $\sim10^{-6}$ from Table II,1. Thus, the supernova shell must have mixed with a mass of about 10^4 times its mass in the interstellar gas. The deuterium to hydrogen ratio in the solar system is $\sim10^{-4}$ so it appears that if sufficient neutrons were available to convert the whole of the hydrogen in a supernova shell to deuterium, then this amount of dilution could explain the observed solar system abundance of this isotope. To produce the lithium, beryllium, and boron, it must be assumed that about 1% of the carbon, nitrogen, and oxygen in the shell was spallated either by high-energy neutrons or alpha particles ejected by the core or by protons into which the neutrons decayed. It is also possible that these latter elements may have been produced by a high-energy tail of the protons which are demanded in the p process. It does not appear probable, however, that a single supernova could account both for the deuterium and the r process elements in the solar system.

A supernova origin for the x-process elements would also suggest that supernovae are the original sources of cosmic radiation. Thus the primary cosmic radiation might be expected to have greater than normal abundances of iron and other abundant elements synthesized in supernovae. There is some evidence in support of this (No57).

D. Preservation of Lithium in Stars

Finally, we discuss an observational result which may suggest yet another region where lithium may be synthesized, and where it is certainly preserved. We summarized in Sec. X A the evidence that lithium is present in many kinds of late-type stars. Though no relative abundances of this element in different classes of late-type stars have yet been determined, it seems highly probable that the lithium abundance is variable, and also in some stars it is probably far more abundant than it is in the interstellar gas. This suggests strongly that there is some mechanism by which it can be preserved and even synthesized in stellar interiors. For example, in one S-type star, R Andromedae (Me56), both technetium and lithium are observed. Hence in this case there must be mixing between the helium-burning core where the technetium is synthesized and the surface. We have emphasized in Sec. X B that lithium cannot survive in a hydrogen-burning zone. Cameron (Ca55) attempted to show that Li^7 can be built in a hydrogen-burning zone through $He^3(\alpha,\gamma)Be^7(K)Li^7$, the Li^7 reaching the surface of the star because it is preserved in the form of Be^7, whose half-life against K capture is lengthened because of the comparative rarity of s-state electrons at the densities of production. Unfortunately his calculation of the rate of the reaction $He^3(\alpha,\gamma)Be^7$ is based on an estimate given by Salpeter (Sa52a) which was incorrectly printed, and it seems also that the increase of the half-life against K capture has been considerably overestimated.

Lithium does not react as rapidly with helium as it does with hydrogen, and it appears possible that it can exist in a helium-burning zone long enough for it to be able to reach the surface from the deep interior. Thus we conclude that the presence of lithium in the atmospheres of late-type stars suggests that these stars can have no hydrogen-burning zones. This implies that the helium cores must be large enough, and the stars' evolution sufficiently advanced, so that the hydrogen envelopes extend only to depths where the temperatures are less than $\sim10^6$ degrees. Reactions which may synthesize lithium in a helium-burning core will be discussed elsewhere.

XI. VARIATIONS IN CHEMICAL COMPOSITION AMONG STARS, AND THEIR BEARING ON THE VARIOUS SYNTHESIZING PROCESSES

Different processes of element synthesis take place at different epochs in the life-history of a star. Thus

the problem of element synthesis is closely allied to the problem of stellar evolution. In the last few years work from both the observational and theoretical sides has led to a considerable advance in our knowledge of stellar evolution. Theoretical work by Hoyle and Schwarzschild (Ho55) has been repeatedly mentioned since it affords estimates of temperatures in the helium core and in the hydrogen-burning shell of a star in the red-giant stage. However, the calculated model is for a star of mass 1.2 solar masses and a low metal content (~1/20 of the abundances given by Suess and Urey), and is thus intended to apply to Population II stars.

From the observational side, the attack has been through photometric observations of clusters of stars, from which their luminosities and surface temperatures have been plotted in color-magnitude or Hertzsprung-Russell (HR) diagrams, by many workers. We refer here only to two studies, by Johnson (Jo54) and by Sandage (Sa57a). A cluster may be assumed to consist of stars of approximately the same age and initial composition, and hence its HR diagram represents a "snapshot" of the stage to which evolution has carried its more massive members, once they have started to evolve fairly rapidly off the main sequence after their helium cores have grown to contain 10 to 30% of the stellar mass. Clusters of different ages will have main sequences extending upwards to stars of different luminosity, and the point at which its main sequence ends can be used to date a cluster; the rate of use of nuclear fuel, given by the luminosity, depends on the mass raised to a fairly high power (3 or 4).

Figure XI,1 is due to Sandage (Sa57a), and is a composite HR diagram of a number of galactic (Population I) clusters together with one globular cluster, M3 (Population II). The right-hand ordinate gives the ages corresponding to main sequences extending upwards to given luminosities. This diagram gives an idea of the way in which stars of different masses (which determine their position on the main sequence) evolve into the red-giant region. The most massive stars evolve into red supergiants (e.g., the cluster h and χ Persei); the difference between the red giants belonging to the Population I cluster M67 and the Population II cluster M3 should also be noted. Since stars evolve quite rapidly, compared with the time they spend on the main sequence, the observed HR diagram may be taken as nearly representing the actual evolutionary tracks in the luminosity-surface-temperature plane.

A feature of Population II stellar systems is that their HR diagrams contain a "horizontal branch" [see, for example, the work by Arp, Baum, and Sandage (Ar53)] which probably represents their evolutionary path subsequent to the red-giant stage. This feature is not included in the diagram of M3 in Fig. XI,1, although it is well represented by that cluster, since this diagram is intended to show just the red-giant branches of clusters. The old Population I cluster M67 has a sparse distribution of stars which may lie on the Population I
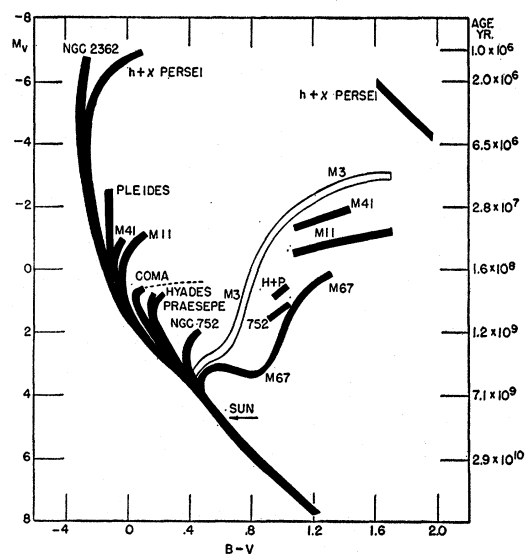

FIG. XI,1. Composite Hertzsprung-Russell diagram of a number of galactic (Population I) star clusters, together with one globular cluster, M3 (Population II), by Sandage (Sa57a). The abscissa measures the color on the B-V system, and defines surface temperature (increasing from right to left). The left-hand ordinate gives the absolute visual magnitude, M_v, of the stars (thus luminosity increases upwards). The heavy black bands (Population I) and unfilled band (Population II) represent the regions in the temperature-luminosity plane which are occupied by stars. The names of each cluster are shown alongside the appropriate band. The right-hand ordinate gives the ages of the clusters, corresponding to main sequences extending upwards to given luminosities. Note that the clusters all have a common main sequence below about $M_v = +3.5$. Note also that the red giants have different luminosities, according to the luminosities they had while on the main sequence (which are defined by their masses). *Diagram reproduced by courtesy of the Astrophysical Journal.*

analogy of the horizontal branch; the other Population I clusters in Fig. XI,1 do not show such a feature. Presumably the evolutionary history of a more massive Population I star subsequent to its existence as a a red giant is more rapid.

Whenever reference is made in different parts of this paper to particular epochs in a star's evolutionary life, we are referring to a schematic evolutionary diagram for the star which has the same general characteristics as the HR diagrams in Fig. XI,1. With this background in mind, we turn now to astrophysical observations which provide many indications of element synthesis in stars. This is either taking place at the present time or else it has occurred over a time-scale spanned by the ages of nearby Population II stars. These indications may be divided into the following groups.

A. Hydrogen Burning and Helium Burning

It appears theoretically probable that some stars, perhaps delineated by their initial mass and amount of mass loss during their existence on the red-giant branch of their evolutionary path, may still exist as stable configurations for a time after they have ex-

hausted almost all of their hydrogen. Such stars would be expected to be very rich in helium and perhaps the products of helium burning. Alternatively, stars may develop inner cores in which helium burning takes place, while still possessing hydrogen-burning shells and envelopes with a normal hydrogen content. If mixing (large-scale convection) then sets in, in such a star, core material which has been modified by hydrogen burning may appear on the stellar surface. While a star is in the red-giant stage, the temperature of the hydrogen-burning zone may be as high as 30 or 40×10^6 degrees, at least in Population II stars with masses of 1.2 $M_\odot$. At 30×10^6 degrees there may be considerable destruction of oxygen through the reactions $O^{16}(p,\gamma)F^{17}(\beta^+\nu_+)O^{17}(p,\alpha)N^{14}$ (cf. Table III,2 and Fig. III,2), if the evolutionary time-scale is as long as 10^5 years at this stage. If the onset of energy generation by helium burning in a partially degenerate core leads to some instability and consequent mixing (Ho55), then the star may settle down into a new structure in which hydrogen burning occurs at a lower temperature, in material which may or may not have been appreciably enriched in C^{12}.

As was pointed out in Sec. III F(1), any stars in which the products of helium burning mix through a hydrogen-burning zone to the surface should appear rich in nitrogen and neon, as well as in helium, and considerably depleted in hydrogen. The equilibrium abundances of C^{13}, N^{14}, and N^{15} relative to C^{12} will be approached if sufficient time is spent in the hydrogen zone for the CN reactions to have gone through several cycles. On the basis of the most recent cross-section values N^{14} will be by far the most abundant of the carbon and nitrogen isotopes if equilibrium is attained even though C^{12} is the nucleus produced in the helium burning. O^{16} will also be converted to N^{14} (without cycling) if the temperature is great enough. Ne^{20} will mainly be converted to Ne^{21} and Ne^{22} and a very small amount of Na so that the element neon survives hydrogen-burning.

Greenstein (Gr54a), using the older rates of the CN cycle, discussed the connection between the operation of the CN cycle at various temperatures, the amount of mixing, and the abundance of nitrogen observed on the surface. We wish to elaborate on this argument at this point. If equilibrium is attained the ratio N/C will be given by 0.82 N^{14}/C^{12} since N^{15} is very rare and $C^{12}/C^{13}=4.6$ by number independently of temperature. The rough temperature dependence given for N^{14}/C^{12} in Sec. III F(1) is not sufficiently

accurate for our present purposes and in Table XI,1 we give various equilibrium ratios as a function of temperature. In the last row of the table we list the logarithm of the time t in years for the N/C ratio to approach the equilibrium value at a given temperature from a not too greatly different value at another temperature. This time is of the order of magnitude of the sum of the mean lifetimes of C^{12} and C^{13} which is 22% greater than that of C^{12} alone and is thus easily calculable from the entries in Table III,2. In Table XI,1 we have taken $\rho x_H = 10$ g/cc since this value is representative of the density and hydrogen concentrations in hydrogen-burning zones in giant stars. These characteristic times required to reach the equilibrium ratio for N/C are relevant to our problem. Only if the CN isotopes remain at the temperatures listed in the first row of Table XI,1 for times comparable to those listed in the last row will the N/C ratios given in the intervening rows be reached. The last and thus lowest temperature at which the CN isotopes spend sufficient time in mixing to the surface will determine the observed surface ratios. This assumes that the mixed-in CN outweighs that in the original envelope material. An inspection of the table indicates that this last, lowest temperature is probably about 15×10^6 degrees since the time required for N/C to reach its equilibrium value is $\sim 10^7$ years at this temperature. We estimate that 10^7 years is the maximum time available for transport of the original C^{12} from the core through a significant portion of the envelope.

Figure XI,2 gives a schematic representation of the way in which the N/C ratio varies in the hydrogen-burning regions of a star of approximately four solar masses. During the initial condensation of the star, this ratio might be about 1 or 2, as in the solar system material and in young stars like 10 Lacertae and τ Scorpii (see Table XI,2). As hydrogen burning becomes established at central temperatures $20-30 \times 10^6$ degrees, the ratio rapidly reaches an equilibrium value in the range 100–50. When the star leaves the main sequence, gravitational contraction of the core occurs, the temperature of the hydrogen-burning shell rises and N/C decreases. At the onset of helium-burning, C^{12} is produced in the core and eventually some of this new carbon will be mixed into the hydrogen-burning regions. There will be a relatively short period during which the N/C ratio decreases to a minimum, followed by a rapid rise as N/C reaches its equilibrium value at the temperature at which the hydrogen burns in the star, which by now is in a highly evolved stage, per-

TABLE XI,1. Equilibrium nitrogen-carbon ratios as a function of temperature ($\rho x_H = 10$).

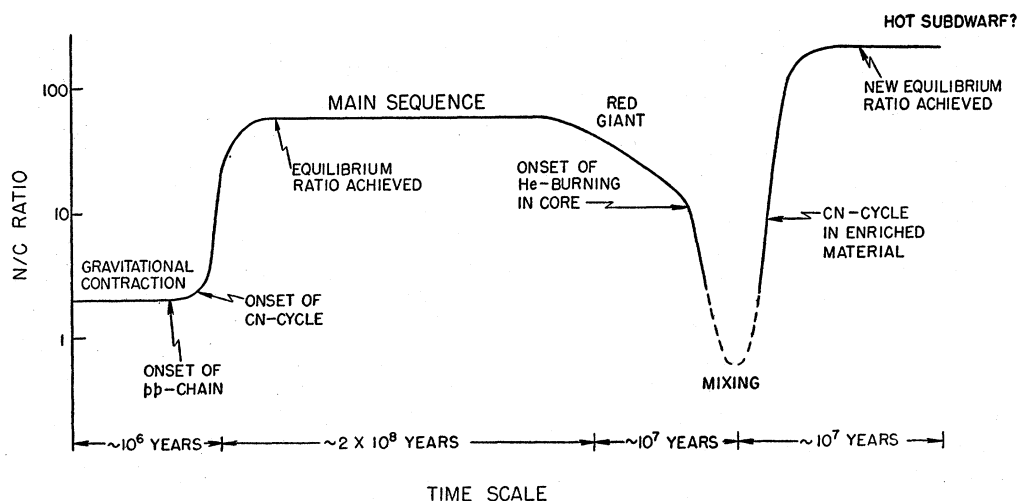| $T(10^6$ degrees)	10	12	15	20	30	40	50	70	100
N^{14}/C^{12} by number	470	250	200	110	58	38	28	17	14
N/C by number	380	210	160	90	47	31	23	14	12
N/C by mass	440	240	180	100	54	36	26	16	13
$\log_{10} t$ (years)	10.6	9.0	7.2	5.1	2.4	0.8	−0.4	−2.1	−3.6

TIME SCALE

FIG. XI,2. Schematic representation of the variation of the N/C ratio in regions where the hydrogen burning occurs in a star of approximately four solar masses. An initial ratio of $\sim$2, as in the solar system, is assumed. The time scales for different phases of the star's evolution are schematically marked as abscissas. With the onset of the CN cycle, an equilibrium ratio in the range $\sim$50–100 is rapidly reached; when the star leaves the main sequence the temperature increases and the ratio drops. The onset of helium burning in the core reduces the ratio to an unknown lower limit defined by the onset of mixing. Passage of the core C^{12} through an outer hydrogen-burning region increases the ratio again to a new equilibrium value.

haps that of a hot subdwarf. The hydrogen-burning zone may be far out from the star's center and thus at a fairly low temperature, say 15×10^6 degrees. In this case we would estimate N/C to be $\sim$160 with an upper limit from uncertainties in cross sections of $\sim$250.

Several groups of stars exist whose spectra give evidence that hydrogen burning and helium burning have been occurring under the various possible conditions that we have just considered. These are as follows:

(i) Some stars, classified by other criteria as being of spectral types O or B, have no hydrogen lines; the stars HD 124448 (Po47), HD 160641 (Bi52), and HD 168476 (Th54) are examples. Helium and carbon lines are strong in all three; the oxygen lines usually prominent at this temperature are completely lacking in HD 168476. A preliminary determination of abundances in HD 160641 (Al54) has shown that carbon, nitrogen, and neon are all more abundant, relative to oxygen, than in normal stars, while helium has completely replaced hydrogen. These three stars have high velocities and may have originated in another part of the Galaxy than the solar neighborhood; they are probably Population II objects. The comparative rarity of such stars among surveys of B-type stars seems to indicate that they do not spend long in this evolutionary stage, or else the conditions under which stars evolve in this way are actually rare.

(ii) Münch and Greenstein have studied seven hot subdwarf stars with peculiar abundances of the light elements, and especially with an apparent excess of nitrogen. An analysis by Münch (Mu57a) of one such star, HZ 44, which is a high-temperature subdwarf, has shown that helium is more abundant than hydrogen.

Nitrogen is about 200–300 times as abundant as carbon. Two determinations of the relative abundances of the elements, by mass, are given in Table XI,2, corresponding to the range of temperature and pressure given by the analysis. Aller's results for HD 160641 [see (i) above], are also given, together with the "normal" abundances by Suess and Urey, the abundances in the main-sequence (unevolved) young stars τ Scorpii and 10 Lacertae obtained by Traving (Tr55, Tr57), and the abundances in τ Scorpii obtained by Aller, Elste, and Jugaku (Al57c) (we have arbitrarily assumed here that the H/He ratio is the same as that determined by Traving). Since numbers of atoms are not conserved during element synthesis ($4H^1 \rightarrow He^4$, $3He^4 \rightarrow C^{12}$ etc.), only percentage abundances by mass are meaningful in considering the amount of increase or decrease in a given element, as compared with its normal abundance. In HZ 44 there appears to have been a slight increase in the sum of the elements heavier than helium, most of which is due to an increase in nitrogen by a factor between 10 and 25. The earlier discussion indi-

TABLE XI,2. A comparison between the chemical compositions of evolved stars and young stars.

		Percentage mass			
Element	Suess and Urey (Su56)	Main sequence young stars Traving	Aller	HZ 44 (Range)	HD 160641
H	75.5	58.6	[58.7]	9.0 – 9.1	0
He	23.3	39.8	[39.8]	88.7 –83.8	95.4
C	0.080	0.17	0.03	0.0047– 0.014	0.31
N	0.17	0.19	0.15	1.66 – 4.85	0.47
O	0.65	0.55	0.40	0.12 – 0.34	0.75
Ne	0.32	0.62	0.84	0.47 – 1.38	3.00
Si	0.053	0.10	0.07	0.17 – 0.48	0.065

cates that this increase is probably due to modification of C^{12}, part of which was present in the star when it condensed, and part of which was produced by helium burning. The following schematic picture may explain the observations. The star has had a helium-burning core in which at least some C^{12} was built, and probably some O^{16} and Ne^{20} (depending on the time-scale and temperature, according to Fig. III,3). Mixing then occurred, and the core material passed out through a hot hydrogen-burning region (30–40×10^6 degrees) in which a good proportion of the oxygen could have been destroyed (depending on the time the material spent at this temperature). The neon isotopes cycled and were not destroyed even if the temperature was high enough for neon to interact. Further modification of the star's structure occurred, and the most recent hydrogen-burning region through which the internal material passed, on being mixed to the surface, was a cool one ($\sim15\times10^6$ degrees), in which the ratio N/C in the enriched material became ~160 by number on the basis of our previous equilibrium estimates and ~300 by observation. Since each of these values has errors of the order of $\pm50\%$ it would seem that they are in satisfactory agreement.

Münch has suggested that HZ 44 (and some other similar stars which he is studying at present) may be of Population I; they have low velocities and differ in other respects from "horizontal branch" stars of Population II, and may be analogous objects in Population I. The absolute magnitude of HZ 44 is in the range $+3$ to $+5$; the surface gravity seems high, and its mass may be considerably larger than 1 $M\odot$.

(iii) The "classical" Wolf-Rayet stars, of both the carbon and the nitrogen groups, belong to Population I. A discussion, which includes references to earlier work, is given by Aller (Al43). There is still disagreement on the extent to which the characteristic broad emission features in the spectra are due to ejection of material, but there seems no doubt that these stars have reached a late evolutionary stage (Sa53). One example is a member of the binary system V 444 Cygni, in which the other component is an early-type massive star. The mass of the WR component is apparently less than the main-sequence component, but is still large (~10 $M\odot$); if the star has reached a later evolutionary stage then its mass may originally have been larger. The lifetime on the main sequence may have been only a few million years. The WR stars are apparently deficient in hydrogen, but upper limits to its abundance have not been set. Helium is apparently the main constituent. In the WC stars the ratios by number of helium: carbon: oxygen are 17:3:1: (Al57a), and nitrogen is not seen at all. In the WN stars the ratios by number of helium: carbon: nitrogen: are about 20:1/20:1 (Al43, Al57a). All these estimates are rough, because of difficulties in abundance determinations, arising through large departures from thermodynamic equilibrium, stratification, etc. However, it

seems probable that in WN stars the surface material has been through the CN cycle (Ga43); according to the dependence of N^{14}/C^{12} as a function of T, the temperature would be quite high, $\sim50\times10^6$ degrees. In WC stars, on the other hand, the products of helium burning have probably reached the surface without being modified by hydrogen burning (Sa53, Gr54a).

(iv) Planetary nebulae are Population II objects (Mi50). The composition of the nebulae is quite similar to that of young stars (Al57d), but the central stars, which can be of WR, Of, or absorption-line O type, are often apparently deficient in hydrogen. Many authors (e.g., Sw52) have pointed out that, among the central stars of WR type, there is not a clear-cut distinction between a carbon and a nitrogen sequence, as there is in Population I WR stars. Apparently the abundance ratio of carbon/nitrogen can take a whole range of values: the balance between the onset of mixing and the extent and temperature of a hydrogen-burning zone would seem not to be so critical as in the case of the Population I WR stars. The masses of the central stars of planetary nebulae are about 1 $M\odot$ (Al56), and their absolute magnitudes are about 0 or $+1$. Bidelman (Bi57) and Herbig (St57) have suggested that the hydrogen-poor carbon stars of the R Coronae Borealis class [see (viii) below] may be the ancestors of some planetary nebulae.

(v) The A-type stars v Sagittarii (Gr40, Gr47) and HD 30353 (Bi50) have anomalously weak hydrogen lines and appear to be rather similar to, although slightly cooler than, HZ 44 [see (ii)]. While helium, nitrogen, and neon are all strong in v Sagittarii, carbon is weak. In Plate 1 (see pages 611–614 for plates) spectra are shown of the region near the Balmer limit in this star and in the A-type supergiant η Leonis (which it resembles in temperature and pressure), obtained by Greenstein at the McDonald Observatory. The comparison between the two stars is striking, the remarkable absence of the Balmer discontinuity in v Sagittarii, and the strength of helium lines while at the same time ionized metals are strong, are impossible to explain other than by an abnormal composition. The great strength of lines other than hydrogen has been explained by the reduced opacity (mainly due to hydrogen in a stellar atmosphere of this temperature), but possibly the temperature is somewhat lower than has been estimated. Both v Sagittarii and HD 30353 are spectroscopic binaries; this might be significant in view of work by Struve and Huang on mass-loss from close binaries (St57a), since one possibility for their evolutionary history is that the stars might have lost most of their hydrogen-containing atmospheres in this way.

(vi) Some white dwarfs, i.e., stars near the end of their life, show strong lines of helium and no hydrogen. These stars must have degenerate cores and the only nuclear fuel remaining must be in the surface layers. In Plate 1 we show Greenstein's spectra of three white dwarfs. One has nothing but strong helium

lines; one with very broad hydrogen lines is shown for comparison, together with one which is discussed in subdivision B of this section.

(vii) The carbon stars, in which bands due to carbon molecules dominate the spectrum instead of bands due to oxides, as in M and S stars, have an abnormally high abundance of carbon relative to oxygen, which will all be used in forming the spectroscopically inaccessible CO molecule. It has therefore not been possible so far to determine the ratio of carbon relative to hydrogen. Bouigue (Bo54a) has found that nearly equal abundances of carbon and oxygen, i.e., a carbon/oxygen ratio between 3 and 6 times normal, could account for the spectroscopic appearance (see Bi54). The carbon/oxygen ratio may vary among the carbon stars (Ke41).

The majority of carbon stars have an apparently normal atmospheric abundance of hydrogen. They may have a higher than normal abundance of the heavy elements (Bi54, Gr54a) (cf. paragraph D (iii) of this section], but no abundance determinations are yet available; technetium has been observed (Me56a). Again, the majority of these stars show bands of $C^{12}C^{13}$ and $C^{13}C^{13}$, indicating that the C^{12}/C^{13} ratio is about 3 or 4 (Mc48), which is near the equilibrium ratio produced in the CN cycle. Thus these stars may be ones in which helium burning ($3He^4 \rightarrow C^{12}$) has been taking place in the core (together, probably, with some neutron production leading to the s process). Large-scale mixing may then have set in *before* all the hydrogen in the envelope had been exhausted; the C^{12} passed through a hydrogen-burning shell on its way out to the surface, and the equilibrium ratio of C^{13} was thus produced. As many authors have noted, nitrogen should be abundant in these stars. Two examples of this kind of star, X Cancri (an irregular variable) and HD 54243, will be seen in Plate 2. Such stars at a later stage in their evolutionary history might look like WN stars or the star studied by Münch, HZ 44. However, the increased carbon/oxygen ratio might possibly be due to destruction of oxygen in a sufficiently hot hydrogen-burning region.

(viii) Some rare specimens among the carbon stars have weak or absent CH bands and hydrogen lines, and have been suggested to be deficient in hydrogen (Wu41, Bi53, Bu53). There is no evidence to suggest that in these stars the C^{12}/C^{13} ratio is smaller than that in the solar system ($\sim$90). Most of the group are variables of the R CrB type; RCrB itself was analyzed by Berman (Be35) and found to be very rich in carbon and deficient in hydrogen. There are a few nonvariable examples, two of which are shown in Plate 2. A spectrum of HD 137613 (Sa40, Bi53) has been borrowed from the Mount Wilson files and is shown alongside the two normal carbon stars; absence of C^{13} bands and weakness of H_β are striking. The stars are not a good match in temperature, and hence differences in their line spectra will be seen; however, HD 137613 is hotter than the

other two so that H_β would be expected to be stronger in it. Greenstein's spectra of the peculiar carbon star HD 182040, first discussed by Curtiss (Cu16), and the normal carbon star HD 156074, which have similar temperatures, are shown together; the weakness of the CH band and H_γ in the former, while C_2 can be seen, is notable. HD 182040 has no detectable C^{13}.

Such stars are too cool to show helium even if it is in high abundance, although Herbig (He49a) suggested tentative identification of an emission feature at λ 3888.4 in the spectrum of R CrB near minimum light with HeI. Possibly the $3He^4 \rightarrow C^{12}$ reaction has been going on in the core and the products were not mixed to the surface until almost all of the hydrogen in the star had been used up, and no hydrogen-burning shell existed, and hence no C^{13} was produced. The R CrB stars probably belong to Population II. Stars of this sort at a later evolutionary stage might look, for example, like HD 124448, or like those central stars of planetary nebulae which are of WC type, as discussed in (iv) above.

Two stars with a large C^{12}/C^{13} ratio, HD 76396 and HD 112869 (Mc48), have excessively strong CH; they belong to the high-velocity group of CH stars studied by Keenan (Ke42). Another star of the same sort is HD 201626 (No53). If C^{12} has actually mixed out to the surface, then it cannot have gone through a hydrogen-burning region. Nitrogen should then be less abundant than in normal carbon stars. One possibility is that these stars do not possess a hydrogen-burning shell, but have a relatively thin surface region in which hydrogen still exists. Another possibility is that the temperature of an outer hydrogen-burning zone was not high enough. The high-velocity (Population II) character of the CH stars means that they may, at the beginning of their lives, have had a ratio of carbon, nitrogen, and oxygen to hydrogen which was much lower than in Population I stars.

(ix) Miss Roman (Ro52) has found that certain G- and K-type giants having high velocities have a peculiar appearance in the cyanogen band; she has designated these the "4150" stars. Bidelman (Bi57) suggested that these stars may have a higher than normal carbon abundance. However, he has commented recently that, although these stars have strong cyanogen (CN), they do not show C_2 bands (private communication). Perhaps they are also examples of stars whose surface layers contain material that has recently passed through the CN cycle; the nitrogen/carbon ratio may be larger than normal.

A peculiar G-type giant, HD 18474 (Bi53, Hu 57a) and two similar stars studied by Greenstein and Keenan, have weak CH and somewhat weakened CN absorption; these seem to have a low carbon/hydrogen ratio, while the abundance of the metals seems to be normal in two of the stars and low in one which has a high velocity (Gr57a).

To summarize, we conclude that the spectroscopic

indications of the occurrence of hydrogen burning and helium burning in stars show great diversity. Hydrogen burning is demonstrated by complete hydrogen exhaustion (e.g., HD 160641, some white dwarfs); partial hydrogen exhaustion and high nitrogen abundance (e.g., HZ 44, WN stars, v Sagittarii); occurrence of C^{13} in the equilibrium ratio with C^{12} (e.g., normal carbon stars). Knowledge of the masses of the various stars mentioned here is scanty, but a wide range may be involved, leading to a range in evolutionary tracks and time-scales (see Fig. XI,1). The general evolutionary sequence, however, is probably as follows: (a) the carbon stars (red giants); (b) stars like HD 160641, the WN stars, and HZ 44 ("horizontal branch" stars and their analogy in Population I); (c) the white dwarfs (exhaustion of fuel, end of life).

Evidence for helium burning is less direct. The main problem is that in cool stars the depletion of oxygen during hydrogen burning will always lead to an apparent increase of carbon, because less CO will be formed. Further study of dissociation equilibria of the various molecules, together with a knowledge of the opacity of carbon stars, may throw more light on the problem. However, the WC stars and possibly HD 124448 may have a large increase in carbon; in HZ 44 a smaller increase may have occurred (see Table XI, 2).

The way in which conditions for hydrogen and helium burning depend on the initial mass of the star is at present quite uncertain, and more computed evolutionary tracks, carried through the onset of helium burning, are needed.

B. α Process

A peculiar white dwarf, Ross 640 (Gr56), has strong features attributed to magnesium and calcium. Greenstein's spectrum of this star is reproduced in Plate 1. Although analyses of white dwarf atmospheres, with their extremely large surface gravities, have not been carried out, it seems hard to explain such a spectrum except by the actual presence of large amounts of the α-process elements magnesium and calcium.

One peculiar and perhaps unique white dwarf has no recognizable spectral features except very broad absorptions at $\lambda\lambda$ 3910, 4135, and 4470. Greenstein (Gr56a) has suggested that these may be the helium lines $\lambda\lambda$ 3889 +3965, 4121+4144, and 4438+4472, arising under conditions of extreme pressure, with the obliteration of atomic orbits which would give rise to other lines normally expected. Burbidge and Burbidge (Bu54) have suggested that the features at $\lambda\lambda$ 3910 and 4135 may be due to Si II $\lambda\lambda$ 3854–3863 and 4128–4131, and that the feature at λ 4470 may be due to Mg II 4481, again under very high pressure, and have proposed that the star has a high abundance of the α-process elements magnesium and silicon.

C. Synthesis of Elements in the Iron Peak of the Abundance Curve, and the Aging Effect as It Is Related to this and Other Types of Element Synthesis

Stars which have evolved so far as to have the central temperatures and densities necessary for the equilibrium production of elements in the iron peak become unstable (see Sec. XII). Thus if they spend only a short time in this stage, specimens in which it is occurring or has recently taken place would be expected to be rare (unless stellar remnants—white dwarfs—are left after the explosion). However, if element synthesis has been going on throughout the life-history of our galaxy we might expect to observe an aging effect in that the oldest stars might have the lowest metal abundances. The following observations support this.

(i) Some stars in whose spectra metallic lines are strikingly weak have been observed. Analysis by Chamberlain and Aller (Ch51) of the so-called subdwarfs, HD 19445 and HD 140283, led to an iron abundance 1/10 of normal and a calcium abundance 1/30 of normal for these stars. A recent more detailed analysis of HD 19445 by Aller and Greenstein (Al57b) has confirmed the low iron abundance, which they find to be 1/20 of normal. Plate 2 shows the photographic region of the spectrum of HD 19445 together with the normal $F7$ V star ξ Peg; HD 19445 actually has a slightly lower temperature than ξ Peg (Gr57), and if it were compared with a $G0$ or $G2$ star (where its temperature places it) the difference in the strength of the metallic lines would be even more striking than illustrated in Plate 2. The absolute magnitude of HD 19445, about +5, is very near to the main sequence at the true temperature of the star; certainly the departure from the main sequence is within the error in the trigonometric parallax. The name "subdwarf" is thus seen to be misleading. Most of the "subdwarfs" in this temperature range have been so designated from spectroscopic parallaxes, which are uncertain since the spectral peculiarities of these stars have caused them to be classified too early on low-dispersion spectrograms.

HD 19445 and HD 140283 have high space velocities and belong to Population II. The implication is that they are members of a spherical distribution of stars which condensed before the Galaxy assumed its present flattened form and hence are old stars. Similar extreme weak-line stars, presumably belonging to Population II, e.g., HD 122563 (Gr57), may have low velocities. The fact that calcium is weakened as well as the iron-peak elements means that this aging effect shows, as would be expected, in other element-building processes besides the e process. Plate 2 shows that a line of Sr II is also weak (strontium is produced by the s process).

Five more stars which have some of the characteris-

tics of Population II were analyzed by Burbidge and Burbidge (Bu56a), by the curve-of-growth method without allowing for the effect of a lowered metal abundance on the opacity. In each star the abundances of a selection among the elements magnesium, aluminum, calcium, scandium, titanium, chromium, manganese, iron, strontium, yttrium, zirconium, and barium were determined. The stars showed a spread in the ratio of the abundances of these elements relative to hydrogen which indicated a range in ages; the most extreme case had a similar ratio to those in HD 19445 and HD 140283. The abundance ratios for strontium, yttrium, and zirconium showed no significant differences from those for iron, but tentative results for barium gave smaller ratios than those for iron (this result was however, uncertain).

(ii) Stars with high space velocities do not belong to the solar neighborhood, and in particular those with high z velocities may be presumed to belong to an older more spherical population. The so-called subdwarfs have very high space motions, but Miss Roman (Ro50, Ro52) and Keenan and Keller (Ke53) found a general correlation between space motion and spectral peculiarities in that high-velocity stars tend to have strong CH and weak CN and metallic lines. A recent analysis of a group of high-velocity stars by Schwarzschild, Schwarzschild, Searle, and Meltzer (Sc57b) has shown that the most extreme example measured by them, ϕ^2 Orionis, has ratios of the metals to hydrogen and of carbon, nitrogen, and oxygen to hydrogen, that are both one quarter of the solar values. The heavy elements also are under-abundant by the same factor as iron. Thus if the different compositions of the so-called subdwarfs, the less extreme high-velocity stars, and the solar-neighborhood stars are due to an aging effect, then elements produced by hydrogen burning, helium burning and the α, e, and s processes are all affected, and in the high-velocity stars the factors are all about the same. Seven high-velocity G-type giants analyzed by Greenstein and Keenan (Gr57a) have values for the metals/hydrogen ratio varying from 0.4 to 0.6 times normal.

(iii) The globular clusters may contain the oldest stars in our galaxy. The age of M3 has been given as 6×10^9 years by Johnson and Sandage (Jo56). It might therefore be expected that the stars in such a cluster would have lower abundances of the metals and other elements than normal. Also, theoretical evolutionary tracks can be made to agree with the observed color-magnitude diagram only if a low metal abundance is used (Ho55). Unfortunately, the brightest main-sequence stars of this cluster (in which turbulence and opacity should have only small effects on abundance determinations) are too faint for spectrophotometric analysis. However, information may be derivable from the colors. The two-color (U−B, B−V) plot for M3 lies well above the normal solar-neighborhood plot throughout its length, while the so-called

subdwarf HD 19445 [see C (i)] lies very near to the M3 plot. This position of HD 19445 may be the result of different "blanketing" of the continuous spectrum by the spectrum lines. All lines are weakened in HD 19445; the metallic lines are more numerous in the blue (B) than in the visual (V) spectral region, and still more numerous in the ultraviolet (U). The effect of weakened metallic lines would therefore be to increase the blue intensity relative to the visual, and to increase the ultraviolet relative to the blue. Qualitatively therefore, as discussed by Johnson and Sandage (Jo56), this is in the same sense as that required to explain the abnormal position of HD 19445 on the U−B, B−V diagram. An accurate evaluation of the effect is currently being made by Sandage, Burbidge, and Burbidge. If this explanation is found to be satisfactory then we shall have indirect proof that the stars of M3 have low metal abundances. Sandage has shown by an approximate calculation that if the amount of light subtracted from the sun's continuum by the spectrum lines is added in the appropriate regions (without allowing for any redistribution of energy caused by blanketing), the effect is to shift the sun on to the M3 line in the (U−B, B−V) plot, at a value of B−V corresponding to a normal F5 star.

(iv) Studies of colors and spectra of external galaxies are still too uncorrelated for us to make deductions concerning abundance variations. It may, however, be worth entertaining the possibility that some of the elliptical galaxies which have much earlier-type spectra than would correspond to their color classes may prove to have low calcium and iron abundances, relative to hydrogen.

(v) Apart from the foregoing discussion of possible aging effects (in other processes besides the e process), no undoubted examples of stars exhibiting the e-process abundances predominantly are known. However, a speculative possibility may be considered. The white dwarf van Maanen 2 shows strong, very broadened lines of iron (Gr56); possibly it has a high abundance of iron. Such stars may be the remnants (perhaps after large mass loss) of stars which reached a central temperature sufficient to build the iron peak, but did not suffer complete catastrophic explosion.

D. s Process

Three groups of giant stars have abundance anomalies that indicate the occurrence of the s process in their interiors. These are (i) the S stars; (ii) the Ba II stars; and (iii) the carbon stars.

(i) The S stars probably have luminosities in the range of normal giants. Elements with neutron magic-numbers appear more predominantly in the spectra of S stars than in M stars of the same temperature (Me47, Al51, Bu52, Bi53a, Me56, Te56). It has been realized for some time that this must be a real atmospheric abundance effect and not an ionization,

TABLE XI,3. Overabundance ratios for the sum of the s-process isotopes of each element in HD 46407, calculated on the assumption that the observed overabundance ratios are due solely to building of the s-process isotopes.

Element	Observed ratio y	Suess and Urey abundances s	$r+p$	Calculated ratio for s-isotopes y'	$\langle\sigma N\rangle y'$
Strontium	4.7	18.79	0.106	4.7	381
Yttrium	7.8	8.9	...	7.8	1326
Zirconium	4.8	52.92	1.53	4.9	884
Niobium	5.2	1.00	...	5.2	832
Molybdenum	3.2	1.4185	1.0015	4.8	343
Ruthenium	7.8	0.6445	0.8452	16.7	1837
Barium	14	3.4326	0.2253	14.9	281
Lanthanum	9.8	2.00	0.0018	9.8	647
Cerium	9.6	2.00	0.2601	10.7	407
Praseodymium	28	0.40	...	28	672
Neodymium	14	1.276	0.1630	15.7	443
Samarium	13	0.3080	0.3448	26.4	4050
Gadolinium	3.0	0.0147	0.668	93	3255
Ytterbium	2.0	0.12346	0.0944	2.8	78
Tungsten	9	0.326	0.1646	13.0	914

TABLE XI,4. Search for r-process elements in HD 46407.

Element	Whether observed in the sun	Sensitive lines: whether accessible	Whether strengthened in HD 46407
Selenium	No	No	No evidence
Bromine	No	No	No evidence
Krypton	No	No	No evidence
Tellurium	No	No	No evidence
Iodine	No	No	No evidence
Xenon	No	No	No evidence
Osmium	Yes	Yes	Inconclusive[a]
Iridium	Yes	Yes	Probably no[b]
Platinum	Yes	Yes	Very probably no[c]
Gold	Yes	Yes	No evidence[d]

[a] All lines in the observed wavelength range of HD 46407 are too badly blended for any identifications to be made.

[b] At the wavelengths of the strongest lines in the observed range, *no lines* are visible, either in HD 46407 or in the standard star.

[c] There are four possible identifications, for all of which the lines in HD 46407 are equal to those in the standard star.

[d] Sensitive line is outside the observed range in HD 46407. Other lines are not seen.

dissociation, or excitation effect. Fujita (Fu39, Fu40, Fu 41) suggested that the S stars have carbon abundances intermediate between M and the carbon stars. The appearance of strong lines of Tc I in S stars (Me52) has been previously described as a good indicator of current nuclear activity and mixing on a time scale $\sim10^5$ years in these stars. In Plate 3 we show two portions of the spectrum of the S-type long-period variable star R Andromedae obtained by Merrill, together with a standard $M5$ III star; this spectrum was taken from the plate files at Mount Wilson Observatory. The first portion shows the lines of Tc I in R Andromedae; the second shows a region where ZrO bands are present in R Andromedae, and TiO bands are seen in the M-type star. The strength of Ba II λ 4554 in R Andromedae will also be noted. The two stars are not a perfect match in temperature, so that some differences in the line spectra will also be noted. R Andromedae is somewhat cooler than the M-type star, and since it is a long-period variable, emission lines will be seen in its spectrum, notably at H_γ.

(ii) From the spectroscopic point of view the rarer Ba II stars (Bi51) represent an easier problem to analyze, since their temperatures are considerably higher, their spectra being of types G-K, while their spectral peculiarities link them closely with the S stars. They have a greater-than-normal abundance of carbon, probably intermediate between the M and the carbon stars. A recent curve-of-growth analysis of HD 46407, a typical Ba II star (Bu57a), has yielded abundances of a large number of elements relative to those in the standard $G8$ III star κ Geminorum, which is very similar in temperature and luminosity and was used as a comparison. Portions of the spectra of HD 46407 and κ Geminorum are shown in Plate 3; the most prominent of the features that are strengthened in the Ba II star are marked. Abundances of all elements which

could be studied, lighter than $A=75$, and in particular elements in the iron peak, are normal. Most of the elements with $A>75$, which are spectroscopically observable, are overabundant; this includes in particular those with neutron magic-numbers. The observed abundance ratios, relative to normal, are given in column 2 of Table XI,3. With the possible exception of gadolinium, all these elements have a large proportion of their isotopes produced in the s process, as is shown in the appendix. On the other hand, with the possible exception of ytterbium, all of the elements with $A>75$ which we have assigned mainly to the s process, and which are spectroscopically observable, are found to be overabundant.

The observations in HD 46407 refer only to the sum of all isotopes of each element, and we wish to derive the true overabundances of those isotopes actually built by the s process. From the appendix we have obtained the sum of the solar-system abundances of the isotopes of each element in Table XI,3 which are built by the s process, and by the r and p processes together. If these sums are denoted by s and $r+p$, respectively, and if the observed and true overabundances are y and y', respectively, then we have

$$y(s+r+p)=y's+r+p.$$

Values of s, $r+p$, and y' are given in columns 3, 4, and 5 of Table XI,3.

Finally, we have taken the mean vale of σN for all the s-process isotopes of each element, and the product of this and y' is given in the last column. Under conditions of steady flow this product should be constant (see Sec. VI), and this is the case to within a factor of about 2, if we exclude ruthenium, samarium, gadolinium, ytterbium. Of these, only samarium has a well-determined abundance, and the possibility that cross sections for this element in the appendix are too large was discussed in Sec. VI. The estimates of σ for Gd^{154}, Gd^{155}, and Yb^{89} may also be too large, while

that for Ba¹³⁴ may be too low. If further abundance determinations confirm the low value of y for ytterbium then it may be found that a smaller proportion of its abundance should be assigned to the s process.

Europium, both of whose isotopes have been assigned to the r process, turned out not to be overabundant in HD 46407. A search for the most abundant of the r process elements in the spectrum of HD 46407 was inconclusive; most of these elements cannot be identified in HD 46407 or in the standard star. However, none were found to be strengthened in HD 46407. The results of this search are given in Table XI,4. This table is given in order to show how difficult it is to identify spectrum lines due to many of the r-process heavy elements, let alone determine abundances, in stars other than the sun.

The elements copper, zinc, gallium, and germanium are all produced predominantly by the s process, yet the first two and probably the last are not overabundant in HD 46407 (we have no evidence concerning gallium). These elements fall on the steep part of σN versus A plot in Fig. VI,3, and this suggests, therefore, that there is a plentiful supply of neutrons produced in Ba II stars, giving the shorter of the two capture-time-scales discussed in Sec. II, and leading to building of elements according to the flat part of the curve in Fig. VI,3. If this process occurs in a volume containing $10^{-2}-10^{-3}$ of the mass of the star, then subsequent mixing could produce the observed overabundances; normal abundances would be expected to be observed for copper, zinc, gallium, and germanium, and depletion of the iron-peak elements would not be detectable. Such a copious flux of neutrons means that interior temperatures of $\sim10^8$ degrees must have been reached. However, we have independent indications, from the presence of an excess amount of carbon in this and other Ba II stars (as also in the S stars), that a temperature sufficient for the reaction 3He⁴→C¹² to occur has been achieved.

Tc I lines have not been observed in Ba II stars; before it can certainly be said that technetium is absent a search should be made for Tc II in the ultraviolet. Possibly the Ba II stars represent a later evolutionary stage than the S stars, or they may evolve from stars in a different mass range in which mixing to the surface takes a time $\gg10^5$ years.

HD 26 is a Ba II star with Population II characteristics (abnormally strong CH, weak metallic lines, and a high velocity). The strongest spectrum lines include those of the rare earths [Vrabec, quoted by Greenstein (Gr54a)]. This suggests that the s process is also taking place in the oldest stars.

(iii) As was mentioned in paragraph A(vii), the carbon stars also have apparent overabundances of the heavy elements, less striking than in the S stars, together with the presence of technetium. Actual abundances have not been determined, but it seems as though the s process has been occurring here also,

perhaps in a smaller volume of the star, while a core containing more carbon is developed. More abundance determinations, together with computations of evolutionary tracks of stars, will be helpful in elucidating the evolutionary differences between M, C, S, and Ba II stars.

E. r Process

The outstanding piece of observational evidence that this takes place is given by the explanation of the light curves of supernovae of Type I as being due to the decay of Cf²⁵⁴ (Bu56, Ba56), together with some other isotopes produced in the r process. Further evidence can be obtained only by interpreting the spectra of Type I supernovae, a problem which has so far remained unsolved.

F. p Process

No astrophysical evidence is at present available for the occurrence of this process. The present theory might suggest that isotopes built in this way should be seen in the spectra of supernovae of Type II.

G. x Process

The situation as far as the astrophysical circumstances of the x process are concerned has been discussed in Sec. X.

H. Nuclear Reactions and Element Synthesis in the Surfaces of Stars

The peculiar A stars, in which large magnetic fields have recently been found (see Ba57), have long been known to have anomalously strong (and often variable) lines of certain elements in their spectra. Abundances of all the observable elements have been determined in two magnetic stars, α^2 Canum Venaticorum and HD 133029, and in one peculiar A star, HD 151199, in which a magnetic field has not been detected, owing to the greater intrinsic width of the spectrum lines, but may well be present (Bu55, Bu55a, Bu56b). The results are given in Table XI,5, which should be compared with Table XI,3 and the discussion of the Ba II star HD 46407. At first glance the results are very similar, particularly in the fact that predominantly the elements with neutron magic-numbers are overabundant, but there are some striking differences, as follows: (a) barium is overabundant in HD 46407, and normal in the peculiar A stars; (b) europium is the most prominently overabundant element in the peculiar A stars, and is normal in HD 46407; (c) silicon, calcium, chromium, and manganese are normal in HD 46507 while calcium is underabundant and the rest are overabundant in the peculiar A stars; and (d) the overabundance ratios of the strontium group and the rare earth group differ by factors of about 2 in HD 46407 and by factors varying from 2 in HD 151199 to 40 in α^2 Canum Venaticorum.

TABLE XI,5. Abundances of the elements in three "peculiar A" stars, relative to those in a normal star.

Element	Magic number isotope (A,N) for anomalous elements	α^2CVn	HD 133029	HD 151199
Magnesium		0.4	1.4	1.2
Aluminum		1.1	2.2	
Silicon	28, 14	10	25	1.3
Calcium	40, 20	0.02	0.05	2.6
Scandium		0.7		
Titanium		2.6	2.3	
Vanadium		1.3	3.2	
Chromium	52, 28	5.2	10.3	1.8
Manganese		16	15:	9
Iron		2.9	4.1	1.1
Nickel		3.0	2	
Strontium	88, 50	14	11.5	65
Yttrium	89, 50	20:		
Zirconium	90, 50	30	40	
Barium	138, 82	$\leq$0.9		0.6
Lanthanum	139, 82	1020:	200:	
Cerium	140, 82	400	190	
Praseodymium	141, 82	1070	630	
Neodymium	142, 82	250	200	
Samarium	144, 82	410	260	
Europium		1910	640	130
Gadolinium		810	340	
Dysprosium		760	460	
Lead	208, 126	1500:	1500:	

Clearly, some kind of element synthesis has been taking place in the peculiar A stars (Fo55a, Bu57). Since it is unlikely that the products of any nuclear reaction in the interior could have mixed to the surface, and since an energy source is available in the atmosphere in the form of the magnetic fields, we have suggested that this represents a special process of element synthesis which can only take place in stellar atmospheres where there is acceleration of nucleons by electromagnetic activity to energies far above thermal. The predominance of magic-number nuclei among the overabundant elements indicates that the type of synthesis probably involves neutrons; in fact, it may be essentially an s process taking place in a proton atmosphere. However, the buildup may be by deuteron stripping reactions (d,p) as well as or instead of by (n,γ) processes; (α,n), $(\alpha,2n)$, and $(\alpha,3n)$ may also occur. Free neutrons are thought to be produced by (p,n) processes on the light nuclei, and their presence in a hydrogen atmosphere means that equilibrium abundances of both deuterium and He^3 will be produced. Evidence for the presence of deuterium in magnetic stars is at present lacking; evidence for the possible presence of He^3 in one of them, 21 Aquilae, has been discussed by Burbidge and Burbidge (Bu56c).

The activity in magnetic stars is thought to take place in "spot" regions, with a duration of only a few seconds (the time-scale is limited by the rate of energy loss by bremsstrahlung), but must continue over long time-scales comparable with the lifetime of the stars in order to build the observed anomalies of the heavy elements, so that each gram of the surface layer is

processed many times. An important condition for the detection of the anomalies is that no mixing between the surface layer and the interior should occur, or it would dilute the products of nuclear activity so that they would not be detectable. This condition happens to be fulfilled in the A-type stars, where the convective layer extends from the photosphere inwards to a depth of only 1000 km (cf. Fo55a).

XII. GENERAL ASTROPHYSICS

A. Ejection of Material from Stars and the Enrichment of the Galaxy in Heavy Elements

Table XII,1 gives a tentative assessment of the production of elements in the Galaxy, the table being subdivided in accordance with the various processes described in the previous sections.

The values given in the third column were obtained in the following way. The fractions by weight of the various groups of elements in the solar system have already been given in Table II,1. These fractions were reduced by a factor 2 (except for hydrogen) to make allowance for the lower concentrations of the heavy elements, relative to the sun, in the stars which are believed to comprise the main mass of the Galaxy. It is clear that some such reduction must be made, and the factor 2, although somewhat uncertain, is based on the work of Schwarzschild et al. (Sc57b; cf. also earlier work mentioned therein). The resulting fractions, when taken together with a total mass of 7×10^{10} $M \odot$ for the Galaxy (Sc56), yield the values shown in the third column of Table XII,1.

The products of the synthesizing processes must be distributed in space. Emission from stellar atmospheres apart, two ejection mechanisms are mentioned in the fourth column of Table XII,1, supernovae, and red giants and supergiants. These are believed to be of main importance, but matter is also ejected from novae, close binary systems (St46, Wo50, St57a), P Cygni and WR stars, and planetary nebulae (cf. Gu54, St57). Leaving aside the x process, the association between the second and fourth columns of Table XII,1 was made on the basis that only in supernovae are temperatures of thousands of millions of degrees reached. Reasons for this view have been given in Sec. III,F. In contrast, temperatures of hundreds of millions of degrees may be expected in red giants and supergiants (Sec. V, B), and in the other contributors, novae, binaries, etc. Thus, processes of synthesis requiring temperatures of order 10^8 degrees have been associated with the giants, whereas processes requiring temperatures of order 10^9 degrees have been associated with supernovae.

Estimates of the total amount of material which may have been distributed in space by supernovae and red giants and supergiants, assuming a constant

TABLE XII,1.

Elements	Mode of production	Total mass in galaxy ($M_\odot$ as unit)	Astrophysical origin	Total mass of all material ejected over lifetime of galaxy ($M_\odot$ as unit)	Required efficiency
He	H burning	8.1×10^9	Emission from red giants and supergiants	2×10^{10}	0.4
D	x process?	7.5×10^6?	Stellar atmospheres? Supernovae?	?	?
Li, Be, B	x process	8.5×10^2	Stellar atmospheres	?	?
C, O, Ne	He burning	4.3×10^8	Red giants and supergiants	2×10^{10}	2×10^{-2}
Silicon group	α process	4.0×10^7	Pre-Supernovae	2×10^8	0.2
Silicon group	s process	8.5×10^6	Red giants and supergiants	2×10^{10}	4×10^{-4}
Iron group	e process	2.4×10^7	Supernovae	2×10^8	0.1
$A>63$	s process	4.5×10^4	Red giants and supergiants	2×10^{10}	2×10^{-6}
$A<75$	r process	5×10^4	Supernovae Type II	1.7×10^8	3×10^{-4}
$A>75$	r process	10^4	Supernovae Type I	3×10^7	3×10^{-4}
$A>63$	p process	1.3×10^2	Supernovae Type II	1.7×10^8	10^{-6}

rate of star formation and death during the lifetime of the Galaxy, are given in the fifth column of Table XII,1 and were made in the following way.

The rates of supernovae were taken to be 1 per 300 years for Type I and 1 per 50 years for Type II, as estimated by Baade and Minkowski (Ba57a), and the age of the Galaxy was taken as 6×10^9 years. The average mass emission per supernova is not easy to estimate (see Sec. XII,C), but we have taken it to be 1.4 $M\odot$. The exponential-decay light curve is characteristic of Type I and not of Type II supernovae; this has been taken to indicate that the rapid production and capture of neutrons, leading to synthesis of the heaviest r-process elements, occurs only in Type I supernovae. The lighter r-process elements are probably made in Type II supernovae, while the products of the α and e processes may perhaps be made in either type.

The estimate for the ejection of mass by red giants and supergiants was based on the assumption that such stars shed most of their material into space during the giant phases of their evolution. Thus Deutsch (De56) has shown that matter is streaming rapidly outwards from the surface of an M-type supergiant, and he considers from the spectroscopic data that probably all late-type supergiants are also ejecting material at a comparably rapid rate. There is also some evidence that normal giant stars are ejecting matter, although probably on a smaller scale. Hoyle (Ho56b) has indicated that mass loss may have a more important effect on the evolution of giants and supergiants of very low surface gravity than have nuclear processes. With these considerations in mind, it is necessary to estimate the fraction of the mass of the Galaxy that has been condensed into stars which have gone through their whole evolutionary path.

The luminosity and mass functions for solar-neighborhood stars have been studied by Salpeter (Sa55a). He has shown that stars which lie on the main sequence now with absolute visual magnitudes fainter than $+3.5$ (which form the bulk of stars at present in ex-

istence) make up 55% of the total mass. Stars which formed with magnitudes brighter than $+3.5$ (the majority of which have gone through their whole evolutionary path) make up the remaining 45%. We find from his mass function that the average mass of the stars brighter than $+3.5$ was 4 $M\odot$. Since the upper limit to the mass of a white dwarf is about 1.4 $M\odot$, we find that, of the remaining 45%, 16% may lie in white dwarfs and 29% in the form of ejected gas. Thus the division of mass between stars which have not evolved, white dwarfs, and material which has been processed by stars is approximately 4:1:2. Extrapolating these results to the Galaxy as a whole, we find that 2×10^{10} $M\odot$ has been processed by stars. Some of this is included in the estimate of matter ejected by supernovae, but the majority will have been processed at temperatures $\lesssim10^8$ degrees, and ejected by red giants and supergiants.

The efficiency of production of each group of elements in the total ejected material that is necessary to explain the abundances in column 3 of Table XII,1 is obtained by dividing column 3 by column 5, and is given in the last column. It must be emphasized here that the estimates given in Table XII,1 are very preliminary. Even on an optimistic view they might well prove incorrect by as much as a factor 3. It is noteworthy, however, that the emission seems adequate to explain the synthesis requirements, except possibly in the case of deuterium, and helium, which is the only element needing an efficiency near to unity for its production. It will be clear from the foregoing that our estimates are not accurate enough to establish whether or not it is necessary to assume some helium in the original matter of the Galaxy.

The efficiency necessary to produce the r-process elements is considerably smaller than that required to give the observed supernova light curves (see Sec. XII,C). It should, in addition, be reiterated that we have no evidence at all concerning the abundances of the r-only and p-process isotopes outside the solar system, as we pointed out in Sec. XI.

If the universal value of the deuterium to hydrogen ratio turns out to be of order 10^{-4}, it will be difficult to provide for an adequate abundance of deuterium by processes of an electromagnetic nature occurring in stellar atmospheres, as has already been pointed out in Sec. X,C. The possible alternative process of origin, also discussed in Sec. X,C, rests on considerations to be given in Sec. XII,B. At sufficiently high temperatures $(T > 7 \times 10^9$ degrees) elements of the iron group break down into α particles and neutrons. For example, $Fe^{56} \to 13\alpha + 4n$. In Sec. XII,B the onset of a supernova is associated with such breakdown reactions developing in the central regions of a star. In Type II supernovae, hydrogen is present in the outer expanding envelope, and capture of the neutrons by relatively cool hydrogen yields deuterium without subsequent disintegration. As was pointed out in Sec. X,C, if one supernova converted one solar mass of its envelope into deuterium and was then diluted by mixture with 10^4 solar masses, the terrestrial abundance would result. These estimates of production and dilution are not at all unreasonable. On this basis the galactic abundance of deuterium would not necessarily be as large as in the solar system.

The balance between the observed solar-system abundances and the material ejected from stars has been made on the assumption of a constant rate of star formation and death during 6×10^9 years. There are some considerations which suggest that the rate may have been greater in the early history of the Galaxy.

First, recent work on the 21-cm radiation by hydrogen, reviewed by van de Hulst (Hu56), has shown that neutral atomic hydrogen makes up only a few percent of the total mass of both our Galaxy and M31 (and it probably comprises the major part of the gas and dust). Star formation is currently occurring only in Population I regions, which comprise about 10% of the mass of the Galaxy (by analogy with the ratio found by Schwarzschild (Sc54) in M31). Originally the Galaxy must have been composed entirely of gas. Thus it would seem probable that star formation and element synthesis would have occurred at a greater rate early in the life of the Galaxy, and, as a larger and larger fraction of the mass became tied up in small stars and in white dwarfs, so nuclear activity would have been a decreasing function of the age of the Galaxy.

Second, the solar system is 4.5×10^9 years old, and the uranium isotope ratio (Sec. VIII) gives 6.6×10^9 years as the minimum age of the r-process isotopes. Thus the abundances that we are discussing (which are half the solar system abundances) must have been formed (by all 8 synthesizing processes) in a time less than the age of the Galaxy, say $1-2 \times 10^9$ years. Also, there are apparently large abundance differences between extreme Population II stars such as the globular clusters M92 (and M3) and, for example, the old galactic cluster M67, while the ages that have been given do not differ correspondingly and are both $\sim 6 \times 10^9$ years (Jo56, Sa57a). It is of interest to mention recent investigations of the color-magnitude diagram of the nearby stars by Sandage (Sa57b) and by Eggen (Eg57), based on the data of Eggen (Eg55, Eg56) and the Yale Parallax Catalogue (Ya52). There are a few stars to the right of the main sequence at $M = 3.5$ to 4; if the parallaxes are accurate then they may be either stars which are still contracting and have not yet reached the main sequence, or they may have evolved off the main sequence. In the latter case, their ages would be $\gtrsim 8 \times 10^9$ years.

These facts may be reconciled if we suppose that star formation and death in the originally spherical gaseous Galaxy occurred at a sufficient rate to produce element abundances which then recondensed into the oldest star systems that we see today in the halo. The initial differentiation of Populations I and II was interpreted as one of location in the Galaxy and of comparative youth (spiral arms) and age (halo, nucleus). However, it is clear that a number of subclassifications are demanded (Pa50, We51, Bu56a). While the oldest halo stars that we see today were condensing, we may suppose that concentration towards the center and the equatorial plane was occurring, and the formation of stars was favored by conditions in the flattening higher-density region, leading to a rapid gradient of heavy-element enrichment so that star systems forming in the disk at nearly the same time as the globular clusters had higher abundances of heavy elements. Only gas will contract in this way; stars, once formed, become "frozen" in the shape of the system at the time of their formation. The remaining gas became concentrated into the spiral arms, so that these were the only places where any star formation could any longer occur. If, during the first $1-2 \times 10^9$ years in the life of the Galaxy, the average proportion of the mass in which star formation was occurring is taken as 50% (instead of 10% as now), then the increased rate of nuclear activity would compensate for the shorter time scale for element synthesis.

Finally, it is of some importance to discuss the cosmological background to this problem. In an evolutionary explosive cosmology we have that, if T is the age of a system, $T_{universe} > T_{galaxy} > T_{some\ clusters} > T_{sun}$. Apart from the products of an initial ylem, if this type of initial condition is proposed, the Galaxy will condense out of primeval hydrogen, and the synthesis will go on as we have already described it. It is of interest that possibly the ylem production of deuterium could be incorporated in a model of this sort. Alternatively, in a steady-state cosmology we have only that $T_{galaxy} > T_{some\ clusters} > T_{sun}$, and we should expect that the initial condensation of the Galaxy would take place out of gas which already had a weak admixture of the heavy elements that had been synthesized in other galaxies. Thus it might be that a search for low-mass stars of pure hydrogen would present

a possible cosmological test, although such stars might take so long to condense (He55) that they would have become contaminated with the products of the death of massive stars before they had been able to contract themselves into self-contained stars.

It is also of interest to remark on the final stages of galactic evolution. Although, as remarked in the Introduction, the lowest energy state of the elements would be reached when the galaxy was transmuted to iron, it appears that the astrophysical circumstances lead to the matter being finally all contained in white dwarfs (degenerate matter), so that such an extreme condition as an iron galaxy may never be reached.

It should be emphasized that the present value of $1/H$ determined from the red-shift measurements by Humason, Mayall, and Sandage (Hu56a) is 5.4×10^9 years, and this in the evolutionary cosmologies is a time of the order of the age of the universe. However, this value is in conflict with the ages of some star clusters in our galaxy. Thus any attempt to relate the synthesis of the elements in the galaxy through a number of necessarily complex steps to a particular cosmological model must await the resolution of this dilemma.

B. Supernova Outbursts

In the following discussion we consider the course of evolution that in our view leads to the outbursts of supernovae. According to a well-known calculation by Chandrasekhar the pressure balance in a star cannot be wholly maintained by degeneracy for masses greater than a certain critical mass. For pure He^4 this critical mass turns out to be $1.44\ M\odot$, while for pure iron the value is $1.24\ M\odot$.

It follows that stars with masses greater than the critical value cannot be in mechanical support unless there is an appreciably temperature contribution to their internal pressures. Mechanical support therefore demands high internal temperatures in such stars.

Our arguments depend on these considerations. We are concerned with stars above the Chandrasekhar limit, and assume that mechanical support is initially operative to a high degree of approximation. This is not a restriction on the discussion, since our eventual aim will be to show that mechanical support ceases to be operative. A discussion of catastrophic stars would indeed be trivial if a lack of mechanical support were assumed from the outset.

The next step is to realize that a star (with mass greater than the critical value) must go on shrinking indefinitely unless there is some process by which it can eject material into space. The argument for this startling conclusion is very simple. Because of the high internal temperature, energy leaks outwards from the interior to the surface of the star, whence it is radiated into space. This loss of energy can be made good either by a slow shrinkage of the whole mass of the star (the shrinkage being "slow" means that mechanical support is still operative to a high

degree of approximation), or by a corresponding gain of energy from nuclear processes. But no nuclear fuel can last indefinitely, so that a balance between nuclear energy generation and the loss from the surface of the star can only be temporary. For stars of small mass the permissible period of balance exceeds the present age of the galaxy, but this is not so for the stars of larger mass now under consideration. Hence for these stars shrinkage must occur, a shrinkage that is interrupted, but only temporarily, whenever some nuclear fuel happens for a time to make good the steady outflow of energy into space.

Shrinkage implies a rising internal temperature, since mechanical support demands an increasing thermal pressure as shrinkage proceeds. It follows that the internal temperature must continue to rise so long as the critical mass is exceeded, and so long as mechanical support is maintained. The nuclear processes consequent on the rise of temperature are, first, production of the α-particle nuclei at temperatures from $1-3 \times 10^9$ degrees and, second, production of the nuclei of the iron peak at temperatures in excess of 3×10^9 degrees. It is important in this connection that the temperature is not uniform inside a star. Thus near the center, where the temperature is highest, nuclei of the iron peak may be formed, while outside the immediate central regions would be the α-particle nuclei, formed at a somewhat lower temperature, and still further outwards would be the light nuclei together with the products of the s process, formed at a much lower temperature. Indeed some hydrogen may still be present in the outermost regions of the star near the surface. The operation of the r process turns out to depend on such hydrogen being present in low concentration. The p process depends, on the other hand, on the outer hydrogen being present in high concentration.

Turning now to the nuclei of the iron peak, the statistical equations given in Sec. IV show that the peak is very narrow at $T \sim 3 \times 10^9$ degrees, the calculated abundances falling away sharply as the atomic weight either decreases or increases from 56 by a few units. At higher temperatures the peak becomes somewhat wider, ranging to copper on the upper side and down to vanadium on the lower side. Beyond these limits the abundances still fall rapidly away to negligible values with one exception, the case of He^4. From (6) in Sec. IV we find that the statistical equations yield the following relation between the abundances of He^4 and Fe^{56}

$$\log n(4,2) = 34.67 + \tfrac{3}{2} \log T_9$$

$$+ \frac{1}{14} \{\log n(56,26) - 36.40 - \tfrac{3}{2} \log T_9\} - \frac{34.62}{T_9} + \frac{\theta}{7}.$$

or

$$\log n(4,2) - \frac{\log n(56,26)}{14} = 32.08 + 1.39 \log T_9 - \frac{34.62}{T_9} + \frac{\theta}{7}.$$

Under the conditions of the present discussion the densities of free protons and neutrons are comparable and small compared with the helium and iron densities, so that the θ term is small and is neglected.

We consider the application of this equation for a fixed value of the total density equal to 10^8 g/cm^3. This is a plausible value for $T \simeq 7 \times 10^9$ degrees ($T_9 \simeq 7$), and is the mean density of a stellar core of $1 M \odot$ with a radius of 1.7×10^8 cm. Supposing that conditions in this core are such that the mass is equally divided between He^4 and Fe^{56}, then $\log (4,2) = 30.88$ and $\log n(56,26) = 29.73$, since no other nucleus makes an appreciable contribution to the density. Substituting in the equation above we find that then $T = 7.6 \times 10^9$ degrees. Thus when T rises above about 7×10^9 degrees there is a very considerable conversion of iron into helium.

This result is not very dependent on the particular value of 10^8 g/cm^3 used above, since the critical temperature at which the masses of helium and iron are comparable increases only slowly with the density (Ho46). The density cannot differ very much from 10^8 g/cm^3. Thus a value much less than 10^6 g/cm^3 would be most implausible for $T \sim 7 \times 10^9$ degrees, while a value appreciably greater than 10^8 g/cm^3 is forbidden by the condition that there must be an appreciable thermal contribution to the pressure.

The argument now runs as follows. Let us suppose that the temperature increases to 8.2×10^9 degrees. In this case the right-hand side of the equation increases by 0.4 and in order that the equation is satisfied, the difference between $\log n(4,2)$ and $(1/14) \log n(56, 26)$ must also increase by 0.4. However, $\log n(4,2)$ can only increase by 0.3 since at this point the total mass of the core will be in the form of helium. Thus an increase in temperature of 0.6×10^9 degrees implies that the numerical value of the term $(1/14) \log n(56,26)$ is decreased by at least 0.1, and this implies a drop in the amount of iron of at least a factor of 25. So we conclude that an increase in temperature from 7.6 to 8.2×10^9 degrees causes nearly all of the iron to be converted to helium; i.e., from the situation that the mass is equally divided between helium and iron we reach conditions in which $\sim 98\%$ of the mass is helium and $\sim 2\%$ is iron. A similar conclusion follows for other values of the total density. However, for much higher temperatures the term in θ becomes important, reflecting the approach toward a neutron core which would be achieved at extremes of density and temperature.

To convert 1 g of iron into helium demands an energy supply of 1.65×10^{18} ergs. This may be compared with the total thermal energy of 1 gram of material at 8×10^9 degrees which amounts to only 3×10^{17} ergs. Evidently the conversion of iron into helium demands a supply of energy much greater than the thermal content of the material. The supply must come from gravitation, from a shrinkage of the star, and clearly

the shrinkage must be very considerable in order that sufficient energy becomes available. This whole energy supply must go into the conversion and hence into nuclear energy, so that very little energy is available to increase the thermal content of the material. However, instantaneous mechanical stability in such a contraction would demand a very large increase in the internal temperature. Thus we conclude that in this contraction, in which the thermal energy is, by hypothesis, only increased by a few percent, there is no mechanical stability, so that the contraction takes place by free fall inward of the central parts of the star. At a density of 10^8 g/cm^3, this implies an implosion of the central regions in a time of the order of 1/5 of a second ($\tau \simeq (4/3\pi G\rho)^{-\frac{1}{2}}$ and in our view it is just this catastrophic implosion that triggers the outburst of a supernova.

Before considering the consequences of implosion, it is worthwhile emphasizing that loss of energy by neutrino emission, the urca process (Ga41), is very weak compared to the process described above. Neutrino emission does not rob a star of energy at a sufficiently rapid rate to demand catastrophic implosion, though at temperatures in excess of $\sim 3 \times 10^9$ degrees it does promote a much more rapid shrinkage of the star than would otherwise arise from the loss of energy through normal radiation into space. The reaction Mn$^{56}(\beta^-\nu)$Fe^{56} with a half-life of 2.58 hr probably gives the main contribution to the loss of energy through neutrino emission. The binding energy of Mn^{56} is less than that of Fe^{56} by 2.895 Mev. Thus, under conditions of statistical equilibrium near $T = 5 \times 10^9$ degrees, this implies that Mn^{56} is less abundant than Fe^{56} by a factor $\sim 10^3$. Hence, it is reasonable to suppose that a fraction of about 10^{-3} of the mass is in the form of Mn^{56}. The beta decay of this nucleus leads to an energy loss of about 3×10^{12} ergs per gram of Mn^{56}. Thus a time-scale of about 10^8 sec is demanded to produce an energy loss by neutrino emission comparable with the thermal energy possessed by the stellar material. Hence we conclude that under these conditions in the stellar core, the urca process is quite ineffective as compared with the refrigerating action of the conversion of Fe^{56} to He^4.

The last question to be discussed is the relationship between the *implosion* of the central regions of a star and the *explosion* of the outer regions. Two factors contribute to produce explosion in the outer regions. The temperature in the outer regions is very much lower than the central temperature. Because of this the outer material does not experience the same extensive nuclear evolution that the central material does. Particularly, the outer material retains elements that are capable of giving a large energy yield if they become subject to sudden heating, e.g., C^{12}, O^{16}, Ne^{20}, Ne^{21}, He^4, and perhaps even hydrogen. The second point concerns the possibility of the outer material experiencing a sudden heating. Because under normal

conditions the surface temperature of a star is much smaller than the central temperature, material in the outer regions normally possesses a thermal energy per unit mass that is small compared with the gravitational potential energy per unit mass. Hence any abnormal process that causes the thermal energy suddenly to become comparable with the gravitational energy must lead to a sudden heating of the outer material. This is precisely the effect of an implosion of the central regions of a star. Consequent on implosion there is a large-scale conversion of gravitational energy into dynamical and thermal energy in the outer zones of the star.

One last point remains. Will the gravitational energy thus released be sufficient to trigger a thermonuclear explosion in the outer parts of the star? The answer plainly depends on the value of the gravitational potential. Explosion must occur if the gravitational potential is large enough. In a former paper (Bu56) it was estimated that a sudden heating to 10^8 degrees would be sufficient to trigger an explosion. This corresponds to a thermal energy $\sim 10^{16}$ ergs per gram. If the gravitational potential per gram at the surface of an imploding star is appreciably greater than this value, explosion is almost certain to take place. For a star of mass 1.5 $M\odot$, for instance, the gravitational potential energy per unit mass appreciably exceeds 10^{16} ergs per gram at the surface if the radius of the star is less than 10^{10} cm. At the highly advanced evolutionary state at present under consideration it seems most probable that this condition on the radius of the star is well satisfied. Hence it would appear as if implosion of the central regions of such stars must imply explosion of the outer regions.

Two cases may be distinguished, leading to the occurrence of the r and p processes. A star with mass only slightly greater than Chandrasekhar's limit can evolve in the manner described above only after almost all nuclear fuels are exhausted. Hence any hydrogen present in the outer material must comprise at most only a small proportion of the total mass. This is the case of hydrogen deficiency that we associate with Type I supernovae, and with the operation of the r process. In much more massive stars, however, the central regions may be expected to exhaust all nuclear fuels and proceed to the point of implosion while much hydrogen still remains in the outer regions. Indeed the "central region" is to be defined in this connection as an innermost region containing a mass that exceeds Chandrasekhar's limit. For massive stars the central region need be only a moderate fraction of the total mass, so that it is possible for a considerable proportion of the original hydrogen to survive to the stage where central implosion takes place. This is the case of hydrogen excess that in the former paper we associated with the Type II supernovae, where the p process may occur. However, the rarity of the p-process isotopes, and hence the small amount of

material which must be processed to synthesize them, suggests that if Type II supernovae are responsible, the p process is a comparatively rare occurrence even among them. On the other hand, in any supernova in which a large flux of neutrons was produced, a small fraction of those having very high energies might escape to the outer parts of the envelope, and after decaying there to protons, might interact with the envelope material and produce the p-process isotopes.

Energy from the explosive thermonuclear reactions, perhaps as much as fifty percent of it, will be carried inwards, causing a heating of the material of the central regions. It is to this heating that we attribute the emission of the elements of the iron peak during the explosion of supernovae.

C. Supernova Light Curves

The left-hand side of Plate 4 shows the Crab Nebula, the remnant of a supernova which exploded in 1054 A.D. The right-hand side of Plate 4 shows three exposures of the galaxy IC 4182 during the outburst and fading of the supernova of 1937. The first exposure (20 min) shows the supernova at maximum brightness; the second (45 min) shows it about 400 days after maximum; on the third (85 min) the supernova is too faint to be detected.

Throughout this paper we have proposed that the production of the e-process, r-process, and p-process isotopes takes place immediately preceding or during such outbursts of supernovae. This is the only type of astrophysical process that we know of, apart from an initial state in an evolutionary cosmology, in which it can be presumed that the necessary high-energy, rapidly evolving conditions can be expected. Thus while we were searching for such an astrophysical situation the discovery that the half-life for decay by spontaneous fission of Cf^{254} was equal to the half-life for decay of the light curve of the supernova in IC 4182 (Bu56, Ba56) led us to make the detailed calculations which are described in Secs. VII and VIII.

Since this original work was carried out, there has been further investigation of the half-life of Cf^{254} (see Sec. VIII). Also we have re-examined the evidence concerning the light curves of supernovae. Results of the calculations have allowed us to re-examine the basic assumption made in our earlier papers, that the energy released in the decay of Cf^{254} must dominate over all of the other possible sources of decay energy.

The half-life of 55 ± 1 days was obtained from Baade's result on the supernova in IC 4128. In Fig. XII, 1 we show Baade's light curve of the supernova in IC 4182, and the light curves of Tycho Brahe's nova and Kepler's nova (Ba43, Ba45), together with estimated points for the supernova of 1054 (the Crab Nebula) (Ma42). For SN IC 4182 the observations have been made for as long as 600 days after maximum. The absolute magnitude of this supernova at maximum has been
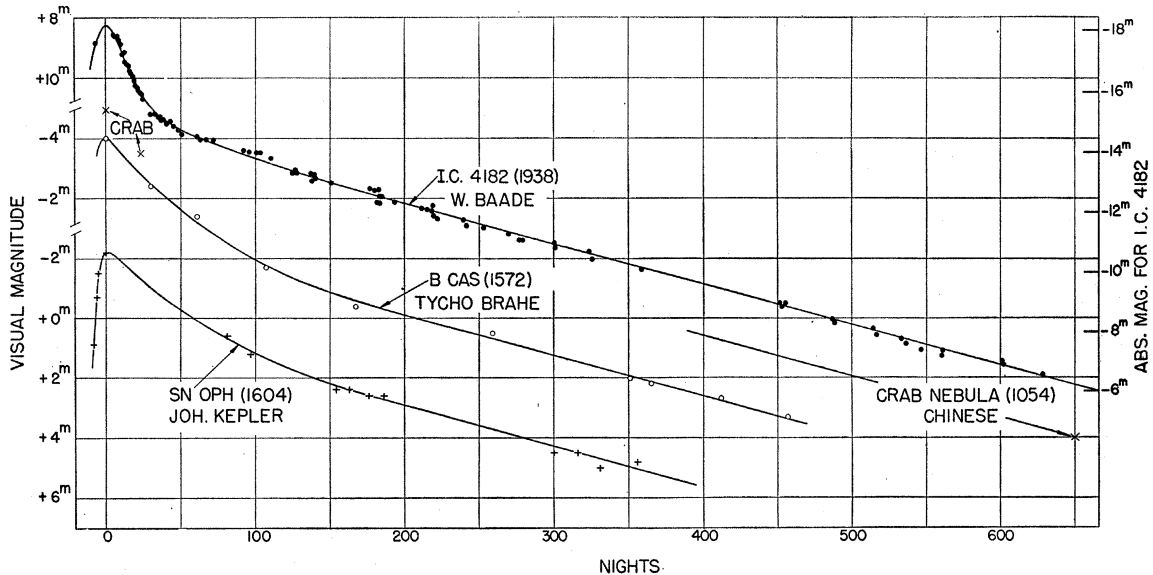
Fig. XII,1. Light curves of supernovae by Baade (Ba43, Ba45, Ba56). Measures for SN IC 4182 are by Baade; those for B Cassiopeiae (1572) and SN Ophiuchi (1604) have been converted by him to the modern magnitude scale from the measures by Tycho Brahe and Kepler. The three points for the supernova of 1054 are uncertain, being taken from the ancient Chinese records (Ma42). The abscissa gives the number of nights after maximum; the left-hand ordinate gives the apparent magnitude (separate scale for each curve); the points for the Crab Nebula belong on the middle scale, i.e., that for B Cassiopeiae. The right-hand ordinate gives the absolute magnitude for SN IC 4182 (Ba57a) derived by using the current distance scale. Compare with Fig. VIII,3.

estimated, with the best current value for the distance scale correction, to be −18.1 (Ba57a). The absolute magnitude of the Crab at its maximum in 1054 has been estimated to be −17.5 to −16.5 (To1355, Ma42, Ba57a). The value of 55 days for the half-life of SN IC 4182 was derived mainly from the points far out in the light curve where apparent magnitudes fainter than +19 had to be measured. Any systematic errors in measuring the faint magnitudes in this region would have the effect of changing the estimated value of this half-life and the possibility that such errors are present cannot be ruled out (Ba57a). The uncertainties in the measurements of other supernovae, which are not described here, are such that either all supernovae have true half-lives of 55 days, or they may have a unique half-life slightly different from 55 days, but lying in the range 45–65 days. Alternatively there may be an intrinsic variation between different light curves. These observational uncertainties must be borne in mind when considering the following discussion.

The only comparisons that we shall attempt to make will be between the total radiant energy emitted by a supernova and the form of the light curve, and the total energy emitted and the energy decay curves based on the calculations in Sec. VIII. No direct comparison between the early parts of the supernova light curve and the energy decay curve are possible, since the energy-degradation processes and the energy-transfer processes in the shell of the supernova will distort the relation between the two. Some aspects

of this part of the problem have recently been studied by Meyerott and Olds (Me57).

Astrophysical arguments concerning the amounts of the r-process elements which are built in supernovae come from three different directions:

(i) The supernova or the supernovae which synthesized the r-process material of the solar system.

(ii) The Crab Nebula, the only remnant of a supernova which has been studied in any detail.

(iii) The light curves of supernovae which enable us to estimate how much material has been involved in the outburst, either on the assumption that the energy released by one or two of the isotopes dominates, and defines the light curve, or on the assumption that all of the decay activity is important.

Let us suppose that a total mass $mM\odot$ is ejected in a particular supernova outburst and that a fraction f of this mass is in the form of r-process elements. Further, let us suppose that a fraction g of the heavy elements is in the form of Cf^{254}, or alternatively that a fraction g' of the heavy elements is in the form of Fe^{59}. In Sec. VIII it was shown that under specific conditions this was the only other isotope which could be expected to contribute an amount of energy comparable with Cf^{254}. Since it has a half-life of 45 days it cannot be *a priori* excluded from the discussion, particularly if, as has been stated above, some of the supernova light curves may have half-lives which are near to 45 days.

On the basis that Cf^{254} is responsible for the total

energy released in the light curve after this curve has reached its exponential form, an approximation which will be corrected in what follows, we have, since the energy release per Cf^{254} nucleus is 220 Mev, that the total energy available in the Cf^{254} is $gfm \times 1.67 \times 10^{51}$ ergs. Of the unknowns m, f and g, m is unknown for all supernovae except the Crab which may have a mass of about 0.1 $M \odot$ (Os57) so that $m \simeq 0.1$. The uncertainties in this value are discussed later. The value of f is determined by the conditions in the outer envelope of the star which have developed in its evolution to the supernova stage, while g is determined by the degree of building in the r process.

We consider the possible values of f. The most favorable situation that can be attained is reached when there are equal amounts by number of hydrogen, helium, and carbon, oxygen, and neon taken as a group, and about 1% of iron by number. In schematic terms, the sequence of events is as follows. The protons are captured by the C^{12}, O^{16}, Ne^{20} to form, after beta decay, C^{13}, O^{17}, Ne^{21}. Each of these now captures an alpha particle and releases a single neutron, so that we end with O^{16}, Ne^{20}, and Mg^{24}, together with a source of free neutrons. To build into the heavy element region, about 100 neutrons per Fe^{56} nucleus are required. These neutrons have come, via the steps that we have outlined, from the original hydrogen. Thus by number the necessary ratio of hydrogen to iron is 100:1, and the mass ratios of the material are hydrogen: helium: carbon: oxygen: neon: iron = 1:4:4:5.33:6.67: 0.56, so that the iron comprises about 2% of the envelope by mass, and after the outburst about 6% of the mass is transformed into heavy elements. The maximum value of f is then 0.06. This situation is probably unrealistic because we have assumed essentially that the efficiency of the process is 1, since all of the hydrogen has been converted to neutrons, and each light nucleus has produced one neutron. As a more conservative value we will take $f_{max} = 0.01$.

A number of values of g are possible; $g = 1$ corresponds to the situation in which all of the heavy elements are transmuted to Cf^{254}. We can see no reason from the standpoint of nuclear physics why this should occur and consequently we are inclined to disregard it.

If all of the r-process material is transformed into material lying in the range of atomic weight $230 < A < 260$, then we see from Fig. VII,4 that $g \simeq 0.04$. This is also a very unreal situation, since while no material resides in the region below $A \simeq 230$, it is also supposed that no fission has taken place to terminate the r process and hence to begin to cycle the material between $A = 110$ and $A = 260$.

We can consider a third situation in which, starting from iron, the material has been driven so that all of the r-process peaks have been produced in the way that has been described in Sec. VII. Further nuclear activity results in the following situation. The material begins to cycle between $A = 110$ and $A = 260$, because,

following fission of the heaviest isotopes, the fission fragments help to build in the regions $A = 110$ and $A = 150$, and the total amount of material which resides in the region $110 < A < 260$ is determined by the amount of cycling which can take place. Sufficient cycling reduces the amount of material in the region < 110, and in the extreme case we suppose that no iron is left and also no material is left in the $N = 50$ peak. Under these conditions we estimate, from Figs. VII,3 and VII,4, that $g \simeq 0.011$. Here we have supposed that only half of the abundance follows the part of the cycle between $A \simeq 110$ and $A \simeq 150$.

A fourth situation is just that which has been supposed to give rise to the solar-system abundances of the r-process isotopes. In this case a steady state is reached and no appreciable cycling has taken place. Reference to Fig. VII,3 and VII,4 shows that $g \simeq 0.002$.

A fifth situation is that in which the r-process isotopes are built from a base material which is very much lighter than iron. In this case we have only been able to make a guess concerning the amount of material residing in r-process elements with $A \lesssim 45$. We then find that $g \simeq 0.0004$.

Thus the largest value of g which appears to be plausible is obtained when cycling takes place and $g = 0.011$, and it is this value which we use in the following calculations.

There is a spread in absolute magnitudes at maximum of supernovae and probably also a spread in the difference between the maximum absolute magnitude and the magnitude at which the exponential form of the light curve sets in. Let us suppose that this difference is δM. Then the total energy emitted under the exponential tail of the light curve is given by

$$E_t = 3.8 \times 10^{33} \times 10^{0.4(4.6-M-\delta M)} \times 8.64 \times 10^4 \times \tau_m \text{ ergs,}$$

where M is the absolute magnitude of the supernova at maximum and τ_m days is the mean life of the radioactive element responsible. The energy emitted by the sun and its absolute magnitude have been taken as 3.8×10^{33} erg/sec and 4.6, respectively. Thus for Cf^{254},

$$E_t = 2 \times 10^{42} \times 10^{0.4(-M-\delta M)}$$

where the half-life of $Cf^{254} = 61$ days has been used. If the half-life is 56 days, then the value of E_t must be reduced by about 8%. We have shown in Sec. VIII that the total energy release parallels the spontaneous fission release over the time when the Cf^{254} predominates. Thus when making this calculation we must include the contribution which the other radioactive elements apart from Cf^{254} make to the curve. From Fig VIII,1 we find that the ratio of the total energy release to the Cf^{254} energy release is 8:7. On including this correction factor, we have that the total energy release from the mass $mM \odot = gfm \times 1.91 \times 10^{51}$ ergs. Thus putting $g = 0.011$, $f = 0.01$, we have that

$$m \times 1.07 \times 10^{+5} = 10^{0.4(-M-\delta M)}$$

or

$$\log m = 0.4(-M-\delta M)-5.029.$$

For the Crab, in which $M \simeq -17.5$ and δM is arbitrarily taken as $+3$,

$$m = 5.9,$$

while for SN IC 4182, in which $M = -18.1$ and $\delta M = +2.5$,

$$m = 16.1.$$

The mass of the Crab Nebula is estimated to be $0.1\ M\odot$ (Os57). This result was based on the assumption that, although the hydrogen/helium ratio was abnormally small, in that their number densities were approximately equal, the remainder of the elements had normal abundances, as given, for example, in the appendix. The situation regarding the elements other than hydrogen and helium in the Crab is still very unclear. For example, there appear to be no identifications or information on iron, though we should expect that the iron/hydrogen or iron/helium ratio would be abnormally large. The mass is actually derived by obtaining the density of free electrons per unit of mean atomic weight, and finally by making the assumption about the composition described above. Thus the total mass estimated is approximately a linear function of the mean atomic weight which is assumed. Hence if the material in the shell had the initial composition which we consider to be typical of a highly-evolved star, the mean atomic weight would be about ten times that assumed in Osterbrock's calculation. Hence a mass $\simeq 1\ M\odot$ would not be unreasonable. This leaves a discrepancy between the calculated and observed mass of this supernova shell of a factor of ~ 5. This may be partly or completely accounted for by uncertainties in estimating the absolute magnitude of the Crab supernova at maximum. Baade (Ba57a) has estimated that the absolute magnitude was -17.5 at maximum by using the observation that the star vanished from naked eye visibility about 650 days after maximum, and assuming that the total drop in brightness was the same as that for the supernova in IC 4182. Mayall and Oort (Ma42) have estimated that it reached -16.5 by using the observation that the supernova ceased to be visible in daylight after 23 days. If the supernova did reach only -16.5 at maximum, the mass needed to be ejected in the envelope is $\sim 2.4\ M\odot$. An alternative explanation is that the Crab never did show that exponential light curve which is typical of supernovae in which Cf^{254} is produced.

For IC 4182, a mass of $\sim 10\ M\odot$ is not unreasonable, particularly if it is supposed that the amount of mass ejected is roughly proportional to the maximum luminosity of the supernova.

It is of some interest to carry out a calculation similar to that made for Cf^{254} on the assumption that Fe^{59} is alone responsible for the light curve, particularly since we have earlier pointed out that this isotope will dominate the energy decay among the isotopes apart from Cf^{254}, and also since some supernova light curves have half-lives possibly nearer to 45 than to 55 days.

In this case the total energy released by Fe^{59} is given by

$$E_t = g'fm \times 8.6 \times 10^{49}\ \text{ergs.}$$

The most favorable situation which can be envisaged is that as before there is about 2% by mass of iron in the envelope, so that $f \simeq 0.01$, but that there is a paucity of neutrons so that perhaps only 5 neutrons per iron nucleus are made available. On this assumption the proportion of the material which captures 3 neutrons to form Fe^{59} can easily be calculated, as indicated in Sec. VIII, if it is assumed that the capture cross section remains constant, and we find that about 20% of the original Fe^{56} will be transformed to Fe^{59}. In this case $g' = 0.2$ (see Sec. VIII). Thus we obtain the result that

$$g'fm \times 4.44 \times 10^{49} = 1.48 \times 10^{42} \times 10^{0.4(M-\delta M)}$$

or

$$\log m = 0.4(-M-\delta M)-4.78.$$

This equation for m has a numerical constant which differs by a factor of 0.25 in the logarithm from that for the Cf^{254} decay. Thus we conclude that if the physical conditions described above are plausible, the large-scale production of Fe^{59} will be able to explain a light curve with a half-life of 45 days if the mass ejected is about 1.8 times greater than that demanded if Cf^{254} is responsible. However, if sufficient neutrons were available to build the r-process elements in the same proportions that they appear in the solar system the relative amount of Fe^{59} can only be estimated rather uncertainly, as has been done in Sec. VIII, but the value of g becomes much smaller than 0.2 and the mass required in the envelope becomes unreasonably large.

The relatively low efficiency of conversion of the material into either Cf^{254} or Fe^{59} arises from the small values of g, g', and f which seem to be plausible. The values of g and g' are determined by the nuclear physics of the situation. However, as previously stated, f is in essence determined by the initial composition of the envelope material. The maximum efficiency would be achieved when $f = 1$, i.e., when the whole of the material was initially composed of iron and was changed to heavy elements in the supernova explosion. Such a condition does not seem very plausible. However, if a situation could arise in which some of the outer core material has been converted to isotopes in the iron peak by the equilibrium process (Sec. IV) while the inner core material has evolved to its last equilibrium configuration consisting of a pure neutron core, an instability in which the neutrons were mixed into the iron would result in the production of the r-process isotopes, and since there would be a plentiful supply of neutrons, cycling in the range $110 \lesssim A \lesssim 260$ would

take place. Under these conditions the total amount of mass demanded to produce the curves from Cf^{254} would be only about 0.06 $M\odot$ in the case of the Crab, and only about 0.16 $M\odot$ in the case of SN IC 4182.

Finally, mention must be made of the possible distortion of the light curve by the decay of other isotopes with longer half-lives than those responsible for the regions considered. The most important case appears to be that of Cf^{252}, which has a half-life of 2.2 years. From Fig. VIII,3 this should begin to make the curve flatten out after about 500 days. This flattening is very gradual and could well be masked by the small systematic errors in magnitude measurement which may be present in the light curve of the supernova in IC 4182. If no distortions occur through the energy transfer processes in the envelope at this late stage, very accurate measurements by photoelectric techniques of the very faint end of the next supernova light curve which can be followed may provide a good experimental test of this supernova theory. In the same way further observations may be able to determine whether all supernovae have exactly the same decay curves, a question which may also have some bearing on the problem of whether or not the r-process component of the solar-system material was built in a single supernova outburst.

D. Origin of the r-Process Isotopes in the Solar System

As mentioned in Sec. VII, the forms of the back sides of the abundance peaks of the r-process isotopes might suggest that the conditions obtaining in a single supernova were responsible for their synthesis. Though this conclusion remains highly uncertain at the present time, it is worthwhile considering its astrophysical implications.

A possible sequence of events in the origin of the r-process isotopes in the solar system might then be as follows. The isotopes which are made by the other processes have already been synthesized and a cloud of such material is present. Inside this cloud a supernova outburst takes place. About $10^{-2} M\odot$ is converted by this process to isotopes built in the r process, and this material is gradually diluted by the other material present. The material will be diluted first by expansion of the supernova shell into the surrounding medium and second by effects of galactic rotation and turbulence in the interstellar gas. Thus the total volume in which this occurs may be crudely estimated in the following way. The volume of a supernova shell (the Crab Nebula) is about 1 psc³ after about 10^3 years. Since a shell probably decelerates, it may be supposed that after about 10^4 years its volume is about 25 psc³ and its expansion velocity has reached a numerical value equal to the mean random velocity of the interstellar clouds.

One time-scale of interest is that for the formation of the solar system, i.e., $10^7 - 10^8$ years, and one epoch of interest is a period of this length occurring some 5×10^9 years ago. However the more important time scale for this argument is the time in which the material can disperse, between the time at which the supernova outburst occurred and the epoch at which the solar system condensed. From the argument based on the U^{235}/U^{238} ratio this time interval is of the order of 10^9 years. At an epoch more than 5×10^9 years ago, it is probable that effects of galactic shear and of turbulent motion were different from their present values, so that no very good estimates of the total dilution volume can be made from this standpoint. On the other hand we can estimate the dilution factor by the following method.

On the basis of discussion in Sec. XII, we can suppose that the r-process isotopes originally comprised a total of about 2 percent of a solar mass in the supernova outburst. At present in the solar system the ratio by mass of the r-process isotopes to hydrogen is $\sim 10^{-6}$ (Table II,1). Thus the amount of hydrogen into which the shell expanded was $\sim 2 \times 10^4 M\odot$. If we suppose that the mean density of this gas was about 10^{-24} g/cm³, the total volume was $\sim 4 \times 10^{61}$ cm³ so that the dimension of this volume was about 75 psc. This is a fraction of approximately 10^{-6} of the total volume of the galaxy. The total number of supernovae that would explode in $\sim 10^9$ years is $\sim 3 \times 10^6$, so that we might expect that, on an average, 3 might have gone off in this volume, so that one only is entirely possible. It does not appear unreasonable from this point of view, therefore, that a single supernova has been responsible for all of the material built by the r process currently present in the solar system.

XIII. CONCLUSION

In Secs. III to X we have discussed the details of the various synthesizing processes which are demanded to produce the atomic abundances of all of the isotopes known in nature, while in Secs. II, XI, and XII we have attempted to describe the astrophysical theory and observations which are relevant to this theory.

It is impossible in a short space to summarize the advantages and disadvantages of a theory with as many facets as this. However, it may be reasonable to conclude as follows. The basic reason why a theory of stellar origin appears to offer a promising method of synthesizing the elements is that the changing structure of stars during their evolution offers a succession of conditions under which many different types of nuclear processes can occur. Thus the internal temperature can range from a few million degrees, at which the pp chain first operates, to temperatures between 10^9 and 10^{10} degrees when supernova explosions occur. The central density can also range over factors of about a million. Also the time-scales range between billions of years, which are the normal lifetimes of

stars of solar mass or less on the main sequence, and times of the order of days, minutes, and seconds, which are characteristic of the rise to explosion. On the other hand, the theory of primeval synthesis demands that all the varying conditions occur in the first few minutes, and it appears highly improbable that it can reproduce the abundances of those isotopes which are built on a long time-scale in a stellar synthesis theory.

From the standpoint of the nuclear physics of the problem, a major advance in the last few years has been the gradual realization through the interplay between experiment and theory that the helium-burning reaction $3He^4 \rightarrow C^{12}$ will take place in stellar interiors; theoretical work on stellar evolution has shown that in the interiors of red giant stars the conditions are right for such a reaction to take place. Another major advance has been the realization that under suitable stellar conditions the (α,n) reactions on certain nuclei can provide a source of neutrons; these are needed to synthesize the heavy isotopes beyond the iron peak in the abundance distribution and also to build some of the isotopes lighter than this.

The recent analysis of the atomic abundances (Su56) has enabled us to separate the isotopes in a reasonable scheme depending on which mode of synthesis is demanded. In particular, the identification of the r-process peaks was followed by the separation of the heavy isotopes beyond iron into the s-, r-, and p-process isotopes, and has enabled us to bring some order into the chaos of details of the abundance curve in this region. The identification of Cf^{254} in the Bikini test and then in the supernova in IC 4182 first suggested that here was the seat of the r-process production. Whether this finally turns out to be correct will depend both on further work on the Cf^{254} fission half-life and on further studies of supernova light curves, but that a stellar explosion of some sort is the seat of r-process production there seems to be little doubt.

From the observational standpoint, the gradual establishment in the last few years that there are real differences in chemical composition between stars is the strongest argument in favor of a stellar synthesis theory. Details of this argument, and the attempts to show that some stars are going through, or have gone through, particular synthesizing processes, while others are simply condensed out of material which has been processed earlier, and have not yet had time to modify any of their own material, have been given in Sec. XI.

Many problems remain. Although we have given a tentative account of the events leading up to a supernova outburst, we have no detailed dynamical theory of such an explosion. Neither can we explain the principal features of supernova spectra. Further, we do not yet understand the way in which stars evolve to this stage. In fact, the whole problem of stellar evolution beyond the red-giant stage is beset on the theoretical side by problems which are very difficult to handle with the present computational techniques. From the observational side we can estimate the time taken for a star to move through a particular evolutionary stage by making counts of the number of stars in that part of the HR diagram of a star cluster, but these diagrams alone cannot tell us, for example, whether the evolutionary track is in the sense of increasing or decreasing surface temperature at a particular point, i.e., from right to left or from left to right in the diagram.

The whole question of the chemical compositions of stars is complicated by the problem of mixing, since in many cases it cannot be supposed that the atmospheric composition of a star is identical with that of its interior. Also, attempts to determine compositions of very distant or very faint stars are a challenging problem. However, the term "universal abundance" will remain meaningless in the astronomical sense until a reasonable sample of the material in different parts of our own galaxy has been investigated, with the determination of abundances of the heavier elements. It might be pointed out here that on the basis of this theory there may be nothing universal in the isotope ratios. In many cases different isotopes of an element are built by different processes, and the isotope ratios which are observationally known are almost entirely obtained from solar-system material. Thus, for example, another solar system might have condensed out of material consisting mainly of hydrogen and gas ejected from stars which had gone through hydrogen burning, helium burning, the s process, the α process, and the e process, but not the r process. In this case, among the heavy elements the s-process isotopes would be present but the r-process isotopes would be absent, so that those elements which are predominantly built by the r process would be in very low abundance. Thus in such a solar system, the inhabitants would have a very different sense of values, since they would have almost no gold and, for their sins, no uranium.

The question of the composition of the material in other galaxies is not likely to be settled in the near future, except for coarse estimates. Perhaps the only sample of such material which we are able to obtain is contained in the extremely high-energy cosmic-ray particles ($\geq 10^{18}$ ev) which may have been accelerated and escaped from extragalactic nebulae (Ro57, Bu57b).

We have attempted to show that the interchange of material between stars and the interstellar gas and dust will be sufficient to explain the observed abundances relative to hydrogen. This attempt has been reasonably successful, though the aging problems have demanded that we do not consider that synthesis has gone on at a uniform rate since our galaxy condensed. It appears that successive generations of stars are demanded, if all eight processes are to contribute, although it is conceivable that, in a particular star,

one part or another can go through each process, ending with a catastrophic explosion.

We have made some attempt to explain possible modes of production of deuterium lithium, beryllium, and boron, but at present we must conclude that these are little more than qualitative suggestions.

In the laboratory, it is probable that the next steps to be taken are studies of the further reactions in helium burning, i.e., $C^{12}(\alpha,\gamma)O^{16}$ and $O^{16}(\alpha,\gamma)Ne^{20}$, work on the neutron-producing reactions, and particularly on neutron capture cross sections, and accurate work on nuclear masses and binding energies, particularly of the nuclei in the rare-earth region.

In astrophysical observations it is important that evidence for the operation of the s process and of the r process be sought spectroscopically. In giant stars where the s process may operate, the elements most overabundant should be those in general with a stable, "magic number" isotope having a closed shell of neutrons. These elements are strontium, yttrium, zirconium, barium, lathanum, cerium, praseodymium, neodymium, lead, and bismuth. All of these except bismuth have been found to be overabundant in the only such star analyzed up to the present time (Table XI,3). In supernova remnants, such as the Crab nebula, the r process may have operated to enhance the abundance of the following heavy elements: selenium, bromine, krypton, tellurium, iodine, xenon, caesium, osmium, iridium, platinum, gold, thorium, and uranium. The effect of the r process on the abundance of the iron-group elements and of the lighter elements from carbon to calcium is very difficult to estimate. The iron-group elements will be depleted by neutron capture in the original envelope material but material from the core (e process) injected during the explosion may yield an over-all enhancement in the final expanding shell. The over-all abundance of the lighter elements is not appreciably changed by the supernova explosion but the ratio to hydrogen and helium will rise to a value considerably greater than that in unevolved matter. This is because in our model we require that hydrogen and helium originally be comparable in abundance by number to carbon, oxygen, and neon, and then that they be depleted by the energy generation and the neutron-releasing processes.

An important key to the solution of problems in stellar nucleogenesis lies in the determination of relative isotopic abundances in stars. It is realized that this is a very difficult problem spectroscopically, but nonetheless every possible technique of isotope analysis should be brought to bear in this regard. Relative isotopic abundances are many times as informative as relative element abundances.

In concluding we call attention to the minimum age of the uranium isotopes derivable from their relative production in the r process. Our calculations place this minimum age at 6.6×10^9 years with a limit of error on the low side of at most 0.6×10^9 years. This small limit of error comes directly from the relatively short half-life of U^{235}. We feel that this minimum age is significantly greater than the currently accepted value for the geochemical age of the solar system, 4.5×10^9 years. It is, indeed, comparable with the ages assigned to the oldest globular clusters so far discovered. Since it is a minimum, it will not be unexpected if still older objects exist in our galaxy. In fact the stars discussed by Sandage and Eggen, mentioned in Sec. XII A, whose ages may be $\gtrsim 8 \times 10^9$ years, might be such examples.

ACKNOWLEDGMENTS

APPENDIX

We give in the appendix all of the information that we have been able to collect which is relevant to the synthesis problem. A detailed explanation of the format of this table is given in Sec. II C. The abundances (N) of the isotopes have been taken predominantly from the work of Suess and Urey (Su56), though in a few cases the solar abundances of Goldberg et al. (Go57) have been given in parentheses below those of Suess and Urey. The neutron capture cross sections (σ) have been discussed in Sec. V B, while the method of assignment of the nuclei among the eight synthesizing processes has been described in Sec. II B. The designation m means "magic," i.e., the nucleus has a closed shell of neutrons and thus a small neutron capture cross section in the s process. The designation m' means that the progenitor in the r process is "magic." When m is used as a superscript, as in Eu^{152m}, it designates an isomeric state. A process which returns material back down the neutron capture chain is designated by the word *returns*.

A	Main line	$\sigma(n,\gamma)$ in mb or $\tau_{\frac{1}{2}}$	N	σN	Process	A	Weak line or bypassed	$\sigma(n,\gamma)$ in mb or $\tau_{\frac{1}{2}}$	N	Process
1	$_1$H	0.3(0.1%th)	4.00×10^{10}		Primeval					
2	$_1$H$_1$	$\lesssim2\times10^{-4}$ (0.1%th)	5.7×10^6		x					
3	$_1$H$_2(\beta^-)$	12.26 yr			τ_β too long					
3	$_2$He$_1$	5000 (n,p) (extr.)			H burning					
4	$_2$He$_2$		3.08×10^9		H burning					
5	$_2$He$_3(n)$	2×10^{-21} sec			returns					
6	$_2$He$_4(\beta^-)$	0.82 sec								
6	$_3$Li$_3$	2000(n,α)(exp)	7.4		x, returns					
7	$_3$Li$_4$	0.33(1%th)	92.6		x					
8	$_3$Li$_5(\beta^-)$	0.84 sec								
8	$_4$Be$_4(\alpha)$	$\sim2\times10^{-16}$ sec			returns					
9	$_4$Be$_5$	0.085(1%th)	20		x	9	$_3$Li$_6(\beta^-)\rightarrow n,\,2$He^4	0.17 sec		returns
10	$_4$Be$_6(\beta^-)$	2.7×10^6 yr				10	$_5$B$_5$	1000(n,α) (0.1%th)	4.5	returns
11	$_4$Be$_7(\beta^-)$	Not known								
11	$_5$B$_6$	<0.5(1%th)	19.5		x					
12	$_5$B$_7(\beta^-)$	0.025 sec								
12	$_6$C$_6$	0.047(1%th)	3.50×10^6		He burning					
13	$_6$C$_7$	0.009(1%th)	3.92×10^4		H burning					
14	$_6$C$_8(\beta^-)$	5600 yr								
14	$_7$N$_7$	1.0(n,γ)(1%th) 1.7(n,p)(0.1%th)	6.58×10^6		H burning					
15	$_7$N$_8$	0.00024(1%th)	2.41×10^4		H burning	15	$_6$C$_9(\beta^-)$	2.4 sec		
16	$_7$N$_9(\beta^-)$	7.4 sec								
16	$_8$O$_8$	0.01(1%th)	2.13×10^7		He burning					
17	$_8$O$_9$	1.0(n,α)(0.1%th)	8.00×10^3		H burning returns	17	$_7$N$_{10}(\beta^-)\rightarrow n,$ O^{16}	4.14 sec		returns
18	$_8$O$_{10}$	0.0021(1%th)	4.36×10^4		H burning					
19	$_8$O$_{11}(\beta^-)$	29 sec								
19	$_9$F$_{10}$	0.094(1%th)	1600		H burning					
20	$_9$F$_{11}(\beta^-)$	11 sec								
20	$_{10}$Ne$_{10}$	0.02	7.74×10^6		He burning					
21	$_{10}$Ne$_{11}$	0.6 (also n,α)	2.58×10^4		H burning returns					
22	$_{10}$Ne$_{12}$	0.36(1%th)	8.36×10^5	3.0×10^5	H burning					
23	$_{10}$Ne$_{13}(\beta^-)$	40 sec								
23	$_{11}$Na$_{12}$	3.5	4.38×10^4	1.5×10^5	H burning, s					
24	$_{11}$Na$_{13}(\beta^-)$	15.0 hr								
24	$_{12}$Mg$_{12}$	1.8	7.21×10^5	1.3×10^6	He burning, α					
25	$_{12}$Mg$_{13}$	6 (also n,α)	9.17×10^4	5.5×10^5	s					
26	$_{12}$Mg$_{14}$	2.0	1.00×10^5	2.0×10^5	$s(m)$					
27	$_{12}$Mg$_{15}(\beta^-)$	9.5 min								
27	$_{13}$Al$_{14}$	5.3 (exp)	9.48×10^4	5.0×10^5	$s(m)$					
28	$_{13}$Al$_{15}(\beta^-)$	2.30 min								
28	$_{14}$Si$_{14}$	1.8($\frac{1}{3}\times$Al^{27})	9.22×10^5	1.7×10^6	α, $s(m)$					
29	$_{14}$Si$_{15}$	12 (also n,α)	4.70×10^4	5.6×10^5	s					
30	$_{14}$Si$_{16}$	8	3.12×10^4	2.5×10^5	s					
31	$_{14}$Si$_{17}(\beta^-)$	2.62 hr								
31	$_{15}$P$_{16}$	32	1.00×10^4	3.2×10^5	s					
32	$_{15}$P$_{17}(\beta^-)$	14.5 day								
32	$_{16}$S$_{16}$	12 (also n,α)	3.56×10^5	4.3×10^6	α, s					
33	$_{16}$S$_{17}$	36 (also n,α and n,p)	2.77×10^3	1.0×10^5	s					
34	$_{16}$S$_{18}$	12	1.57×10^4	1.9×10^5	s					
35	$_{16}$S$_{19}(\beta^-)$	87 days								
35	$_{17}$Cl$_{18}$	33	6670	2.2×10^5	s	36	$_{16}$S$_{20}$	12	51	$r(m)$
36	$_{17}$Cl$_{19}(\beta^-)$	3.1×10^5 yr 100				36	$_{17}$Cl$_{19}(\beta^-)$	3.1×10^5 yr		α, s
						36	$_{18}$A$_{18}$	15	1.26×10^5 [1.9×10^6]	α, s s decay
						37	$_{18}$A$_{19}$(EC)	35 day		
37	$_{17}$Cl$_{20}$	10	2180	2.2×10^4	$s(m)$	37	$_{17}$Cl$_{20}$	10	2180 [2.2×10^4]	$s(m)$
38	$_{17}$Cl$_{21}(\beta^-)$	37.3 min								
38	$_{18}$A$_{20}$	2	2.4×10^4	4.8×10^4	$s(m)$					

A	Main line	$\sigma(n,\gamma)$ in mb or $\tau_{\frac{1}{2}}$	N	σN	Process	A	Weak line or bypassed	$\sigma(n,\gamma)$ in mb or $\tau_{\frac{1}{2}}$	N	Process
39	$_{18}A_{21}(\beta^-)$	260 yr				39	$_{18}A_{21}(\beta^-)$	260 yr		
39	$_{19}K_{20}$	8	2940	2.4×10^4	$s(m)$	40	$_{18}A_{22}$	15	$(+K^{40}\ \text{decay})$	s / s decay
40	$_{19}K_{21}$ (EC, 11%, β^- 89%)	1.3×10^9 yr, 100	0.38		s only	41	$_{18}A_{23}(\beta^-)$	1.82 hr		
41	$_{19}K_{22}$	25	219	5.5×10^3	s	41	$_{19}K_{22}$	25	219 $[5.5 \times 10^3]$	s
42	$_{19}K_{23}(\beta^-)$	12.5 hr				40	$_{20}Ca_{20}$	4	4.75×10^4 $[1.9 \times 10^5]$	$\alpha(m)$ / s decay
42	$_{20}Ca_{22}$	12	314	3.8×10^3	s					
43	$_{20}Ca_{23}$	20	64	1.3×10^3	s					
44	$_{20}Ca_{24}$	8	1040	8.3×10^3	α, s					
45	$_{20}Ca_{25}(\beta^-)$	160 days								
45	$_{21}Sc_{24}$	16	2.8 (63)	45 (1.0×10^3)	s					
46	$_{21}Sc_{25}(\beta^-)$	85 days								
46	$_{22}Ti_{24}$	10	194 (290)	1.9×10^3 (2.9×10^3)	s only; e	46	$_{20}Ca_{26}$	4	1.6	r only
47	$_{22}Ti_{25}$	12	189 (280)	2.3×10^3 (3.4×10^3)	s; e, r					
48	$_{22}Ti_{26}$	6	1790 (2600)	10.7×10^3 (1.6×10^4)	α, s; e, r	48	$_{20}Ca_{28}$	4	87.7	r only (m)
49	$_{22}Ti_{27}$	8	134 (200)	1.1×10^3 (1.6×10^3)	s; e, r					
50	$_{22}Ti_{28}$	4	130 (190)	5.2×10^2 (7.6×10^2)	$s(m)$; r, e	50	$_{23}V_{27}$	10	0.55 (1.1)	e
51	$_{22}Ti_{29}(\beta^-)$	5.80 min				50	$_{24}Cr_{26}$	8	344 (1800)	e
51	$_{23}V_{28}$	30	220 (430)		$e(m)$					
52	$_{23}V_{29}(\beta^-)$	3.77 min								
52	$_{24}Cr_{28}$	8	6510 (3.3×10^4)		$e(m)$					
53	$_{24}Cr_{29}$	31	744 (3800)		e					
54	$_{24}Cr_{30}$	8	204 (1000)		e	54	$_{26}Fe_{28}$	29	3.54×10^4 (1.3×10^4)	$e(m)$
55	$_{24}Cr_{31}(\beta^-)$	3.6 min								
55	$_{25}Mn_{30}$	124	6850 (7900)		e					
56	$_{25}Mn_{31}(\beta^-)$	2.58 hr								
56	$_{26}Fe_{30}$	29	5.49×10^5 (2.1×10^5)		e					
57	$_{26}Fe_{31}$	96	1.35×10^4 (5100)		e					
58	$_{26}Fe_{32}$	29	1980 (760)		e	58	$_{28}Ni_{30}$	40	1.86×10^4 (1.7×10^4)	e
59	$_{26}Fe_{33}(\beta^-)$	45 day								
59	$_{27}Co_{32}$	248	1800 (2200)		e					
60	$_{27}Co_{33}(\beta^-)$	5.2 yr								
60	$_{28}Ni_{32}$	40	7170 (6600)		e					
61	$_{28}Ni_{33}$	104	342 (310)		e					
62	$_{28}Ni_{34}$	40	1000 (910)		e					
63	$_{28}Ni_{35}(\beta^-)$	80 yr				63	$_{28}Ni_{35}(\beta^-)$	80 yr		
63	$_{29}Cu_{34}$	48	146 (1500)	7.0×10^3 (7.2×10^4)	s	64	$_{28}Ni_{36}$	40	318 $[1.3 \times 10^4]$ (290) $[(1.2 \times 10^4)]$	s
64	$_{29}Cu_{35}$ (EC 42%; β^+ 19%)	12.8 hr				64	$_{29}Cu_{35}$ (β^- 39%)	12.8 hr		
64	$_{28}Ni_{36}$	40(0.61)	318 (290)	7.8×10^3 (7.1×10^3)	s	64	$_{30}Zn_{34}$	49(0.39)	238 $[4.5 \times 10^3]$	s only
65	$_{28}Ni_{37}(\beta^-)$	2.56 hr				65	$_{30}Zn_{35}$ (EC, β^+)	245 day		
65	$_{29}Cu_{36}$	48	66 (680)	3.2×10^3 (3.3×10^4)	s	65	$_{29}Cu_{36}$	48	66 $[3.2 \times 10^3]$ (680) $[(3.3 \times 10^4)]$	s

A	Main line	$\sigma(n,\gamma)$ in mb or $\tau_{\frac{1}{2}}$	N	σN	Process	A	Weak line or bypassed	$\sigma(n,\gamma)$ in mb or $\tau_{\frac{1}{2}}$	N	Process
66	$_{29}Cu_{37}(\beta^-)$	5.1 min								
66	$_{30}Zn_{36}$	49	134	6.6×10³	s					
67	$_{30}Zn_{37}$	64	20.0	1.3×10³	s					
68	$_{30}Zn_{38}$	49	90.9	4.5×10³	s					
69	$_{30}Zn_{39}(\beta^-)$	52 min								
69	$_{31}Ga_{38}$	84	6.86	576	s					
70	$_{31}Ga_{39}(\beta^-)$	21 min								
70	$_{32}Ge_{38}$	82	10.4	849	s only	70	$_{30}Zn_{40}$	49	3.35	r only
71	$_{32}Ge_{39}(EC)$	12 day								
71	$_{31}Ga_{40}$	84	4.54	381	s					
72	$_{31}Ga_{41}(\beta^-)$	14.1 hr								
72	$_{32}Ge_{40}$	82	13.8	1130	s					
73	$_{32}Ge_{41}$	148	3.84	568	s					
74	$_{32}Ge_{42}$	82	18.65	1520	s	74	$_{34}Se_{40}$	96	0.649	p
75	$_{32}Ge_{43}(\beta^-)$	82 min								
75	$_{33}As_{42}$	240	4.0(⅔)	640	sr					
76	$_{33}As_{43}(\beta^-)$	26.7 hr								
76	$_{34}Se_{42}$	96	6.16	591	s only	76	$_{32}Ge_{44}$	82	3.87	r only
77	$_{34}Se_{43}$	360	5.07		rs					
78	$_{34}Se_{44}$	96	16.0		r(m')	78	$_{36}Kr_{42}$	107	0.175	p
79	$_{34}Se_{45}(\beta^-)$	7×10⁴ yr 360				79	$_{34}Se_{45}(\beta^-)$	7×10⁴ yr		
80	$_{34}Se_{46}$	96	33.8		r(m')	79	$_{35}Br_{44}$	480	6.78	r(m') s decay
81	$_{34}Se_{47}(\beta^-)$	18 min				80	$_{35}Br_{45}$ (β⁻ 92%; EC 5%; β⁺ 3%)	18 min		
81	$_{35}Br_{46}$	480	6.62		r(m')	80	$_{36}Kr_{44}$	107	1.14 [122]	s only
82	$_{35}Br_{47}(\beta^-)$	36 hr				81	$_{36}Kr_{45}(EC)$	2×10⁵ yr 440		
82	$_{36}Kr_{46}$	107	5.90	630	s only	82	$_{36}Kr_{46}$	107	5.90 [630]	s only
83	$_{36}Kr_{47}$	440	5.89		r(m')	82	$_{34}Se_{48}$	96	5.98	r only (m')
84	$_{36}Kr_{48}$	107	29.3		r(m')	84	$_{38}Sr_{46}$	48	0.106	p
85	$_{36}Kr_{49}(\beta^-)$	10.4 yr								
85	$_{37}Rb_{48}$	112	4.73		rs(m')					
86	$_{37}Rb_{49}(\beta^-)$	18.6 day								
86	$_{38}Sr_{48}$	48	1.86	89	s only	86	$_{36}Kr_{50}$	2.4	8.94	r only (m)
87	$_{38}Sr_{49}$	60	1.33	80	s only	87	$_{37}Rb_{50}(\beta^-)$	4.3×10¹⁰ yr 9	1.77	r only (m)
88	$_{38}Sr_{50}$	4.8	15.6	75	s(m)					
89	$_{38}Sr_{51}(\beta^-)$	54 day								
89	$_{39}Y_{50}$	19	8.9	170	s(m)					
90	$_{39}Y_{51}(\beta^-)$	64.0 hr								
90	$_{40}Zr_{50}$	12	28.0	336	s(m)					
91	$_{40}Zr_{51}$	24	6.12	147	s					
92	$_{40}Zr_{52}$	18	9.32	118	s	92	$_{42}Mo_{50}$	24	0.364	p(m)
93	$_{40}Zr_{53}(\beta^-)$	9×10⁵ yr 24				93	$_{40}Zr_{53}(\beta^-)$	9×10⁵ yr		
94	$_{40}Zr_{54}$	18	9.48	121	s	93	$_{41}Nb_{52}$	160	1.00	r, s decay
95	$_{40}Zr_{55}(\beta^-)$	65 day				94	$_{41}Nb_{53}{}^m(\beta^-)$	6.6 min		
						94	$_{41}Nb_{53}(\beta^-)$	2×10⁴ yr		
95	$_{41}Nb_{54}(\beta^-)$	35 day				94	$_{42}Mo_{52}$	240	0.226	p, s
95	$_{42}Mo_{53}$	324	0.382	124	s	95	$_{42}Mo_{53}$	324	0.382 [124]	s
96	$_{42}Mo_{54}$	240	0.401	96	s only	96	$_{40}Zr_{56}$	6.0	1.53	r only
						96	$_{44}Ru_{52}$	432	0.0846	p
97	$_{42}Mo_{55}$	324	0.232	75	s					
98	$_{42}Mo_{56}$	240	0.581(½)	70	s≈r	98	$_{44}Ru_{54}$	432	0.0331	p
99	$_{42}Mo_{57}(\beta^-)$	67 hr								
99	$_{43}Tc_{56}(\beta^-)$	2.1×10⁵ yr 120				99	$_{43}Tc_{56}(\beta^-)$	2.1×10⁵ yr		
100	$_{43}Tc_{57}(\beta^-)$	16 sec				99	$_{44}Ru_{55}$	1160	0.191	sr s decay
100	$_{44}Ru_{56}$	432	0.189	82	s only	100	$_{44}Ru_{56}$	432	0.189 [82]	s only s decay
101	$_{44}Ru_{57}$	1160	0.253		rs	100	$_{42}Mo_{58}$	240	0.234	r only

A	Main line	$\sigma(n,\gamma)$ in mb or $\tau_{\frac{1}{2}}$	N	σN	Process
102	$_{44}$Ru$_{58}$	432	0.467($\frac{1}{2}$)	100	$r \approx s$
103	$_{44}$Ru$_{59}(\beta^-)$	40 day			
103	$_{45}$Rh$_{58}$	760	0.214		r
104	$_{45}$Rh$_{59}(\beta^-)$	42 sec			
104	$_{46}$Pd$_{58}$	504	0.0628	32	s only
105	$_{46}$Pd$_{59}$	880	0.1536		r
106	$_{46}$Pd$_{60}$	504	0.1839		r
107	$_{46}$Pd$_{61}(\beta^-)$	7×10^6 yr 880			
108	$_{46}$Pd$_{62}$	504	0.180		r
109	$_{46}$Pd$_{63}(\beta^-)$	13.6 hr			
109	$_{47}$Ag$_{62}$	1000	0.126		r
110	$_{47}$Ag$_{63}(\beta^-)$	24 sec			
110	$_{48}$Cd$_{62}$	432	0.111	48	s only
111	$_{48}$Cd$_{63}$	1160	0.114($\frac{1}{2}$)	66	$r \approx s$
112	$_{48}$Cd$_{64}$	432	0.212($\frac{1}{2}$)	46	$r \approx s$
113	$_{48}$Cd$_{65}$	1160	0.110($\frac{1}{2}$)	64	$r \approx s$
114	$_{48}$Cd$_{66}$	432	0.256($\frac{1}{2}$)	55	$r \approx s$
115	$_{48}$Cd$_{67}(\beta^-)$	54 hr			
115	$_{49}$In$_{66}(\beta^-)$	1320 (6×10^{14} yr)	0.105($\frac{1}{2}$)	70	$s \approx r$
115	$_{49}$In$_{66}{}^m(\beta^-)$	4.5 hr $- - - \rightarrow$			
116	$_{49}$In$_{67}(\beta^-)$	13 sec			
116	$_{50}$Sn$_{66}$	84	0.189	16	s only
117	$_{50}$Sn$_{67}$	280	0.102	29	s
118	$_{50}$Sn$_{68}$	84	0.316	27	s
119	$_{50}$Sn$_{69}$	280	0.115	32	s
120	$_{50}$Sn$_{70}$	84	0.433	36	s
121	$_{50}$Sn$_{71}(\beta^-)$	~28 hr			
121	$_{51}$Sb$_{70}$	348	0.141	49	s
122	$_{51}$Sb$_{71}(\beta^-)$	2.8 day			
122	$_{52}$Te$_{70}$	156	0.115	18	s only
123	$_{52}$Te$_{71}$	520	0.0416	22	s only
124	$_{52}$Te$_{72}$	156	0.221	34	s only
125	$_{52}$Te$_{73}$	520	0.328		$r(m')$
126	$_{52}$Te$_{74}$	156	0.874		$r(m')$
127	$_{52}$Te$_{75}(\beta^-)$	9.3 hr			
127	$_{53}$I$_{74}$	880	0.80		$r(m')$
128	$_{53}$I$_{75}(\beta^-\ 95\%)$	25.0 min			
128	$_{54}$Xe$_{74}$	360	0.0764	28	s only
129	$_{54}$Xe$_{75}$	1400	1.050$\blacktriangleleft$		$r(m')$
130	$_{54}$Xe$_{76}$	360	0.162	58	s only
131	$_{54}$Xe$_{77}$	1400	0.850		r
132	$_{54}$Xe$_{78}$	360	1.078		r
133	$_{54}$Xe$_{79}(\beta^-)$	5.27 day			
133	$_{55}$Cs$_{78}$	480	0.456		rs
134	$_{55}$Cs$_{79}(\beta^-)$	2.3 yr			
134	$_{56}$Ba$_{78}$	37.2	0.0886	3.3	s only
135	$_{56}$Ba$_{79}$	124	0.241($\frac{2}{3}$)	20	sr
136	$_{56}$Ba$_{80}$	37.2	0.286	11	s only
137	$_{56}$Ba$_{81}$	124	0.414($\frac{2}{3}$)	34	sr
138	$_{56}$Ba$_{82}$	10	2.622	26	$s(m)$
139	$_{56}$Ba$_{83}(\beta^-)$	85 min			
139	$_{57}$La$_{82}$	32	2.00	66	$s(m)$
140	$_{57}$La$_{83}(\beta^-)$	40.2 hr			
140	$_{58}$Ce$_{82}$	19	2.00	38	$s(m)$

A	Weak line or bypassed	$\sigma(n,\gamma)$ in mb or $\tau_{\frac{1}{2}}$	N	Process
102	$_{46}$Pd$_{56}$	504	0.0054	p
104	$_{44}$Ru$_{60}$	432	0.272	r only
106	$_{48}$Cd$_{58}$	432	0.0109	p
107	$_{46}$Pd$_{61}(\beta^-)$	7×10^6 yr		
107	$_{47}$Ag$_{60}$	1000	0.134	r s decay
108	$_{47}$Ag$_{61}$ (β^-, 98.5%; EC, 1.5%)	2.3 min		
108	$_{48}$Cd$_{60}$	432	0.0079	p, s
109	$_{48}$Cd$_{61}$(EC)	1.3 yr		
109	$_{47}$Ag$_{62}$	1000	0.126	r
110	$_{46}$Pd$_{64}$	504	0.0911	r only
112	$_{50}$Sn$_{62}$	84	0.0134	p
113	$_{48}$Cd$_{65}{}^m(\beta^-)$	5 yr		
113	$_{49}$In$_{64}$	1320	0.0046	ps
114	$_{49}$In$_{65}(\beta^-)$	72 sec		
114	$_{50}$Sn$_{64}$	84	0.0090	ps
115	$_{50}$Sn$_{65}$	280	0.00465	ps
116	$_{50}$Sn$_{66}$	84	0.189 [16]	s only
116	$_{48}$Cd$_{68}$	432	0.068	r only
120	$_{52}$Te$_{68}$	156	0.00420	p
122	$_{50}$Sn$_{72}$	84	0.063	r only
123	$_{51}$Sb$_{72}$	348	0.105	r only (m')
124	$_{50}$Sn$_{74}$	84	0.079	r only (m')
124	$_{54}$Xe$_{70}$	360	0.00380	p
126	$_{54}$Xe$_{72}$	360	0.00352	p
128	$_{53}$I$_{75}$(EC$+\beta^+$ 5%)	25.0 min		
128	$_{52}$Te$_{76}$	156	1.48	$r(m')$
129	$_{52}$Te$_{77}(\beta^-)$	72 min		
129	$_{53}$I$_{76}(\beta^-)$	1.7×10^7 yr		
130	$_{53}$I$_{77}(\beta^-)$	12.6 hr		
130	$_{54}$Xe$_{76}$	360	0.162 [58]	s only
130	$_{52}$Te$_{78}$	156	1.60	r only (m')
130	$_{56}$Ba$_{74}$	37.2	0.00370	p
132	$_{56}$Ba$_{76}$	37.2	0.00356	p
134	$_{54}$Xe$_{80}$	360	0.420	r only
136	$_{54}$Xe$_{82}$	4.9	0.358	r only (m)
136	$_{58}$Ce$_{78}$	82	0.0044	p
138	$_{57}$La$_{81}$(EC, β^-)	57.6 (2×10^{11} yr)	0.0018	p
138	$_{58}$Ce$_{80}$	82	0.00566	p

A	Main line	$\sigma(n,\gamma)$ in mb or $\tau_{\frac{1}{2}}$	N	σN	Process	A	Weak line or bypassed	$\sigma(n,\gamma)$ in mb or $\tau_{\frac{1}{2}}$	N	Process
141	$_{58}Ce_{83}(\beta^-)$	32 day								
141	$_{59}Pr_{82}$	60	0.40	24	$s(m)$					
142	$_{59}Pr_{83}(\beta^-)$	19.1 hr								
142	$_{60}Nd_{82}$	36	0.39	15	s only (m)	142	$_{58}Ce_{84}$	82	0.250	r only
143	$_{60}Nd_{83}$	180	0.175	33	s					
144	$_{60}Nd_{84}$	120	0.344	42	s	144	$_{62}Sm_{82}$	72	0.0108	$p(m)$
145	$_{60}Nd_{85}$	180	0.119	21	s					
146	$_{60}Nd_{86}$	120	0.248	30	s					
147	$_{60}Nd_{87}(\beta^-)$	11.6 day								
147	$_{61}Pm_{86}(\beta^-)$	2.6 yr								
147	$_{62}Sm_{85}$	4800	0.100		rs					
148	$_{62}Sm_{86}$	1440	0.0748	108	s only	148	$_{60}Nd_{88}$	120	0.0824	r only
149	$_{62}Sm_{87}$	4800	0.0920		rs					
150	$_{62}Sm_{88}$	1440	0.0492	71	s only	150	$_{60}Nd_{90}$	120	0.0806	r only
151	$_{62}Sm_{89}(\beta^-)$	80 yr 4800				151	$_{62}Sm_{89}(\beta^-)$	80 yr		
152	$_{62}Sm_{90}$	1440	0.176 ← – – – – – – – –		rs	151	$_{63}Eu_{88}$	5600	0.0892	rs
						152	$_{63}Eu_{89}$(EC, 72%; β^-, 28%)	13 yr or 9.2 hr		
153	$_{62}Sm_{91}(\beta^-)$	47 hr				152	$_{63}Eu_{89}^{m}(\beta^-$, 78%; EC, 22%)	13 yr or 9.2 hr		
						152	$_{64}Gd_{88}$	2400	0.00137	ps
						153	$_{64}Gd_{89}$(EC)	236 day		
153	$_{63}Eu_{90}$	5600	0.0976		rs	153	$_{63}Eu_{90}$	5600	0.0976	rs
154	$_{63}Eu_{91}(\beta^-)$	16 yr								
154	$_{64}Gd_{90}$	2400	0.0147	35	s only	154	$_{62}Sm_{92}$	1440	0.150	r only
155	$_{64}Gd_{91}$	6800	0.101		r					
156	$_{64}Gd_{92}$	2400	0.141		r	156	$_{66}Dy_{90}$	1320	0.00029	p
157	$_{64}Gd_{93}$	6800	0.107		r					
158	$_{64}Gd_{94}$	2400	0.169		r	158	$_{66}Dy_{92}$	1320	0.000502	p
159	$_{64}Gd_{95}(\beta^-)$	18 hr								
159	$_{65}Tb_{94}$	6000	0.0956		r					
160	$_{65}Tb_{95}(\beta^-)$	72 day								
160	$_{66}Dy_{94}$	1320	0.0127	17	s only	160	$_{64}Gd_{96}$	2400	0.149	r only
161	$_{66}Dy_{95}$	4400	0.105		r					
162	$_{66}Dy_{96}$	1320	0.142		r	162	$_{68}Er_{94}$	1116	0.000316	p
163	$_{66}Dy_{97}$	4400	0.139		r					
164	$_{66}Dy_{98}$	1320	0.157		r	164	$_{68}Er_{96}$	1116	0.00474	p? Too abundant
165	$_{66}Dy_{99}(\beta^-)$	2.32 hr								
165	$_{67}Ho_{98}$	2800	0.118		r					
166	$_{67}Ho_{99}(\beta^-)$	27.2 hr >30 yr								
166	$_{68}Er_{98}$	1116	0.104		r					
167	$_{68}Er_{99}$	1840	0.0770		r					
168	$_{68}Er_{100}$	1116	0.0850		r	168	$_{70}Yb_{98}$	1080	0.00030	p
169	$_{68}Er_{101}(\beta^-)$	9.4 day								
169	$_{69}Tm_{100}$	1400	0.0318		r					
170	$_{69}Tm_{101}(\beta^-)$	129 day								
170	$_{70}Yb_{100}$	1080	0.00666	7.2	s	170	$_{68}Er_{102}$	1116	0.0470	r only
171	$_{70}Yb_{101}$	1200	0.0316($\frac{1}{3}$)	19	$s \approx r$					
172	$_{70}Yb_{102}$	1080	0.0480($\frac{2}{3}$)	35	sr					
173	$_{70}Yb_{103}$	1200	0.0356($\frac{1}{3}$)	29	sr					
174	$_{70}Yb_{104}$	1080	0.0678($\frac{2}{3}$)	49	sr	174	$_{72}Hf_{102}$	520	0.00078	p
175	$_{70}Yb_{105}(\beta^-)$	4.2 day								
175	$_{71}Lu_{104}$	1040	0.0488($\frac{2}{3}$)	34	sr	176	$_{70}Yb_{106}$	1080	0.0278	r only
176	$_{71}Lu_{105}^{m}(\beta^-)$	3.7 hr				176	$_{71}Lu_{105}(\beta^-)$	Large σ $(7.5 \times 10^{10}$ yr)	0.0013	p
176	$_{72}Hf_{104}$	520	0.0226	12	s only	177	$_{71}Lu_{106}(\beta^-)$	6.8 day		
177	$_{72}Hf_{105}$	1040	0.0806($\frac{2}{3}$)	56	sr	177	$_{72}Hf_{105}$	1040	0.0806	sr
178	$_{72}Hf_{106}$	520	0.119	62	s					
179	$_{72}Hf_{107}$	1040	0.0604	63	s					
180	$_{72}Hf_{108}$	520	0.155	81	s	180	$_{74}W_{106}$	480	0.0006	p
181	$_{72}Hf_{109}(\beta^-)$	46 day								
181	$_{73}Ta_{108}$	1320	0.065	86	s					
182	$_{73}Ta_{109}(\beta^-)$	112 day								
182	$_{74}W_{108}$	480	0.13	62	s					
183	$_{74}W_{109}$	1640	0.070($\frac{1}{3}$)	77	sr					
184	$_{74}W_{110}$	480	0.15	72	s	184	$_{76}Os_{108}$	1176	0.00018	p
185	$_{74}W_{111}(\beta^-)$	74 day								
185	$_{75}Re_{110}$	2040	0.0500($\frac{1}{3}$)	51	$s \approx r(m')$					

A	Main line	$\sigma(n,\gamma)$ in mb or $\tau_{\frac{1}{2}}$	N	σN	Process	A	Weak line or bypassed	$\sigma(n,\gamma)$ in mb or $\tau_{\frac{1}{2}}$	N	Process
186	$_{75}$Re$_{111}$ ($\beta^-\sim95\%$)	91 hr				186	$_{75}$Re$_{111}$ (EC $\sim5\%$)	91 hr		
186	$_{76}$Os$_{110}$	1176	0.0159	19	s only	186	$_{74}$W$_{112}$	480	0.14	$r(m')$
						187	$_{74}$W$_{113}(\beta^-)$	24 hr		
187	$_{76}$Os$_{111}$	2480	0.0164	41	s only	187	$_{75}$Re$_{112}(\beta^-)$	2040 ($\sim5\times10^{10}$ yr)	0.0850	$r(m')$
						188	$_{75}$Re$_{113}(\beta^-)$	17 hr		
188	$_{76}$Os$_{112}$	1176	0.133		$r(m')$	188	$_{76}$Os$_{112}$	1176	0.133	
189	$_{76}$Os$_{113}$	2480	0.161		$r(m')$					
190	$_{76}$Os$_{114}$	1176	0.264		$r(m')$	190	$_{78}$Pt$_{112}$	384	0.0001	p
191	$_{76}$Os$_{115}(\beta^-)$	16 day								
191	$_{77}$Ir$_{114}$	3160	0.316		$r(m')$					
192	$_{77}$Ir$_{115}$ (β^- 96.5%)	74 day				192	$_{77}$Ir$_{115}$ (EC 3.5%)	74 day		
192	$_{78}$Pt$_{114}$	384	0.0127	4.9	s only	192	$_{76}$Os$_{116}$	1176	0.410	$r(m')$
193	$_{78}$Pt$_{115}$	long				193	$_{76}$Os$_{117}(\beta^-)$	31 hr		
193	$_{78}$Pt$_{115}^{(m)}$(EC)	3.4 day								
193	$_{77}$Ir$_{116}$	3160	0.505		$r(m')$	193	$_{77}$Ir$_{116}$	3160	0.505	$r(m')$
194	$_{77}$Ir$_{117}(\beta^-)$	19 hr								
194	$_{78}$Pt$_{116}$	384	0.533		$r(m')$					
195	$_{78}$Pt$_{117}$	1240	0.548		$r(m')$					
196	$_{78}$Pt$_{118}$	384	0.413		r	196	$_{80}$Hg$_{116}$	240	0.00045	p
197	$_{78}$Pt$_{119}(\beta^-)$	19 hr								
197	$_{79}$Au$_{118}$	1200	0.145		r					
198	$_{79}$Au$_{119}(\beta^-)$	2.70 day								
198	$_{80}$Hg$_{118}$	240	0.0285	6.8	s only	198	$_{78}$Pt$_{120}$	384	0.117	r only
199	$_{80}$Hg$_{119}$	680	0.0481		rs					
200	$_{80}$Hg$_{120}$	240	0.0656($\frac{2}{3}$)	11	sr					
201	$_{80}$Hg$_{121}$	680	0.0375		rs					
202	$_{80}$Hg$_{122}$	240	0.0844($\frac{2}{3}$)	14	sr					
203	$_{80}$Hg$_{123}(\beta^-)$	48 day								
203	$_{81}$Tl$_{122}$	276	0.0319($\frac{2}{3}$)	6	sr					
204	$_{81}$Tl$_{123}$ ($\beta^-\sim98\%$)	4.1 yr				204	$_{81}$Tl$_{123}$ (EC $\sim2\%$)	4.1 yr		
204	$_{82}$Pb$_{122}$	50	0.0063 (0.26)	0.32 (13)	s only	204	$_{80}$Hg$_{124}$	240	0.0194	r
205	$_{82}$Pb$_{123}$(EC)	$\sim5\times10^7$ yr 100				205	$_{80}$Hg$_{125}(\beta^-)$	5.2 min		
						205	$_{81}$Tl$_{124}$	276	0.0761($\frac{2}{3}$) [14]	sr s decay
						206	$_{81}$Tl$_{125}(\beta^-)$	4.20 min		
206	$_{82}$Pb$_{124}$	25	0.122($\frac{1}{3}$) (5.0)	1.5 (62)	s cycles r decay	206	$_{82}$Pb$_{124}$	25	0.122($\frac{1}{3}$) (5.0) [1.5] [(62)]	s cycles r decay
207	$_{82}$Pb$_{125}$	50	0.0995($\frac{1}{3}$) (4.1)	2.5 (100)	s cycles r decay					
208	$_{82}$Pb$_{126}$	10	0.243 (10)	2.4 (100)	$s(m)$ cycles (r decay)					
209	$_{82}$Pb$_{127}(\beta^-)$	3.3 hr								
209	$_{83}$Bi$_{126}$	15	0.144(?)	1.2(?)	$s(m)$ cycle (r decay)					
210	$_{83}$Bi$_{127}^m$ (β^- 56%) (RaE)	5.0 day				210	$_{83}$Bi$_{127}$ (α 44%)	(2.6$\times10^6$ yr) 5		
210	$_{84}$Po$_{126}(\alpha)$	138.40 day			(m)	211	$_{83}$Bi$_{128}(\alpha)$	2.15 min		
206	$_{82}$Pb$_{124}$	cycles				207	$_{81}$Tl$_{126}(\beta^-)$	4.78 min		
						207	$_{82}$Pb$_{125}$	cycles		

BIBLIOGRAPHY

(References are arranged and designated by the first two letters of the first-mentioned author's name, and year. Otherwise duplicate designations are distinguished by postscript letters.)

Ad57   R. L. Adgie and J. S. Hey, Nature 179, 370 (1950).

Aj55   F. Ajzenberg and T. Lauritsen, Revs. Modern Phys. 27, 136 (1955).

Al57   Alder, Stech, and Winther, Phys. Rev. 107, 728 (1957).

Al43   L. H. Aller, Astrophys. J. 97, 135 (1943).

Al51   L. H. Aller and P. C. Keenan, Astrophys. J. 113, 72 (1951).

Al54   L. H. Aller, Mem. soc. roy. sci. Liège 14, 337 (1954).

Al56   L. H. Aller, Gaseous Nebulae (John Wiley and Sons, Inc., New York, 1956), p. 217.

Al57a L. H. Aller, Preprint for *Handbuch der Physik* (Springer-Verlag, Berlin, 1957).

Al57b L. H. Aller and J. L. Greenstein (private communication).

Al57c Aller, Elste, and Jugaku, Astrophys. J. Suppl. **3**, 1 (1957).

Al57d L. H. Aller, Astrophys. J. **125**, 84 (1957).

Al50 R. A. Alpher and R. C. Herman, Revs. Modern Phys. **22**, 153 (1950).

Al53 R. A. Alpher and R. C. Herman, Ann. Rev. Nuclear Sci. **2**, 1 (1953).

Ar53 Arp, Baum, and Sandage, Astron. J. **58**, 4 (1953).

Aw56 M. Awschalom, Phys. Rev. **101**, 1041 (1956).

Ba43 W. Baade, Astrophys. J. **97**, 119 (1943).

Ba45 W. Baade, Astrophys. J. **102**, 309 (1945).

Ba56 Baade, Burbidge, Hoyle, Burbidge, Christy, and Fowler, Publ. Astron. Soc. Pacific **68**, 296 (1956).

Ba57a W. Baade (private communication).

Ba57 H. W. Babcock, *Proceedings of the Stockholm Symposium on Electromagnetic Phenomena in Cosmical Physics* (to be published).

Ba50 C. L. Bailey and W. R. Stratton, Phys. Rev. **77**, 194 (1950).

Be35 L. Berman, Astrophys. J. **81**, 369 (1935).

Be39 H. A. Bethe, Phys. Rev. **55**, 103, 434 (1939).

Bi50 W. P. Bidelman, Astrophys. J. **111**, 333 (1950).

Bi51 W. P. Bidelman and P. C. Keenan, Astrophys. J. **114**, 473 (1951).

Bi52 W. P. Bidelman, Astrophys. J. **116**, 227 (1952).

Bi53 W. P. Bidelman, Astrophys. J. **117**, 25 (1953).

Bi53a W. P. Bidelman, Astrophys. J. **117**, 377 (1953).

Bi54 W. P. Bidelman, Mem. soc. roy. sci. Liège **14**, 402 (1954).

Bi57 W. P. Bidelman, *Vistas in Astronomy*, edited by A. Beer (Pergamon Press, London, 1957), Vol. II, p. 1428.

Bl52 J. M. Blatt and V. F. Weisskopf, *Theoretical Nuclear Physics* (John Wiley and Sons, Inc., New York, 1952), p. 390.

Bo39 N. Bohr and J. A. Wheeler, Phys. Rev. **56**, 426 (1939).

Bo53 A. Bohr and B. R. Mottelson, Kgl. Danske Videnskab. Selskab, Mat.-fys. Medd. **27**, No. 16 (1953).

Bo48 H. Bondi and T. Gold, Monthly Notices Roy. Astron. Soc. **108**, 252 (1948).

Bo57 Booth, Ball, and MacGregor, Bull. Am. Phys. Soc. Ser. II, **2**, 268 (1957).

Bo54 Bosman-Crespin, Fowler, and Humblet, Bull. soc. sci. Liège **9**, 327 (1954).

Bo54a R. Bouigue, Ann. astrophys. **17**, 104 (1954).

Br37 British Association Mathematical Tables, Vol. VI.

Br52 British Association Mathematical Tables, Vol. X.

Br49 H. Brown, Revs. Modern Phys. **21**, 625 (1949).

Br57 Bromley, Almqvist, Gove, Litherland, Paul, and Ferguson, Phys. Rev. **105**, 957 (1957).

Bu53 W. Buscombe, Astrophys. J. **118**, 459 (1953).

Bu52 W. Buscombe and P. W. Merrill, Astrophys. J. **116**, 525 (1952).

Bu54 G. R. Burbidge and E. M. Burbidge, Publ. Astron. Soc. Pacific **66**, 308 (1954).

Bu55 G. R. Burbidge and E. M. Burbidge, Astrophys. J. Suppl. **1**, 431 (1955).

Bu55a E. M. Burbidge and G. R. Burbidge, Astrophys. J. **122**, 396 (1955).

Bu56 Burbidge, Hoyle, Burbidge, Christy, and Fowler, Phys. Rev. **103**, 1145 (1956).

Bu56a E. M. Burbidge and G. R. Burbidge, Astrophys. J. **124**, 116 (1956).

Bu56b G. R. Burbidge and E. M. Burbidge, Astrophys. J. **124**, 130 (1956).

Bu56c E. M. Burbidge and G. R. Burbidge, Astrophys. J. **124**, 655 (1956).

Bu57 Burbidge, Burbidge, and Fowler, *Proceedings of the Stockholm Symposium of Electromagnetic Phenomena in Cosmical Physics* (to be published).

Bu57a E. M. Burbidge and G. R. Burbidge, Astrophys. J. **126**, 357 (1957).

Bu57b G. R. Burbidge, Phys. Rev. **107**, 269 (1957).

Ca54 A. G. W. Cameron, Phys. Rev. **93**, 932 (1954).

Ca55 A. G. W. Cameron, Astrophys. J. **121**, 144 (1955).

Ch51 J. W. Chamberlain and L. H. Aller, Astrophys. J. **114**, 52 (1951).

Co53 C. D. Coryell, Ann. Rev. Nuclear Sci. **2**, 308 (1953).

Co56 C. D. Coryell, Laboratory for Nuclear Studies, Annual Report (1956).

Co56a Cowan, Reines, Harrison, Kruse, and McGuire, Science **124**, 103 (1956).

Co57 Cook, Fowler, Lauritsen, and Lauritsen, Phys. Rev. **107**, 508 (1957).

Co57a C. L. Cowan, Jr., and F. Reines, Phys. Rev. **107**, 1609 (1957).

Cr53 J. Crawford, Publ. Astron. Soc. Pacific **65**, 210 (1953).

Cu16 R. H. Curtiss, Publs. Observatory Univ. Mich. **2**, 182 (1916).

Da56 R. Davis, Bull. Am. Phys. Soc. Ser. II, **1**, 219 (1956).

De56 A. J. Deutsch, Astrophys. J. **123**, 210 (1956).

Du51 D. B. Duncan and J. E. Perry, Phys. Rev. **82**, 809 (1951).

Eg55 O. J. Eggen, Astron. J. **60**, 401 (1955).

Eg56 O. J. Eggen, Astron. J. **61**, 360 (1956).

Eg57 O. J. Eggen, Astron. J. **62**, 45 (1957).

Fa57 R. A. Farrell (private communication).

Fe54 Feshbach, Porter, and Weisskopf, Phys. Rev. **96**, 448 (1954).

Fi56 Fields, Studier, Diamond, Mech, Inghram, Pyle, Stevens, Fried, Manning, Ghiorso, Thompson, Higgins, and Seaborg, Phys. Rev. **102**, 180 (1956).

Fo47 Fowler, Hornyak, and Cohen (unpublished, 1947). Quoted in W. E. Siri, *Isotopic Tracers and Nuclear Radiations* (McGraw-Hill Book Company, New York, 1949), p. 11.

Fo54 W. A. Fowler, Mem. soc. roy. sci. Liège **14**, 88 (1954).

Fo55 Fowler, Burbidge, and Burbidge, Astrophys. J. **122**, 271 (1955).

Fo55a Fowler, Burbidge, and Burbidge, Astrophys. J. Suppl. **2**, 167 (1955).

Fo56 W. A. Fowler and J. L. Greenstein, Proc. Natl. Acad. Sci. U. S. **42**, 173 (1956).

Fo56a Fowler, Cook, Lauritsen, Lauritsen, and Mozer, Bull. Am. Phys. Soc. Ser. II, **1**, 191 (1956).

Fo57 P. Fong, preprint (1956); Phys. Rev. (to be published).

Fr55 J. H. Fregeau and R. Hofstadter, Phys. Rev. **99**, 1503 (1955).

Fr56 J. H. Fregeau, Phys. Rev. **104**, 225 (1956).

Fu39 Y. Fujita, Japanese J. Astron. Geophys. **17**, 17 (1939).

Fu40 Y. Fujita, Japanese J. Astron. Geophys. **18**, 45 (1940).

Fu41 Y. Fujita, Japanese J. Astron. Geophys. **18**, 177 (1941).

Fu56 Y. Fujita, Astrophys. J. **124**, 155 (1956).

Ga41 G. Gamow and M. Schoenberg, Phys. Rev. **59**, 539 (1941).

Ga43 G. Gamow Astrophys. J. **98**, 500 (1943).

Gh55 A. Ghiorso, UCRL Report No. 2912, and Geneva conference report (1955).

Go37 V. M. Goldschmidt, Skrifter Norske Videnskaps-Acad. Oslo. I. Mat.-Naturv. Kl. No. 4 (1937).

Go57 Goldberg, Aller, and Müller, preprint (1957).

Go54 Good, Kunz, and Moak, Phys. Rev. **94**, 87 (1954).

Go54a K. Gottstein, Phil. Mag. **45**, 347 (1954).

Gr54b A. E. S. Green, Phys. Rev. **95**, 1006 (1954).

Gr40 J. L. Greenstein, Astrophys. J. **91**, 438 (1940).

Gr47　J. L. Greenstein and W. S. Adams, Astrophys. J. **106**, 339 (1947).

Gr51　J. L. Greenstein and R. S. Richardson, Astrophys. J. **113**, 536 (1951).

Gr54　J. L. Greenstein, *Modern Physics for Engineers*, editor L. Ridenour (McGraw-Hill Book Company, Inc., New York, 1954), p. 267.

Gr54a　J. L. Greenstein, Mem. soc. roy. sci. Liège **14**, 307 (1954).

Gr54c　J. L. Greenstein and E. Tandberg-Hanssen, Astrophys. J. **119**, 113 (1954).

Gr56　J. L. Greenstein, Publ. Astron. Soc. Pacific **68**, 501 (1956).

Gr56a　J. L. Greenstein, *Third Berkeley Symposium on Statistics* (University of California Press, Berkeley, 1956), p. 11.

Gr57　J. L. Greenstein, (private communication).

Gr57a　J. L. Greenstein and P. C. Keenan (to be published).

Gr55　G. M. Griffiths and J. B. Warner, Proc. Phys. Soc. (London) **A68**, 781 (1955).

Gu54　G. A. Gurzadian, *Dynamical Problems of Planetary Nebulae* (Erivan, USSR, 1954).

Ha50　R. N. Hall and W. A. Fowler, Phys. Rev. **77**, 197 (1950).

Ha56　C. Hayashi and M. Nishida, Progr. Theoret. Phys. **16**, 613 (1956).

Ha56a　Halbert, Handley, and Zucker, Phys. Rev. **104**, 115 (1956).

Ha56b　Hayakawa, Hayashi, Imoto, and Kikuchi, Progr. Theoret. Phys. **16**, 507 (1956).

Ha56c　C. B. Haselgrove and F. Hoyle, Monthly Notices Roy. Astron. Soc. **116**, 527 (1956).

Ha57　Hagedorn, Mozer, Webb, Fowler, and Lauritsen, Phys. Rev. **105**, 219 (1957).

Ha57a　E. C. Halbert and J. B. French, Phys. Rev. **105**, 1563 (1957).

Ha57b　J. A. Harvey (private communication).

He48　A. Hemmendinger, Phys. Rev. **73**, 806 (1948).

He49　A. Hemmendinger, Phys. Rev. **75**, 1267 (1949).

He49a　G. H. Herbig, Astrophys. J. **110**, 143 (1949).

He55　Henyey, Lelevier, and Levée, Publ. Astron. Soc. Pacific **67**, 154 (1955).

He57　L. Heller, Astrophys. J. **126**, 341 (1957).

He57a　G. H. Herbig and K. Hunger (unpublished).

Ho46　F. Hoyle, Monthly Notices Roy. Astron. Soc. **106**, 343 (1946).

Ho49　F. Hoyle, Monthly Notices Roy. Astron. Soc. **109**, 365 (1949).

Ho54　F. Hoyle, Astrophys. J. Suppl. **1**, 121 (1954).

Ho55　F. Hoyle and M. Schwarzschild, Astrophys. J. Suppl. **2**, 1 (1955).

Ho56　Hoyle, Fowler, Burbidge, and Burbidge, Science **124**, 611 (1956).

Ho56b　F. Hoyle, Astrophys. J. **124**, 482 (1956).

Ho56c　R. Hofstadter, Revs. Modern Phys. **28**, 214 (1956).

Hu51　H. Hurwitz and H. A. Bethe, Phys. Rev. **81**, 898 (1951).

Hu55　J. R. Huizenga, Physica **21**, 410 (1955).

Hu55a　"Neutron cross sections," by D. J. Hughes and J. A. Harvey, Brookhaven National Laboratory (1955).

Hu56　H. C. van de Hulst, Verslag Gewone Vergader. Afdel. Natuvrk. Koninkl. Ned. Akad. Wetenschap. **65**, No. 10, 157 (1956).

Hu56a　Humason, Mayall, and Sandage, Astron. J. **61**, 97 (1956).

Hu56b　J. R. Huizenga and J. Wing, Phys. Rev. **102**, 926 (1956).

Hu57　J. R. Huizenga and J. Diamond, Phys. Rev. **107**, 1087 (1957).

Hu57a　J. A. Humblet (unpublished).

Hu57b　J. R. Huizenga and J. Wing, Phys. Rev. **106**, 91 (1957).

Hu57c　K. Hunger and G. E. Kron, Publ. Astron. Soc. Pacific **69**, 347 (1957).

Jo54　H. L. Johnson, Astrophys. J. **120**, 325 (1954).

Jo56　H. L. Johnson and A. R. Sandage, Astrophys. J. **124** 379 (1956).

Jo57　W. H. Johnson, Jr., and V. B. Bhanot, Phys. Rev. **107**, 1669 (1957).

Ka54　Kaplon, Noon, and Racette, Phys. Rev. **96**, 1408 (1954).

Ka56　R. W. Kavanagh, thesis, California Institute of Technology, and private communication.

Ke41　P. C. Keenan and W. W. Morgan, Astrophys. J. **94**, 501 (1941).

Ke42　P. C. Keenan, Astrophys. J. **96**, 101 (1942).

Ke53　P. C. Keenan and G. Keller, Astrophys. J. **117**, 241 (1953).

Ke56　P. C. Keenan and R. G. Teske, Astrophys. J. **124**, 499 (1956).

Ki56　T. D. Kinman, Monthly Notices Roy. Astron. Soc. **116**, 77 (1956).

Kl47　O. Klein, Arkiv Mat. Astron. Fysik **34A**, No. 19 (1947); F. Beskow and L. Treffenberg, Arkiv Mat. Astron. Fysik **34A**, Nos. 13 and 17 (1947).

Ko56　O. Kofoed-Hansen and A. Winther, Kgl. Danske Videnskab. Selskab, Mat.-fys. Medd. **30**, No. 20 (1956).

La57　W. A. S. Lamb and R. E. Hester, Phys. Rev. **107**, 550 (1957).

La57a　W. A. S. Lamb and R. E. Hester, Report No. UCRL/4903 (May, 1957).

La57b　Lagar, Lyon, and Macklin, Bull. Am. Phys. Soc. Ser. II, **2**, 15 (1957), and private communication.

Le56　T. D. Lee and C. N. Yang, Phys. Rev. **104**, 254 (1956).

Ma42　N. U. Mayall and J. H. Oort, Publ. Astron. Soc. Pacific **54**, 95 (1942).

Ma49　M. G. Mayer and E. Teller, Phys. Rev. **76**, 1226 (1949).

Ma57　J. B. Marion and W. A. Fowler, Astrophys. J. **125**, 221 (1957).

Mc40　A. McKellar, Publ. Astron. Soc. Pacific **52**, 407 (1940).

Mc41　A. McKellar, Observatory **64**, 4 (1941).

Mc44　A. McKellar and W. H. Stillwell, J. Roy. Astron. Soc. Canada **38**, 237 (1944).

Mc48　A. McKellar Publs. Dominion Astrophys. Observatory, Victoria, B. C. **7**, 395 (1948).

Me47　P. W. Merrill, Astrophys. J. **105**, 360 (1947).

Me52　P. W. Merrill, Science **115**, 484 (1952).

Me56　P. W. Merrill and J. L. Greenstein, Astrophys. J. Suppl. **2**, 225 (1956).

Me56a　P. W. Merrill, Publ. Astron. Soc. Pacific **68**, 70 (1956).

Me57　R. E. Meyerott and J. Olds, paper in preparation.

Mi50　R. Minkowski, Publs. Observatory Univ. Mich. **10**, 25 (1950).

Mu57　C. O. Muehlhause and S. Oleska, Phys. Rev. **105**, 1332 (1957).

Mu57a　G. Münch, Astrophys. J., in preparation.

Na56　Nakagawa, Ohmura, Takebe, and Obi, Progr. Theoret. Phys. **16**, 389 (1956).

Ni55　S. G. Nilsson, Kgl. Danske Videnskab. Selskab, Mat.-fys. Medd. **29**, No. 16 (1955).

No53　R. J. Northcott, J. Roy. Astron. Soc. Canada **47**, 65 (1953).

No55　J. H. Noon and M. F. Kaplon, Phys. Rev. **97**, 769 (1955).

No57　Noon, Herz, and O'Brien, Nature **179**, 91 (1957).

Op39　J. R. Oppenheimer and J. S. Schwinger, Phys. Rev. **56**, 1066 (1939).

Op51　E. J. Öpik, Proc. Roy. Irish Acad. **A54**, 49 (1951).

Op54　E. J. Öpik, Mem. soc. roy sci. Liège **14**, 131 (1954).

Os57　D. E. Osterbrock, Publ. Astron. Soc. Pacific **69**, 227 (1957).

Pa50　P. P. Parenago, Astron. Zhur. **27**, 150 (1950).

Pa53　Patterson, Brown, Tilton, and Inghram, Phys. Rev. **92**, 1234 (1953).

Pa55　C. C. Patterson, Geochim. Cosmochim. Acta **7**, 151 (1955).

Pa55a Patterson, Brown, Tilton, and Inghram, Science **121**, 69 (1955).
Pi57 R. E. Pixley (private communication).
Pi57a Pixley, Hester, and Lamb (private communication).
Po47 D. M. Popper, Publ. Astron. Soc. Pacific **59**, 320 (1947).
Re53 F. Reines and C. L. Cowan, Phys. Rev. **92**, 830 (1953).
Re56 Reynolds, Scott, and Zucker, Phys. Rev. **102**, 237 (1956).
Ro50 N. G. Roman, Astrophys. J. **112**, 554 (1950).
Ro52 N. G. Roman, Astrophys. J. **116**, 122 (1952).
Ro57 B. Rossi (private communication).
Ru29 H. N. Russell, Astrophys. J. **70**, 11 (1929).
Sa40 R. F. Sanford, Publ. Astron. Soc. Pacific **52**, 203 (1940).
Sa44 R. F. Sanford, Astrophys. J. **99**, 145 (1944).
Sa52 E. E. Salpeter, Astrophys. J. **115**, 326 (1952).
Sa52a E. E. Salpeter, Phys. Rev. **88**, 547 (1952).
Sa53 E. E. Salpeter, Ann. Rev. Nuclear Sci. **2**, 41 (1953).
Sa54 E. E. Salpeter, Australian J. Phys. **7**, 373 (1954).
Sa55 E. E. Salpeter, Phys. Rev. **97**, 1237 (1955).
Sa55a E. E. Salpeter, Astrophys. J. **121**, 161 (1955).
Sa57 E. E. Salpeter, Phys. Rev. **107**, 516 (1957).
Sa57a A. R. Sandage, Astrophys. J. **125**, 435 (1957).
Sa57b A. R. Sandage (unpublished).
Sc56 M. Schmidt, Bull. Astron. Soc. Netherlands **13**, 15 (1956).
Sc57a R. P. Schuman, unpublished.
Sc54 M. Schwarzschild, Astron. J. **59**, 273 (1954).
Sc57 Schwarzschild, Howard, and Härm, Astrophys. J. **125**, 283 (1957).
Sc57b Schwarzschild, Schwarzschild, Searle, and Meltzer, Astrophys. J. **125**, 123 (1957).
Sn55 T. Snyder *et al.*, Geneva Conference Reports **5**, 162 (1955).
Sm48 J. S. Smart, Phys. Rev. **74**, 1882 (1948).
Sm49 J. S. Smart, Phys. Rev. **75**, 1379 (1949).
Sp49 L. Spitzer, Astrophys. J. **109**, 548 (1949).
Sp55 L. Spitzer and G. B. Field, Astrophys. J. **121**, 300 (1955).
St56 E. J. Stanley and R. Price, Nature **177**, 1221 (1956).
St46 O. Struve, Observatory **66**, 208 (1946).
St57 O. Struve, Sky and Telescope **16**, 262 (1957).
St57a O. Struve and S. S. Huang, Occ. Notices Roy. Astron. Soc. **3**, 161, No. 19 (1957).
Su56 H. E. Suess and H. C. Urey, Revs. Modern Phys. **28**, 53 (1956).

Sw56 C. P. Swann and E. R. Metzger, Bull. Am. Phys. Soc. **1**, 211 (1956); see also Amsterdam Conference Proceedings (1956).
Sw52 P. Swings and J. W. Swensson, Ann. astrophys. **15**, 290 (1952).
Ta57 N. Tanner, Phys. Rev. **107**, 1203 (1957).
Ta57a N. Tanner and R. E. Pixley (private communication).
Te56 R. G. Teske, Publ. Astron. Soc. Pacific **68**, 520 (1956).
Th52 R. G. Thomas, Phys. Rev. **88**, 1109 (1952).
Th54 A. D. Thackeray, Monthly Notices Roy. Astron. Soc. **114**, 93 (1954).
Th57 S. G. Thompson and A. Ghiorso (private communication).
To1355 T'o-t'o Sung-Shih, *History of the Sung Dynasty*, Treatise on Astronomy, paragraph on guest-stars (Po-na edition), Chap. 56, p. 25a.
To49 Tollestrup, Fowler, and Lauritsen, Phys. Rev. **76**, 428 (1949).
Tr55 G. Traving, Z. Astrophys. **36**, 1 (1955).
Tr57 G. Traving, Z. Astrophys. **41**, 215 (1957).
Tu56 Turkevitch, Hamaguchi, and Read, Gordon Conference Report (1956).
Ur56 H. C. Urey, Proc. Natl. Acad. Sci. U. S. **42**, 889 (1956).
Wa55 A. H. Wapstra, Physica **21**, 367, 387 (1955).
Wa55a Way, King, McGinnis, and van Lieshout, Nuclear Level Schemes, National Academy of Sciences, Washington (1955).
Wa55b G. J. Wasserburg and R. J. Hayden, Nature **176**, 130 (1955).
We35 C. F. von Weizsäcker, Z. Physik **96**, 431 (1935).
We38 C. F. von Weizsäcker, Physik. Z. **39**, 633 (1938).
We51 C. F. von Weizsäcker, Astrophys. J. **114**, 165 (1951).
We57 J. Weneser, Phys. Rev. **105**, 1335 (1957).
We57a V. F. Weisskopf, Revs. Modern Phys. **29**, 174 (1957).
Wh41 J. A. Wheeler, Phys. Rev. **59**, 27 (1941).
Wo50 F. B. Wood, Astrophys. J. **112**, 196 (1950).
Wo49 Woodbury, Hall, and Fowler, Phys. Rev. **75**, 1462 (1949).
Wo52 E. J. Woodbury and W. A. Fowler, Phys. Rev. **85**, 51 (1952).
Wu41 K. Würm, Naturwissenschaften **29**, 686 (1941).
Wu57 Wu, Ambler, Hudson, Hoppes, and Hayward, Phys. Rev. **105**, 1413 (1957).
Ya52 *Yale Parallax Catalogue* (Yale University Observatory, 1952), third edition.
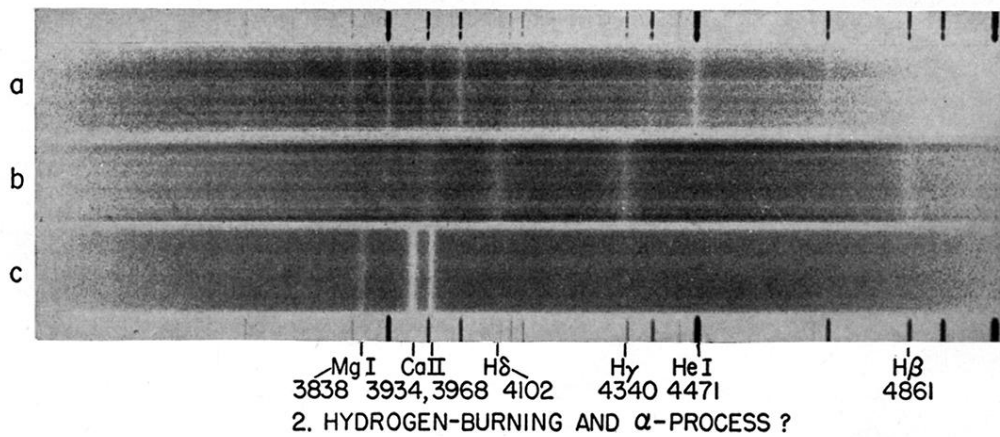
STARS SHOWING RESULTS OF:

I. HYDROGEN-BURNING

NiII   FeII CoII   CrII H18   HII,VII   He I   SiII HeI,H8   CaII HeI
3577   3621   3678 3692   3771   3820   3856 3889   3934 3965

2. HYDROGEN-BURNING AND α-PROCESS ?

    MgI CaII   Hδ   Hγ   HeI   Hβ
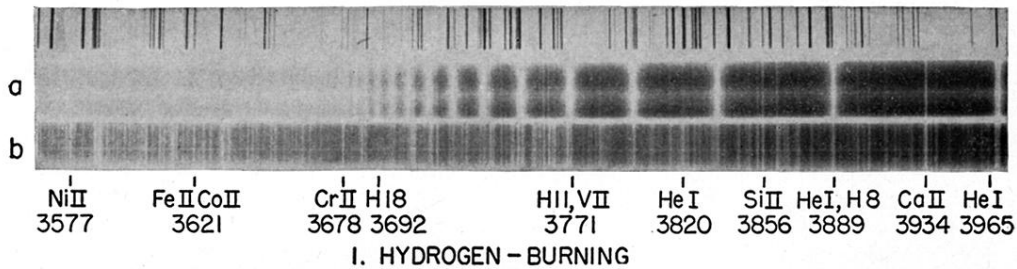3838 3934,3968 4102   4340 4471   4861

PLATE I.

PLATE 1. Portions of the spectra of stars showing the results of hydrogen burning and possibly the α process. Upper: (a) Normal A-type star, η Leonis, showing strong Balmer lines of hydrogen and a strong Balmer discontinuity at the series limit. (b) Peculiar star, υ Sagittarii, in which hydrogen has a much smaller abundance than normal. Lower: (a) White dwarf, L 1573–31, in which hydrogen is apparently absent. The comparison spectrum above the star is of a helium discharge tube; note the lines of helium in the star's spectrum. (b) White dwarf, L 770–3, which shows broad lines due to hydrogen only, for comparison with (a) and (c). (c) White dwarf, Ross 640, which shows only the two lines due to Ca II and a feature due to Mg I. All the spectrograms in this plate were obtained by J. L. Greenstein; the upper two are McDonald Observatory plates and the lower three are Palomar Observatory plates.
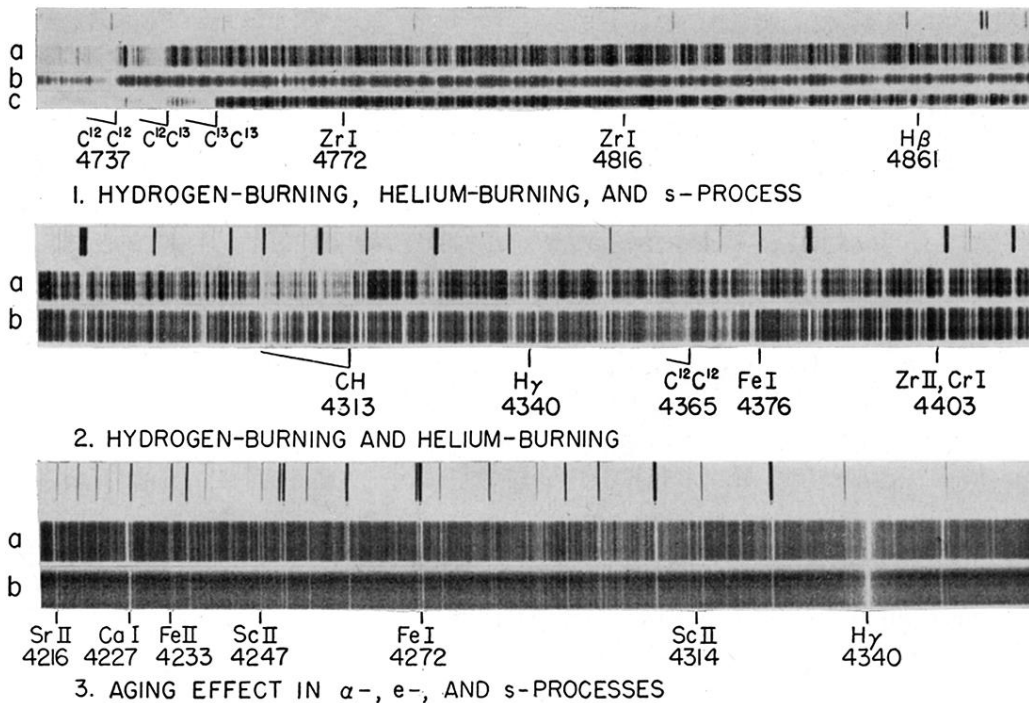
STARS SHOWING RESULTS OF:

a
b
c

C¹² C¹² C¹²C¹³ C¹³C¹³   ZrI   ZrI   Hβ
4737   4772   4816   4861

1. HYDROGEN-BURNING, HELIUM-BURNING, AND s-PROCESS

a
b

            CH   Hγ   C¹²C¹² FeI   ZrII,CrI
            4313   4340   4365 4376   4403

2. HYDROGEN-BURNING AND HELIUM-BURNING

a
b

Sr II   Ca I   Fe II   Sc II   Fe I   Sc II   Hγ
4216   4227   4233   4247   4272   4314   4340

3. AGING EFFECT IN α-, e-, AND s-PROCESSES

PLATE 2.

PLATE 2. Portions of the spectra of stars showing different aspects of element synthesis. Upper: (a) Normal carbon star, X Cancri, which has $C^{12}/C^{13}\sim3$ or 4. (b) Peculiar carbon star, HD 137613, which shows no C^{13} bands, and in which hydrogen is apparently weak. (c) Normal carbon star, HD 52432, which has $C^{12}/C^{13}\sim3$ or 4. Note that ZrI lines appear to be strongest in (a). Middle: (a) Normal carbon star, HD 156074, showing the CH band and Hγ. (b) Peculiar carbon star, HD 182040, in which CH is not seen, although the weak band of C_2 at λ 4365 is visible. Hγ is also very weak, indicating that hydrogen has a low abundance. Lower: (a) Normal F-type star, ξ Pegasi. (b) Peculiar star, HD 19445, which has a slightly lower temperature than ξ Pegasi, yet all lines but hydrogen are much weakened, showing that the abundances of α-, e-, and s-process elements are much lower than normal ("aging" effect). The middle two spectra were obtained by J. L. Greenstein, the remainder, with the exception of HD 137613, by E. M. and G. R. Burbidge.
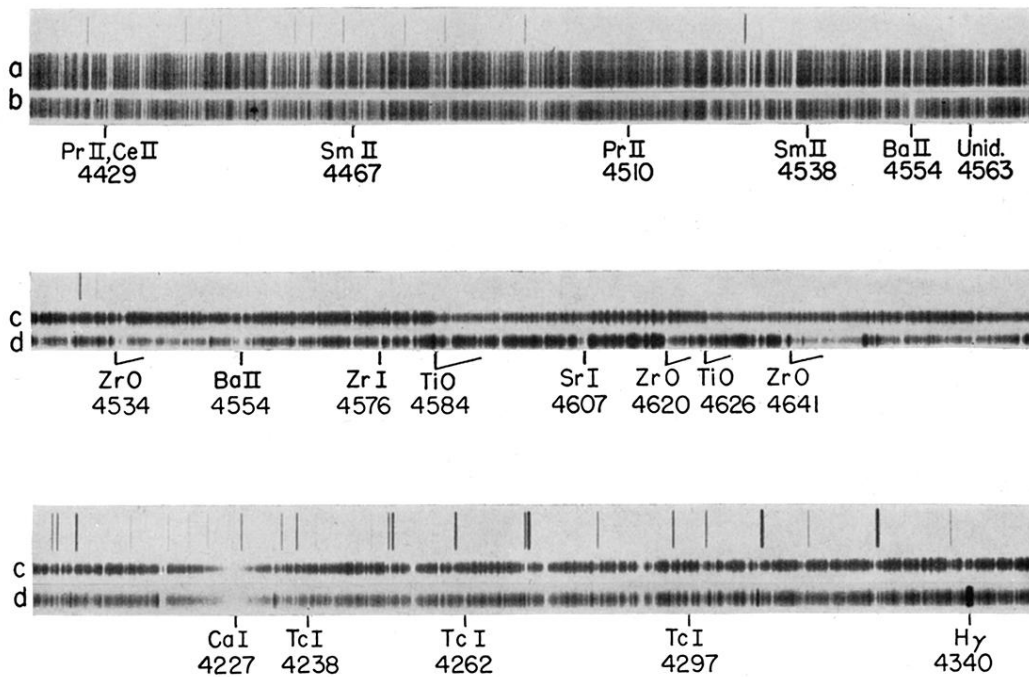
STARS SHOWING RESULTS OF s-PROCESS

PLATE 3.

PLATE 3. Portions of the spectra of stars showing the results of the s process. Upper: (a) Normal G-type star, κ Geminorum. (b) Ba II star, HD 46407, showing the strengthening of the lines due to the s-process elements barium and some rare earths. Middle: (c) M-type star, 56 Leonis, showing TiO bands at λλ 4584 and 4626. (d) S-type star, R Andromedae, showing ZrO which replace the TiO bands. Lines due to Sr I, Zr I, and Ba II are all strengthened. Lower: (c) Another spectral region of the M-type star, 56 Leonis; note that Tc I lines are weak or absent. (d) R Andromedae; note the strong lines of Tc I. The spectrum of R Andromedae was obtained by P. W. Merrill, and the upper two spectra by E. M. and G. R. Burbidge.

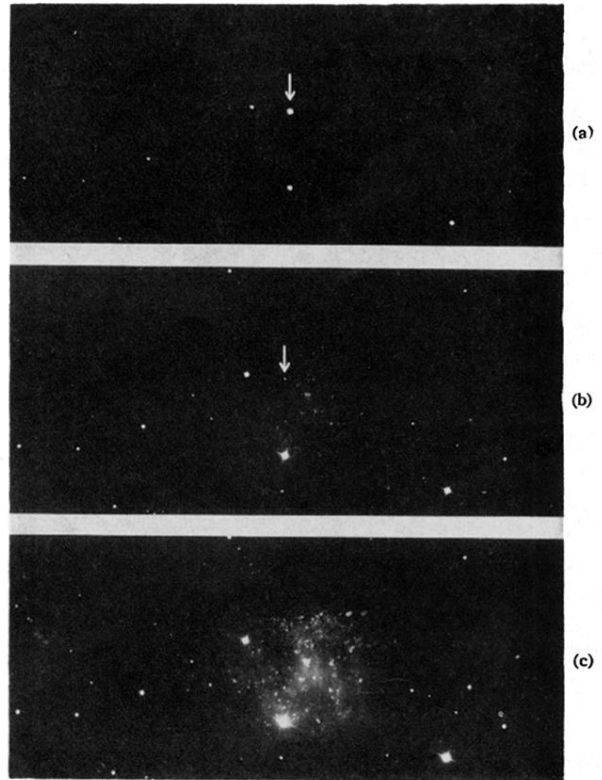Crab Nebula

Supernova in IC 4182

(a)

(b)

(c)

PLATE 4. Left: The Crab Nebula, photographed in the wavelength range λ6300–λ6750. The filamentary structure stands out clearly at this wavelength, which comprises light mainly due to the Hα line. Right: The supernova in IC 4182, photographed (a) September 10, 1937 at maximum brightness—exposure 20 m; (b) November 24, 1938, about 400 days after maximum—exposure 45 m; (c) January 19, 1942, about 1600 days after maximum, when the supernova was too faint to be detected—exposure 85 m. Note that the lengths of the three exposures are different. These plates were taken by W. Baade, to whom we are indebted for permission to reproduce them.